AQRP Project 14-016

Improved Land Cover and Emission Factor Inputs for Estimating Biogenic Isoprene and Monoterpene Emissions for Texas Air Quality Simulations

Final Report

Prepared for:

Elena McDonald-Buller
Project Manager
Texas Air Quality Research Program

Mark Estes
TCEQ Project Liaison

Prepared by:

Haofei Yu and Alex Guenther
Pacific Northwest National Laboratory

Carsten Warneke and Joost de Gouw
NOAA Earth System Research Laboratory

Sue Kemball-Cook, Jaegun Jung, Jeremiah Johnson, Zhen Liu and Greg Yarwood
Ramboll Environ

QA Requirements: Audits of Data Quality: 10% Required

September 2015

CONTENTS

APPENDICES

TABLES

FIGURES

ACKNOWLEDGEMENT

The preparation of this report is based on work supported by the State of Texas through the Air Quality Research Program administered by The University of Texas at Austin by means of a Grant from the Texas Commission on Environmental Quality.

EXECUTIVE SUMMARY

The exchange of gases and aerosols between the Earth's surface and the atmosphere is an important factor in determining atmospheric composition and regional air quality. Accurate quantification of emission fluxes is a necessary step in developing air pollution control strategies. In some cases, emissions can be directly measured (e.g., point sources with continuous emission monitors) or can be estimated with reasonable confidence (e.g., point sources that have well-defined operating parameters). In contrast, large uncertainties are associated with area sources including emissions from vegetation, and in particular, emissions of biogenic volatile organic compounds (BVOCs). Vegetation is the largest source of VOC emissions to the global atmosphere. The oxidation of BVOCs in the atmosphere affects ozone, aerosol and acid deposition. Current BVOC emission estimates are based on measurements for individual plants that must be scaled up to represent landscapes and adjusted for environmental conditions. There is a critical need for independent BVOC emission inputs for air quality models.

Texas Air Quality Research Program (AQRP) Project 14-016 used aircraft observations from the 2013 Southeast Atmosphere Study (SAS) to assess and reduce uncertainties associated with a widely used BVOC emissions model, namely the Model of Emissions of Gases and Aerosol from Nature version (MEGAN; Guenther et al., 2012). The eddy covariance technique was used to directly quantify BVOC emission fluxes for all suitable aircraft observations from the SAS study.

The overall goal of this project is more accurate BVOC emission estimates that can be used in Texas air quality simulations that are critical for scientific understanding and the development of effective regulatory control strategies that will enhance efforts to improve and maintain clean air.

Estimation of Terpenoid Emissions Fluxes from Aircraft Data

Using a wavelet based approach, fluxes of isoprene and total monoterpenes were estimated using turbulence and proton transfer reaction-mass spectrometry (PTR-MS) measurements made onboard the C-130 aircraft during the 2013 SAS field campaign. Uncertainties associated with the estimated fluxes were also quantified. As expected, the highest isoprene fluxes were observed over broadleaf tree dominated woodland areas, while higher monoterpene fluxes were observed over areas such as longleaf pine woodland in Missouri and conifer and hardwood plantations in Louisiana, Texas, Arkansas and Alabama. The forests in these areas generally have higher fractions of high monoterpene emitting trees such as pines. Relatively low isoprene and monoterpene fluxes were observed over non-forested landscapes. These observations are consistent with a previous aircraft flux study in California (Karl et al., 2013; Misztal et al., 2014).

Subsampling was also performed for select C-130 flight legs to simulate the VOC sampling approach during SAS on the P-3 aircraft, which used a much longer sampling interval (15 seconds (s) versus 0.6 s on average for the C-130). The increased sampling interval in the P-3 data added significant uncertainty and error to calculated fluxes for sampling intervals greater

than a few seconds. Therefore, Fast Fourier Transform and wavelet based approaches were determined to be not suitable for analyzing VOC fluxes from the P-3 aircraft data in heterogeneous regions.

Instead, a mass balance approach was used to estimate isoprene emission fluxes from the NOAA P-3 and C-130 data. In a mass balance approach, it is assumed that the measured BVOC mixing ratio in the boundary layer reflects the equilibrium between emissions, chemical removal by hydroxyl (OH) radicals and entrainment out of the boundary layer (Warneke et al., 2010). The mass balance method requires specification of boundary layer height estimated from the aircraft data, k_{OH} is the rate coefficient for the BVOC+OH reaction, and [*OH*] is the concentration of OH radicals. The latter parameter was estimated using a parameterization from (Ehhalt and Rohrer, 2000) based on measured NO_2 mixing ratios, and j_{O1D} and j_{NO2} photolysis rates. The OH number density was measured onboard the C-130 during SAS and those data were used here to verify the validity of the OH estimate used for the mass balance approach. While there were significant differences between measured and calculated OH, the calculated OH, on average, agreed within 11% with the measurements.

The emission fluxes derived from the aircraft measurements using the mass balance approach were compared with emissions calculated using the BEIS and MEGAN models. For the purpose of these comparisons, the emissions were calculated along the flight tracks using the temperature and photoactive radiation (PAR) measured onboard the aircraft. The idea behind the approach is to use the aircraft data to constrain all the physical and chemical parameters that determine BVOC concentrations in addition to their emissions.

Isoprene emissions calculated from BEIS3.12, BEIS3.13, MEGAN2.0 and MEGAN 2.1 were compared to those calculated using the mass balance approach with measured isoprene mixing ratios from the following studies: Southeast Nexus (SENEX; the NOAA contribution to the Southeast Atmosphere Study [SAS] campaign), Nitrogen, Oxidants, Mercury and Aerosol Distributions, Sources and Sinks (NOMADSS), 2000 and 2006 Texas Air Quality Studies (TexAQS2000, TexAQS2006), International Consortium for Atmospheric Research on Transport and Transformation 2004 study (ICARTT2004) and the 1999 Southern Oxidant Study (SOS1999). The comparison showed that in general, MEGAN2.1 gives isoprene emissions that are higher than both BEIS3.12 and BEIS3.12 emissions and higher than fluxes inferred from NOMADSS aircraft measurements. The results from the C-130 (NOMADSS) and P-3 (SENEX) measurements during SAS compared very similarly with the emissions inventories. In general, MEGAN2.1 provides results that are higher than the emissions estimated from the measurements, whereas BEIS3.12 and BEIS3.13 estimates are lower. However, the uncertainties in the emissions estimated from the measurements are significant and do not allow a decision to be made as to which emissions model is more accurate. These conclusions are very similar to the observations made in previous NOAA work (Warneke et al., 2010)

Development of High Resolution Land Cover Data for MEGAN Modeling in Texas and the Southeastern US

Land cover characteristics including Leaf Area Index (LAI) and Plant Functional Type (PFT) are key driving variables for the estimation of biogenic VOC emissions by MEGAN and other biogenic emission models. Land cover and emission factor input data sets are considered the major uncertainties associated with BVOC emission estimates. We developed an updated LAI database for all of North America based on the 2013 MODIS (MOderate Resolution Imaging Spectroradiometer) satellite product (MCD15A2.005) and applied maximum green vegetation fraction from USGS (http://landcover.usgs.gov/green_veg.php), which is also based on MODIS remote sensing products. Spatial resolution of the LAIv data is approximately 900 meters. An updated 30-meter resolution PFT database (PFT16v2015) was developed for the continental US based on various ground survey, remote sensing and land surface model data products.

Emission Factor Database Development

The PFT16v2015 PFT database was developed for this project to provide the starting point for development of a high-resolution (30 m) emission factor (EF) database. An initial EF database, EFvE2015, was created using the same enclosure based emissions data used for the EF database, EFvE2011, described by Guenther et al. (2012) but with the new landcover data developed for this project and used for the new PFT database. The resulting EFvE2015 data were then compared with the EFvE2011 data. An additional database, EFvA2015, was created based on aircraft flux measurements and the new landcover and compared with the other EFs.

Compared with the EFvE2011 data, the EFvE2015 data predicts higher isoprene emission factors in some regions in the southeastern US, with the biggest differences in north Florida, central Texas, Oklahoma and Arkansas. Higher broadleaf deciduous tree coverages are also predicted for these areas in the PFT16v2015 database. On the other hand, lower broadleaf deciduous tree coverages were predicted by the PFT16v2015 database for southeast Missouri and northern Minnesota, which also has lower isoprene emission factors in the EFvE2015 database. The differences are mainly due to the incorporation of the LandFire existing vegetation type (EVT) data, which provides more spatial detail than the land cover dataset used to develop the EFvE2011 dataset.

Development of Airborne Emission Factors

Aircraft observations were used to evaluate and constrain MEGAN emission factors following the method of (Karl et al., 2013; Misztal et al., 2014) with some improvements and were used to develop the EFvA2015 emission factor database. The wavelet based approach provides isoprene and monoterpene flux data at high spatial resolution. However, the calculated fluxes are for the altitude at which the aircraft is flying and must be extrapolated to the surface level in order to be used to estimate EFs for biogenic VOCs. We applied a vertical flux divergence approach to perform this task. Surface fluxes of BVOCs were then calculated using a vertical flux divergence correction method (Misztal et al., 2014) that assumes a linear relationship between fluxes at different altitudes.

Converting the surface fluxes into EFs requires accurate estimates of meteorological conditions such as temperature, solar radiation and, to a lesser degree, other factors including soil

moisture, wind speed and humidity. The MEGAN model calculates BVOC emissions as the product of an EF and an emission activity factor (EAF) that accounts for the impact of driving variables including canopy environment. We calculated the EAF associated with each aircraft flux measurement and applied this factor to the extrapolated surface flux to obtain the emission factor for standard conditions.

EAFs were calculated using two different approaches. For one version, EAFs were calculated by executing a single point version of MEGANv2.1 for every flux measurement, using the LAIv and vegetation cover with meteorological fields extracted from the North American Land Data Assimilation System (NLDAS-2) forcing data and soil moisture data extracted from NLDAS-2 model data (VIC model). For the second version, EAFs were calculated using the regional MEGANv2.1 model with EFvE2011 emission factor database and meteorological driving variables derived from the Weather Research and Forecasting Model (WRF; Skamarock et al., 2008).

The correlation between EFvE2015 and airborne based EF suggest that the land cover data reasonably captures the variations of BVOC emissions among different EVTs. The correlations between airborne EF calculated using different approaches and the landcover based EFvE2015 data range from 0.32 to 0.73.

The airborne EFs calculated using WRF or using NLDAS meteorological data are considerably different. The WRF based EF values are consistently lower due to higher EAF values estimated by WRF. This is likely due to a high bias in solar radiation and temperature due to underestimates of aerosol and clouds. We have used the NLDAS data for our analysis because it includes assimilation of observed meteorology. However, the substantial differences (~37%) between the WRF and NLDAS results demonstrate the importance of having accurate meteorological observations to determine airborne EFs.

Development of MEGAN Biogenic Emission Inventories and Regional Photochemical Modeling

Using the landcover and emission factor databases described above, we prepared three sets of MEGAN v2.1 biogenic emissions for a June 1–July 15, 2013 modeling episode that encompassed the P-3 and C-130 SAS flights. The first inventory was a base-case biogenic emission inventory, which was developed using the MEGANv2.1 default landcover database, PFT16v2011, and default emission factors, EFv2011. This inventory is referred to as EFvE2011 below. Then, a second biogenic emission inventory (denoted by EFvE2015) was derived from updated inputs: the new high-resolution landcover database, PFT16v2015, and the EFvE2015 emission factor database described above. Finally, a third biogenic emission inventory was derived from the new high-resolution landcover database, PFT16v2015, and the EFvA2015 emission factor database; this inventory was used in a sensitivity test described below and is referred to as EFvA2015.

The three MEGAN emissions inventories were developed using temperatures and PAR from a WRF simulation of the June-July 2013 episode performed as part of this study. WRF was run with a new algorithm that accounts for the radiative effects of sub-grid scale cumulus clouds

(Alapaty et al., 2012; Herwehe et al., 2014) and has been shown to reduce surface downward shortwave radiation (DSW) and improve the simulation surface temperature and precipitation relative to the unmodified version of WRF.

Comparison of WRF modeled surface downward shortwave radiation (DSW) with visible satellite images for the C-130 flights and solar radiation measured at TCEQ monitoring sites indicated that, despite the additional cloud-radiation feedback, WRF underestimated the observed cloud field and overestimated DSW. Underestimating clouds and overestimating the available shortwave radiation very likely introduced a high bias in the MEGAN isoprene emissions through a high bias in PAR and affected the partitioning of surface heat and moisture fluxes.

The default (EFvE2011) and updated (EFvE2015) MEGAN biogenic emission inventories were compared against aircraft flux data and then evaluated using a photochemical grid model. The evaluation of the isoprene and monoterpene emissions against aircraft flux data showed that the MEGAN v2.1 isoprene emissions were consistently higher than the aircraft flux data calculated along the C-130 racetrack flight segments. This was true for both the default and updated MEGAN emission inventories. The default and updated MEGAN monoterpene emissions showed closer agreement with the airborne fluxes than the isoprene emissions, but the MEGAN monoterpene emissions were also generally higher than the airborne fluxes. The MEGAN monoterpene emissions had a spatial pattern similar to the airborne fluxes, with high emissions over the Texas-Louisiana border region, Mississippi and Alabama and lower emissions over southern Missouri and western Tennessee. The changes between default and updated inventories varied along the flight tracks, and it is difficult to assess which inventory showed better agreement with the airborne fluxes. The comparison between MEGAN emissions and the airborne fluxes is affected by the use of different meteorological data (WRF and NLDAS) in preparing the emissions flux estimates.

We performed regional photochemical modeling for June 1-July 15, 2013 time period of the C-130 and P-3 aircraft flights using both the default (EFvE2011) and updated (EFvE2015) MEGAN emission inventories. We evaluated modeled concentrations of terpenoid and other species against the aircraft measurements and compared modeled surface layer ozone to ground level ozone measured at rural sites. The Comprehensive Air Quality Model with Extensions (CAMx; Ramboll Environ, 2015) model has a high bias for surface ozone that is most pronounced at coastal sites during periods of onshore flow. This suggests that the model is affected by bias in the model boundary conditions for ozone and/or precursors.

Using both the default (EFvE2011) and updated (EFvE2015) MEGAN inventories, CAMx simulated spatial patterns of high and low isoprene that are similar to those of the aircraft observations. For example, both the modeled and the measured isoprene are relatively high in the region that includes northeast Texas, northwest Louisiana and southwestern Arkansas. Both observed and CAMx isoprene concentrations show hot spots in southeastern Missouri, central Alabama and central Georgia. Areas of low isoprene occur in the model and measurements in northern Indiana, northern Mississippi South Carolina, northeastern Kentucky and central

Texas. CAMx generally overestimates isoprene along the aircraft flight tracks with bias of 84% using the default EFvE2011 MEGAN emissions and 104% in the updated case with the EFvE2015 biogenic inventory.

Although the modeled high bias for isoprene relative to aircraft observations increased in the run using the updated EFvE2015 MEGAN emissions, the CAMx model's performance in simulating ground level ozone improved in the Houston area. The updated MEGAN inventory EFvE2015 has a significantly lower isoprene emissions factor and lower isoprene emissions in the Houston area, and this appears to reduce ground level ozone, bringing the model into closer agreement with observations. Kota et al. (2015) compared the gridded MEGAN isoprene emissions factor for the region north of Houston with isoprene emission factor estimates derived from a field study and found that the MEGAN emission factor was higher. Kota et al. determined that the overestimated isoprene emission factor caused a high bias in modeled isoprene concentrations in their Community Multiscale Air Quality (CMAQ) model simulation, but the isoprene overestimates did not significantly influence modeled ozone; this is in contrast to results of our CAMx simulations, in which changes in Houston area isoprene emissions strongly affected modeled ozone.

In the CAMx simulations, changes in surface ozone due to the change in the MEGAN emission inventory were relatively small outside of the Houston area and monitoring sites near the eastern border of Texas,

In the CAMx runs using default and updated EFvE2015 MEGAN emissions, modeled monoterpene concentrations were generally lower than the observed concentrations along the P-3 and C-130 flight tracks. Values of the coefficient of determination were lower for monoterpenes than for isoprene. In the run with updated EFvE2015 MEGAN emissions, the magnitude of the CAMx model's low bias for monoterpenes was reduced relative to the run with default emissions.

Four additional CAMx sensitivity tests were carried out.

1. We altered the CB6r2 chemical mechanism to increase the production of OH from the breakdown of isoprene following the mechanism of Peeters et al. (2013). The purpose of the test was to gauge the model's response to an isoprene mechanism that represents an upper limit on the production of OH from isoprene. Increasing OH production from isoprene reduces but does not eliminate the high bias in isoprene products.

2. Based on the high bias for isoprene noted in the CAMx run that used default MEGAN emissions, we reduced the MEGAN isoprene emissions by a factor of 2 for all grid cells and times and reran CAMx. For the P-3 data, the CAMx default run high bias for isoprene products (114%) changed to a low bias of -7% in the sensitivity test as a result of the lower isoprene emissions and atmospheric concentrations. For the C-130 data, the CAMx bias for isoprene products changed from 48% to -33%. The reduction in the

magnitude of bias for isoprene products in this sensitivity test suggests that the MEGAN isoprene emissions are overestimated in the default EFvE2011 case.

3. In June 2013, Nguyen et al. (2015) measured dry deposition velocities (V_d) for biogenic trace gases in an Alabama forest during the Southern Oxidant and Aerosol Study (SOAS). Comparison of CAMx V_d against the measurements showed Vd was underestimated in the model. We increased CAMx dry deposition of these species to improve agreement with the SOAS measurements. The effects of this test on modeled ozone and isoprene and monoterpenes species were small.

4. We ran CAMx with the EFvA2015 MEGAN emission inventory that used isoprene emission factors developed using SAS aircraft data. In the CAMx run with EFvA2015 MEGAN emissions, the high bias for isoprene decreased from 84%-113% in the default (EFvE2011) run and 104%-132% in the EFvE2015 sensitivity test to the range -5% to -16% in the CAMx EFvA2015 sensitivity test. The use of the EFvA2015 emission factors for isoprene in MEGAN improved the CAMx model's ability to reproduce the isoprene concentrations measured by the P-3 and C-130 aircraft. Although the high bias seen in the default EFvE2011 and EFvE2015 CAMx runs is reduced in the EFvA2015 sensitivity test, there was no improvement in correlation between observed and modeled values. R^2 values decreased slightly in the EFvA2015 sensitivity test relative to the CAMx runs using the default and EFvE2015 MEGAN emissions.

The best overall performance among all CAMx runs for a subset of species (isoprene, isoprene products, sum of monoterpenes, ozone, OH) occurred in the sensitivity test in which CAMx was run with the EFvA2015 MEGAN emissions that used emissions factors developed using the aircraft data. The CAMx bias for ozone was nearly unchanged across all CAMx runs. In the CAMx run with updated EFvE2015 MEGAN emissions, the CAMx bias for monoterpenes improved, but the overall bias for isoprene, isoprene products and OH increased. These results, taken together with the high bias in MEGAN isoprene emissions compared to the aircraft fluxes, suggest that MEGAN isoprene emissions are overestimated in both the default EFvE2011 and updated EFvE2015 inventories.

Conclusions

Below, we present conclusions drawn from the results of this study.

- Accurate meteorological input data, especially PAR and temperature, are critical for accurate BVOC emission calculations. Bias in weather model simulation of clouds and shortwave radiation introduces bias into the MEGAN emissions. Standard WRF simulations may result in considerable high bias in solar radiation and temperature due to model treatment of clouds. NLDAS appears to be better but also leads to overestimates. It should also be noted that bias in the PAR and temperature used to estimate emission factors from measured emissions will also introduce bias into the calculated emission factors. Data assimilation approaches (satellite and/or in-situ observations) are recommended for improving these inputs and they should be evaluated by comparison to observations.

- Landcover inputs (LAI and vegetation type) are also critical for BVOC emission modelling. LAI can vary considerably between years and we recommend using the provided 2013 LAI data for 2013 simulations and use the provided scripts and approach to calculate LAI for other years. We also recommend using the vegetation type distributions developed for this project.
- Emission factors are another key variable for BVOC emission modelling. We recommend using the new (aircraft based) isoprene emission factors (EFvA2015) developed for this project for BVOC emission modelling since both the eddy covariance and mixed layer approaches indicate this. However, more work still needs to be done to verify these emission factors and reconcile the substantial differences between leaf based, tower based, aircraft based and satellite based emission estimates. There is less evidence that the monoterpenes should be changed so we do not recommend changing the emission factors for monoterpenes from EFvE2015 to EFvA2015 at this time.

Recommendations

- We need to reconcile the substantial differences between leaf-scale, tower-scale and aircraft-scale emission estimates as well as comparisons to satellite based emission estimates.
- As is the case with most BVOC studies, we have focused on only a few compounds but there is evidence that other "unmeasured" compounds play an important role in atmospheric chemistry (e.g. Di Carlo et al., 2004; Goldstein and Galbally, 2007; Park et al., 2013; Jardine et al., 2015). New analytical techniques provide an opportunity for determining whether there are other important compounds and also for characterizing the contribution of these compounds (Pankow et al., 2012). New techniques include high sensitivity, high resolution, accurate mass, full scan mass spectrometry (time of flight and Orbitrap) and better approaches to minimize artifacts and losses (whole air sampling, removing oxidants with reactive alkenes).
- BVOC response to stress is recognized as potentially important but not well known component of BVOC emission models. These processes could lead to extreme (low or high) emission rates that could have an impact on air quality model results and should be quantified and evaluated.
- A good understanding of hydroxyl (OH) radical concentrations in forest environments is essential for modelling BVOC concentrations and for the interpretation of the measurements of BVOC fluxes. However, several detailed measurements have yielded significantly higher concentrations than can be explained using the known chemical reactions. Resolving this issue is important to advance the understanding of the effect of BVOC emissions on radical levels and ozone formation.
- Accurate meteorological data (PAR and temperature) is critical for accurate BVOC emission calculations. Bias in the WRF model's simulation of clouds and shortwave radiation introduces bias into the MEGAN emissions. The magnitude of this bias can be assessed by comparison of MEGAN emissions calculated along the aircraft flight track using

temperatures and PAR measured aboard the aircraft with MEGAN emissions calculated using WRF model temperatures and PAR. Improvements to the WRF model treatment of clouds and radiation that enable it to provide accurate inputs to MEGAN are needed for development of accurate BVOC emission inventories for photochemical modeling.

- Southern Oxidant and Aerosol Study (SOAS) dry deposition velocity measurements were very useful in constraining CAMx model dry deposition of oxygenated VOCs. Dry deposition measurements for other species/locations would be very helpful in improving models.
- The high resolution (1 m resolution) landcover data should be complemented with geolocated ground surveys of tree species composition and used to improve the MEGAN landcover in urban areas of Texas.

1.0 INTRODUCTION

This document provides the final report for the Texas Air Quality Research Program (AQRP) Project 14-016 "Improved Land Cover and Emission Factor Inputs for Estimating Biogenic Isoprene and Monoterpene Emissions for Texas Air Quality Simulations". The project Co-Principal Investigators (Co-PIs) are Dr. Greg Yarwood of Ramboll Environ, Dr. Alex Guenther of Pacific Northwest National Laboratory (PNNL), and Dr. Joost de Gouw of NOAA's Earth System Research Laboratory. The AQRP project manager is Dr. Elena McDonald-Buller at the University of Texas, Austin. The project liaison for the Texas Commission on Environmental Quality (TCEQ) is Mr. Mark Estes.

The overall goal of this project was to improve quantitative estimates of terpenoid (isoprene and monoterpene) emissions from Texas and the Southeast United States using recent airborne measurements. During the Southeast Atmosphere Study (SAS) 2013 summer field campaign, the NCAR C-130 aircraft and the NOAA P-3 aircraft measured terpenoid (isoprene and total monoterpenes) concentrations over Texas and surrounding states using proton transfer reaction mass spectrometer (PTR-MS) systems and speciated monoterpenes using gas chromatograph mass spectrometry (GC-MS) (in-situ fast-response GC-MS on the NCAR C-130 and canister sampling with laboratory GC-MS analysis for the NOAA P-3). Both aircraft have fast response vertical wind measurements suitable for applying the eddy covariance (EC) technique, which provides a direct measurement of fluxes as described below. Approximately a third of the NCAR C-130 flights were designed to make terpenoid EC flux measurements. Measurement protocols and flight patterns of other NCAR C-130 flights and most NOAA flights were not specifically designed for terpenoid EC flux measurements, but we investigated the possibility of estimating EC fluxes with these measurements. In addition, the availability of direct EC flux measurements and estimates of terpenoid lifetimes (based on measured ozone and OH concentrations) provided an opportunity to examine the utility of using concentration measurements (both mean values and variance measured with fast response PTR-MS) to estimate fluxes in different NOx regimes. This has the potential to greatly expand the observations available for relating terpenoid emissions to land cover distributions because of the large database of NOAA P-3 aircraft measurements. These emission estimates were used to evaluate and update the emission factors used in the Model of Emissions of Gases and Aerosols from Nature (MEGAN) (Guenther et al., 2012). In addition, high-resolution land cover inputs for MEGAN were generated and described in detail. The new and old (default) land cover and emission factor inputs were used to examine the sensitivity of emission and air quality model estimates to uncertainties in these inputs.

The primary outputs of this research are improved land cover and emission factor inputs for the MEGAN biogenic emission model. Outcomes include approaches for quantifying VOC emissions and relating emissions to land cover distributions in order to reduce uncertainties in emissions. The overall benefit of this project is more accurate VOC emission estimates that can be used in Texas air quality simulations that are critical for scientific understanding and the development of regulatory control strategies that will enhance efforts to improve and maintain clean air.

1.1 Background

The exchange of gases and aerosols between the earth's surface and the atmosphere is an important factor in determining atmospheric composition and regional air quality. Accurate quantification and simulation of these fluxes is a necessary step towards developing air pollution control strategies and for attributing observed changes to their causes. Emissions of some compounds, including sulfur dioxide and nitric oxide emitted from electric utilities, are either directly measured or can be estimated with reasonable confidence in the U.S. In contrast, large uncertainties are associated with area source emission estimates including biogenic terpenoid emissions. Current flux estimates are typically based on a few indirect measurements that may not be representative and so could be of limited use for informing regional air quality models. The need for accurate emission estimates requires a transformation of the approaches used to characterize the emissions needed as inputs for air quality models.

1.2 Overview of Approach

We used NCAR C-130 and NOAA P-3 aircraft observations from the 2013 SAS study and NOAA P-3 aircraft observations from the 2006 Texas Air Quality Study to assess and reduce uncertainties associated with the Model of Emissions of Gases and Aerosol from Nature version 2.1 (MEGANv2.1) (Guenther et al. 2012), a widely used biogenic emissions model. In addition, we improved the land cover and emission factor driving variables that are considered the major uncertainties associated with biogenic VOC emission estimates (Guenther 2013).

Our specific objectives included:

1. Use the eddy covariance technique to directly quantify terpenoid emission fluxes for all suitable NCAR C-130 observations during the 2013 SAS study.
2. Using the relationship between terpenoid fluxes and concentrations derived from the NCAR C-130 data, estimate terpenoid fluxes in the southeastern U.S. and Texas using NOAA P-3 aircraft observations from 2013 SAS research program and the 2006 Texas Air Quality Study.
3. Develop high-resolution (30-m) land cover inputs for MEGAN 2.1 (Leaf Area Index, plant functional type and emission factors) for Texas and southeastern U.S. using best available satellite imagery and ground measurements. Provide clear description of methods to ensure reproducibility and future modifications.
4. Use aircraft flux measurements and improved landcover data to a) determine average emission factors for various emission types and investigate variability within emission types, b) identify land cover types with unexpectedly high or low emissions that should be targeted by future studies, c) investigate relationships between foliage density (satellite based Leaf Area Index) and emissions across a given emission type, d) revise emission factors as needed based on aircraft observations.
5. Develop MEGAN biogenic emissions for regional photochemical modeling using updated land cover and emission factors for Texas and the Southeastern U.S. and compare with MEGAN emissions developed using default land cover and emission factors. Evaluate both MEGAN inventories against aircraft flux data.

6. Perform air quality modeling with the MEGAN emission inventory prepared with default inputs and the improved MEGAN emission inventories and evaluate modeled concentrations against measurements in high and low isoprene and NOx regimes.
7. Prepare recommendation as to whether MEGAN inputs developed in 3 and 4 above should be used in future TCEQ modeling.

1.3 Overview of Report

In Section 2, we describe the estimation of terpenoid emission fluxes from C-130 and P-3 aircraft data using wavelet based and mass balance approaches. The development of high-resolution land cover data for MEGAN modeling in Texas and the Southeastern US is discussed in Section 3. Section 4 describes the emission factor database development. Section 5 describes the photochemical modeling with default and updated MEGAN emission inventories and evaluation of modeled concentrations against surface and aircraft measurements. Finally in Section 6, we present conclusions and recommendations for future work.

.

2.0 ESTIMATION OF TERPENOID EMISSION FLUXES FROM AIRCRAFT DATA

Isoprene and total monoterpene fluxes were calculated using turbulence and PTR-MS measurements made onboard the C-130 aircraft during the 2013 SAS field campaign. Subsampling was also performed for select C-130 flight legs to simulate VOC observations as collected on the P-3 aircraft, which used a much longer sampling interval. Methods used in flux estimation, as well as results, evaluation and discussion, are described below.

2.1 Terpenoid Emission Fluxes from C-130 Aircraft Data

Using wavelet based approaches, fluxes of isoprene and total monoterpenes were estimated from PTR-MS measurement data onboard the C-130 aircraft during the 2013 SAS field campaign. Uncertainties associated with the estimated fluxes were also quantified. Section 2.1.1 provides a description of the methods used in flux estimation, followed by results, evaluation and discussions (Section 2.1.2).

2.1.1 Flux Estimation Methods

2.1.1.1 Continuous Wavelet Transform

Wavelet analysis is a powerful mathematical tool for the analysis of trace gas fluxes from airborne measurements data, and this approach has been successfully applied in several airborne field campaigns (Karl et al., 2009;Karl et al., 2013;Mauder et al., 2007;Misztal et al., 2014). Compared with the traditional eddy-covariance method that is based on Fast Fourier Transform (FFT), the wavelet based method relaxes the stationarity requirement and enables investigation of flux contributions from temporally varying spectrums resulting in flux estimates with high spatial resolution. Figure 2-1 provides an example of a comparison between isoprene fluxes estimated using the wavelet and FFT approaches. For an individual flight leg, the FFT approach provides only one flux estimate for the entire 30 km flight leg, while the wavelet approach provides highly resolved flux data. These highly resolved data are very helpful especially for areas with relatively heterogeneous surface topography or land cover.

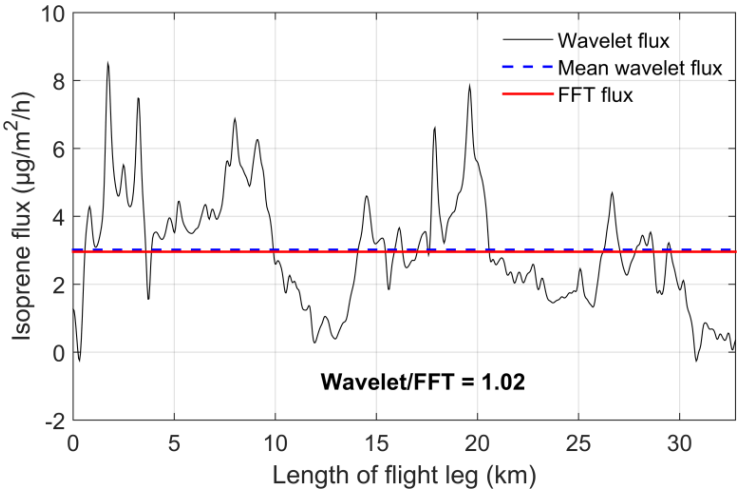

Figure 2-1. An example of a comparison between fluxes estimated using the FFT and wavelet approaches.

In this study, we employed a Continuous Wavelet Transform (CWT) using the Morlet wavelet to quantify temporally resolved isoprene and total monoterpene fluxes from aircraft observation data. Isoprene and monoterpene concentration data collected from the PTR-MS instrument are discrete signals with an average sampling frequency around 1.5 Hz. By assuming the discrete signal is *f(n)*, a wavelet transform of *f(n)* is:

$$W_x(a,b) = \sum_{n=0}^{N} f(n)\overline{\psi_{p,a,b}(n)}$$

$$\psi_{p,a,b} = \frac{1}{a^p}\psi\left(\frac{n-b}{a}\right)$$

where $W_x(a,b)$ is the wavelet coefficient; $\psi_{p,a,b}$ is the "mother wavelet", whose shape is determined by the scale or dilation parameter *a,* and location determined by the translation parameters *b*; and *p* is a normalization factor. For this study, the Morlet wavelet was chosen due to its successful application in previous studies (Karl et al., 2009;Karl et al., 2013;Misztal et al., 2014). Further discussions of the technical details of wavelet based eddy-covariance method can be found elsewhere (Thomas and Foken, 2005;Torrence and Compo, 1998).

The wavelet-based eddy-covariance approach was applied for selected "racetracks" and transect segments of the C-130 research flights 1, 2, 3, 4, 5, 8, 10, 11, 13, 15, 16, 17, 18 and 19 of the SAS campaign. The other research flights were not designed for flux measurements and data from these flights are not considered to be suitable for estimating surface fluxes.

Horizontal flight legs for flux analysis (flux legs) were purposefully selected to exclude sudden aircraft movements such as substantial changes in roll, pitch and yaw angles. In addition, vertical legs were also selected for the determination of planetary boundary layer (PBL) heights, which is needed for wavelet flux analysis and flux divergence corrections. An example of selected flux and PBL legs is shown in Figure 2-2. Vertical profiles of isoprene concentration, potential temperature, virtual potential temperature, water vapor mixing ratio and horizontal wind speed were used to determine PBL height.

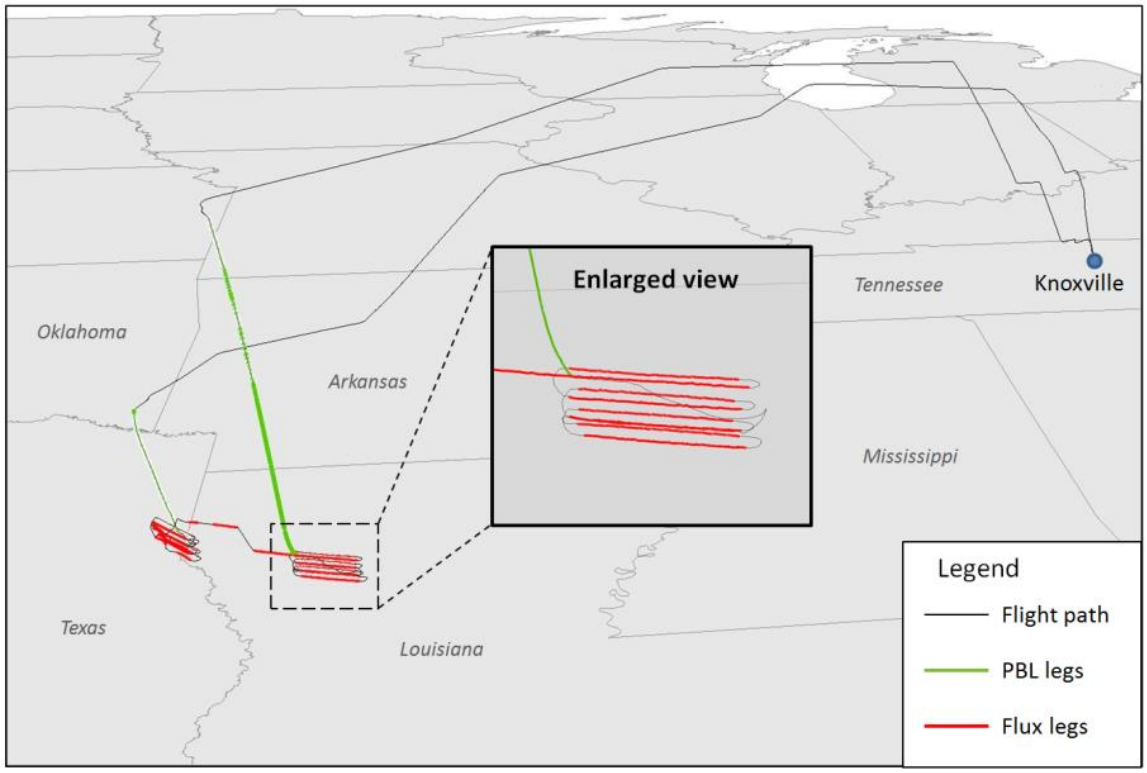

Figure 2-2. Selected flux and PBL legs of research flight 2 that illustrate transects (straight line segments) and stacked racetracks (racetrack shaped segments flown at several different altitudes).

Delay time between concentration data of biogenic VOCs measured by the PTR-MS instrument and the turbulence measurements were determined by examining covariance between vertical wind and BVOC concentrations. Flux legs were rejected if the estimated delay times were outside of expected values or if there was no clear peak in covariance.

2.1.1.2 Quality Assurance

For quality assurance purposes, systematic error (SE), random error (RE) and disjunct errors (DE) (Karl et al., 2013;Lenschow et al., 1994) were calculated for each flux leg as:

$$SE = \frac{2.2 z_i (z / z_i)^{1/2}}{L}$$

$$RE = 1.75 (z / z_i)^{1/4} (z_i / L)^{1/2}$$

$$DE = \frac{\Delta}{T}\left\{\coth\left(\frac{\Delta}{2T_s}\right) - \frac{\Delta}{T}\left[\frac{1 - e^{-T/T_s}}{2\sinh^2(\Delta / 2T_s)}\right]\right\}$$

where z is flight altitude; z_i is the height of the Planetary Boundary Layer (PBL); L is the length of corresponding flux leg in kilometers; Δ is disjunct sampling interval; T is sampling length in

seconds; and T_s is integral time scale, determined from the autocorrelations of VOC sampling data. Flux legs with significantly higher errors, mostly short flight legs, were rejected in later analysis. Further discussions and derivations of the above equations are reported by (Lenschow et al., 1994;Misztal et al., 2014).

Additional quality assurance measures were also performed. First, for each racetrack and transect, isoprene and monoterpene fluxes were estimated using the traditional FFT approach and compared with the mean wavelet flux (see Figure 2-1 for an example). Cross-spectra of the two methods were also calculated and compared. Flux legs that did not have similar values for the two methods were rejected and were not used in further analyses. For the majority of the flux legs, the estimated FFT and mean wavelet fluxes are similar, as well as their cross-spectra.

2.1.2 Results and Discussion of Flux Estimation

Figure 2-3 shows the estimated isoprene flux data for a region near the border of Texas and Louisiana. Data from three research flights (#2, #7 and #13) are shown. Each color in the background represents a unique existing vegetation type (EVT) from the LandFire database (http://www.landfire.gov/). There are approximately 70 EVTs in this region (detailed list not shown). As illustrated in Figure 2-3, the EVT cover in this area is highly heterogeneous. However, the estimated isoprene fluxes generally decrease when approaching water bodies such as the Horseshoe Lake and Red River (with large areas of grassland/agriculture lands along the river), and increases substantially when the aircraft is flying over forested areas.

Figure 2-4 and Figure 2-5 provide an overview of isoprene and monoterpene fluxes estimated for the southeastern US from the SAS C-130 observations. As expected, the highest isoprene fluxes were observed over broadleaf tree dominated woodland areas, especially those with high contributions of high isoprene emitting tree species such as oaks, for example the floodplain forest in Louisiana, Texas and Arkansas, and dry-mesic oak forest in Missouri. The spatial pattern of monoterpene fluxes differs from isoprene, with higher fluxes found over areas such as longleaf pine woodland in Missouri and conifer and hardwood plantations in Louisiana, Texas, Arkansas and Alabama. The forests in these areas generally have higher fractions of high monoterpene emitting trees such as pines. These observations are consistent with a previous aircraft flux study in California (Karl et al., 2013;Misztal et al., 2014).

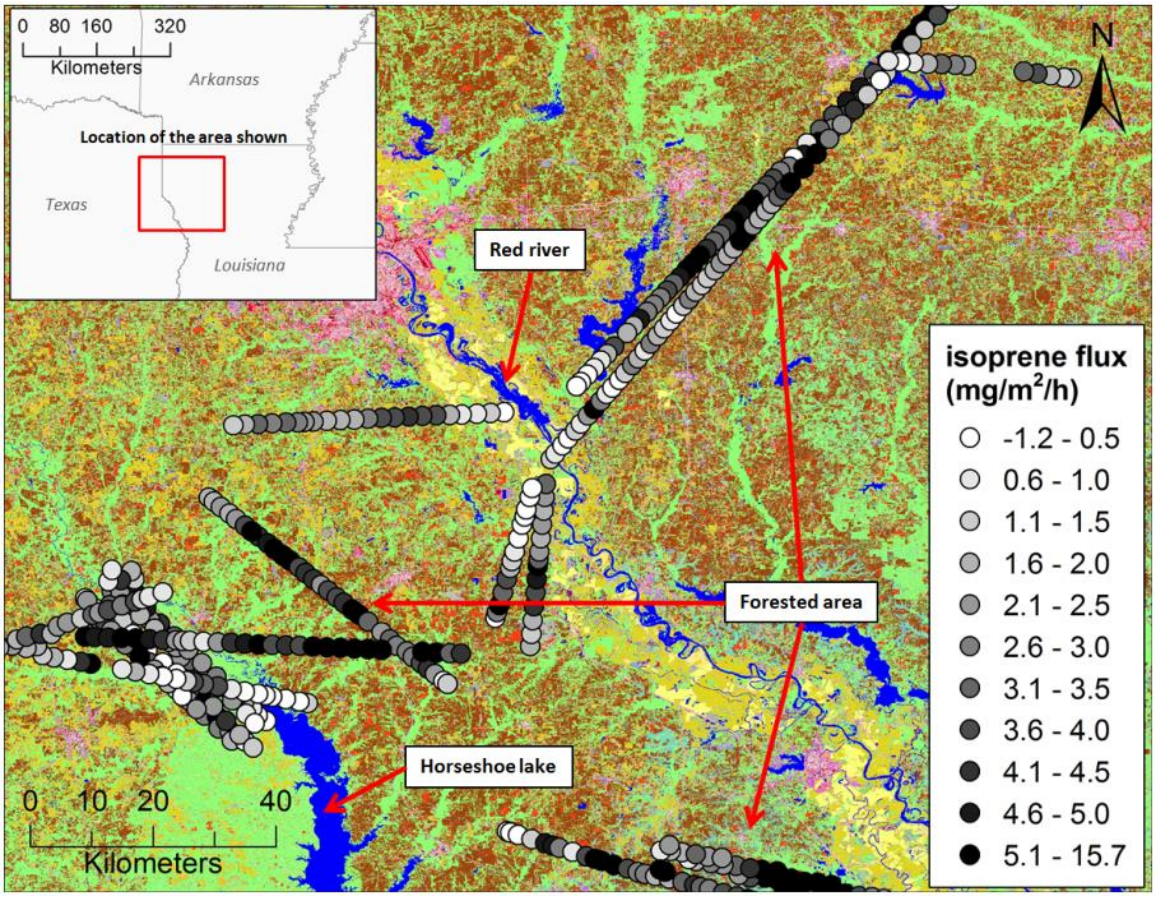

Figure 2-3. Example of the spatial distributions of LandFire existing vegetation types (EVT) and estimated isoprene fluxes. For illustration purposes, isoprene fluxes data were spatially averaged to 2 km for each research flight.

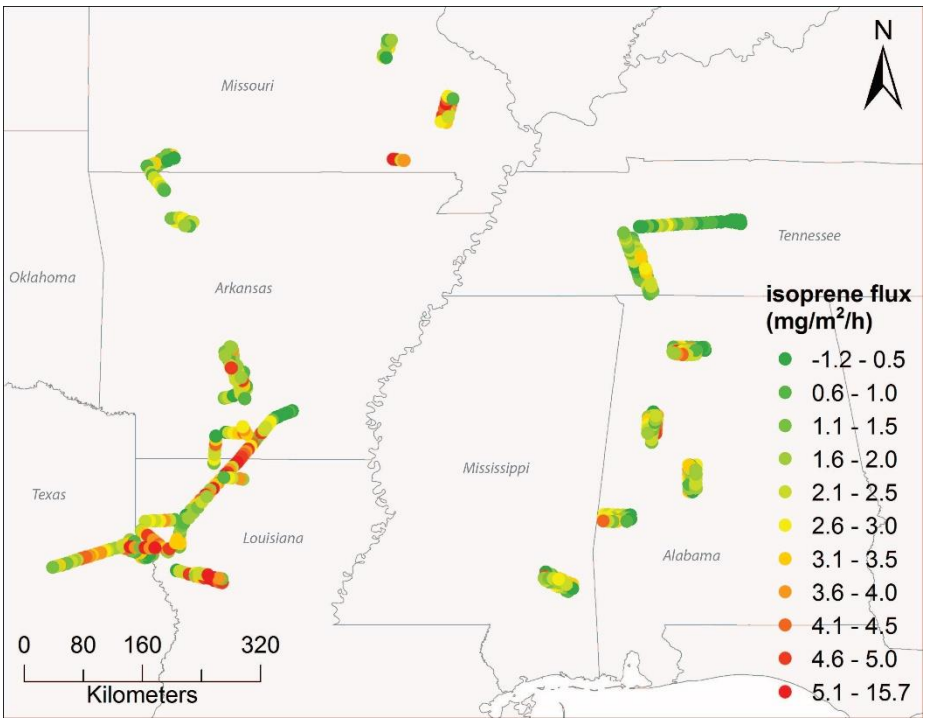

Figure 2-4. Overview of isoprene fluxes estimated for southeastern US. The flux data shown here were spatially averaged to 6 km.

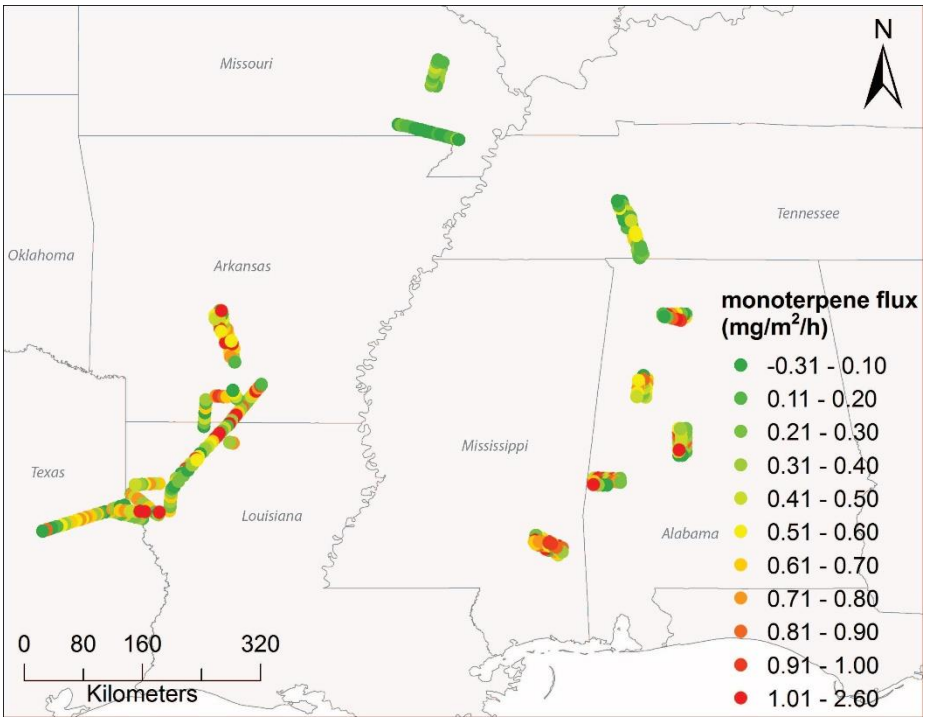

Figure 2-5. Overview of monoterpene fluxes estimated for southeastern US. The flux data shown here were spatially averaged to 6 km.

2.2 Suitability of Wavelet Approach for P-3 Aircraft Data

One of the objectives of this study is to investigate whether biogenic VOC concentration measurements collected by the NOAA P-3 aircraft during the 2013 SAS and the 2006 Texas Air Quality Study are suitable for flux analysis using the wavelet approach. For this task, we sub-sampled the high-resolution BVOC measurements for three selected flux legs (Figure 2-6), applied the same wavelet flux estimation approach to the sub-sampled data and compared the results. The three chosen flux legs are from the C-130 SAS research flights #10, #13 and #15, with lengths around 140 km.

The PTR-MS instrument onboard the P-3 aircraft measures 12 VOC species/categories: acetaldehyde, acetone, acetonitrile, benzene, isoprene, methanol, monoterpenes, methyl vinyl ketone (MVK) plus methacrolein (MACR), methyl ethyl ketone (MEK), toluene, as well as C8 and C9 aromatics. For each individual VOC or category, one measurement was taken every 15 seconds, which is much longer than the sampling interval for the C-130 aircraft (0.6 seconds on average).

Figure 2-7 shows the deviations of FFT flux and mean wavelet flux as a function of sampling intervals for three selected flux legs in comparison to flux results calculated from original high temporal resolution data. With the increase of sampling interval, the calculated mean wavelet flux shows a generally, steady decreasing trend, while the estimated FFT flux fluctuates substantially. At a sampling interval of 15 seconds, the mean wavelet fluxes is less than 50% of actual value and further decreases to near zero when sampling interval exceeds 30 seconds.

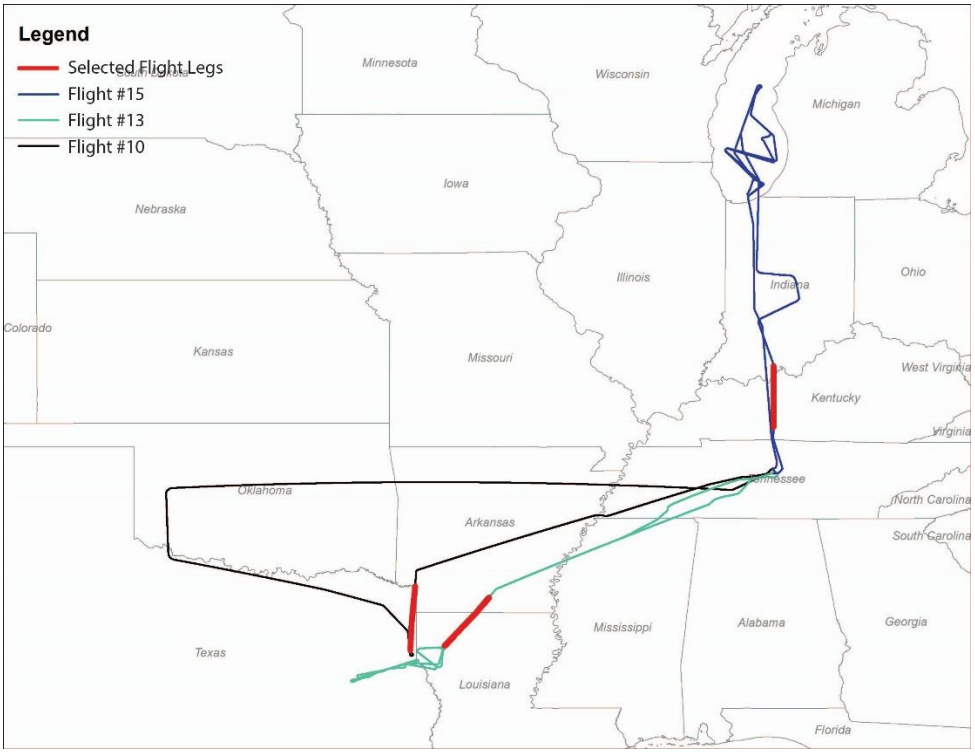

Figure 2-6. Location of the three flux legs selected for sub-sampling

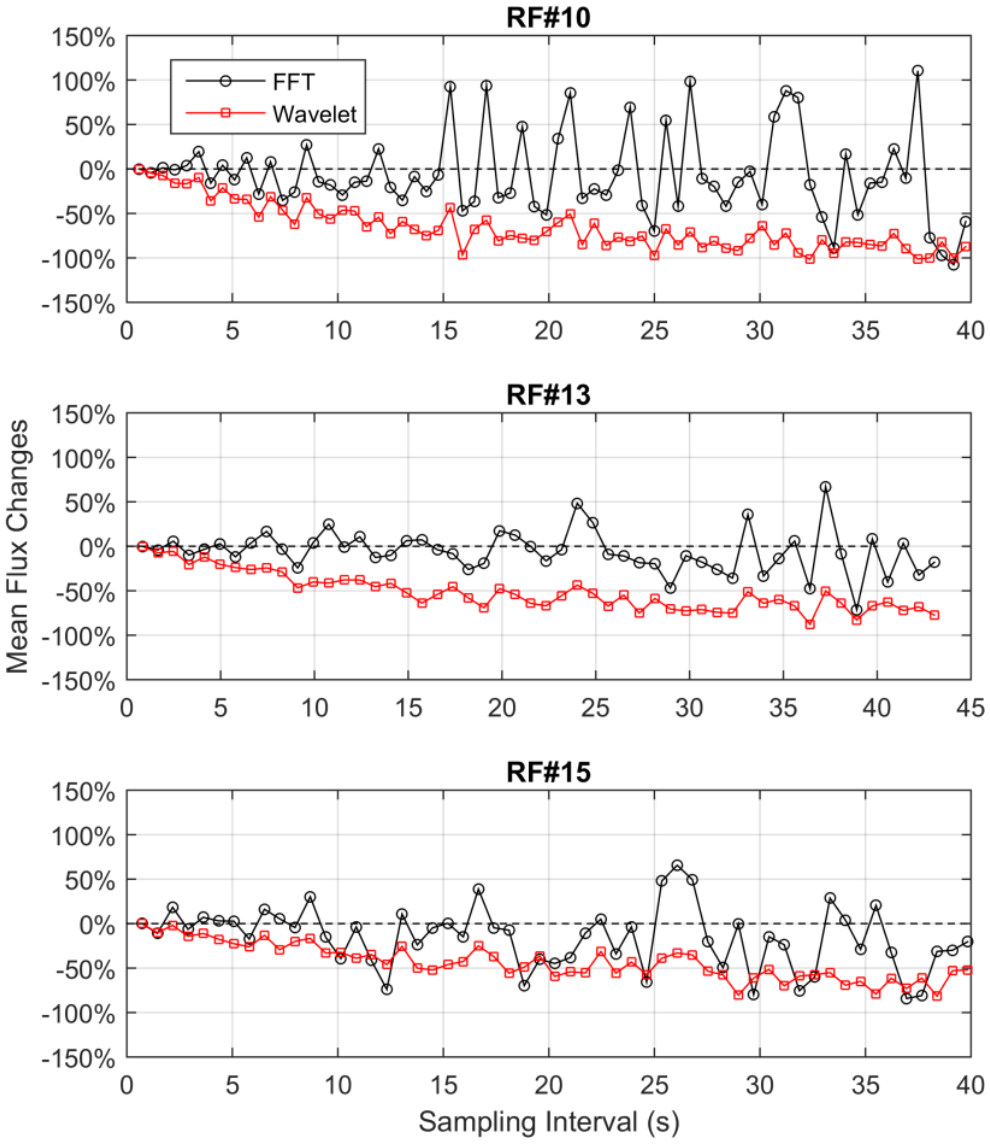

Figure 2-7. Changes of FFT flux and mean wavelet flux as a function of sampling interval.

Furthermore, the increased sampling interval also altered spatial variation patterns of the estimated wavelet fluxes along flight legs (Figure 2-8). The locations where high flux values occur were shifted or, in some cases, the high flux values disappeared altogether. This occurs because increased sampling intervals lead to greater high frequency attenuations, hence higher degrees of signal aliasing. All of which consequently results in spectrum distortions in frequency domain and adds a substantial amount of uncertainties and errors to calculated fluxes for sampling intervals greater than a few seconds. Therefore, the FFT and wavelet based approaches may not be suitable for analyzing VOC fluxes from the P-3 aircraft data in heterogeneous regions and an alternative approach, such as a mass balance approach based on VOC concentrations and lifetimes, is a better alternative for estimating VOC emissions from PTRMS data when sampling intervals are greater than a few seconds.

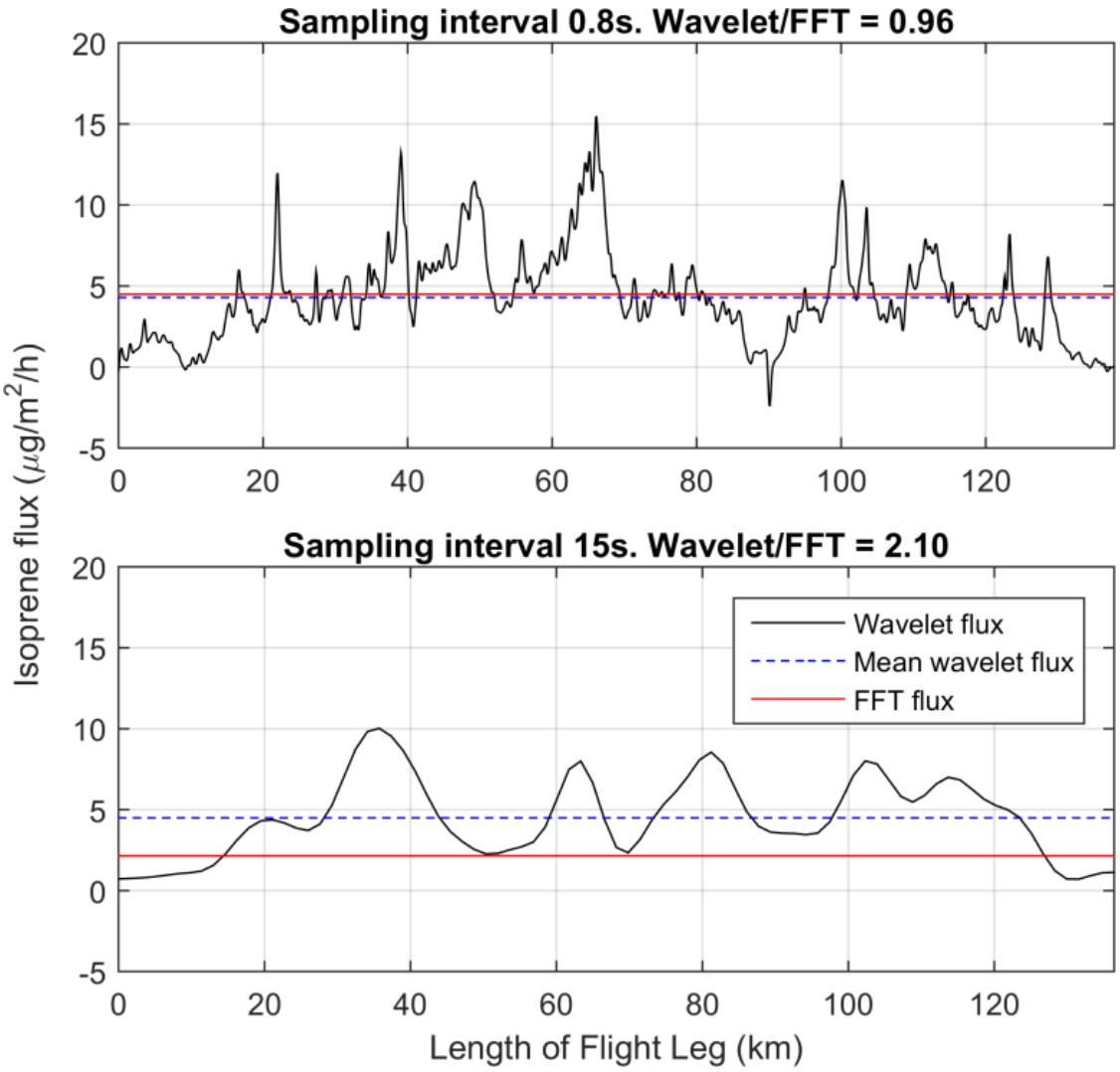

Figure 2-8. Changes in wavelet flux due to increased sampling interval. Data from the selected flux leg from research flight # 13 is shown.

2.3 Isoprene Emission Fluxes from the NOAA P-3 Aircraft Data

A mass balance approach was used to estimate isoprene emission fluxes from the NOAA P-3 and C-130 data. For the NCAR C-130 data, the results were compared with those from the wavelet fluxes described in section 2.1.

2.3.1 Mass Balance Approach for Flux Determination

In the mass balance approach used here, it is assumed that the measured BVOC mixing ratio in the boundary layer reflects the equilibrium between emissions, chemical removal by hydroxyl (OH) radicals and entrainment out of the boundary layer. The approach was first developed in (Warneke et al., 2010), who used the method to estimate fluxes of isoprene and monoterpenes over the eastern U.S. and Texas from four different airborne studies between 1999 and 2006, and compared the results to fluxes calculated from different biogenic emission models.

In (Warneke et al., 2010), BVOC emissions ($Emission_{BVOC}$) were calculated from the measured BVOC concentration ([*BVOC*]) using:

$$Emission_{BVOC} - F_e = [BVOC] \times BL_{height} \times k_{OH} \times [OH]$$

where F_e is the estimated entrainment flux, which is relatively small for most conditions, BL_{height} is the boundary layer height estimated from the aircraft data, k_{OH} is the rate coefficient for the BVOC+OH reaction, and [*OH*] is the concentration of OH radicals. The latter parameter was estimated using a parameterization from (Ehhalt and Rohrer, 2000) based on measured NO_2 mixing ratios, and j_{O1D} and j_{NO2} photolysis rates:

$$[OH] = a(j_{O^1D})^{\alpha} \times b(j_{NO_2})^{\beta} \times \frac{bNO_2 + 1}{cNO_2^2 + dNO_2 + 1}$$

In this equation, the parameters a (4.1×10^9), b (140), c (0.41), d (1.7), α (0.83) and β (0.19) were determined from OH measurements during a campaign in Germany, and the same parameters are used here. Hydroxyl radicals (OH) were measured by Mauldin and co-workers using chemical ionization mass spectrometry onboard the C-130 during SAS. Those data are used here to verify the validity of the above equation. Figure 2-9 shows a comparison between measured and calculated OH. While there are significant differences between the two, on average the calculated OH agreed within 11% with the measurements.

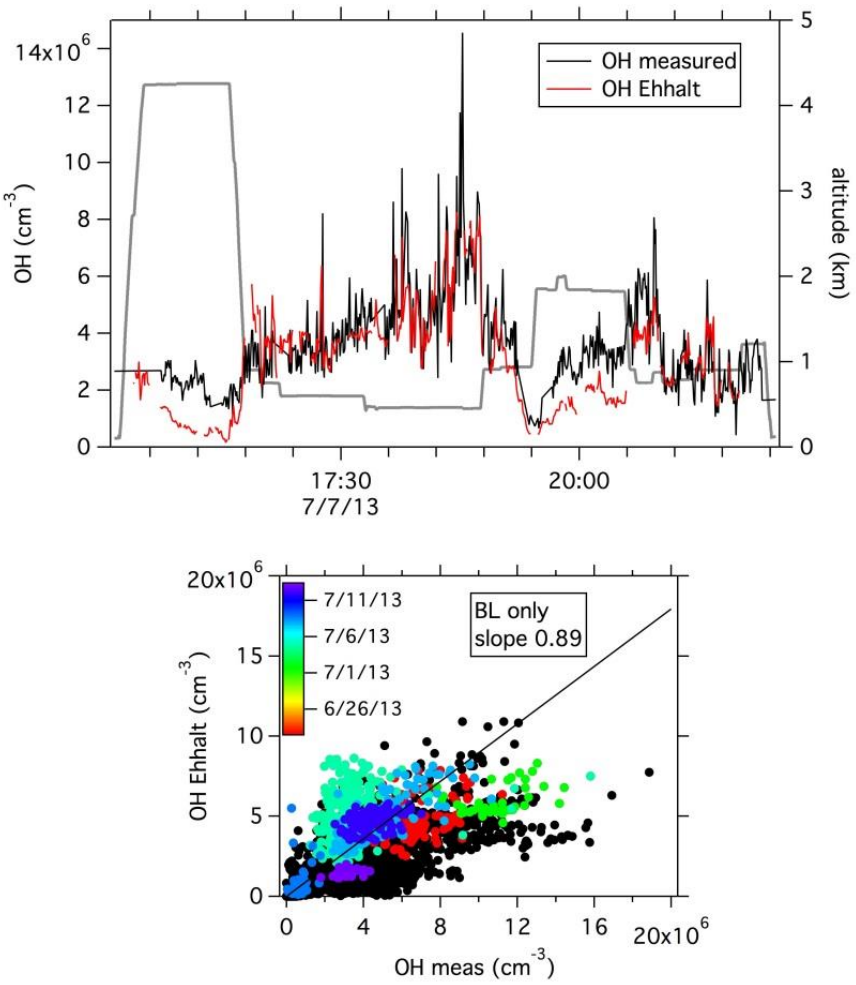

Figure 2-9. Comparison between OH measured by Mauldin and co-workers from the C-130 during SAS, and the OH calculated from the parameterization published by Ehhalt and Rohrer (2000). The top panel shows a time series for the comparison for 1 flight on July 7, 2013

An example of how the mass balance approach is used to calculate isoprene emissions from the June 16 P-3 flight in the Atlanta area is shown in Figure 2.10. Throughout the Atlanta area, enhanced isoprene was observed in the boundary layer. The boundary layer height grew from less than 1 km to about 1.5 km at 21:15 UTC (2nd panel). The calculated OH is shown in the 3rd panel of Figure 2-10 and was highly variable as the aircraft went through different air masses with varying amounts of NOx and as j-values varied underneath broken clouds. Using the above equations, isoprene emissions can now be calculated and are shown in the 4th panel of Figure 2-10, in addition to the 5-min running average, which is used in the following for comparison with the emissions inventories.

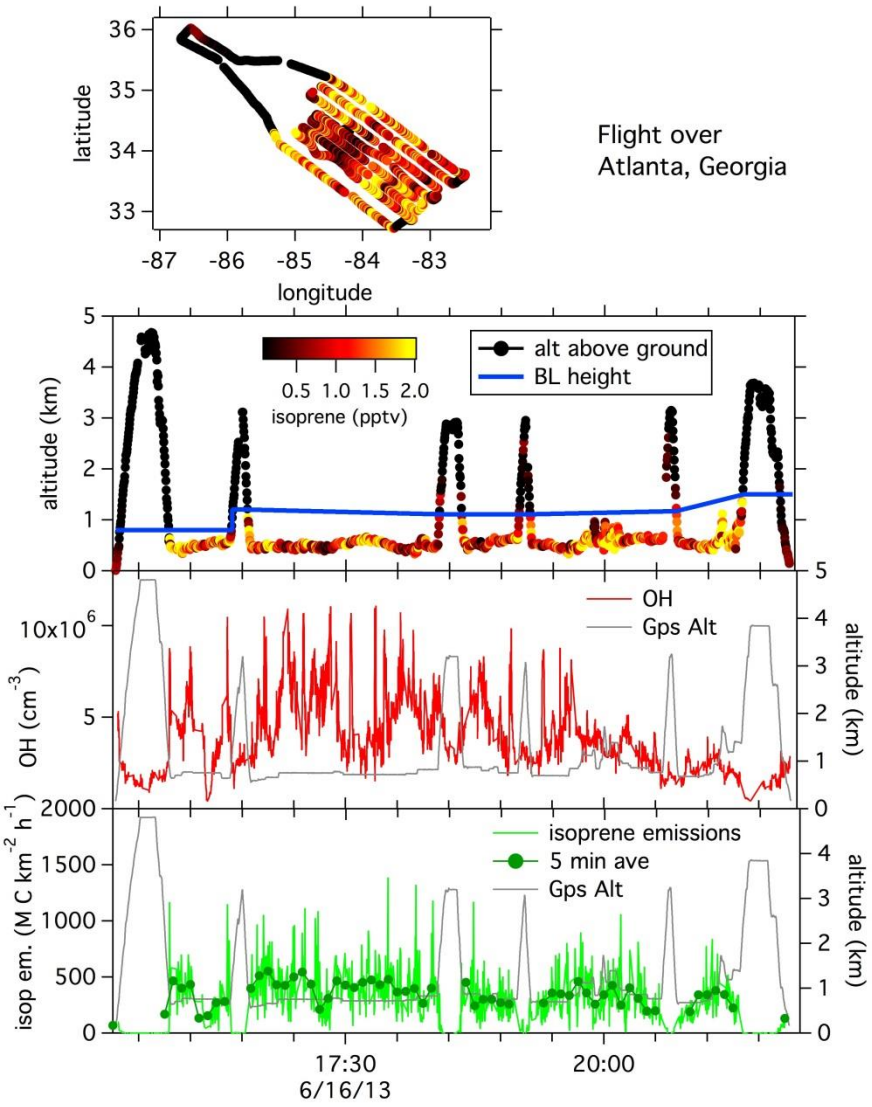

Figure 2-10. Calculation of isoprene emissions using the mass balance approach for the P-3 flight over Atlanta, Georgia, on 16 June 2013.

As part of this project, we also did work to verify the validity of the mass balance approach. In the real atmosphere, surface emissions are turbulently mixed, which leads to horizontal and vertical gradients in the concentration of BVOCs. Also, as the BVOCs are very reactive with OH, this chemistry leads to horizontal and vertical gradients in the concentration of OH. A large-eddy simulation model can be useful to resolve the turbulent mixing of BVOC emissions and the resulting gradients in BVOC and OH concentrations. A large-eddy simulation (LES) for isoprene was published elsewhere (Kim et al., 2012), and the results are used here for verification of the above framework.

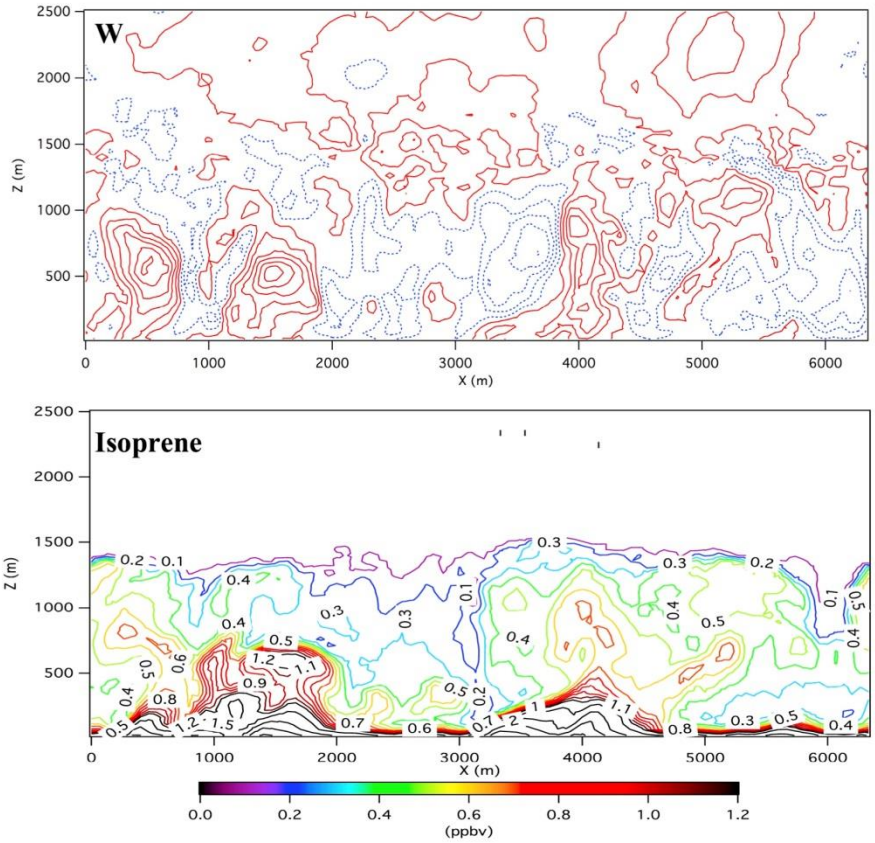

Figure 2-11. Large-eddy simulation of isoprene in the daytime boundary layer. The top panel shows the vertical wind speeds with updrafts in red and downdrafts in blue with the contours ranging from -2.5 m/s to +2.9 m/s in steps of 0.5 m/s. Graph is reproduced from Kim et al. (2012).

An example of an LES result published by Kim et al. (2012) is shown in Figure 2-11. This particular simulation represents the mixing and chemical removal of isoprene in the afternoon boundary layer (2 PM LT) under conditions that are representative for the southern U.S. It can be seen that isoprene is higher in updrafts and lower in downdrafts; these gradients are used in eddy covariance measurements to calculate vertical fluxes. The model uses a chemistry scheme adopted from the global chemical transport model MOZART2.2 (Model for OZone And Related chemical Tracers, Version 2.2) to calculate isoprene mixing ratios, OH concentrations and other species for different NOx conditions.

In this work, we verified that the variance in measured isoprene agrees with the variance calculated from the LES results, and we found good agreement for different NOx regimes. Next, we studied the dependence of average isoprene mixing ratios versus the average OH in the model (Figure 2-12). It was found that there is a simple inverse relationship between mean isoprene and mean OH as a function of NOx. Moreover, the factor between mean isoprene and the inverse of mean OH agrees within 10% with the assumed isoprene emissions in the model. This validates our use of measured BVOC mixing ratios to derive BVOC emissions following the

mass balance approach described above and as used in our previous work (Warneke et al., 2010).

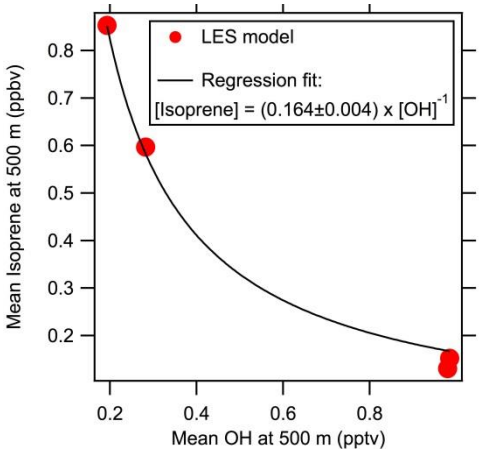

Figure 2-12. Mean isoprene as a function of mean OH at 500 m altitude in the mid-afternoon boundary layer calculated from the large eddy simulation (LES) results published by Kim et al. (2012). The different symbols reflect different NOx conditions.

2.3.2 Comparison with Fluxes from Emission Models

The emission fluxes derived from the measurements using the mass balance approach described in the previous section are subsequently compared with the emissions according to the BEIS and MEGAN models. For the purpose of these comparisons, the emissions are calculated along the flight tracks, and using the temperature and photoactive radiation (PAR) measured onboard the aircraft. The idea behind the approach is to use the aircraft data to constrain all the physical and chemical parameters that determine BVOC concentrations in addition to their emissions. In other words, BVOC concentrations are determined by light- and temperature dependent emissions, boundary layer height, and chemical removal. It is difficult for a 3-D chemical transport model to get all of these parameters correctly represented, and any differences between measured and modeled BVOC concentrations are not necessarily attributable to problems with the base emissions (emission factor). By using the aircraft data to constrain PAR, temperature, boundary layer height and the levels of OH, the comparison is more specifically dependent on the quality of the emissions.

Figure 2-13 illustrates how the isoprene fluxes from the mass balance approach are compared with the emissions calculated along flight tracks from the BEIS3.12 model as an example. Results are shown for the same June 16 flight over Atlanta as was shown earlier. The light and temperature dependent adjustment factors, calculated using the aircraft data, are shown in the 2nd panel of Figure 2-13. Using these adjustment factors, and the base emissions extracted along the flight track from BEIS3.12, the actual isoprene emissions can now be calculated. The results are shown in the 3rd panel and compared with the emissions calculated by the mass balance approach shown previously. In this case, the agreement between the inventory and measurements is very good.

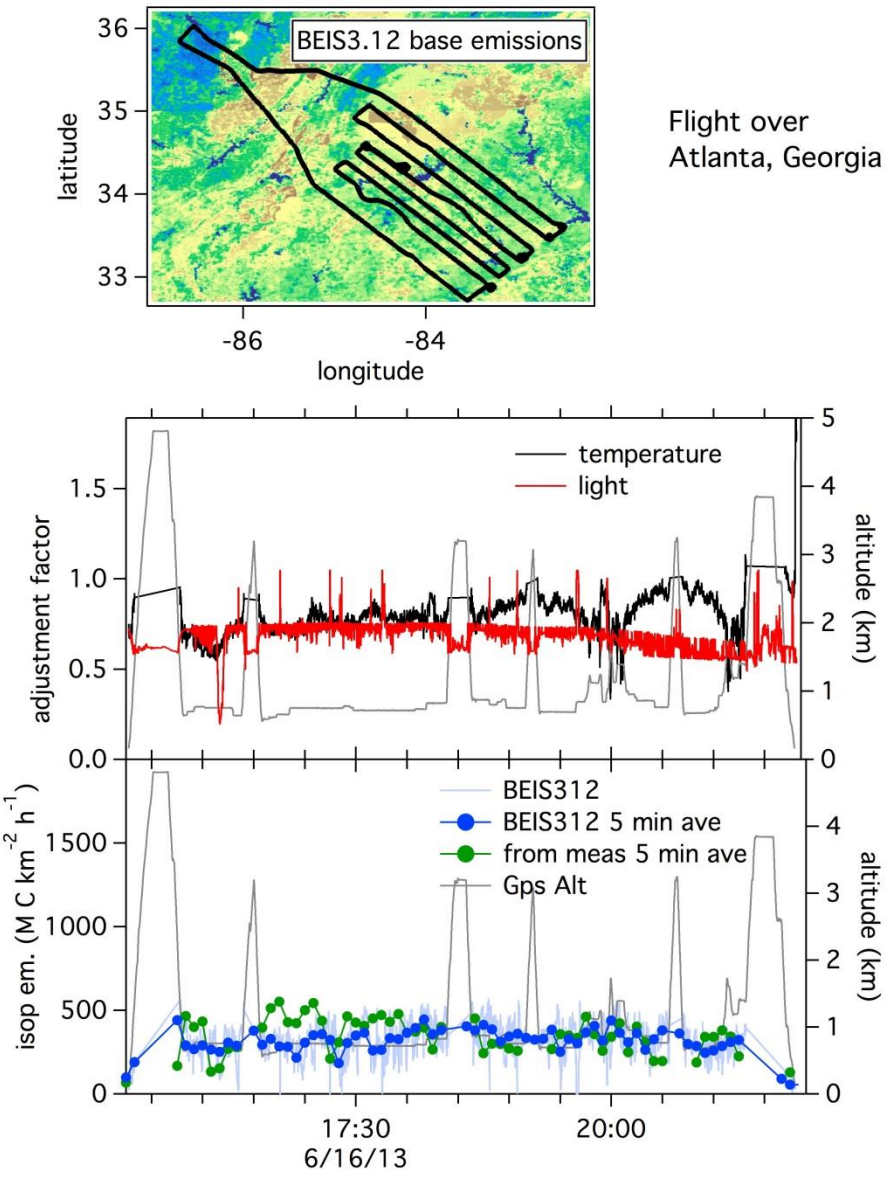

Figure 2-13. Calculation of isoprene emissions along flight tracks using the BEIS3.12 emission model and light and temperature measured from the aircraft.

Figure 2-14 illustrates the same calculation for the MEGAN2.0 model as an example. The light and temperature dependent adjustment factors, calculated using the aircraft data, are shown in the 2nd panel of Figure 2-14. The leaf-area index (LAI), also needed in MEGAN, is extracted along the flight track (2nd panel). Combining all this information, the calculated emissions according to the MEGAN2.0 model are shown in the 3rd panel. One thing to note is the much higher variability in emissions calculated from MEGAN2.0 than from BEIS3.12 (Figure 2-13). Emissions calculated from the mass balance approach are also shown in the 3rd panel of Figure 2-14 and do not agree as well with MEGAN2.0 as they do with BEIS3.12 for this particular flight.

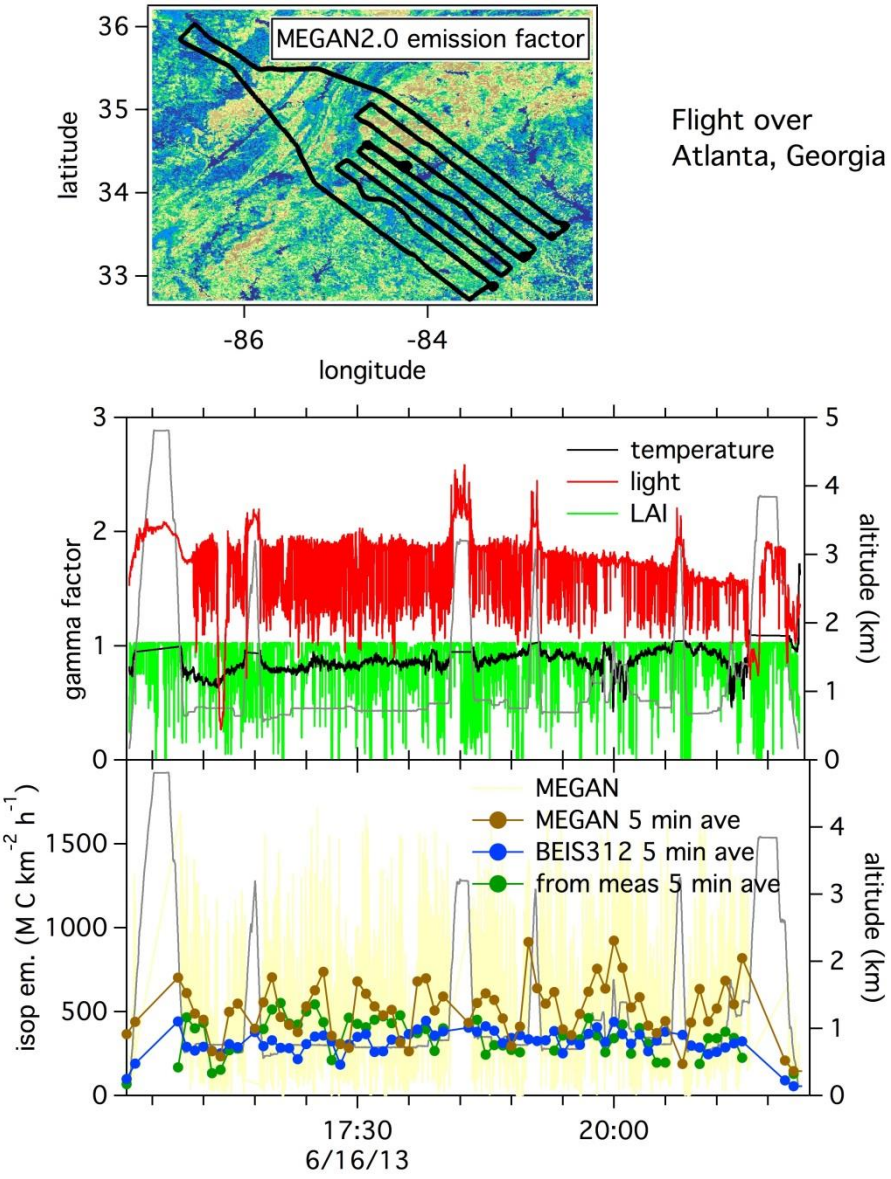

Figure 2-14. Calculation of isoprene emissions along flight tracks using the MEGAN2.0 emission model and light and temperature measured from the aircraft.

A scatter plot of the comparison between measured and calculated emissions for all P-3 flights during SENEX is shown in Figure 2-15. While there are significant differences on a point-to-point basis, on average the agreement is reasonable. The linear correlation coefficient between measurements and model is 0.73, meaning that 53% of the variability in isoprene can be explained by the emission model and parameters measured from the aircraft. On average, the emission inventory was 33% lower than the emissions calculated from the mass balance approach.

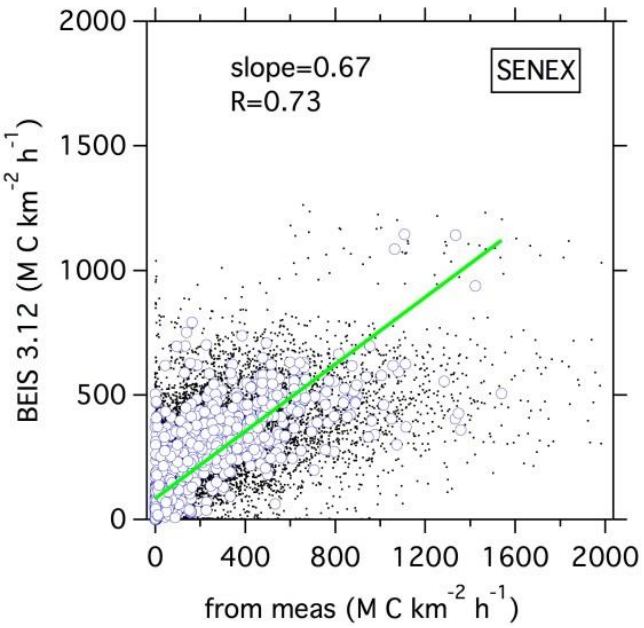

Figure 2-15. Isoprene emissions calculated from BEIS3.12 versus those calculated from the measured isoprene mixing ratios using a mass balance approach. Data included are from all P-3 flights during SENEX.

Similar comparisons between the BEIS3.12, BEIS3.13, MEGAN2.0, MEGAN2.1, and the MEGAN_E2015 and MEGAN_A2015 models developed in this project were made for all six data sets included in this work and are shown in Figure 2-16. Several observations are made here from this graph:

- In general, the emissions according to BEIS are smaller than those from MEGAN, but the MEGAN_E2015 and MEGAN_A2015 models developed here are closest to BEIS.
- The results from the C-130 (NOMADSS) and P-3 (SENEX) measurements during SAS compared very similarly with the emissions inventories.
- The three models that agreed most closely with the emissions estimated from the measurements are BEIS3.12 and the MEGAN_E2015 and MEGAN_A2015 models developed in this project.

Some of these conclusions are very similar to the observations made in our previous work (Warneke et al., 2010), which noted that MEGAN emissions were higher than those from BEIS, and that the emissions estimated from the measurements were in between both emissions models.

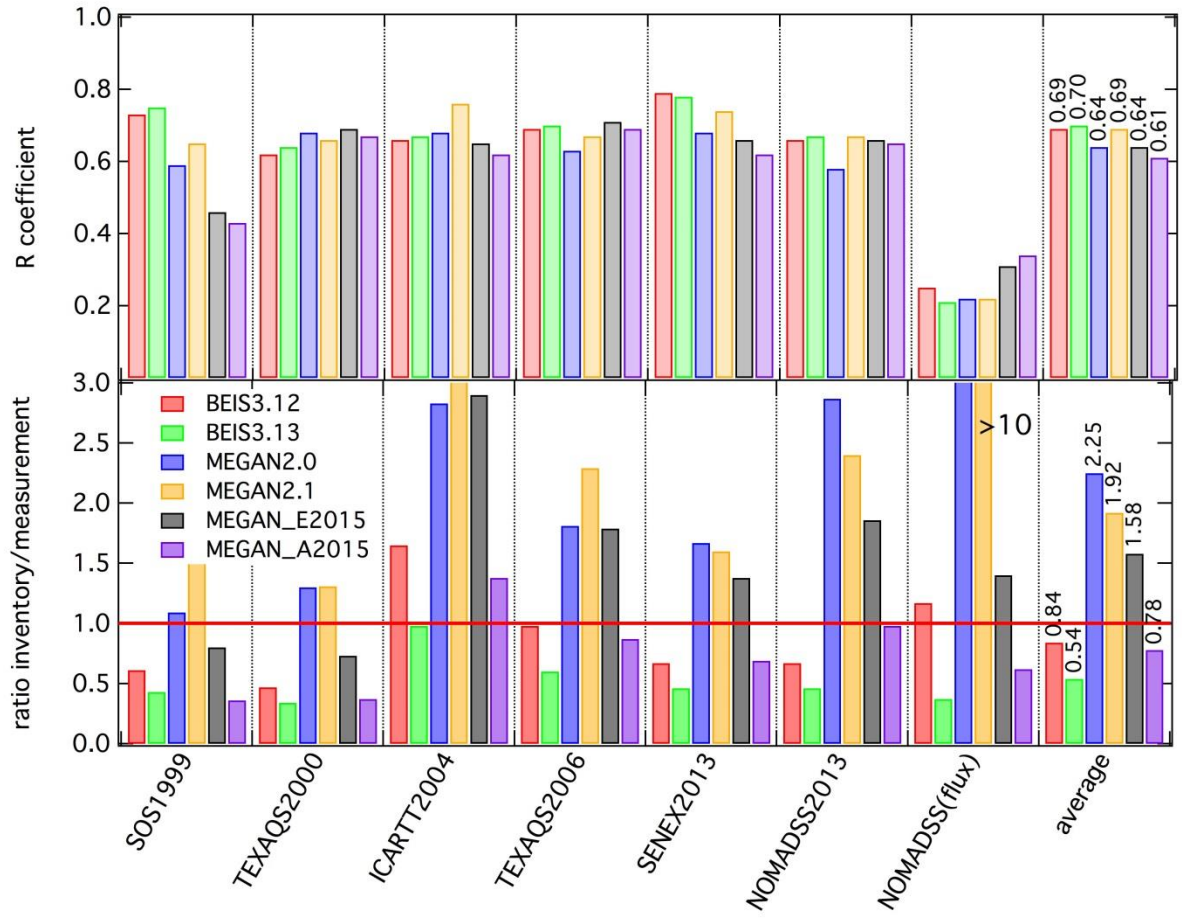

Figure 2-16. Comparison between six different emissions inventories with six different data sets of biogenic emissions.

2.4 Summary of Findings

- Using a wavelet based approach, fluxes of isoprene and total monoterpenes were estimated using turbulence and proton transfer reaction-mass spectrometry (PTR-MS) measurements made onboard the C-130 aircraft during the 2013 SAS field campaign.
- As expected, the highest isoprene fluxes were observed over broadleaf tree dominated woodland areas, while higher monoterpene fluxes were observed over areas such as longleaf pine woodland in Missouri and conifer and hardwood plantations in Louisiana, Texas, Arkansas and Alabama. The forests in these areas generally have higher fractions of high monoterpene emitting trees such as pines.
- Subsampling was also performed for select C-130 flight legs to simulate VOC observations as collected during SAS on the P-3 aircraft, which used a much longer sampling interval (15 s versus 0.6 s on average for the C-130). The increased sampling interval in the P-3 data added significant uncertainty and error to calculated fluxes for sampling intervals greater

than a few seconds. Therefore, Fast Fourier Transform and wavelet based approaches were determined not to be suitable for analyzing VOC fluxes from the P-3 aircraft data in heterogeneous regions.

- Instead, a mass balance approach was used to estimate isoprene emission fluxes from the NOAA P-3 and C-130 data. The emission fluxes derived from the aircraft measurements using the mass balance approach were compared with emissions calculated using the BEIS3 and MEGAN2 models. For the purpose of these comparisons, the emissions were calculated along the flight tracks using the temperature and photoactive radiation (PAR) measured onboard the aircraft.
- Isoprene emissions calculated from BEIS3.12, BEIS3.13, MEGAN2.0, MEGAN2.1 and the MEGAN_E2015 and MEGAN_A2015 models developed in this project were compared to those calculated using the mass balance approach with measured isoprene mixing ratios from the following studies: SENEX (the NOAA contribution to the SAS campaign), NOMADSS, TexAQS2000, TexAQS2006, ICARTT2004 and SOS1999. The comparison showed that in general, MEGAN gives higher emissions than BEIS, but that the MEGAN_E2015 and MEGAN_A2015 models developed here provide emissions that are much closer to BEIS results. The results from the C-130 (NOMADSS) and P-3 (SENEX) measurements during SAS compared very similarly with the emissions inventories. In general, the emissions according to BEIS3.12 and the MEGAN_A2015 and MEGAN_E2015 models are closest to the emissions estimated from the measurements. However, the uncertainties in the emissions estimated from the measurements are significant and do not allow a decision to be made as to which emissions model is more accurate.

3.0 DEVELOPMENT OF HIGH RESOLUTION LAND COVER DATA FOR MEGAN MODELING IN TEXAS AND THE SOUTHEASTERN U.S.

Land cover characteristics including Leaf Area Index (LAI) and Plant Functional Type (PFT) are key driving variables for the estimation of biogenic VOC emissions by MEGAN and other biogenic emission models. We developed an updated LAI and PFT database for Texas and surrounding areas. Methods used in database development are described in Section 3.1, followed by results, evaluation and discussions in Section 3.2.

3.1 LAIv and PFT Database Development

3.1.1 LAIv Database

LAI refers to one-sided green leaf area per unit ground surface area (m^2 of leaf area / m^2 of ground area). The MEGAN model uses LAIv (LAI of vegetation covered surfaces) which has a much smaller range of expected values (Guenther et al., 2006). LAIv is calculated as:

$$LAIv = \frac{LAI}{f_c}$$

where f_c refers to the area fraction that is covered by vegetation. For this project, we retrieved 8 day averaged LAI data for all of North America for 2013 from the MODIS (MOderate Resolution Imaging Spectroradiometer) satellite product (MCD15A2.005) and applied maximum green vegetation fraction from USGS (http://landcover.usgs.gov/green_veg.php), which is also based on MODIS remote sensing products. Spatial resolution of the LAIv data is approximately 900 meters.

3.1.2 PFT Database

Enclosure measurements have clearly shown that different plant species have drastically different BVOC emissions and thus information on vegetation type is needed for BVOC emission modeling. The MEGAN v2.1 model adopted the 16 CLM (Community Land Model) PFT schemes (Table 3-1) to characterize spatial variations of vegetation types (Guenther et al., 2012). For this project, an updated 30 meter resolution PFT database was developed for the continental US based on various ground survey, remote sensing and land surface model data products.

For the eight tree PFTs (PFT #1 - #8), the 30 meter resolution 2012 LandFire Existing Vegetation Type (EVT) data, together with the Forest Inventory and Analysis (FIA) tree species composition data (http://www.fia.fs.fed.us/), were used to derive tree species distributions for each EVT. These species distributions were further evaluated against characteristics of the corresponding EVT (NatureServe, 2009). After excluding non-representative data, each tree species was assigned to one of four aggregated categories: Needleleaf Evergreen Trees, Needleleaf Deciduous Boreal Tree, Broadleaf Evergreen Tree and Broadleaf Deciduous Tree. These categories were further divided into tropical, temperate and boreal trees based on the present day PFT dataset from CLM v4.5 (Oleson et al., 2013), and combined with the 2011 National

Land Cover Database (NLCD) tree canopy cover data (Jin et al., 2013) to obtain final tree PFT cover fractions.

There were no FIA data available for approximately 25% of all the EVTs and tree species distributions for these EVTs were based on MEGAN v2.1 vegetation cover data (Guenther et al., 2012). Non-vegetated EVTs, such as open water and snow-ice covered areas, were assigned a tree cover of zero.

Table 3-1. The 16 CLM PFT scheme used for MEGAN v2.1.

CLM PFT ID	Description
0	Bare
1	Needleleaf Evergreen Temperate Tree
2	Needleleaf Evergreen Boreal Tree
3	Needleleaf Deciduous Boreal Tree
4	Broadleaf Evergreen Tropical Tree
5	Broadleaf Evergreen Temperate Tree
6	Broadleaf Deciduous Tropical Tree
7	Broadleaf Deciduous Temperate Tree
8	Broadleaf Deciduous Boreal Tree
9	Broadleaf Evergreen Temperate Shrub
10	Broadleaf Deciduous Temperate Shrub
11	Broadleaf Deciduous Boreal Shrub
12	Arctic C3 Grass
13	Cool C3 Grass
14	Warm C4 Grass
15	Crop

A similar approach was used for the three shrub PFTs (PFT #9 - #11) and three grass PFTs (PFT #12-14). First, detailed shrub and grass species distributions were estimated based on LandFire EVT and MEGAN v2.1 vegetation cover data (MEGAN v2011 landcover data). Each species was assigned to a specific shrub or grass PFT category using CLM v4.5 present day PFT data, and combined with estimated total shrub and grass cover fractions. The shrub and grass cover fractions were obtained by assigning default maximum vegetation cover fractions to each LandFire EVT based on USGS maximum vegetation cover data minus NLCD tree cover and 2011 NLCD imperviousness (indicating roads and built up areas) cover fraction.

For crops (PFT #15), the LandFire EVT data were used directly since this database includes detailed crop data from the USDA Cropland Data Layer (CDL) database. In addition to these 16 PFTs, an additional vegetation cover for corn was developed using CDL 2013 data, assuming 100% vegetation cover for all corn types including sweet corn, popcorn and assuming that a double crop lands with corn consisted of 50% corn.

3.2 Results and Evaluation of LAIv and PFT database

3.2.1 LAIv Database Evaluation

Figure 3-1 provides an example of the calculated LAIv data for six selected time periods during 2013 (referred to herein as the LAIv2015 database). As expected, LAIv generally increases from January to a peak around August followed by a decline in autumn. Within the United States, LAIv values are generally higher along the west coast and in the southeastern US due to denser evergreen forest cover. In northern and middle US, LAIv values decline from a maximum around August to near zero in winter time.

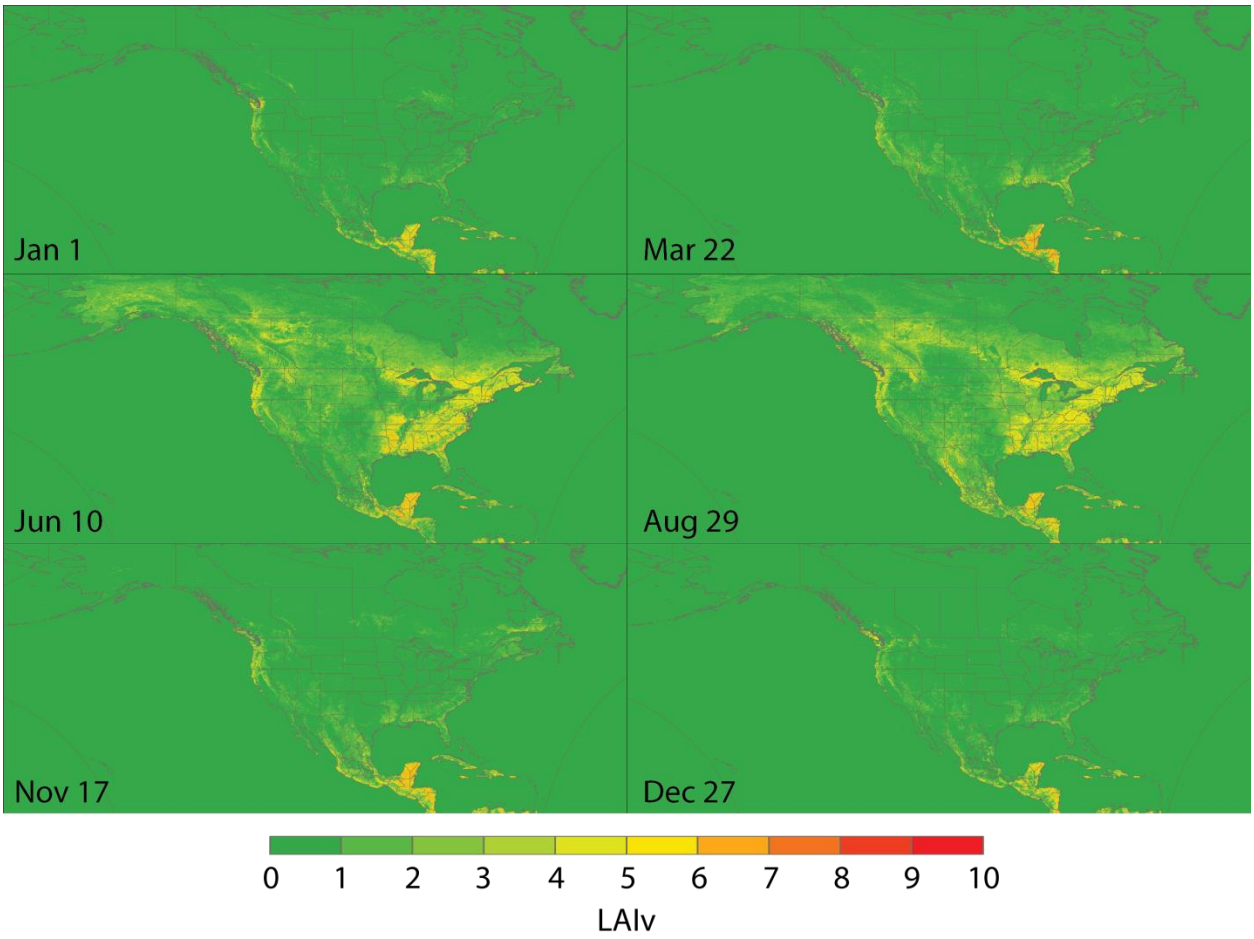

Figure 3-1. Example of calculated LAIv for North America.

Compared with the previous version, LAIv2011 MEGAN LAIv database (Figure 3-2), the LAIv2015 data produced for this project are slightly higher in middle-western US but are generally lower in south-western US, especially for western Texas and along the coastal areas in Louisiana. The observed differences may be due to interannual variation since LAIv2015 data shown are for the year 2013 and the LAIv2011 data shown represent an average for years 2003 to 2011.

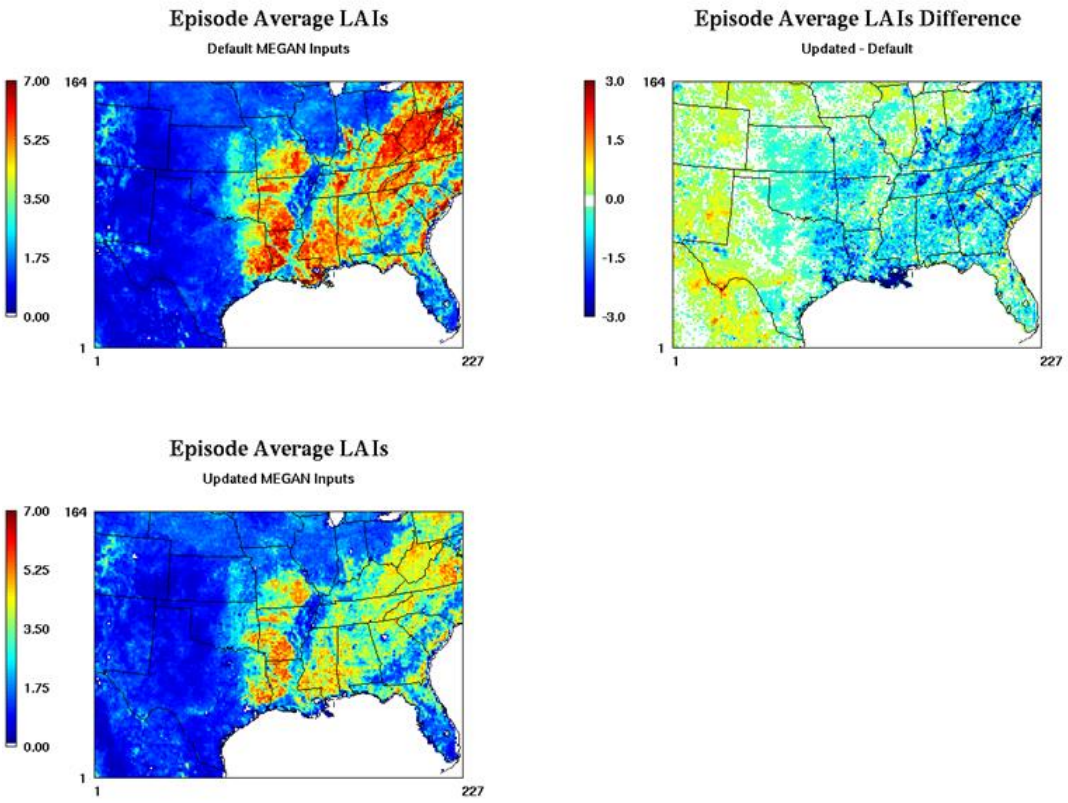

Figure 3-2. Comparison between version 2011 (default) and version 2015 MEGAN LAIv.

3.2.2 PFT Database

The PFT database developed for this project is referred to as the PFT16v2015 data and is compared to three other PFT databases described in Table 3-2. Overall, the PFT16v2015 PFT maps for trees are relatively similar to the PFT16v2011 landcover database, which is not surprising since both were calculated using the same FIA data and NLCD tree cover data. The main difference is that the FIA data was averaged over different zones: v2011 used an ecoregion scheme while v2015 uses the more highly resolved LandFire EVT data. In contrast, the PFT16v2015 and PFT16v2011 shrub and grass distributions are considerably different in both spatial distributions and vegetation cover percentages. The spatial distributions of crops are similar in the PFT16v2011 and PFT16v2011 landcover databases, but not the coverage percentages, which are based on different assumptions.

Table 3-2. PFT Databases used for comparison.

Name	Domain	Resolution	# of PFTs	Reference
PFT5v2007	Global	~900 m (30 second)	5	Guenther et al. 2006
PFT16v2011	North America	60 m	16	Guenther et al. 2012
PFT16v2015	U.S	30 m	16	This Study
CLMv4.5	Global	5000 m	16	Oleson et al. 2013

3.2.2.1 Total Vegetation Cover

Figure 3-3 shows the 30 meter resolution total vegetation cover for the US and Texas, which was obtained by summing all PFT16v2015 PFTs. The overall spatial patterns are consistent with maximum vegetation cover data from USGS as well as PFT5v2007 (Figure 3-4).

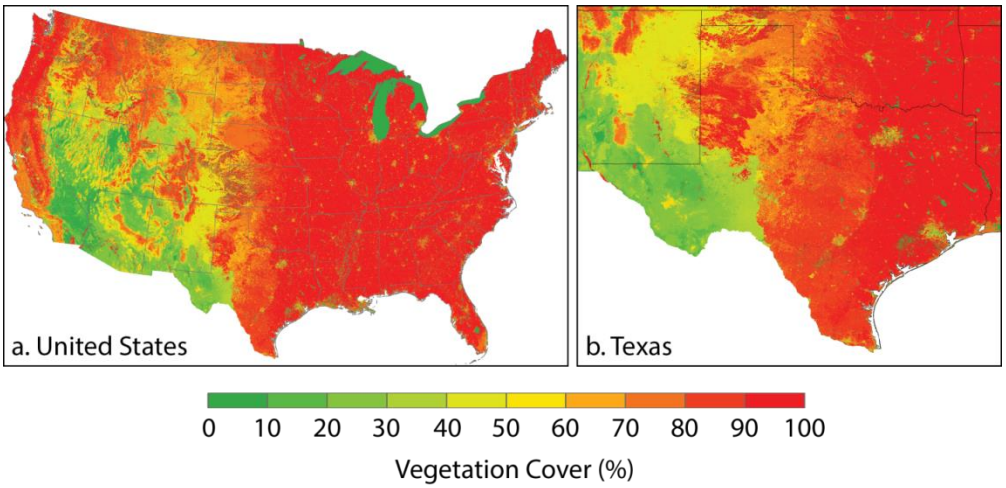

Figure 3-3. Generated 30 meter total vegetation cover for US and Texas.

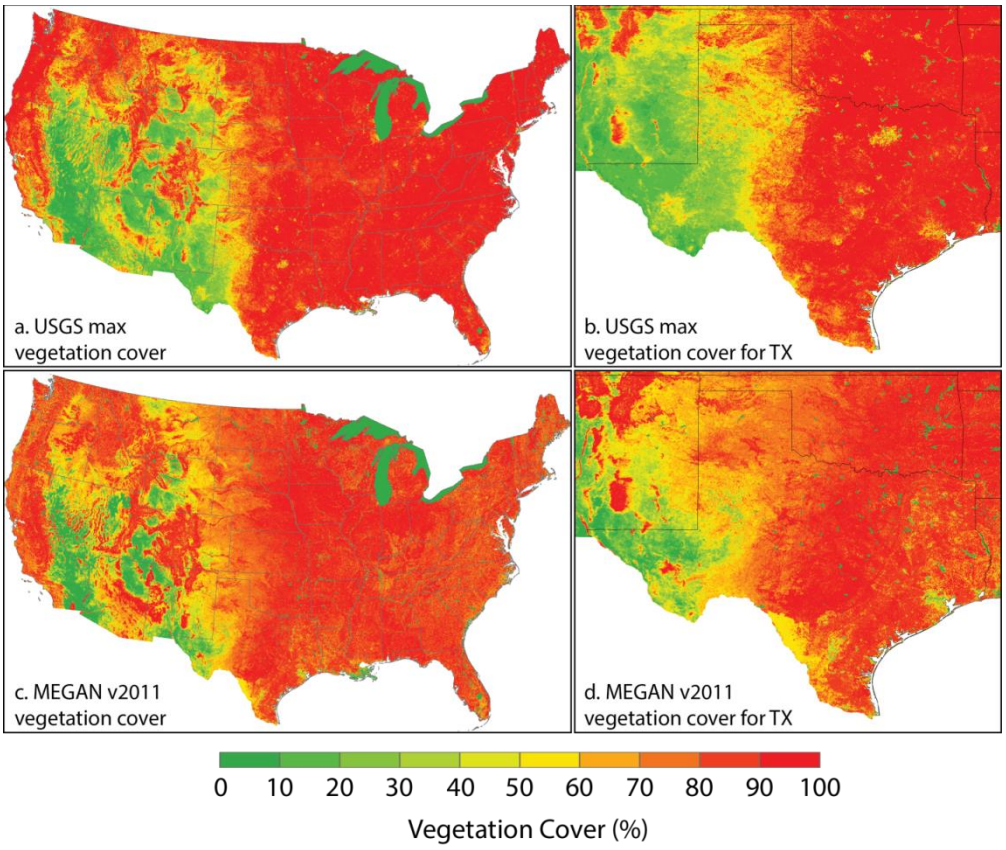

Figure 3-4. Maximum vegetation cover data distributions from USGS (a and b, 1 km resolution) and MEGANPFT5v2007 (c and d, ~900 m resolution) databases.

The PFT16v2015 database was compared with USGS maximum vegetation data by first aggregating the derived vegetation cover data to 900 m and then the USGS max vegetation cover data was subtracted from it (Figure 3-5). The biggest differences are seen in the western US. This includes lower total landcover (i.e., the PFT16v2015 vegetation cover is lower) in urban areas and along water bodies that are not captured well by USGS data due to spatial resolution. The PFT16v2015 total landcover is higher (purple) in northern Texas and western Wyoming which is due to the use of EVT averaged vegetation cover. Within each EVT, total vegetation cover is assumed to have the same value. EVTs that cover large areas, where some of the area has low vegetation cover in the USGS max vegetation map, may lead to overestimates of vegetation cover in these areas.

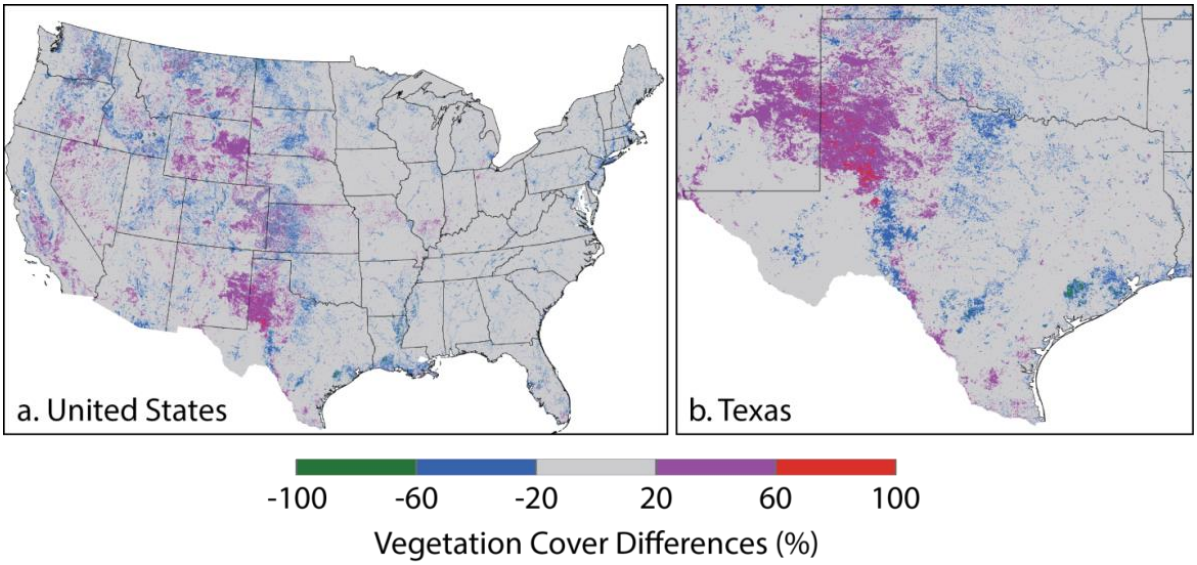

Figure 3-5. Differences between the PFT16v2015 total vegetation cover and USGS max vegetation data (PFT16v2015 – USGS max veg cover).

The PFT16v2015 data and MEGAN PFT16v2011 vegetation cover data were also compared as shown in Figure 3.6. Lower vegetation cover was estimated for PFT16v2015 (purple in Figure 3-6) mainly in the Pacific Northwest and in the eastern US. Lower values are also distributed along water bodies, including coasts, suggesting that the higher resolution of the PFT16v2015 database identifies patches of vegetation distributed along waterways leading to greater estimated vegetation cover. The higher cover estimates for PFT16v2015 (purple in Figure 3-6) were often observed in the southwestern U.S. and in some major urban areas. This may also be due to the ability to account for the patchwork of land cover in arid and urban regions.

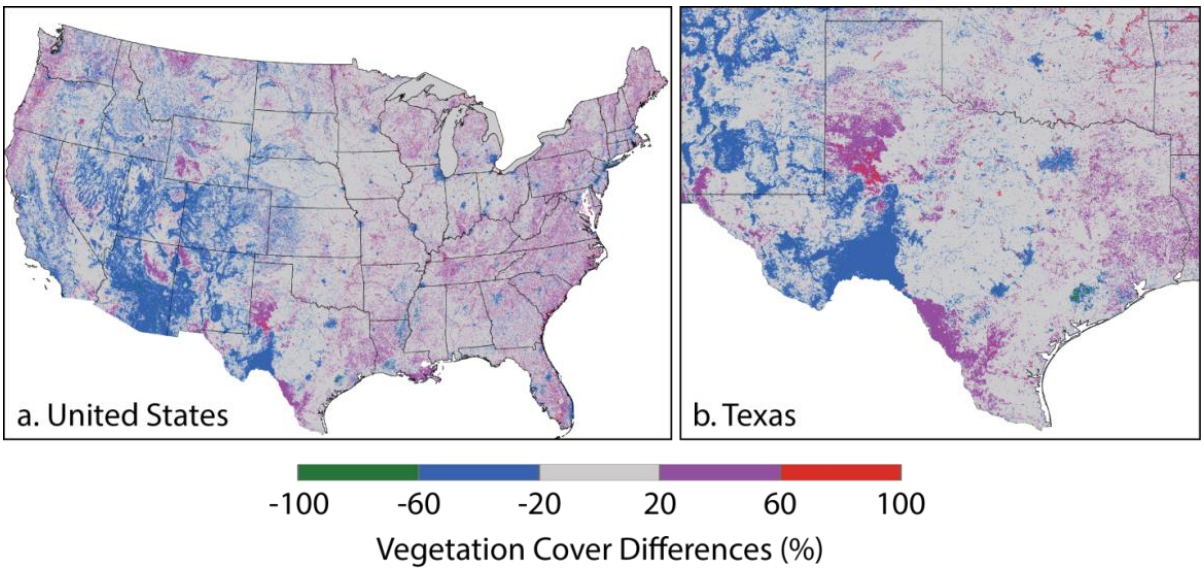

Figure 3-6. Differences between the vegetation cover developed for this project and the v2011 (Guenther et al 2012) vegetation cover data (PFT16v2015-PFT16v2011).

Overall, the PFT16v2015 vegetation cover data is similar or higher in most of Texas. The exception is the Big Bend region where lower vegetation is estimated. The USGS max vegetation cover data does not capture low density vegetation areas in or near small water bodies due to a lack of resolution. The PFT5v2007 database has lower vegetation near water bodies, as well as higher vegetation cover in some urban areas.

Figure 3-7 shows the total PFT vegetation cover from PFT5v2007 and Figure 3-8 shows differences between summed PFTs in the PFT16v2015 database and summed PFTs in the PFT5v2007 database. The differences are relatively small in the eastern US. The PFT16v2015 vegetation cover data has higher cover fraction in southern Texas and lower cover fraction in sparsely vegetated areas in southwestern US.

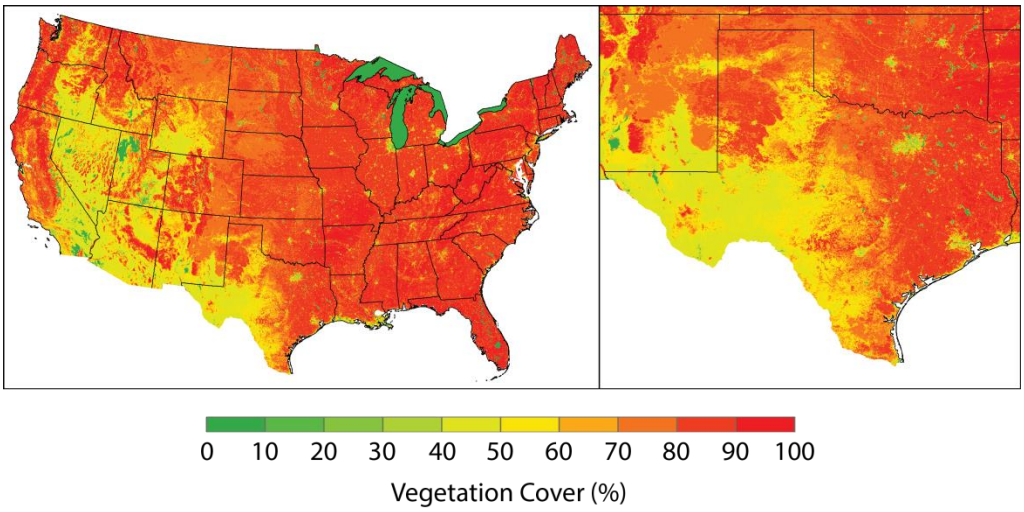

Figure 3-7. Total vegetation cover from sum of all PFT5v2007 PFTs.

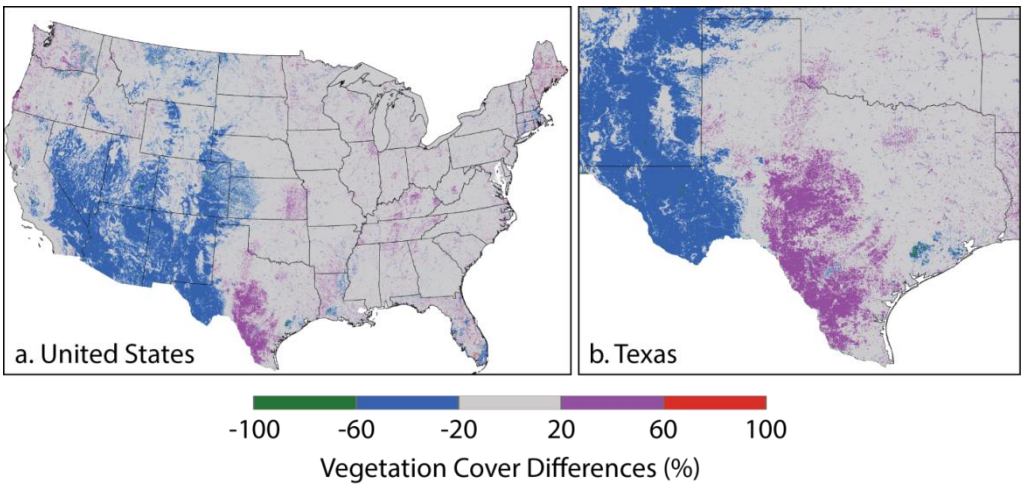

Figure 3-8. Differences between the PFT16v2015 and PFT16v2011 PFT total vegetation cover (PFT16v2015-PFT16v2011).

3.2.2.2 Needleleaf Evergreen Trees: Temperate (PFT #1) and Boreal (PFT#2)

The PFT16v2015 distributions of Needleleaf Evergreen Temperate Tree (PFT#1) and Needleleaf Evergreen Boreal Tree (PFT#2) are shown in Figure 3-9. The Needleleaf Evergreen Temperate trees dominate in the mountains of the US west coast and are an important component of forests in the southeastern US and east Texas. The Needleleaf Evergreen Boreal tree distribution in the US is limited to some alpine conifers in the Rocky Mountains of CO, WY, ID and MT.

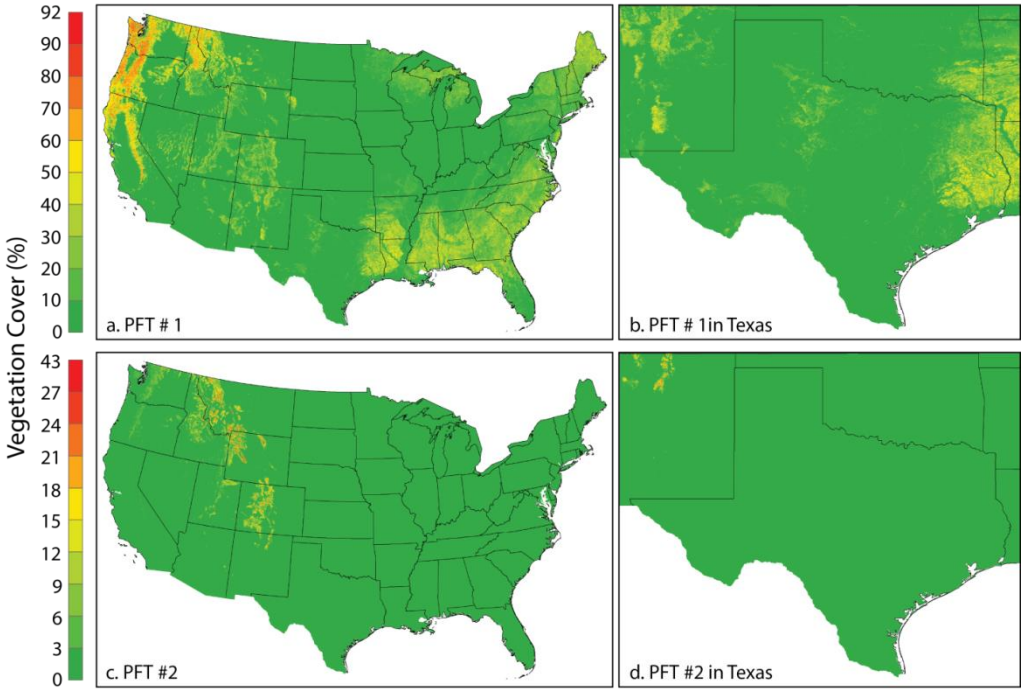

Figure 3-9. PFT16v2015 PFT#1 and #2 distributions.

In the PFT16v2011 database, PFT#1 and #2 are combined and all needleleaf evergreen trees were considered to be PFT#1. Figure 3-10 shows the needleleaf tree cover from PFT16v2011 database and differences between the PFT16v2015 PFT#1 + #2 (aggregated to 900 m) and the PFT16v2011 PFT database. Other than values outside of the US, the biggest differences are mainly observed in the western US, southeast US, (Florida) and northeast US (Maine, New Hampshire, Vermont). PFT16v2015 has fewer needleleaf trees in the Rocky Mountain forests of the western US and in Florida and the northeastern US. Higher values are found in California and the lower Mississippi River valley. The differences are small in Texas.

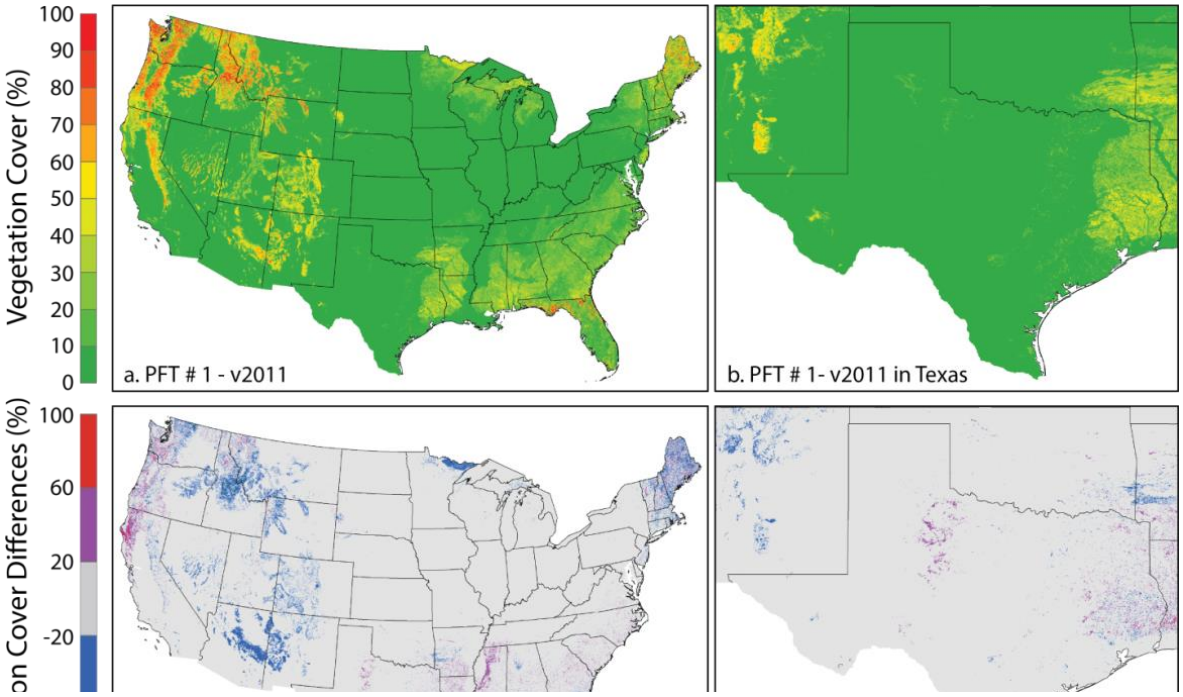

Figure 3-10. Needleleaf evergreen trees from PFT16v2011 database (a and b) and differences between PFT16v2011 (c and d, PFT16v2015-PFT16v2011).

3.2.2.3 Needleleaf Deciduous Boreal Trees: PFT #3

Figure 3-11 shows the PFT16v2015 and PFT16v2011 distributions for needleleaf deciduous boreal trees (PFT#3). There are small areas covered by PFT#3 in the US and they are mainly Taxodium species (bald cypress) located in FL and southern end of LA and Larix species (Larch) in the Pacific Northwest. The Taxodium species are not included in the CLM PFT #3 because CLM considers only Larix species as Needleleaf Deciduous Boreal Trees (Figure 3-9c) and for the U.S. is limited to Minnesota. There are few trees classified as needleleaf deciduous boreal trees in Texas.

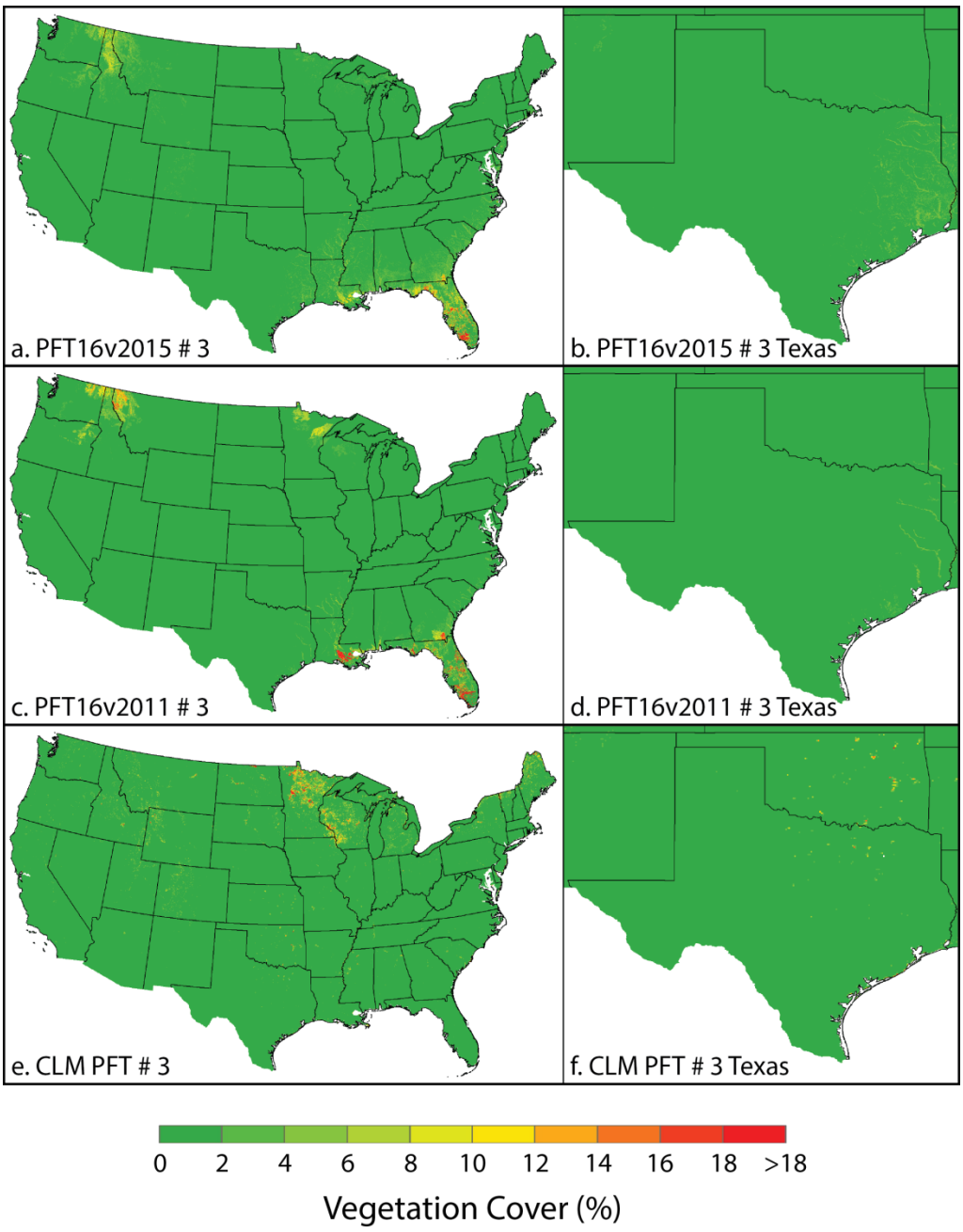

Figure 3-11. PFT16v2015 map for PFT #3 (a and b), PFT16v2011 data for PFT#3 (c and d), and CLM cover percentage for PFT#3 (e and f). Note that in (e and f), the cover percentage refers to percentage of all vegetation in each grid cell, and they do not reflect actual vegetation cover.

3.2.2.4 Broadleaf Evergreen Trees: Tropical (PFT#4) and Temperate (PFT#5)

Figure 3-12 shows a map of PFT16v2015 PFT #4 and #5, PFT16v2011 PFT#5 and CLM v4.5 PFT#5. In the PFT16v2015 PFT dataset, the amount of PFT#4 in the US is minimal while PFT#5 is mainly located in mid-TX and along coastal areas of CA, which is consistent with PFT16v2011 database. However, CLM PFT #5 distributions showed a very different pattern, where most

PFT#5 are located in the southeast corner of US. According to FIA data, the dominant tree species in these areas are actually needleleaf pines, with only small amount of evergreen temperate broadleaf trees. Hence, PFT16v2015 database, as well as the PFT16v2011 PFT data, is expected to be more accurate for this PFT.

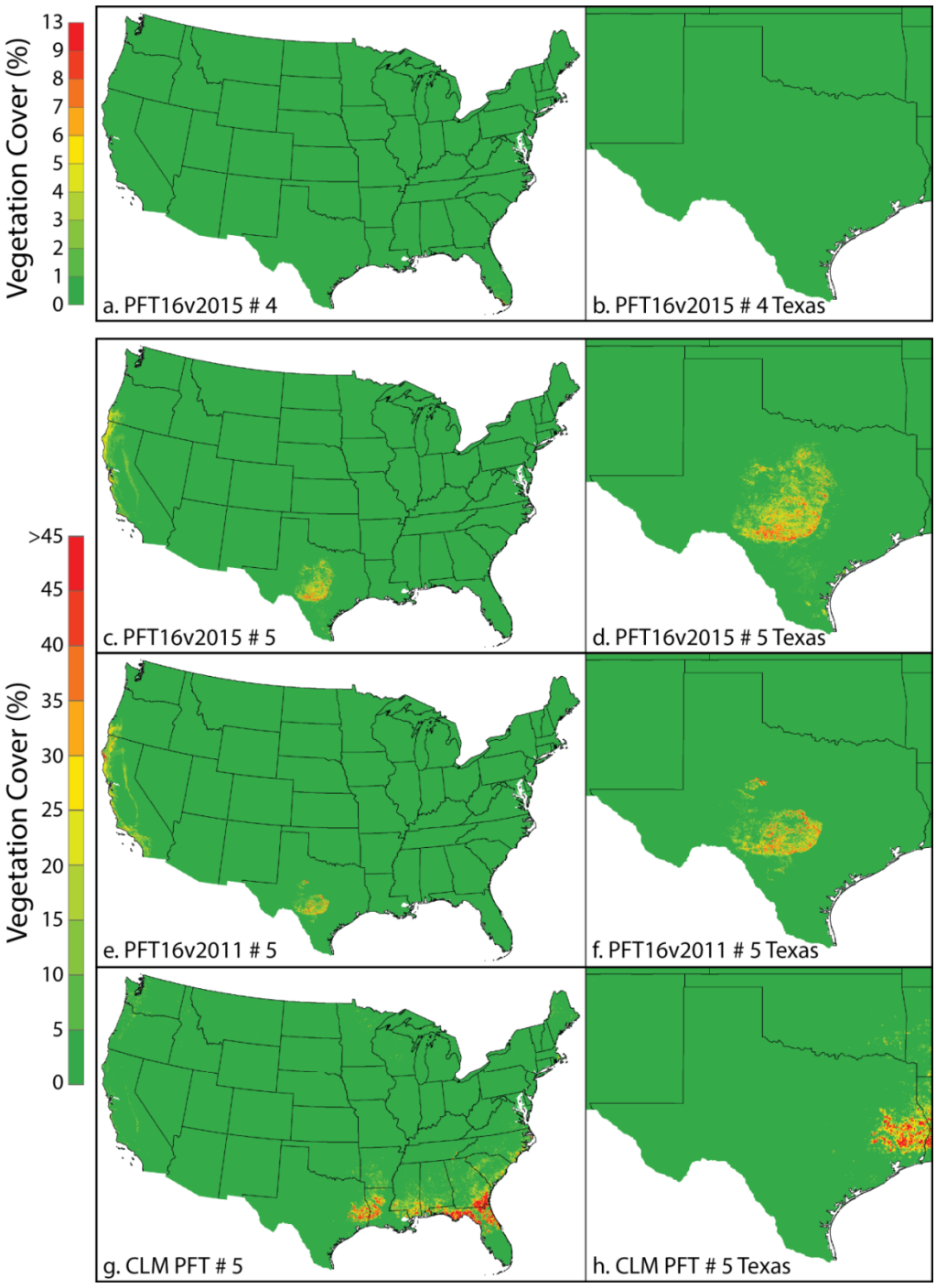

Figure 3-12. Distributions of PFT16v2015 PFT #4 (a and b) and #5 (c and d), PFT16v2011PFT#5 (e and f), and CLM PFT#5 (g and h).

3.2.2.5 Broadleaf Deciduous Trees: Tropical (PFT# 6), Temperate (PFT#7) and Boreal (PFT#8)

Figure 3-13 shows PFT16v2015 broadleaf deciduous tree distributions for individual PFTs (tropical PFT #6, temperate PFT #7, and boreal PFT #8) and for the total broadleaf deciduous trees aggregated to 900m to compare with PFT16v2011. The difference between total broadleaf deciduous trees for PFT16v2015 and PFT16v2011 is shown in Figure 3-14. The spatial distributions of vegetation cover are similar for the PFT16v2015 and PFT16v2011 databases, and the distributions of their discrepancies follow the shape of eco-regions. This is expected since ecoregion averaged values were used to derive PFT16v2015 MEGAN database.

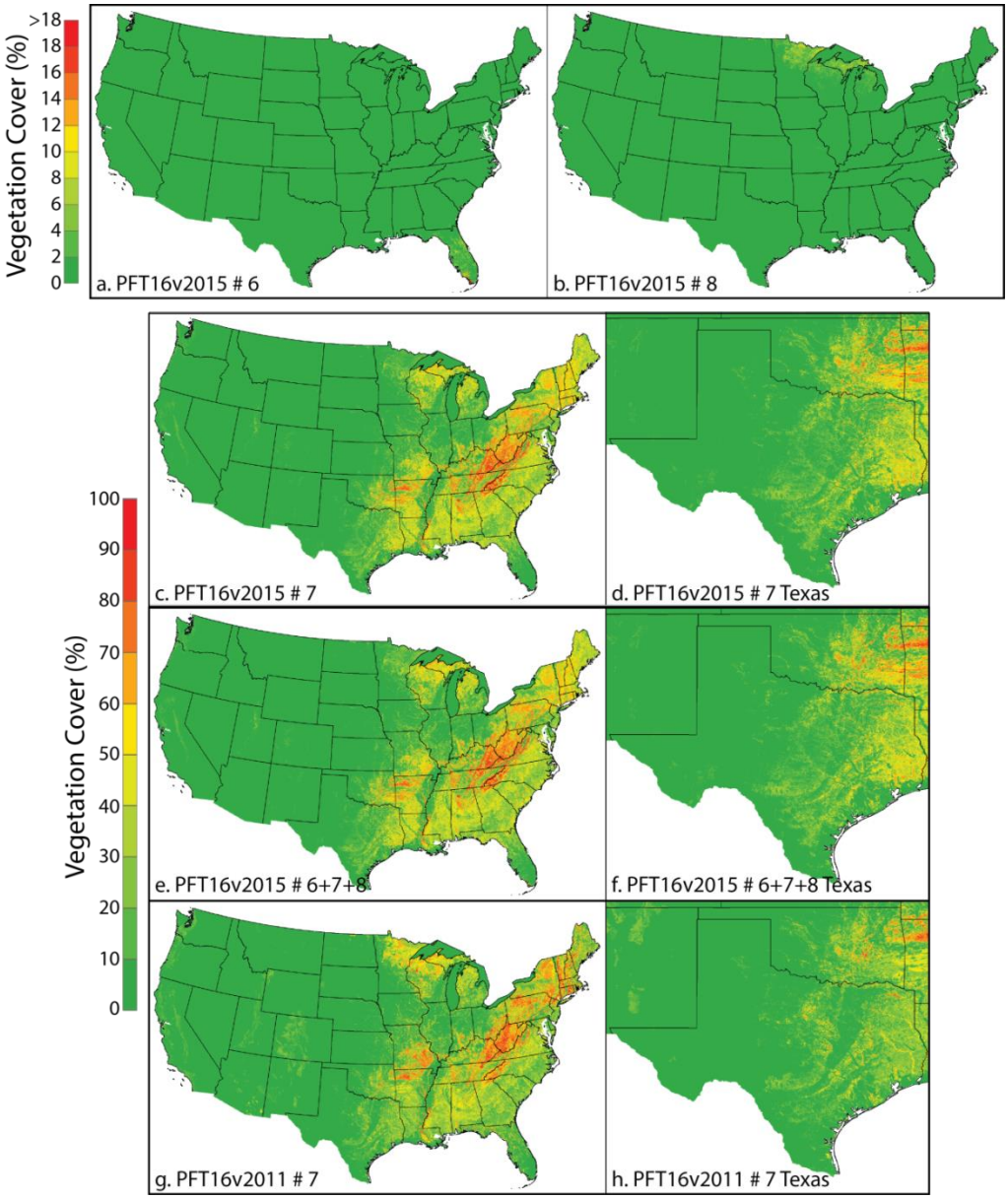

Figure 3-13. PFT16v2015 30 m resolution distribution of PFT #6 (a), #7 (c and d), #8 (b), total (PFT #6+#7+#8) broadleaf deciduous trees aggregated to 900 m resolution (e and f) and PFT16v2011 total broadleaf deciduous trees (g and h).

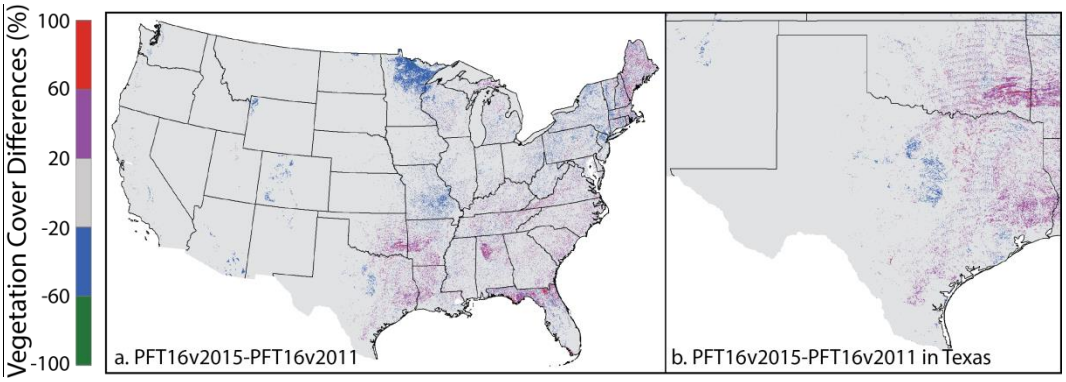

Figure 3-14. Difference in total broadleaf deciduous tree cover fraction (PFT16v2015-PFT16v2011).

3.2.2.6 Shrubs: Broadleaf Evergreen Temperate (PFT #9), Broadleaf Deciduous Temperate (PFT#10) and Broadleaf Deciduous Boreal (PFT #11).

In contrast to the comparison of tree PFTS, the PFT16v2015 shrub PFT database is substantially different from the PFT16v2011 database. This is because shrub cover is not constrained by 30 m satellite cover fraction as is the case for trees. Figure 3-15 shows the PFT16v2015 PFT #9 (a), #10 (b), #11 (c), and total (9+10+11) aggregated to 900m (d and e), along with the PFT16v2011 shrubs (f and g). The difference between PFT16v2015 and PFT16v2011 shrub distributions is shown in Figure 3-16. In the PFT16v2015 database, shrub cover is generally low (mostly less than 30%). However in PFT16v2011 database, shrub cover exceeds 30% in many areas of the mid-west US. Also the biggest differences follow ecoregion patterns and the differences are partly due to different cover estimates for ecoregions and EVTs.

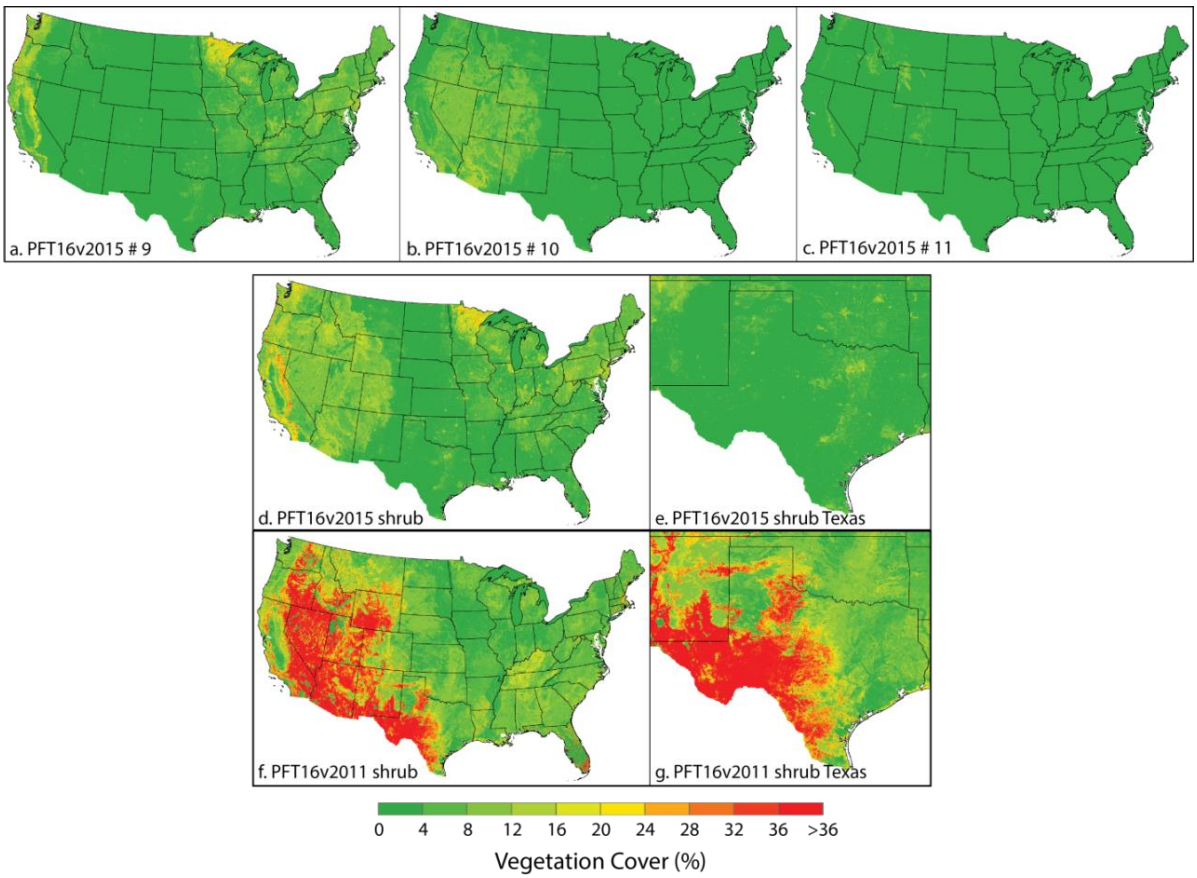

Figure 3-15. PFT16v2015 PFT #9 (a), #10 (b), #11 (c), total shrub (PFT 9+10+11) aggregated to 900m (d and e), and PFT16v2011 shrubs (f and g).

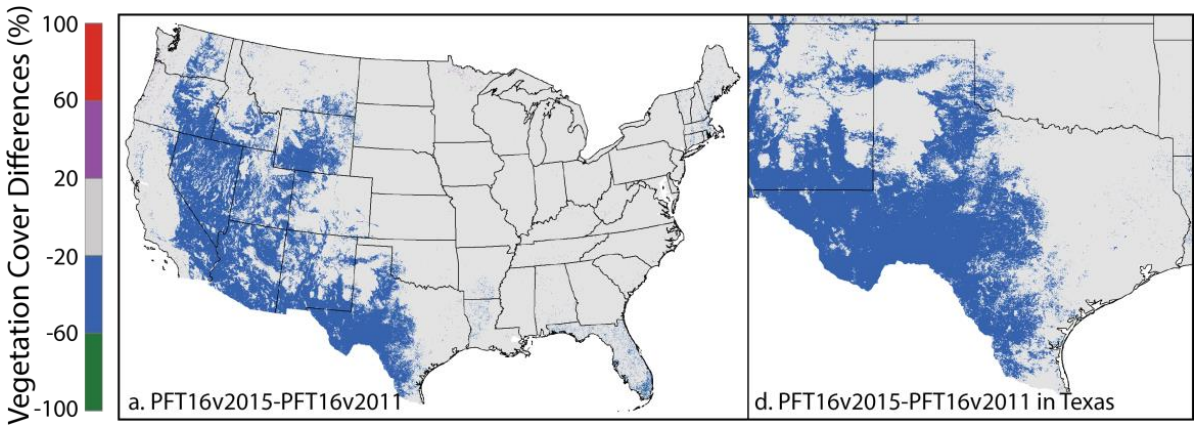

Figure 3-16. Differences between shrub cover fractions in PFT16v2015 and PFT16v2011 databases (PFT16v2015 - PFT16v2011).

3.2.2.7 Grass: Arctic C3 (PFT #12), Cool C3 (PFT #13) and Warm C4 (PFT #14)

Figure 3-17 shows the grass PFT #12 distribution for PFT16v2015 (a) and PFT16v2011 (b) and their differences (c). Overall, the PFT16v2011 database has higher PFT #12 coverage that is likely due to the lower resolution of the CLM data used in the development of the PFT distribution.

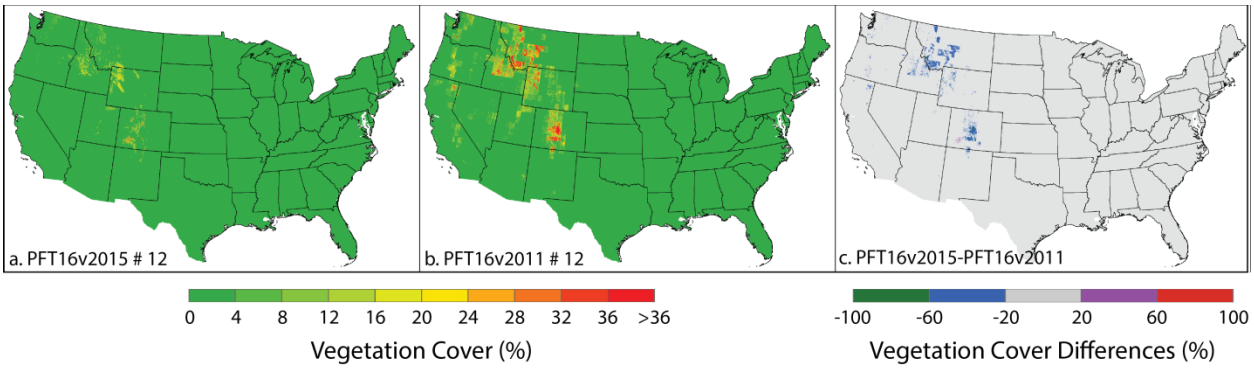

Figure 3-17. Arctic grass (PFT#12) PFT16v2015 (a) and PFT16v2011 (b) distributions and their differences (c).

Figure 3-18 shows the cool C3 grass (PFT#13) distribution for the PFT16v2015 (a and b) and PFT16v2011 (c and d) databases and their differences (e and f). Overall, the PFT16v2011 database has higher cool C3 grass cover fractions in the western US and central Texas and lower cover in the midwestern US.

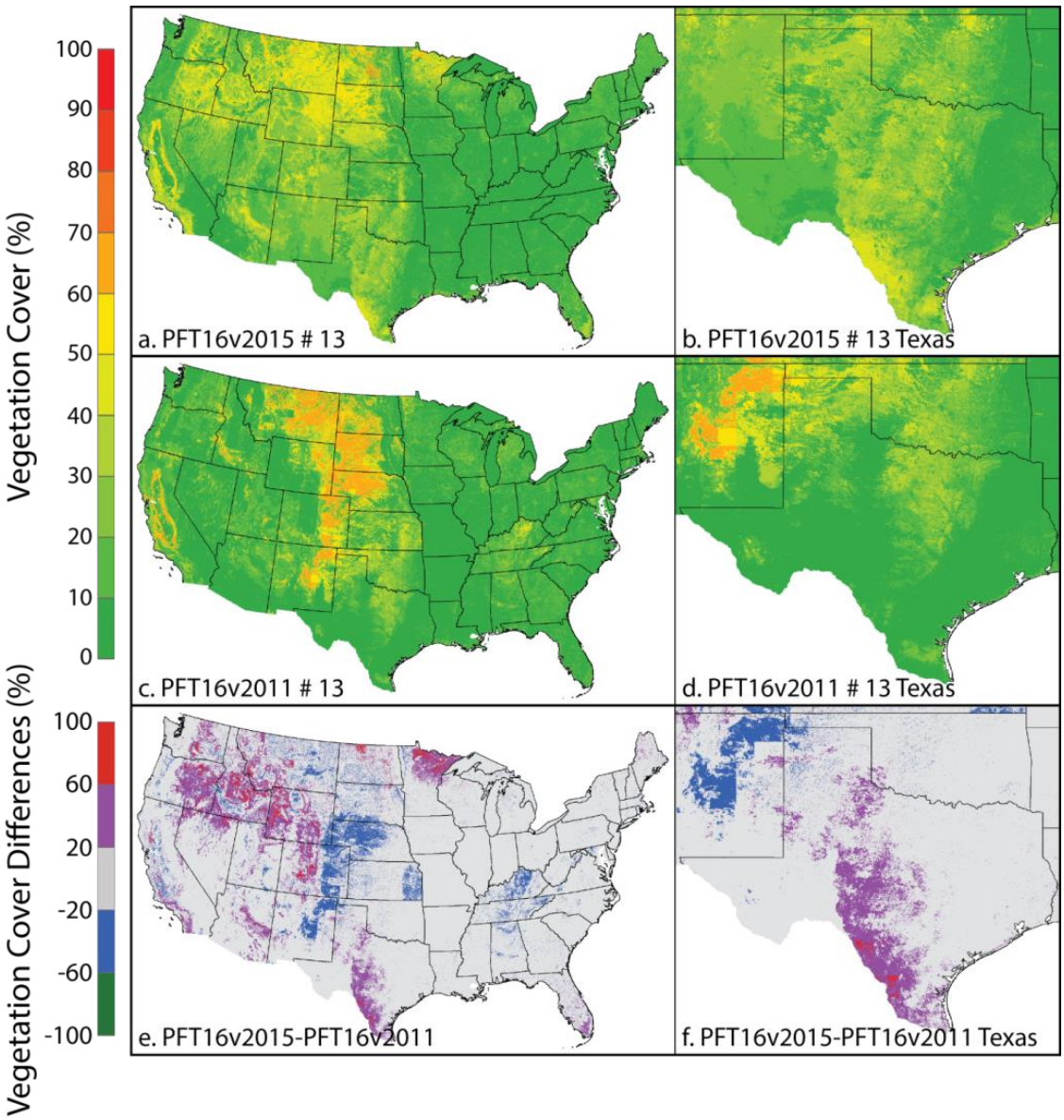

Figure 3-18. Cool C3 grass (PFT#13) distributions for PFT16v2015 (a and b), PFT16v2011 (c and d) and their differences (e and f).

Figure 3-19 shows the warm grass (PFT#14) distribution for PFT16v2015 (a and b), PFT16v2011 (c and d) and their differences (e and f). Overall, the PFT16v2015 database has higher warm C4 Grass cover fractions in the mid-US including Texas. Warm C4 Grass distributions in Oklahoma and Kansas are relatively similar.

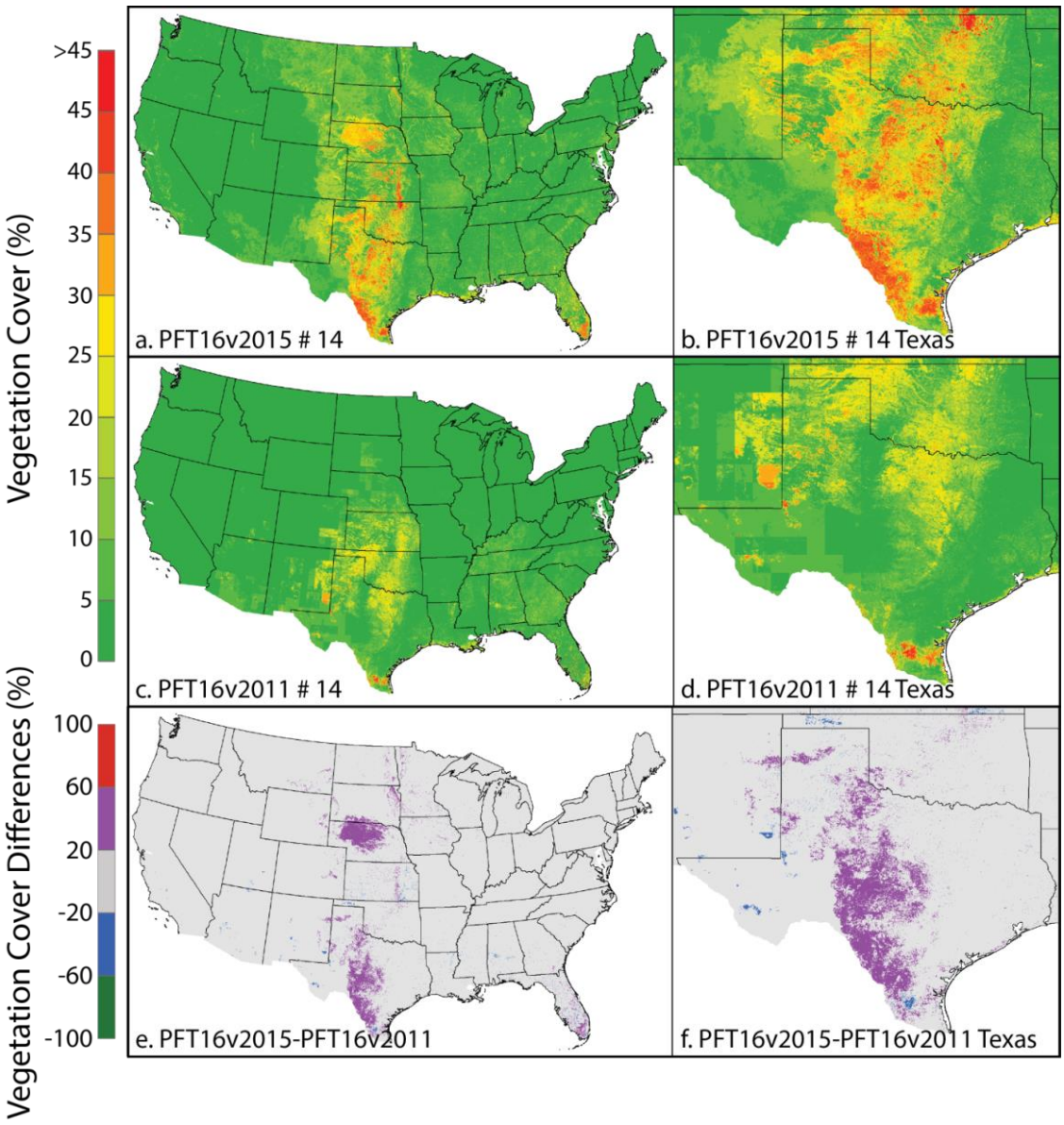

Figure 3-19. Warm C4 grass (PFT#14) distributions for PFT16v2015 (a and b), and PFT16v2011 (c and d) databases and their differences (e and f).

3.2.2.8 Crops: Corn and Other Crops

Figure 3-20 and Figure 3-21 shows the PFT16v2015 and PFT16v2011 database distributions and differences for all crops (Figure 3-20) and just corn (Figure 3-21). Between the PFT16v2015 and PFT16v2011 databases, the spatial distributions of all croplands and cornfields are similar, but the cover fractions are different. This is primarily because the PFT16v2015 database assumes that crop cover fractions are 100% for agriculture EVTs. There are also differences associated with the different years that the databases represent.

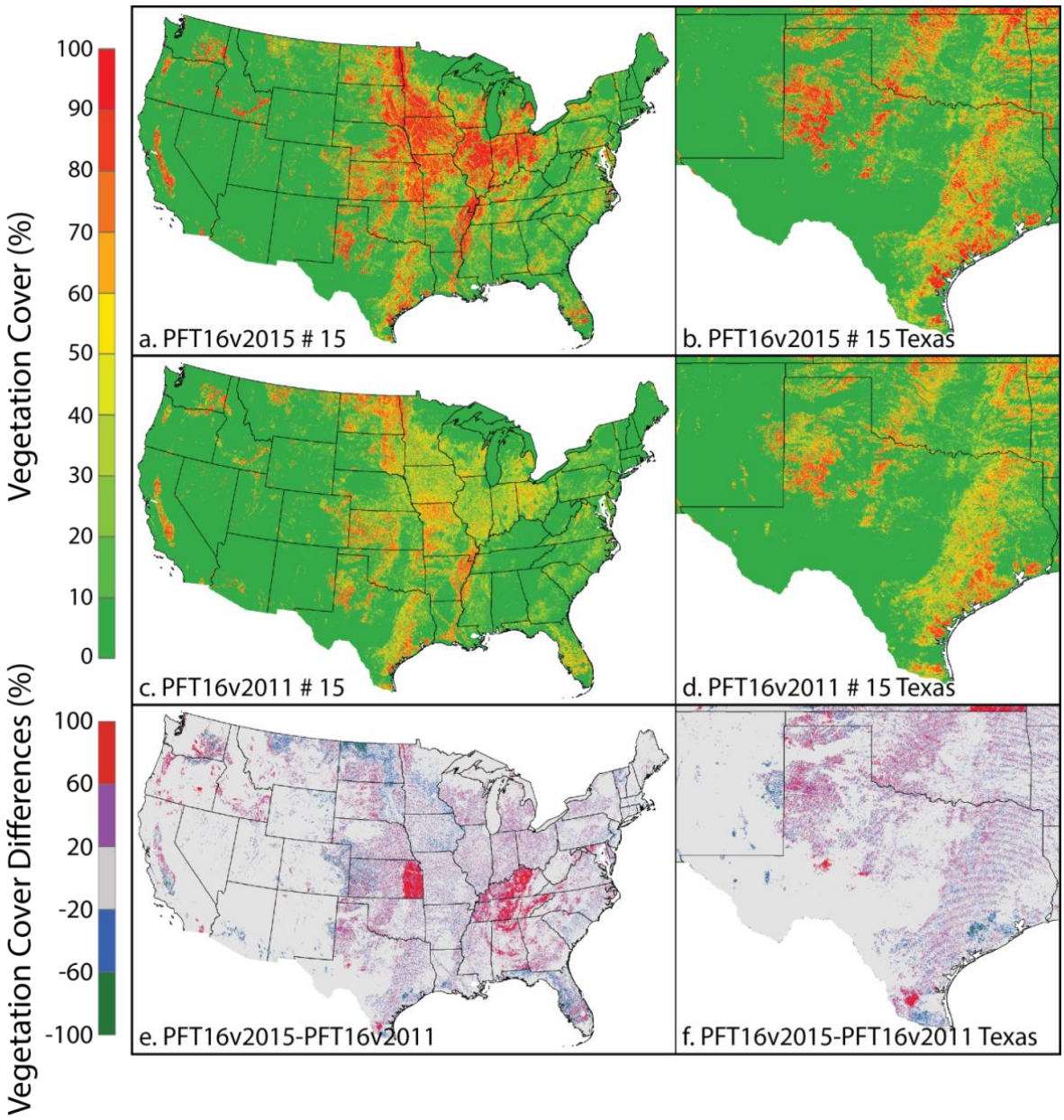

Figure 3-20. PFT16v2015 all crop (a and b) and PFT16v2011 all crop (c and d) distributions and their differences (e and f).

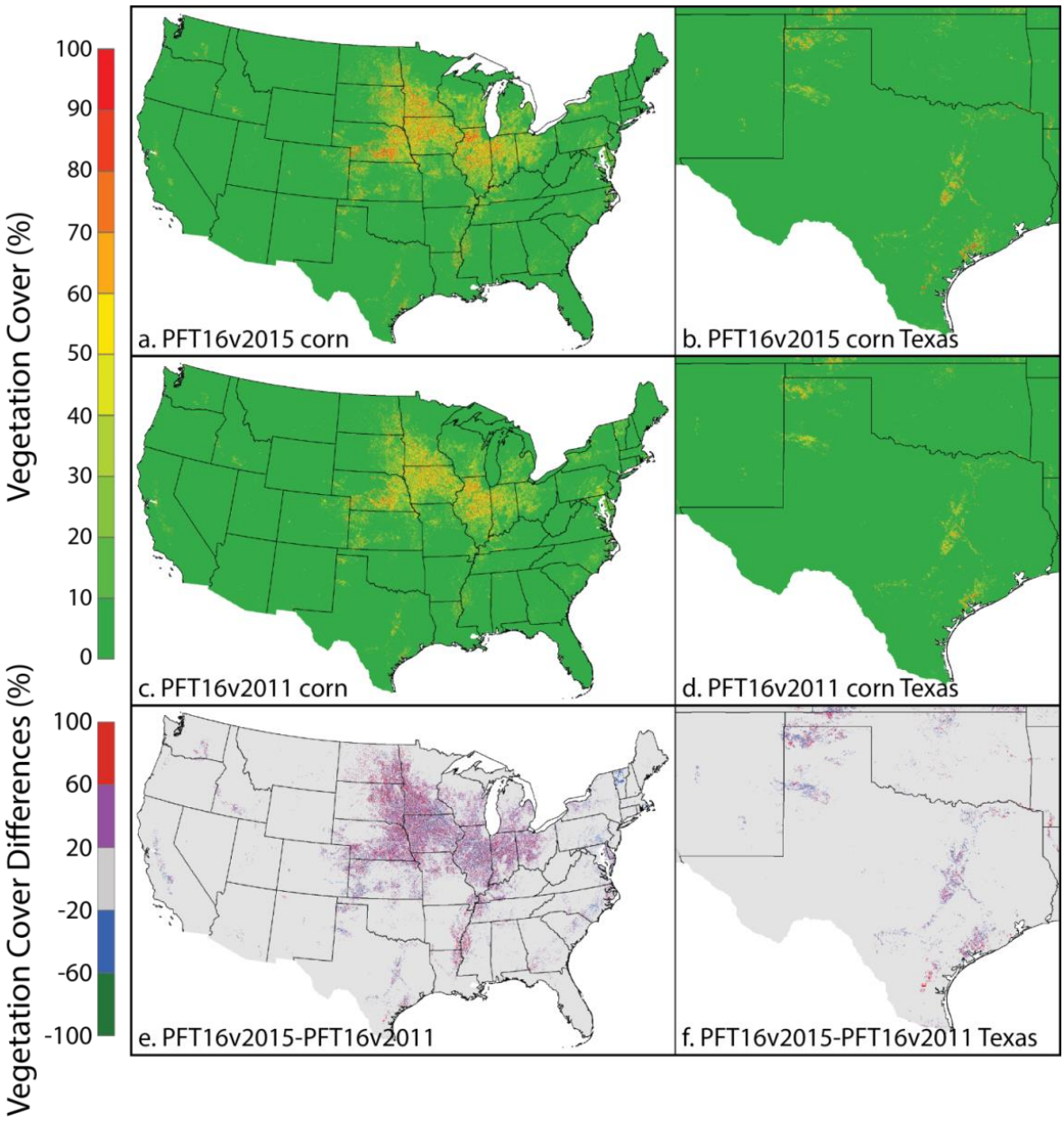

Figure 3-21. PFT16v2015 corn (a and b) and PFT16v2011 corn (c and d) distributions and their differences (e and f).

3.3 Evaluation of Extremely High Resolution Landcover Datasets in Texas Urban Areas

Extremely high resolution (1 m) vegetation data were provided by TCEQ for 12 selected Texas urban areas, including Austin, Beaumont, Corpus, Dallas, El Paso, Houston, Longview, Marshall, San Antonio, Tyler, Victoria and Waco. These detailed datasets were assessed to determine how they could be used to improve vegetation distributions estimates in these Texas urban areas. Substantial differences were identified between the 1 m resolution landcover data and the landcover data described above in sections 3.1 and 3.2 and it was concluded that a better

understanding of the discrepancies was needed before these data are incorporated into the MEGAN landcover.

The high resolution urban landcover data uses a different vegetation classification system (Table 3-3, herein referred as LT) than the 16 PFT scheme as used in the CLM model and MEGAN v2.1 (Table 3-1). The LT classifications were first mapped to PFT scheme using the method shown in Table 3-3. Seven PFTs (PFT #3, 4, 6, 8, 11 and 12) were not mapped here since there are only minimum amount of these PFTs in Texas.

Table 3-3. Mapping method from 1 m landcover type to PFT

Landcover type (LT) ID	Description	Mapping to PFT
1	Barren land	
2	Cold Deciduous Forest/Woodland	PFT #7+#10
3	Broad-leafed Evergreen Forest/Woodland	PFT #5+#9
4	Developed Open, Herbaceous Vegetation	PFT #13+#14+#15
5	Needle-leafed Evergreen Forest/Woodland	PFT #1
6	Shadow	
7	Urban	
8	Water	
9	Mixed Forest	PFT #1+#5+#7+#9+#10

To be consistent with previously developed PFT data, the 1 m resolution urban landcover data were first aggregated to 30 m. Within each aggregated 30 m grid cell, the fractions of 1 m resolution LT types #2, 3, 4, 5 and 9 were tabulated and further decomposed into CLM PFTs. The fractions of corresponding PFTs relative to the total mapped PFTs for corresponding LT type, at corresponding grid cells, were used in the decomposition, which were developed in section 3.1 and 3.2. The decomposed PFTs were then summed together. Since the 1 m resolution data has no fractional vegetation cover information, the summed PFT fractions were also proportionally adjusted using the maximum vegetation cover data as shown in section 3.2.

Figure 3-22 shows the comparison between maximum vegetation cover in the PFT16v2015 database and summed vegetation cover from the 1 m landcover data (fractions of LT #2+3+4+5+9 within 30 m grid cells). The two total vegetation cover datasets show substantial differences, especially in rural areas. The reason was found to be that large areas of grassland/pastures were classified as “barren land” or “urban” in the 1 m resolution urban landcover data (Figure 3-23).

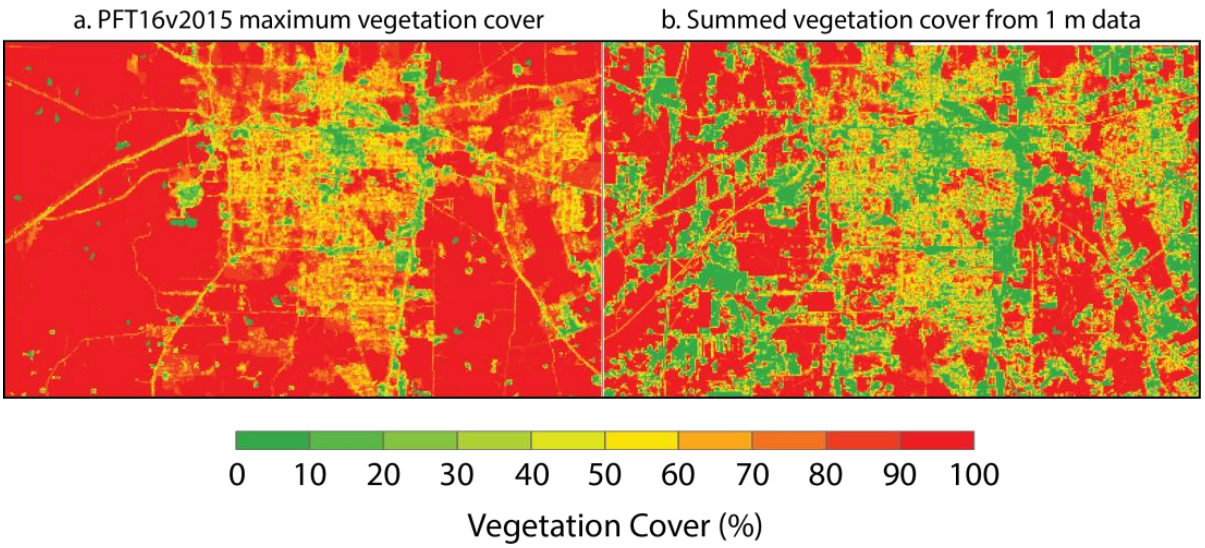

Figure 3-22 Comparison of PFT16V2015 total vegetation cover (a) and summed vegetation cover (b) from 1 m urban landcover data for Marshall, TX area

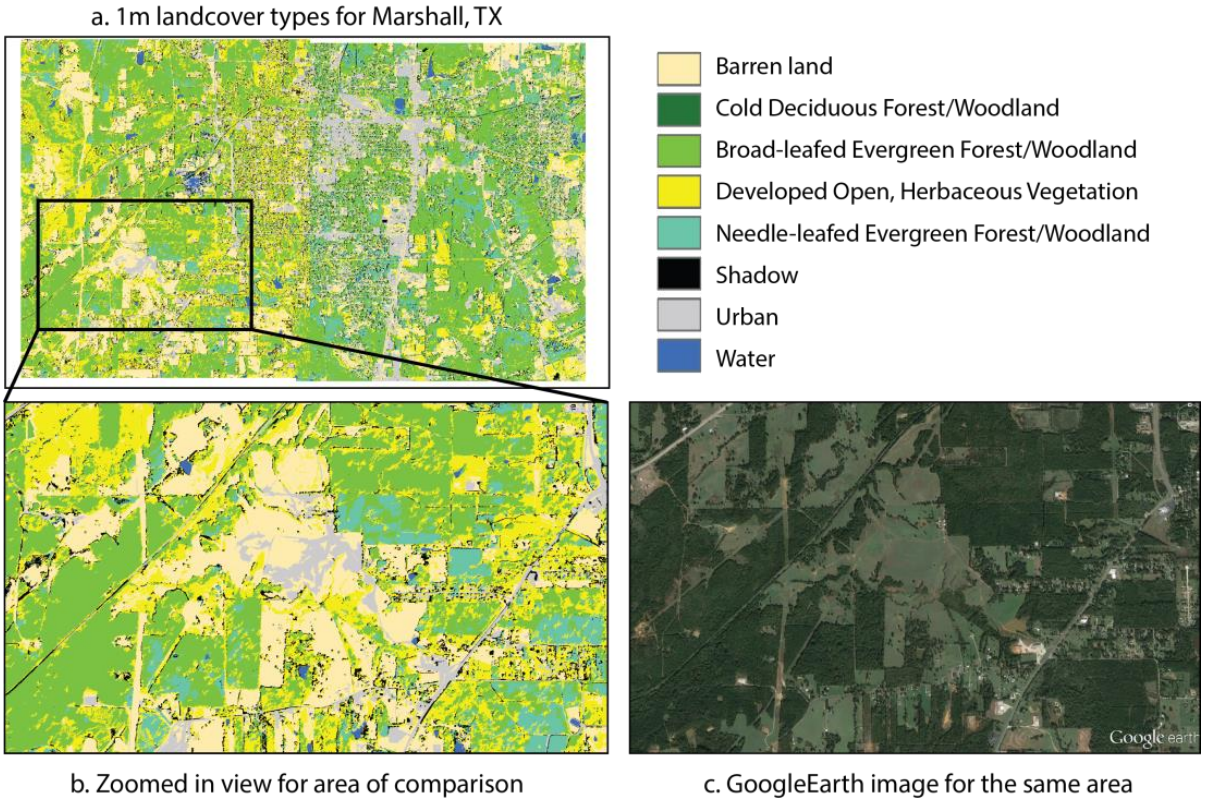

Figure 3-23. Comparison of 1 m resolution urban landcover data (a and b) with Google Earth satellite image (c) for Marshall, TX area

Furthermore, the derived PFT data are also substantially different from those in the MEGAN PFT16v2015 database as shown in previous sections. As an example, Figure 3-24 shows PFT #1 (needleleaf evergreen temperate tree) distribution in the PFT16v2015 database and PFT #1 derived from the 1 m landcover data. The observed differences could be because the 1 m resolution landcover data classified most forests as broadleaf trees/woodlands (Figure 3-23a), while in the PFT16v2015 database, needleleaf evergreen trees dominate.

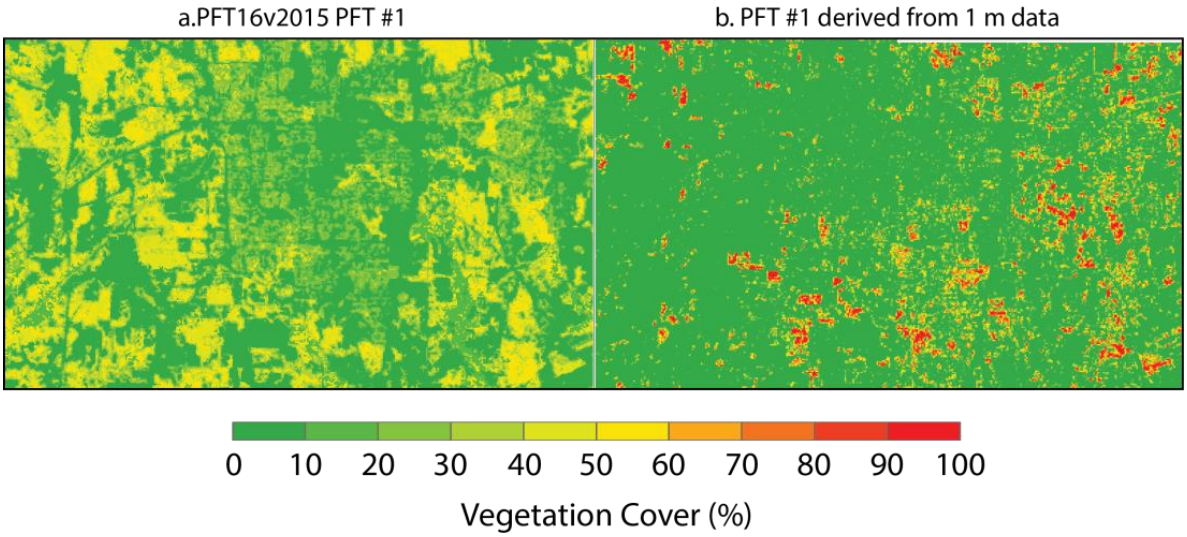

Figure 3-24. Comparison of PFT16v2015 PFT # 1 data (a) and those derived from 1 m resolution urban landcover data for Marshall, TX area

Given the substantial differences as described above, a better understanding of the sources of discrepancies is needed before merging these two datasets together. Therefore, this extremely high resolution urban landcover database has not yet been incorporated into a MEGAN PFT landcover database. This should be done utilizing complementary geolocated ground surveys of tree species composition.

3.4 Summary of Findings

- We developed an updated LAI database for all of North America based on the 2013 MODIS (MOderate Resolution Imaging Spectroradiometer) satellite product (MCD15A2.005) and applied maximum green vegetation fraction from USGS (http://landcover.usgs.gov/green_veg.php), which is also based on MODIS remote sensing products.
- An updated 30-meter resolution PFT database (PFT16v2015) was developed for the continental US based on various ground survey, remote sensing and land surface model data products.

4.0 EMISSION FACTOR DATABASE DEVELOPMENT

The PFT16v2015 database provided the starting point for the high resolution (30 m) EFvE2015 emission factor (EF) database for the continental US using the methods described in Section 4.1.1. The resulting EFs were then compared with the EFvE2011 EF database (Guenther et al. 2012) and the differences are discussed in section 4.1.2. The EFs are then evaluated in section 4.2.2 using the EFvA2015 EF data based on aircraft flux measurements described in section 4.2.1.

4.1 Emission Factor Database

The MEGAN v2.1 emission factor represents the net VOC emission released into the above canopy atmosphere at a set of standard landcover and environmental conditions. The emission factor database described by Guenther et al. (2012) for MEGANv2.1, and referred to here as EFvE2011, includes the following 10 BVOC species: isoprene, myrcene, sabinene, limonene, 3-carene, t-β-ocimene, β-Pinene, α-Pinene, 2-methyl-3-buten-2-ol (232-MBO) and NOx. The EFvE2015 emission factor database developed for this project includes the same 10 VOC species and can also be used to drive MEGAN v2.1. The EFvA2015 data, which incorporates aircraft flux measurements, is for isoprene only.

4.1.1 Methods

MEGAN v2.1 (Guenther et al., 2012) has two alternative approaches for assigning EFs. One approach allows the user to provide PFT distributions and then assigns PFT-specific emission factors to each PFT. We employed this approach and developed the EFvE2015 database as:

$$EF_i = \sum_{p=1}^{15} PFT_{p,i} EF_p$$

Where EF_i is the calculated emission factor for 30 m resolution grid cell *i*; $PFT_{p,i}$ is the fraction of PFT #*p* among all PFTs within corresponding grid cell *i*; and EF_p is PFT-specific emission factors to PFT #*p*, available from (Guenther et al., 2012). Please note that one of the 16 PFTs in CLM is barren land (Table 3-1) and it was not included here.

As discussed in section 3 of this report, the current PFT scheme used in MEGAN v2.1 is the same as used by the CLM4.0 model. This 16 PFT scheme is sufficiently detailed for most land-surface modeling studies, but does not capture all BVOC emission variations. For example, both oak trees and maple trees are classified as broadleaf deciduous temperate trees, although oak trees are high isoprene emitters and maples have negligible isoprene emissions. In order to capture such differences, MEGANv2.1 has a second approach using EF maps that are compiled by combining plant-specific basal emission factors (BEFs) with plant species distributions developed for different eco-regions worldwide. The EFvE2011 and EFvE2015 databases contain EF maps based on species specific distributions and emission factors and can be used in MEGANv2.1 to implement this second approach. The EFvE2011 database is based on ecoregion averaged plant species distributions while the EFvE2015 database used LandFire EVTs. The EFvA2015 database also uses LandFire EVTs and also incorporates aircraft flux measurements.

4.1.2 Results of Emission Factor Database Development

4.1.2.1 Isoprene

Figure 4-1 shows the EFvE2015 and EFvE2011 isoprene emission factors for the contiguous US. For comparison purposes, an emission factor database with PFT-specific BEFs (EF-PFTv2015) was also compiled and presented in Figure 4-1. Note that EFvE2015 data are at 30 meter resolution and then were aggregated to 900 meters for visualization. Overall, the spatial distributions of isoprene EFs are similar across the three datasets. The EF-PFTvE2015 dataset has lower isoprene EFs for oak dominated woodlands in regions including mid-Texas, Arkansas, Missouri, the foothills surrounding California's Central Valley and the high altitude aspen dominated areas in Colorado and Utah. This is expected because aspen and oak trees emit isoprene at substantially higher rates than the average for all broadleaf trees, hence the EF-PFTvE2015 database, which does not distinguish oak and aspen trees from other broadleaf trees, underestimates isoprene emissions in these areas. This result demonstrates the improvement that can be obtained using the plant-specific BEFs.

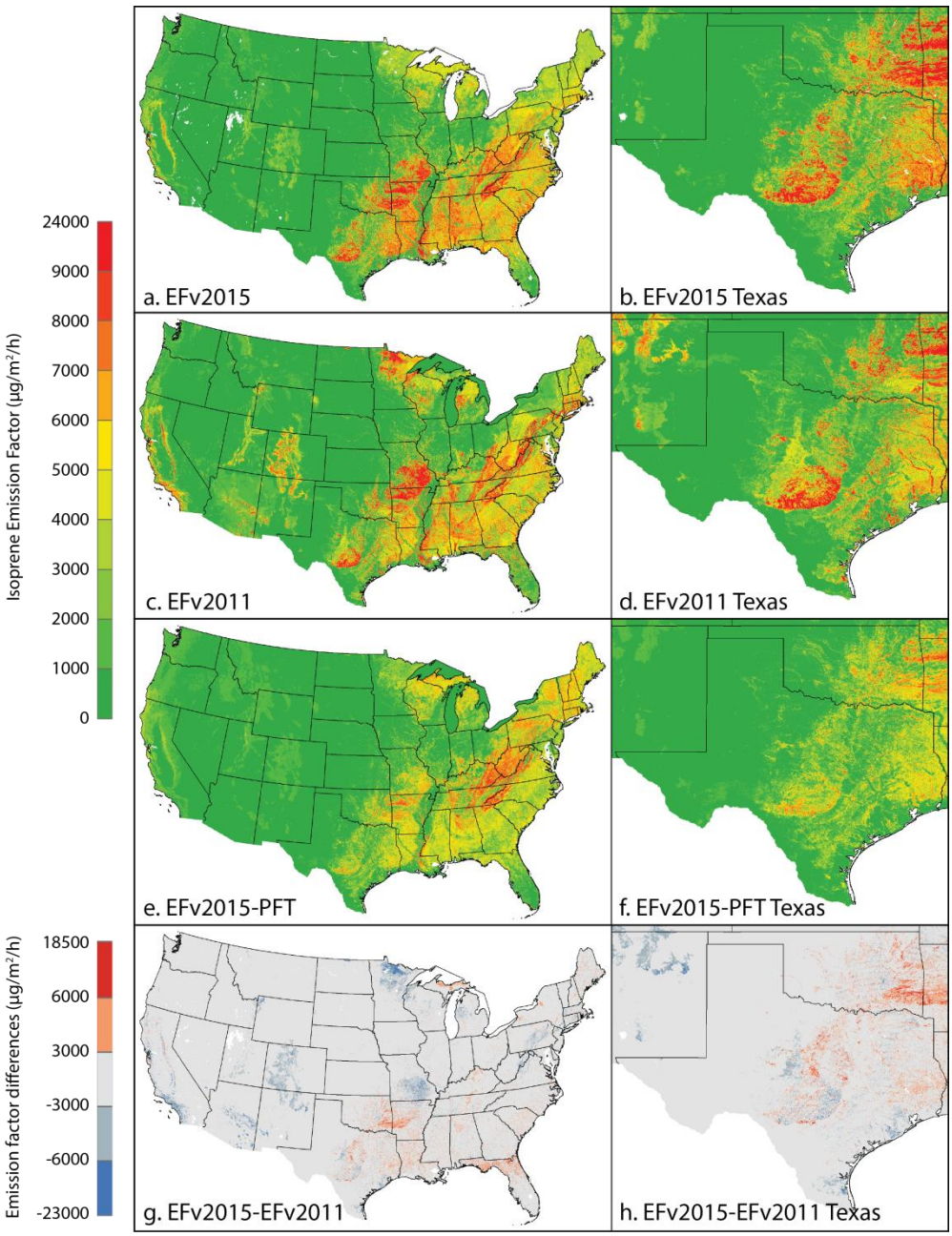

Figure 4-1. EFvE2015 (a and b), EFvE2011 (c and d) and EF-PFTv2015 (e and f) isoprene emission factor datasets for the contiguous US and the differences between the EFvE2015 and EFvE2011 datasets (g and h).

There are noticeable differences between the EFvE2015 and EFvE2011 isoprene datasets (Figure 4-1g and h). Compared with the EFvE2011 data, the EFvE2015 data predicts higher isoprene emission factors in some regions in the southeastern US, with the biggest differences in north Florida, central Texas, Oklahoma and Arkansas. Higher broadleaf deciduous tree coverages are also predicted for these areas in the PFT16v2015 database. On the other hand, lower broadleaf deciduous tree coverages were predicted in PFT16v2015 database for southeast Missouri and northern Minnesota, which also has lower isoprene emission factors in

the EFvE2015 database. The differences are mainly due to the incorporation of the LandFire existing vegetation type (EVT) data, which provides more spatial details than the land cover dataset used to develop the EFvE2011 dataset.

4.1.2.2 Other BVOC Species

Figure 4-2 through Figure 4-10 show emission factors in the EFvE2015 and EFvE2011 datasets, as well as their differences between the two datasets for myrcene, sabinene, limonene, 3-Carene, t-β-ocimene, β-pinene, α-pinene, 232-MBO and NOx, correspondingly. Overall, the spatial distributions of these biogenic VOCs and NOx are consistent in both EFvE2015 and EFvE2011 datasets. In the EFvE2011 dataset for myrcene (Figure 4-2), there are a few isolated high emission factor regions located in central Texas and upper Arizona, due to the use of ecoregion level 4 data in the EFvE2011 dataset. For some VOCs such as myrcene (Figure 4-2), sabinene (Figure 4-3) and limonene (Figure 4-4), the EFvE2015 dataset predicts lower emission factors along river regions in several mid-west states including Iowa, Illinois and Missouri. These riparian ecosystems were not captured well by ecoregion level 4 data and were better characterized with LandFire EVT data. In general, the observed differences in Figure 4-2 through Figure 4-8 are due to the use of the more accurate and detailed LandFire data in the development of EFvE2015 database.

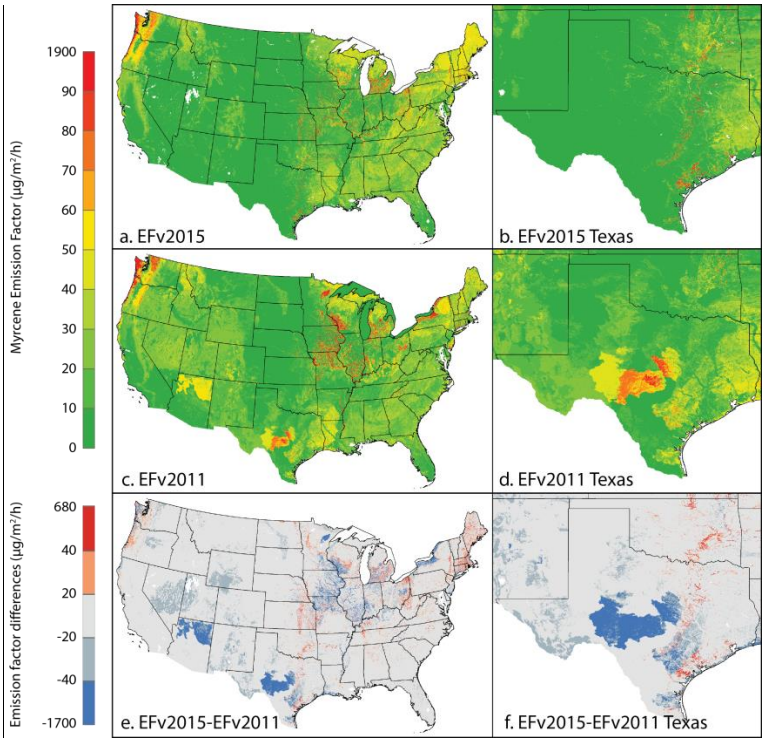

Figure 4-2. Myrcene emission factor datasets (EFvE2015(a), EFvE2011(b)) for contiguous US, and difference between the two datasets (c).

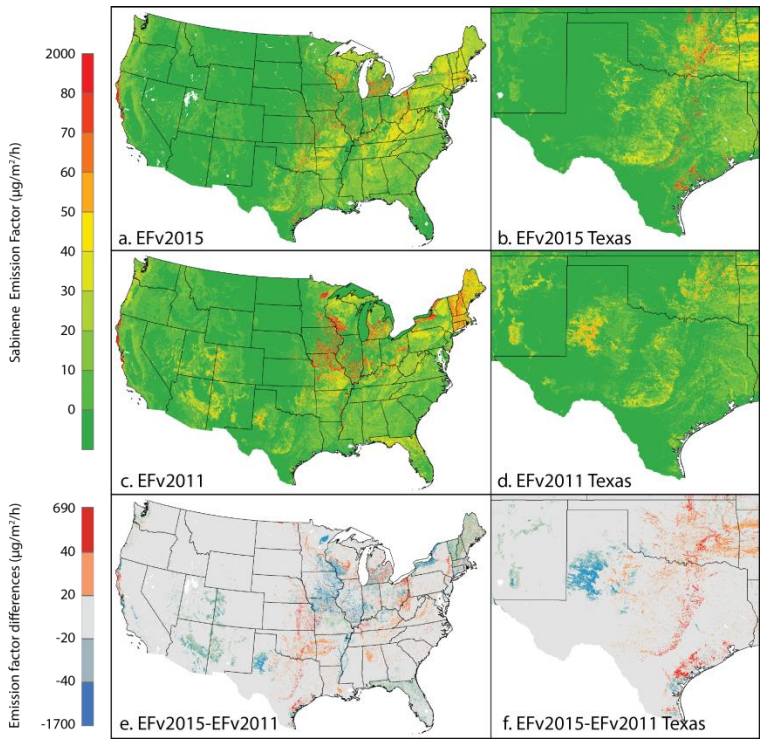

Figure 4-3. Sabinene emission factor datasets (EFvE2015(a), EFvE2011(b)) for contiguous US, and difference between the two datasets (c).

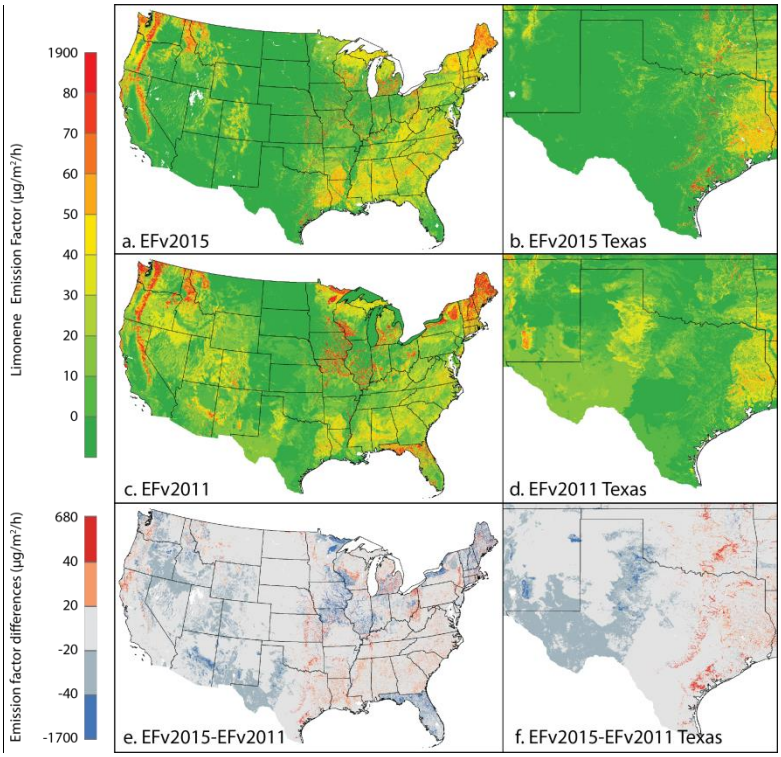

Figure 4-4. Limonene emission factor datasets (EFvE2015(a), EFvE2011(b)) for contiguous US, and difference between the two datasets (c).

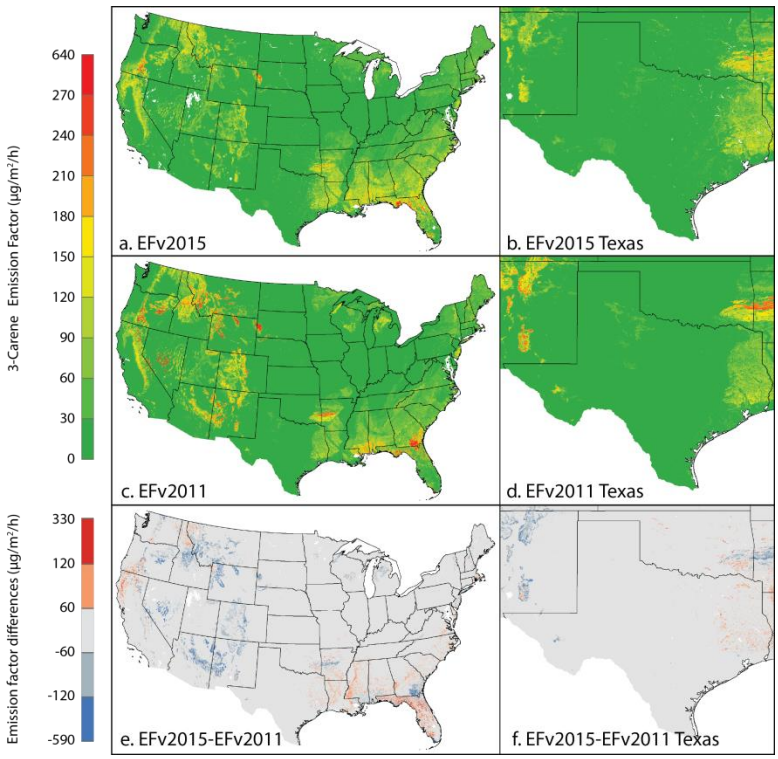

Figure 4-5. 3-Carene emission factor datasets (EFvE2015(a), EFvE2011(b)) for contiguous US, and difference between the two datasets (c).

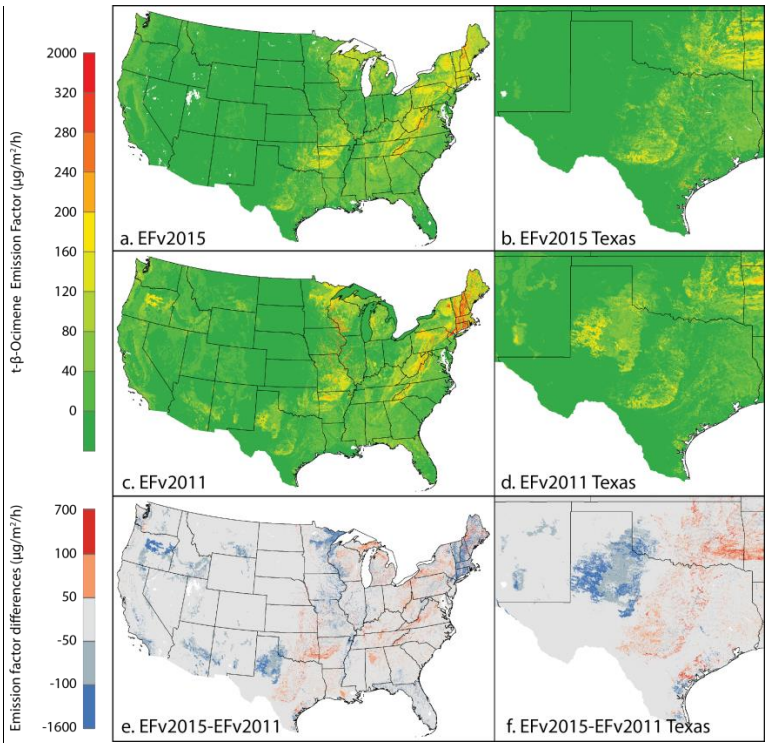

Figure 4-6. t-β-Ocimene emission factor datasets (EFvE2015(a), EFvE2011(b)) for contiguous US, and difference between the two datasets (c).

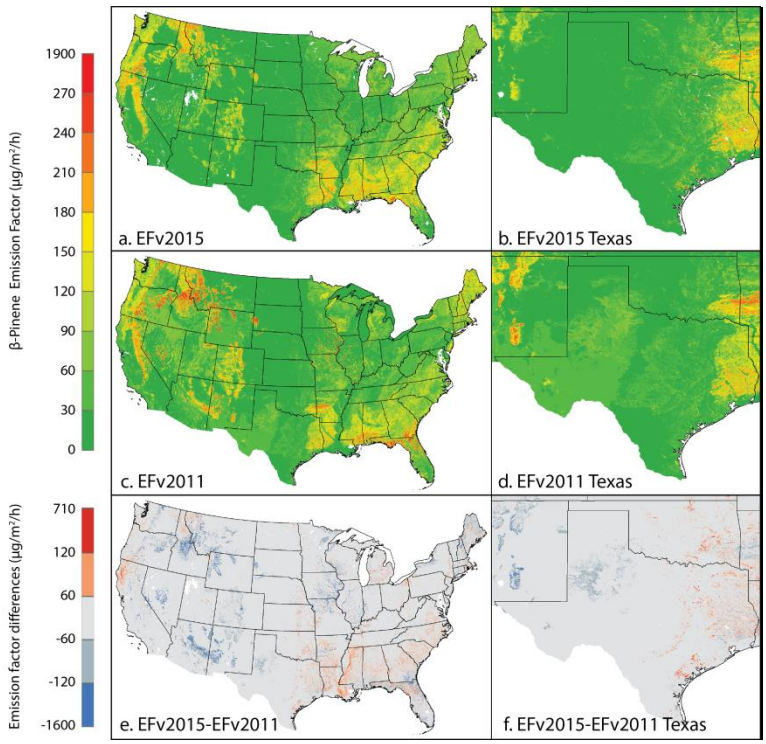

Figure 4-7. β-Pinene emission factor datasets (EFvE2015(a), EFvE2011(b)) for contiguous US, and difference between the two datasets (c).

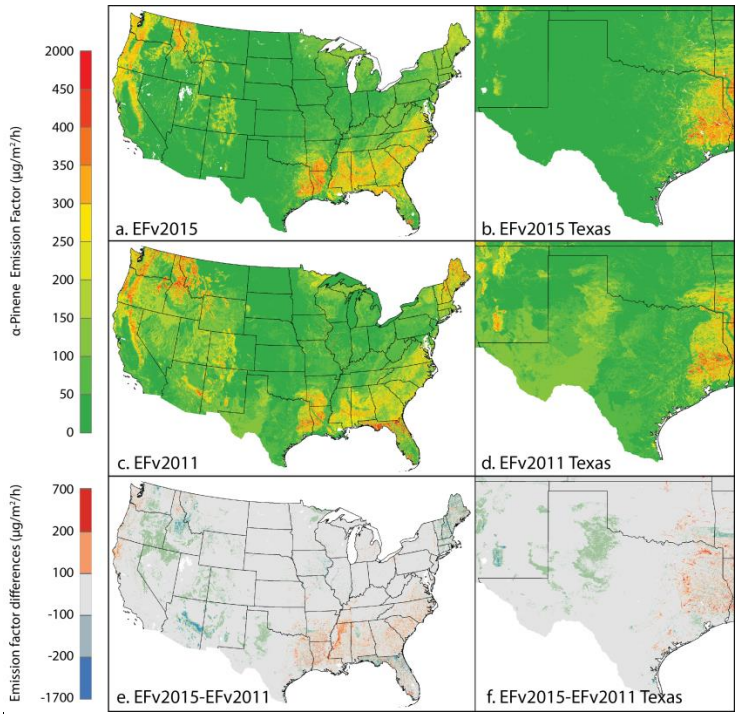

Figure 4-8. α-Pinene emission factor datasets (EFvE2015(a), EFvE2011(b)) for contiguous US, and difference between the two datasets (c).

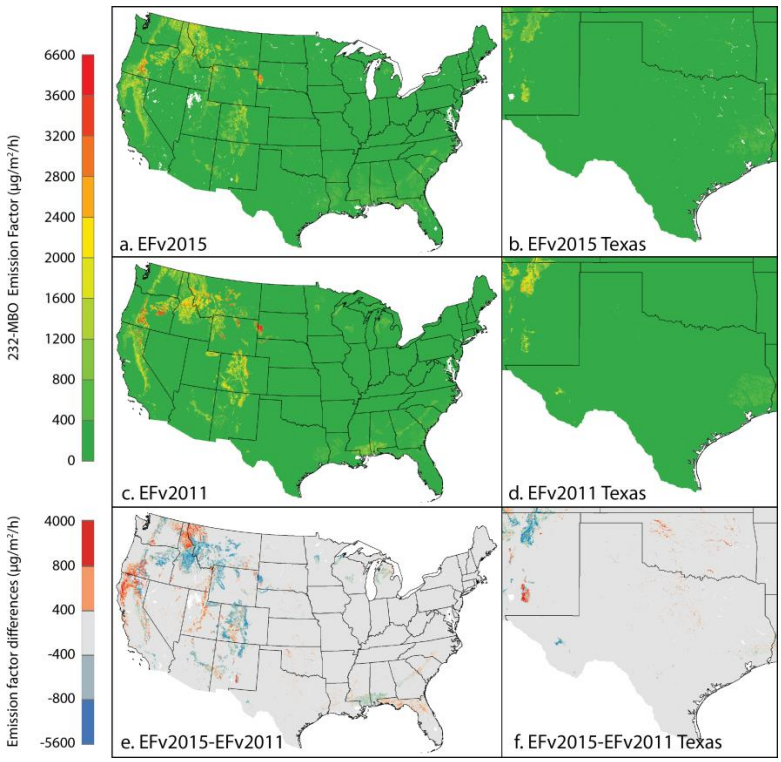

Figure 4-9. 232-MBO emission factor datasets (EFvE2015(a), EFvE2011(b)) for contiguous US, and difference between the two datasets (c).

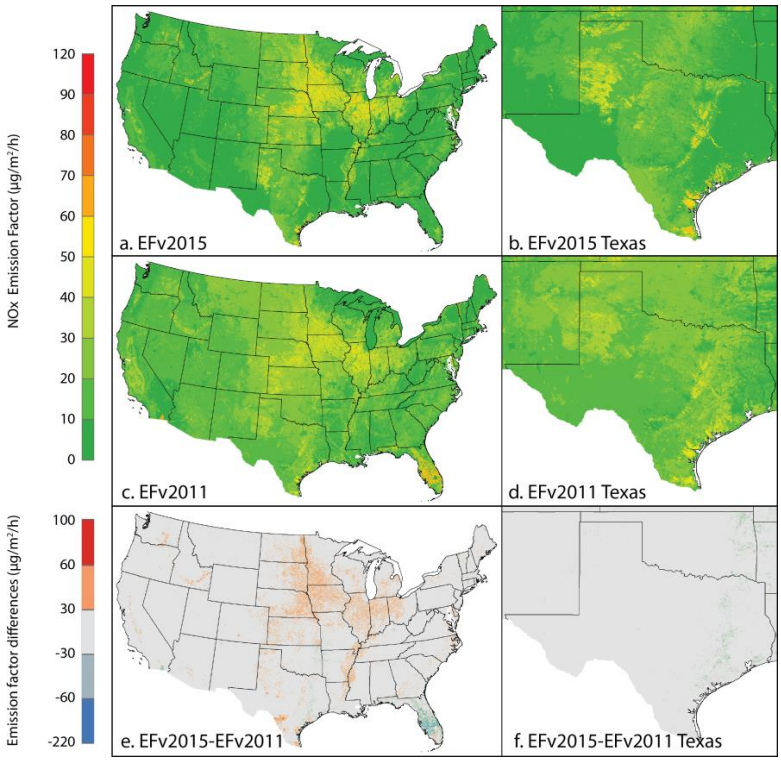

Figure 4-10. NOx emission factor datasets (EFvE2015(a), EFvE2011(b)) for contiguous US, and difference between the two datasets (c).

4.2 Development of Airborne Emission Factors

Aircraft observations were used to evaluate and constrain MEGAN emission factors. A previous pilot study (Karl et al., 2013; Misztal et al., 2014) successfully demonstrated the ability of this approach to characterize isoprene emissions in California oak woodlands. The EFvE2011 data for California were found to be accurate and had high correlations with aircraft observations. For this project, we have improved upon this approach and apply it to the southeastern US and Texas. Section 4.2.1 provides a detailed description of the method and the results are presented in section 4.2.2.

4.2.1 Methods for Developing Airborne Isoprene and Monoterpene EFs

4.2.1.1 Method Using Airborne Eddy Covariance Flux Data

The wavelet based approach provides isoprene and monoterpene flux data at high spatial resolution (see section 2). However the calculated fluxes are for the altitude at which the aircraft is flying and must be extrapolated to the surface level in order to be used to estimate EFs for biogenic VOCs. We applied a vertical flux divergence approach to perform this task.

First, we obtained vertical profiles of BVOC fluxes by averaging the estimated VOC flux at different altitude levels from measurements where the aircraft flew at different altitudes in a stacked racetrack pattern. We then normalized the profile using PBL height to reduce the impact of changing PBL height over time. Surface fluxes of BVOCs were then calculated using a vertical flux divergence correction method (Misztal et al., 2014) that assumes a linear relationship between fluxes at different altitudes. In addition, although the wavelet based approach provides high resolution flux data, there are inevitably considerable uncertainties for such high resolution. Therefore we spatially averaged the extrapolated surface flux to 2 km spatial resolution and performed subsequent analysis based on the spatially averaged data. The spatial resolution of 2 km still provides exceptional information for characterizing emissions in heterogeneous landscapes and it is not achievable if using traditional flux estimation approaches that average over 40 km or more.

Converting the surface fluxes into EFs requires accurate estimates of meteorological conditions such as temperature, solar radiation and wind speed. The MEGAN model calculates BVOC emissions as the product of an EF and an emission activity factor (EAF) that accounts for the impact of driving variables including canopy environment. We calculated the EAF associated with each aircraft flux measurement and applied this factor to the extrapolated surface flux to obtain the emission factor for standard conditions.

EAFs were calculated using two different approaches. For one version, EAFs were calculated by executing a single point version of MEGANv2.1 for every flux measurement, using the LAIv and vegetation cover described in section 3 with meteorological fields extracted from the North American Land Data Assimilation System (NLDAS-2) forcing data and soil moisture data extracted from NLDAS-2 model data (VIC model). For the second version, EAFs were calculated using the EFvE2011 emission factor database and BVOC emission rates calculated using WRF derived meteorological driving variables.

As discussed in section 2, the land cover is highly heterogeneous within the study area, thus it is critical to consider the exact footprint of each aircraft flux measurement. For this project, we improved upon the footprint analysis method used by Misztal et al. (2014) and performed a detailed half-dome footprint analysis. The radius of half-dome footprint was calculated as:

$$dx_{0.5} = 0.9\frac{uz_m^{2/3}h^{1/3}}{w^*}$$

where $dx_{0.5}$ is the half-width of the horizontal footprint (radius); u is horizontal wind speed, extracted from high resolution C-130 data; Z_m is aircraft height above ground, calculated from GPS mean sea level altitude and high resolution ground elevation data; h is PBL height taken from vertical profiles of isoprene concentration, potential temperature, virtual potential temperature, water vapor mixing ratio and horizontal wind speed. If no vertical profiles were available, h was extracted from WRF data provided by the Georgia Institute of Technology; w* is convective velocity scale, derived from vertical latent heat flux, which was also calculated based on the wavelet approach. The direction to which the half-dome is facing was calculated from the C-130 horizontal wind direction data. Vector decompositions were performed to obtain spatially averaged wind speed and wind directions. The estimated half-domes were used to determine the extent of the footprint for each measurement and used to define the area over which to average the 30 meter resolution EFvE2015 isoprene and total monoterpene emission factor data, total vegetation cover (see section 3) and LandFire EVT data. Distributions of these variables within each half-dome area were tabulated for subsequent analysis. An example of the estimated half-dome is shown in Figure 4-11, with the developed 30 m resolution EFvE2015 database (for isoprene) as background. The size and directions of half-domes vary spatially, and the spatial heterogeneity of isoprene emission factors can clearly be seen.

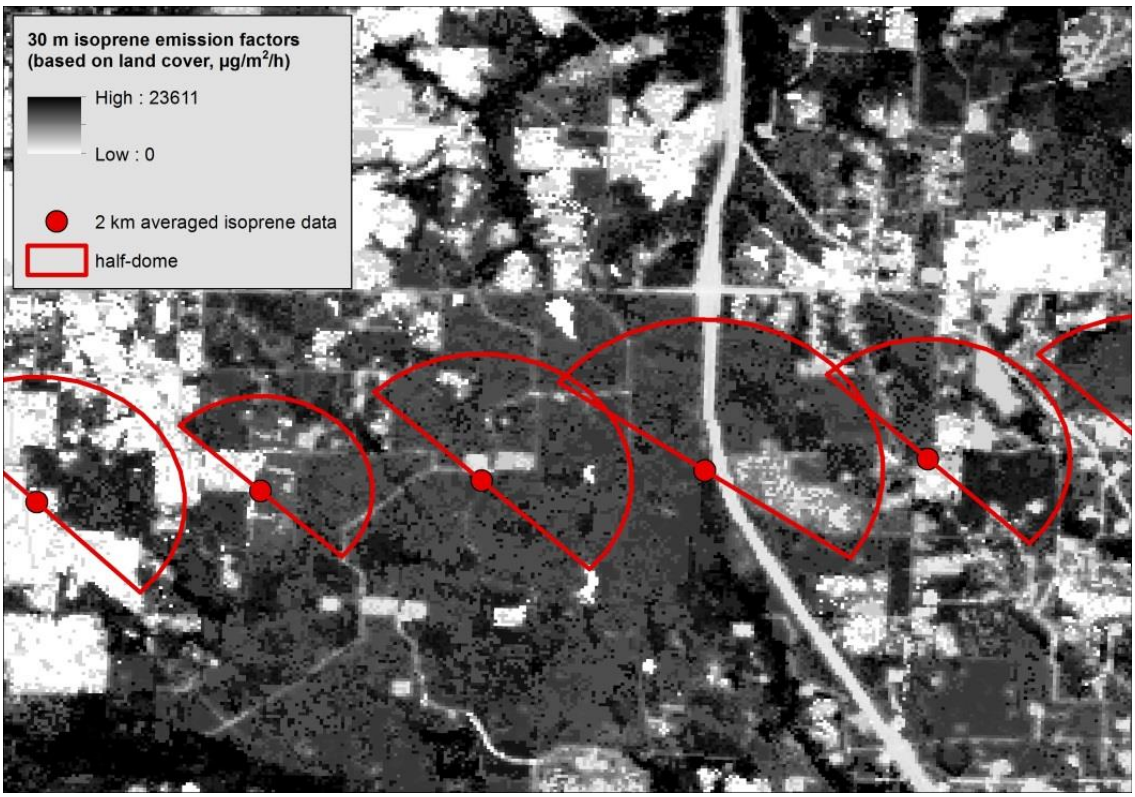

Figure 4-11. Example of the estimated half-dome for spatially averaged surface isoprene data (2 km). The 30 meter resolution EFv2015 isoprene database is shown in the background.

In order to make use of these flux observations to inform, evaluate and constrain BVOC emissions from individual vegetation types, we summarized statistics for individual LandFire EVTs. Several different approaches were tested for this analysis:

a) For each half-dome, the assigned BVOC emission factor was based on the dominant EVT within the footprint area.

b) All EVTs from within any footprint areas (over 200 unique EVTs) were categorized into 11 groups based on their landcover average EF (based on EFEv2015 and LandFire EVT data). Within each half-dome, landcover average EFs were assigned to the dominant EVT group.

Approaches a) and b) are straightforward to implement, however, they do not fully segregate emissions from individual vegetation types and thus will overestimate emissions from low emitting EVTs/groups and underestimate emissions from high emitting EVTs/groups. To overcome this potential issue, additional approaches were tested:

c) Summarize detailed EVT distributions within each footprint area and create a linear system:

$$\begin{bmatrix} f_{1,1} & f_{1,2} & \cdots & f_{1,n-1} & f_{1,n} \\ f_{2,1} & f_{2,2} & \cdots & f_{2,n-1} & f_{2,n} \\ \vdots & \vdots & \ddots & \vdots & \vdots \\ f_{m,1} & f_{m,2} & \cdots & f_{m,n-1} & f_{m,n} \end{bmatrix} \times \begin{bmatrix} BEF_{\varepsilon,1} \\ BEF_{\varepsilon,2} \\ \vdots \\ BEF_{\varepsilon,m} \end{bmatrix} = \begin{bmatrix} BEF_{o,1} \\ BEF_{o,2} \\ \vdots \\ BEF_{o,m} \end{bmatrix}$$

$BEF_{o,1}$ through $BEF_{o,m}$ refers to surface basal emission factor calculated from aircraft observations (subscript *o* denotes observation, and there are *m* data points). *f* denotes area fraction of EVT Ɛ within the half-dome footprint of the corresponding data point ($BEF_{o,1}$ through $BEF_{o,m}$). The first subscript number refers to observation ID, and the second subscript number corresponds to IDs of EVTs. $BEF_{\varepsilon,1}$ through $BEF_{\varepsilon,n}$ refers to BEFs of *n* unique EVTs in the study area (what we are solving for). Since the number of observations is larger than the number of EVTs (m >> n), this system is expected to be overdetermined. This system was solved using least square methods while constraining $BEF_{\varepsilon,1}$ through $BEF_{\varepsilon,n}$ to be positive.

d) Retain the dominant EVT within each footprint area while converting cover fractions of all other EVTs to the dominant EVT cover fraction proportional with their mean EFs from the EFvE2015 database. The same approach was also tested for grouped EVTs.

4.2.1.2 Method Using Mixed Layer Flux Data

As shown in Figure 2-4, BVOC flux data derived from airborne eddy covariance method covers a small fraction of land area in the southeastern US. Isoprene flux calculated using the NOAA P-3 aircraft (see section 2.3) data from the NOMADSS, SENEX and 2006 Texas Air Quality Study (TEXAQS) campaign, covers a much larger area (Figure 4-12) and were also used in this study to derive isoprene EFs.

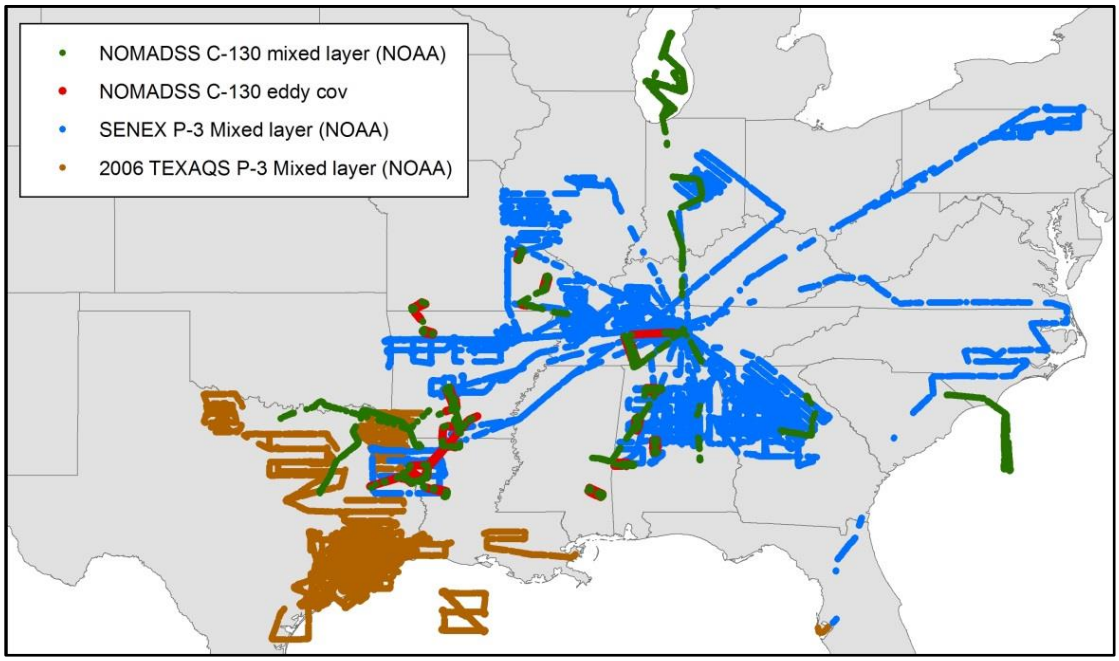

Figure 4-12. Spatial coverage of available flux data from the NOMADSS, SENEX and 2006 Texas Air Quality Study (TEXAQS) campaign calculated using airborne eddy covariance and mixed layer methods.

For mixed layer isoprene flux data, a similar half-dome footprint approach was applied (see section 4.2.1.1), where convective velocity scales were estimated using a wavelet based approach for selected flight legs.

4.2.2 Results and Discussion of Airborne EF Development

4.2.2.1 Results Using Airborne Eddy Covariance Flux Data

4.2.2.1.1 Isoprene

First, we used isoprene flux data derived from airborne eddy covariance method for the NOMADSS campaign alone to evaluate the applicability of the method as described in section 4.2.1.1. The use of different approaches in the estimation of EAF and airborne EF showed consistent results, and they suggest that the EFvE2015 database reasonably captured the variations of BVOC emissions among different EVTs. As an example, Table 4-1 shows the calculated mean airborne EF for isoprene using different approaches and their correlations with EF from the EFvE2015 database. Results for EVTs with too few samples (less than 20) were excluded. The correlations between airborne EF calculated using different approaches and the landcover based EFvE2015 data range from 0.32 to 0.73. It should be noted that when developing the EFvE2015 emission factor database, emission factors for EVT 3997 (agricultural pasture and hayfields) were assumed to be 1, but the calculated airborne EF suggest much higher values except for the results obtained using approach d, which accounted for the relative magnitude of landcover EFs among different EVTs. As expected, if excluding agricultural lands, the R^2 values increase to 0.42 and 0.50 for airborne EF obtained only using dominant EVT within the footprint area (approach a) but decreases slightly for approach d.

Table 4-1. Comparison of EVT averaged airborne isoprene EF calculated using NLDAS data and approaches a and d described in the text. Their correlations with EFvE2015 database EFs and oak percentage of total trees are also shown. Airborne isoprene flux used here are from the airborne eddy covariance method for the NOMADSS campaign

	Mean isoprene emission factor (μg/m2/h)				
EVT ID	Airborne EF (approach a)	Airborne EF (approach d)	EFvE2015 EF	Oak percentage	Vegetation type
3535	3176	3219	6370	17%	Managed Tree Plantation
3304	8450	9783	11500	59%	White Oak-Red Oak-Hickory Forest
3194	3318	3900	7940	23%	Ruderal Forest
3305	4348	5431	7650	35%	Chestnut Oak Forest and Woodland
3473	4246	5619	10000	20%	Eastern Floodplain Forests
3349	2036	1890	5680	16%	Longleaf Pine Woodland
3997	3047	1	1	23%	Agricultural-Pasture and Hayland
3321	5528	5269	7050	30%	Beech-Maple-Basswood Forest
3317	7529	8642	8670	36%	Chestnut Oak Forest and Woodland
3371	3709	3499	6050	16%	Shortleaf Pine Woodland
3307	4656	7475	9980	35%	Coastal Plain Oak Forest
3474	3110	3893	8680	19%	Small Stream Riparian Forests
	0.32	0.73	Correlation (R^2) with land cover BEF (with agricultural)		
	0.42	0.68	Correlation (R^2) with land cover BEF (without agricultural)		
	0.77	0.65	Correlation (R^2) with oak tree percentage		

* Oak percentage refers to percentage that oaks contribute to total tree cover.

In addition, Table 4-1 shows the percentage that oaks trees contribute to total tree cover for each EVT and the correlations between oak tree percentages based on FIA ground surveys and airborne BEFs. These two independent indicators have higher correlations, ranging from 0.65 to 0.77. Since trees dominate isoprene emissions and oak trees are recognized as high isoprene emitters, these high R^2 values provide some confidence in the landcover data, the calculated airborne EFs and the method used.

Approach c, although technically more accurate, was found to perform poorly. The reason is that the established linear system is substantially overdetermined and has too many degrees of freedom. In addition, this approach requires accurate characterizations of the distributions of EVT data within the footprint. Hence this approach was not pursued any further. Similarly, approach d was also discarded ultimately since it also requires accurate characterizations of EVT distributions within footprint areas.

We performed a sensitivity analysis to investigate the impact of the spatial averaging radius on the calculated airborne EF (using approach a) for individual EVTs. Two additional spatial resolutions were tested: 4 km and 6 km (Figure 4-13). The calculated airborne EF varies only slightly with the change in resolution, suggesting a small impact of spatial resolution on the magnitude of airborne BEFs.

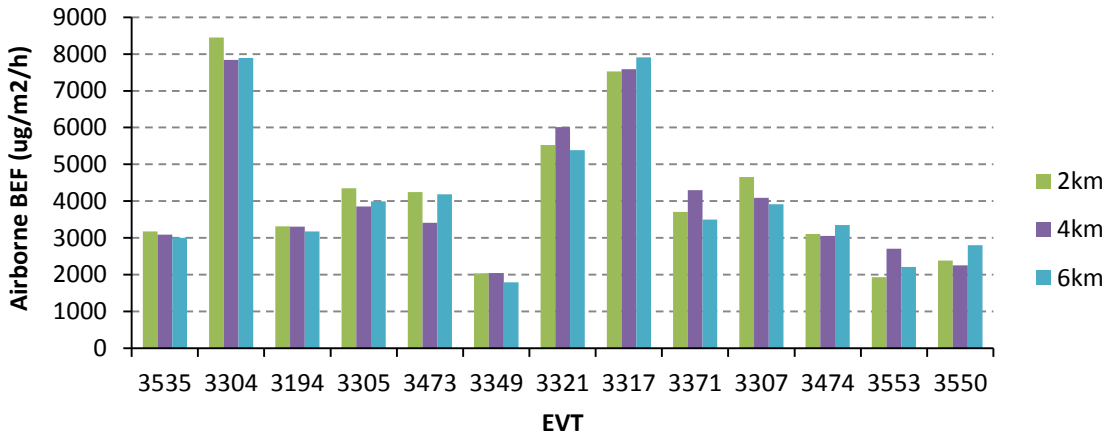

Figure 4-13. Sensitivity study of the impact of spatial averaging resolution on calculated airborne EFs.

In addition, we also evaluated the calculated airborne EFs (approach a) against EF-PFTvE2015 as well as the EFvE2011 database (Figure 4-14), using the same half-dome footprint method. Among the three databases compared, the EFvE2015 database agrees best with the reversely calculated airborne isoprene EFs (R^2 = 0.53), followed by EF-PFTvE2015 (R^2 = 0.46) and EFvE2011 (R^2 = 0.43). The comparison results suggests that the EF-PFTvE2015 database shows improved performance relative to the previous EFvE2011 database, but EFvE2015 best captured spatial variations of isoprene emissions among the three databases.

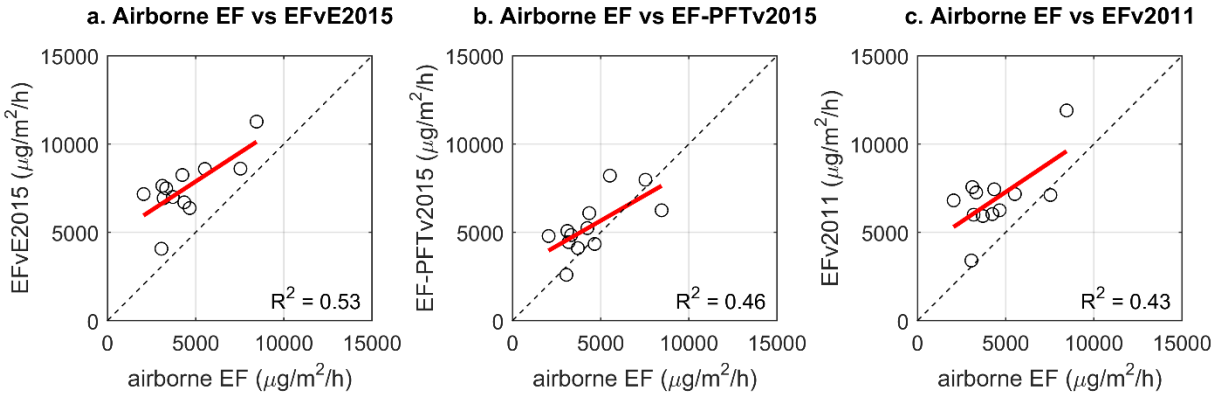

Figure 4-14. Evaluation of airborne isoprene EF versus mean landcover isoprene EF within half-dome footprint from EFv2015, EFv2015-PFT and EFv2011 database. Airborne EFs were derived using airborne eddy covariance method for the NOMADSS campaign.

Mean landcover isoprene EF, within half-dome footprints, from the EFvE2015 dataset for all EVTs (Figure 4-14) are on average 79% higher than the mean airborne isoprene EF. This observation suggests that EFvE2015 may overestimate isoprene in these areas, although the spatial variations of isoprene emissions are well captured. The observed overestimation is less

(59% higher) in the EFvE2011 dataset and the smallest (24% higher) in the EF-PFTvE2015 dataset.

Similar findings are also observed when using approach b. Table 4-2 provides a comparison between EVT group averaged isoprene EF calculated using airborne EFs and enclosure EFs from the EFvE2015 database. Isoprene flux data used in the calculation are from airborne eddy covariance method for the NOMADSS campaign. Results for EVT groups with small sample sizes (less than 20) were excluded. The correlation coefficient (R^2) value between EVT group averaged airborne and enclosure EFs is 0.68 when including EVT group 1, which consists of mostly agriculture EVTs. Due to the assumption used, the average land cover BEFs for agriculture lands are much smaller than airborne EFs. When excluding EVT group 1, the R2 value increases to 0.99. Again, since these two data series were independently developed, this high correlation indicates that the landcover EF (EFv2015 data) captured the variability in isoprene emission between different EVT groups. However, the landcover EFs are on average 57% higher than airborne EF.

Table 4-2. Comparison between EVT group averaged airborne based EFs, based on approach b using NLDAS data, and enclosure based EFs from the EFvE2015 database. Airborne flux data used in the calculation are from airborne eddy covariance method for the NOMADSS campaign.

Mean isoprene basal emission factor (μg/m^2/h)		
EVT group	airborne EF	enclosure EF
1	2500	182
6	2080	5370
7	3220	6480
8	4180	7490
9	5490	8470
11	7370	11000

It should be noted that we expect significant uncertainties in all EVT-specific footprint analysis due to the inherent uncertainties in the 30 meter resolution LandFire EVT data used in the analysis. Lumping EVTs into different groups is expected to reduce this uncertainty to some extent, and this could explain the better correlations obtained when using grouped EVT, instead of individual EVTs.

4.2.2.1.2 Total Monoterpene

Results from airborne eddy covariance flux for total monoterpene suggest that the EFvE2015 dataset also reasonably captured the spatial variations of total monoterpene emissions. Airborne emission factors of total monoterpenes were also calculated using the same approach (Table 4-3). The calculated EVT averaged airborne total monoterpene emission factors correlates reasonably well with mean enclosure emission factors (EFvE2015) within the same

half-dome footprints (R^2 = 0.42). However the mean enclosure EFs (EFvE2015) of total monoterpene are on average 78% higher than airborne EF.

Table 4-3. Comparison of EVT averaged airborne total monoterpene EF calculated using NLDAS data with the approach "a" described in the text, as well as mean landcover emission factors (EFvE2015) within half-dome footprints

	Mean total monoterpene EF (μg/m2/h)		
EVT	Airborne EF (approach a)	Mean EFvE2015 EF within footprint	EVT description
3535	672	1647	Managed Tree Plantation-Southeast Conifer and Hardwood Plantation Group
3194	659	1613	Ruderal Upland-Treed
3349	979	1887	East Gulf Coastal Plain Interior Upland Longleaf Pine Woodland
3305	478	905	Southern Interior Low Plateau Dry-Mesic Oak Forest
3304	421	948	Ozark-Ouachita Dry-Mesic Oak Forest
3473	662	1458	Gulf and Atlantic Coastal Plain Floodplain Systems
3997	629	898	Pasture and Hayland
3321	702	1161	South-Central Interior Mesophytic Forest
3994	309	154	Row Crop
3317	1161	1224	Allegheny-Cumberland Dry Oak Forest and Woodland
3307	599	1068	East Gulf Coastal Plain Northern Dry Upland Hardwood Forest

4.2.2.1.3 Revised Isoprene Emission Factor Database

Current results show that the developed EFvE2015 database may potentially overestimate isoprene emissions. Due to limited information for the majority of EVTs not covered by aircraft isoprene flux data, a detailed and comprehensive modification of existing MEGAN EF database at EVT level is not possible. However, the excellent correlation (R2 = 0.99 when excluding agriculture) as shown in Table 4-2 indicate that revising isoprene EF at grouped EVT level may be promising. We scaled the EFvE2015 database for isoprene proportionally using information from Table 4-2 and developed a revised isoprene database (EFvA2015).

During footprint analysis, all EVTs were categorized into 11 groups and average airborne EFs were calculated for 6 of the 11 groups (section 4.2.2). Scale factors were calculated based on EVT group averaged airborne EF and average land cover EFs in the footprint areas for corresponding EVT groups. For EVT groups with no data available, an average scale factor was applied. The scale factors were then applied to all EVTs within corresponding groups to derive the EFvA2015 dataset.

The developed EFvA2015 dataset for isoprene, as well as differences between EFvE2015 and EFvA2015 data, are shown in Figure 4-15. As expected, the biggest differences are found in the southeastern US, because isoprene emission factors are highest in these areas (Figure 4-1), and they were proportionally scaled down using scale factors, leading to high absolute differences.

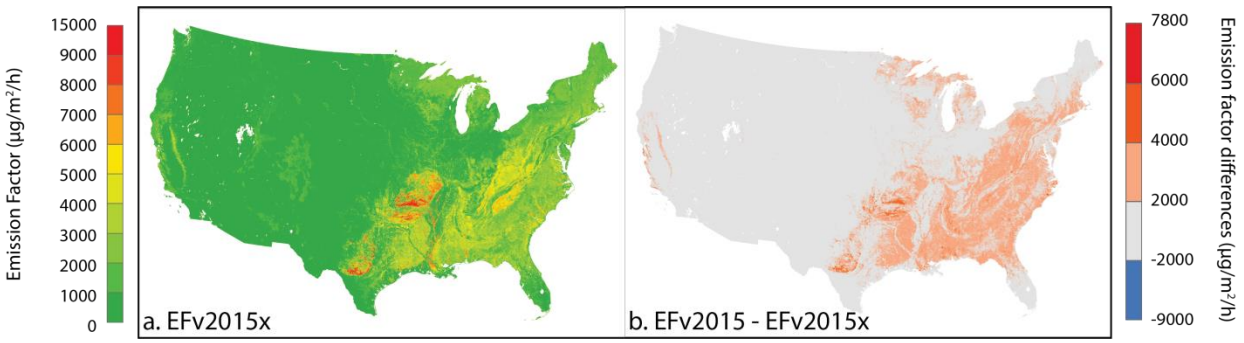

Figure 4-15. Experimental isoprene emission factors (EFvA2015, panel a) and differences between EFvE2015 and EFvA2015 dataset (panel b).

It is also important to note that there are still much room for improvements in the EFvA2015 database for isoprene by increasing the available observations. The success of previous study (Misztal et al., 2014), and also the results as described in previous sections, increase our confidence in the methods used in this project. Efforts are needed to apply this method to other regions, and to incorporate and reconcile more observations from various sources to further refine the developed EFvA2015 database.

4.2.2.2 Results Using Mixed Layer Flux Data

Isoprene flux data derived from the wavelet based airborne eddy covariance approach were also compared with those from the mixed layer method. We found that flux data from the two methods are overall equivalent, with noticeable differences for some flight legs. As an example, Figure 4-16 provides a comparison between the two flux datasets. Profile 1 was flown near the Texas-Louisiana border over Shelby and Panola Counties in Texas. Profile 2 was flown over Natchitoches Parish in Louisiana. Excellent matching was observed for flight profile 2, however isoprene fluxes calculated using the mixed layer approach are higher in flight profile 1. A potential explanation of the observed mismatch is discussed in section 4.3.3.

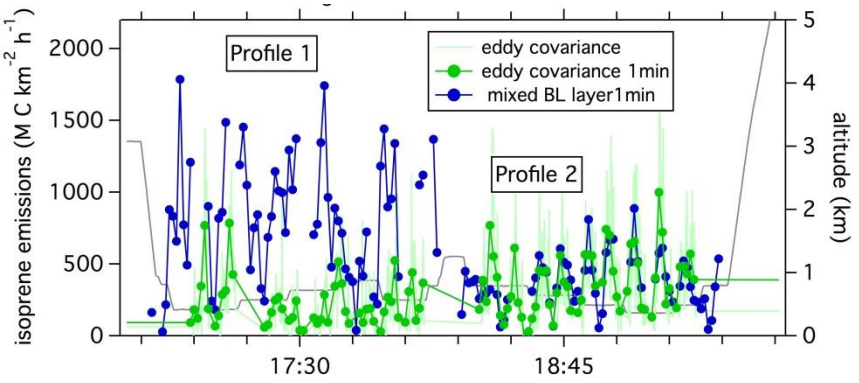

Figure 4-16. Comparison between MBA and wavelet isoprene flux for research flight #2 of the NOMADSS campaign. High resolution wavelet flux data were averaged to MBA flux time stamps.

Despite these noticeable differences, the derived EVT averaged airborne EFs from the two flux database are similar (Figure 4-17), with good correlations, although it seems that isoprene airborne EFs calculated using mixed layer flux and NLDAS data are slightly higher than those calculated using airborne eddy covariance flux data.

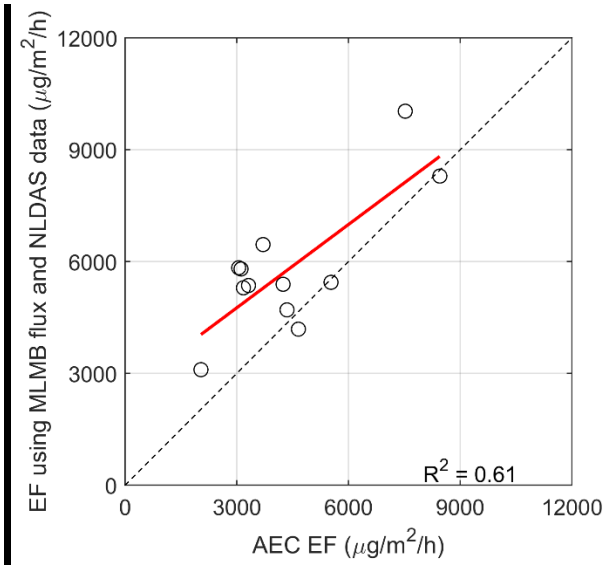

Figure 4-17. Comparison of calculated isoprene airborne emission factors using airborne eddy covariance and mixed layer methods for the NOMADSS campaign.

Using the mixed layer flux data, which covers a much larger area than the airborne eddy covariance flux data (Figure 4-12), we estimated averaged isoprene flux data for 47 EVTs. Figure 4-18 provides a comparison between the calculated EVT averaged mixed layer isoprene flux data from SENEX and the 2006 TEXAQS campaign, and isoprene flux data derived from the EFvE2011 database. Generally, the flux calculated from the EFvE2011 emission factor database captures the spatial variation of isoprene emissions, however the EFvE2011 enclosure based emission factor database was higher for isoprene emissions by 81% on average. The number of EVTs covered by the mixed layer flux data (47) is substantially higher than the 12 EVTs characterized by using airborne eddy covariance flux data alone.

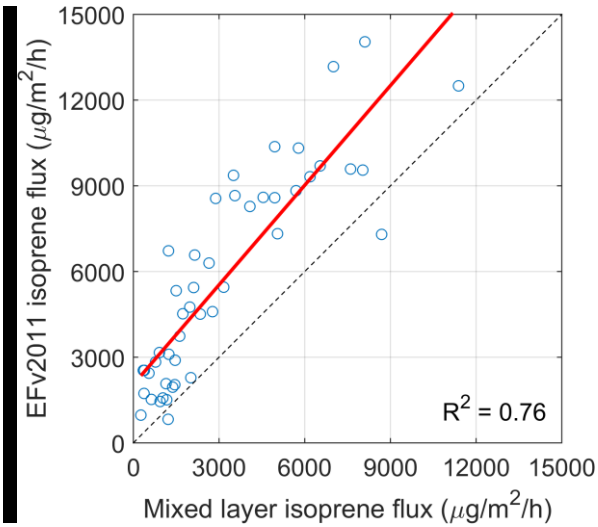

Figure 4-18. Comparison between EVT averaged mixed layer isoprene flux and EFvE2011 isoprene flux data

4.3 Uncertainties and Limitations

The results suggest that the developed EFvE2015 emission factor database captures much of the spatial variations in isoprene emissions in the southeastern US, which has heterogeneous landscapes. Significant improvements were also observed compared with previous database (EFvE2011) and an alternative database developed using PFT-specific emission factors (EF-PFTvE2015). However, current results suggest that even with the updated landcover, the enclosure measurement based EFvE2015 database appears to over-estimate isoprene emissions in southeastern US. To better understand this observation, the uncertainties and limitations of this study are discussed. In this study, the biggest uncertainties could have originated from three sources: emission factors, meteorological driving variables (including solar radiation and temperature), as well as the estimation approaches used.

4.3.1 Uncertainties in the EfvE2015 Emission Factor Database

Enclosure based emission factors have considerable uncertainties. The EFvE2015 database was developed by combining EVT averaged plant species distributions with enclosure measurements for different plant species, and both components are expected to have significant uncertainties.

The LandFire EVT data were developed for the entire US area with 30 meter resolution. The regional distributions of vegetation types may be accurate, but given the substantial degree of spatial heterogeneity (Figure 4-11), naturally, we do not expect perfect match for every 30 meter data point. Therefore, emission factor estimates at a given 30 m data point have a substantial amount of uncertainties, although estimates at larger scale have been shown to be reasonable.

Detailed plant-species distributions were developed from several different sources, including forest and soil surveys. In addition, within each EVT, the distributions of plant species are

assumed to be homogeneous. Realistically, spatial variations of plant species distributions are expected to be considerable even within the same EVT, which would contribute to the overall uncertainties.

Furthermore, enclosure measurement data for BVOCs also contain uncertainties, and they are only available for limited amount of plant and BVOC species. Therefore, assumptions have to be made, such as assigning the same factor to the entire genus of plants, or even family. These assumptions further contribute to uncertainties.

Finally, the aircraft observation based isoprene emission factor database (EFvA2015) is uncertain and is based on limited information on grouped EVTs. There is an urgent need to incorporate and reconcile additional BVOC measurement data from other campaigns that are not included in the scope of this project, such as the 1999 SOS, 2000 TEXAQS, 2004 ICARTT, 2010 Carbonaceous Aerosols and Radiative Effects Study (CARES) and the 2011 California Airborne BVOC Emission Research in Natural Ecosystem Transects (CABERNET) campaign, to further constrain the developed isoprene emission factor database.

4.3.2 Uncertainties in Meteorological Driving Variables

Solar radiation and temperature are among the most important meteorological driving variables. Three meteorological driving variable datasets were used in this study: NLDAS, WRF and aircraft measurements. Each dataset was developed using different methods and assumptions. Inevitably, discrepancies to some degree are expected among the three datasets, as well as real world values.

The airborne EFs calculated using WRF or using NLDAS meteorological data are considerably different. The WRF based EF values are consistently lower due to higher EAF values estimated by WRF. For the reverse calculation of emission factors using airborne eddy covariance data, radiation and temperature data from the NLDAS forcing dataset were used, which is a widely recognized database for North America. Similar with WRF data as used in CAMx modelling, the spatial resolution of NLDAS data is around 12 km. Here, we compared hourly averaged solar radiation data from WRF and NLDAS with measurements data collected from 52 surface sites within Texas (Figure 4-19) during the SAS campaign time period (6/1/2013 to 7/15/2013). Overall, WRF and NLDAS solar radiation data are similar, but both over-estimated solar radiation by approximately 50 W/m^2. Therefore, the modelled isoprene emissions from MEGAN using WRF and NLDAS data are expected to over-estimate. This comparison suggest that the higher airborne EFs calculated using WRF data are likely due to high bias in other meteorological driving variables such as temperature. In addition, it should be noted that this comparison was performed on averaged data from 52 sites but the results differ spatially for individual sites. Random, small and patchy clouds can impact substantially on the measured solar radiations at ground sites, which cannot be captured by meteorological models.

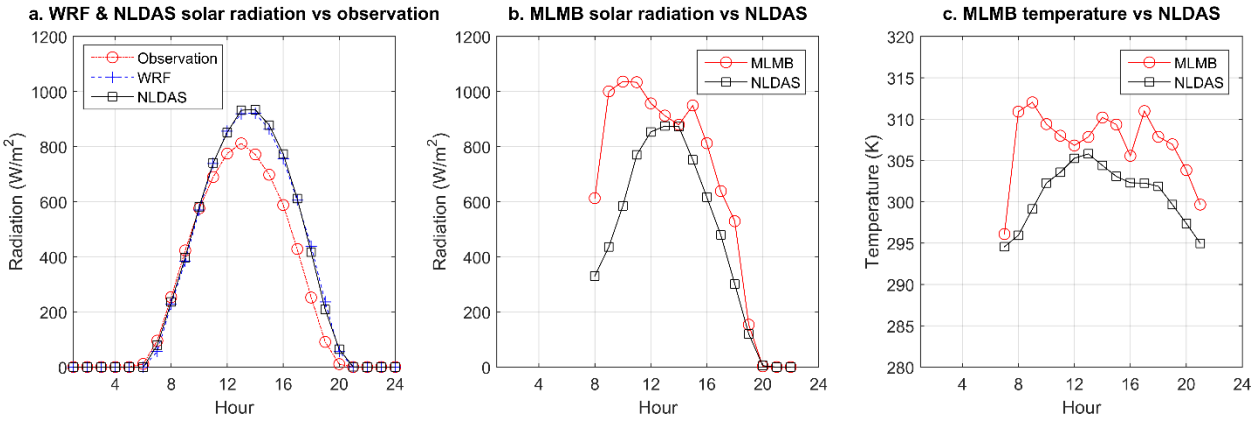

Figure 4-19. Comparison between NLDAS solar radiation with ground measurements at four sites within Texas

We also compared NLDAS solar radiation and temperature data with those calculated from aircraft measurements, which were applied in the calculation of mixed layer isoprene fluxes. On average, solar radiation data used to calculate EF from the mixed layer flux data is 26% higher, and temperature data is 6° K higher than NLDAS data. This suggests that if the mixed layer flux EFs were adjusted with EAFs from NLDAS, consistent with the aircraft eddy covariance data, then there would be an even greater difference in the resulting EFs shown in Figure 4-17. Note that the spatial resolution of NLDAS data is 12 km, with 1 hour temporal resolution, while the resolutions of aircraft measurements are in dozens of meters and at the order of seconds. Therefore we do not expect perfect match between the two. Additionally, despite the differences in meteorological driving variables, the calculated isoprene emission factors still correlate well (Figure 4-17).

These comparisons suggest that the meteorological driving variables used in current isoprene emissions modelling with the MEGAN model could potentially lead to over-estimation of isoprene emissions.

4.3.3 Uncertainties in Aircraft Flux Measurement Approaches

In this study, BVOC flux data were calculated using two distinct approaches: a wavelet based airborne eddy covariance approach, and a mixed layer approach. Surface fluxes were calculated through vertical linear regression in the first approach. Although the assumed linear relationship of vertical BVOC flux is apparent most of the time, exceptions do occasionally occur (Figure 4-20). On vertical profile 2 of NOMADSS research flight #2, a clear linear relationship can be seen, but such linear assumption is less clear on profile 1. For profile 1, the extrapolated surface flux is more uncertain.

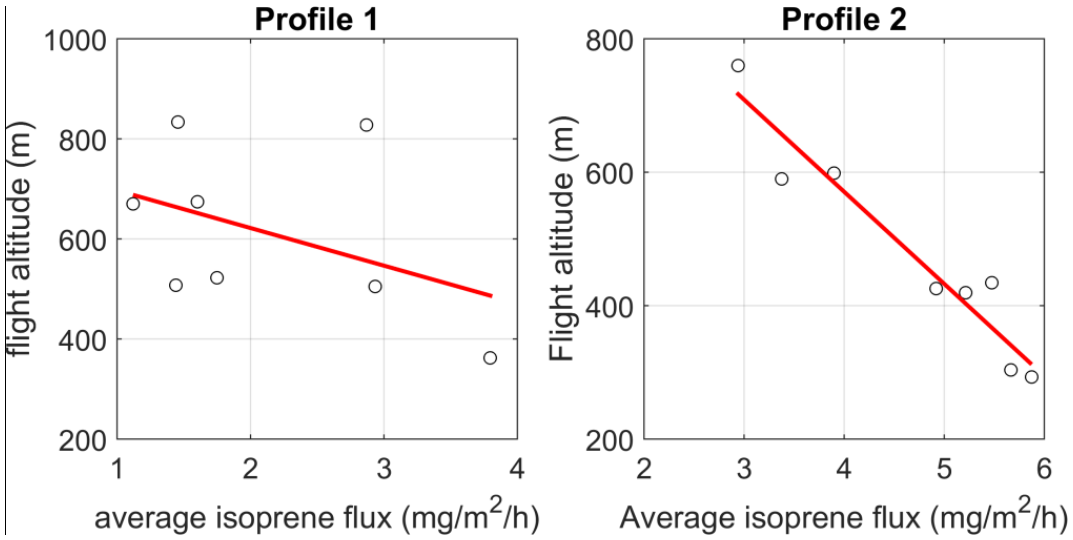

Figure 4-20. Vertical profiles of averaged isoprene flux (calculated using wavelet based airborne eddy covariance) for two selected profiles of NOMADSS research flight #2

A closer examination of the profiles suggests that heterogeneity of ground vegetation below profile 1 may contribute to the observed differences (Figure 4-21). To quantify surface heterogeneity, Figure 4-22 provides semivariogram plots of isoprene EFs from the EFvE2015 database around the two selected profiles, which is a widely accepted metric to characterize spatial heterogeneities (Garrigues et al., 2006). The semivariogram plot shows the variances of quantities between all pairs of sampled locations that are separated by different distances. Higher variances suggest higher spatial heterogeneity. It is apparent from Figure 4-22 that isoprene EFs around profile 1 have substantially more spatial variability than those around profile 2, as indicated by the higher "nugget" (non-zero variances at small separation distances) and semi-variance of profile 1. The variability becomes similar when distance increases to approximately 10 km, the same order as the footprint size of MLMB isoprene flux data. The observations from Figure 4-21 and Figure 4-22 may indicate that landcover heterogeneity could explain some of the differences observed between results from the two approaches for specific flight legs. Furthermore, these observations could also explain the flux mismatch as seen on Figure 4-16.

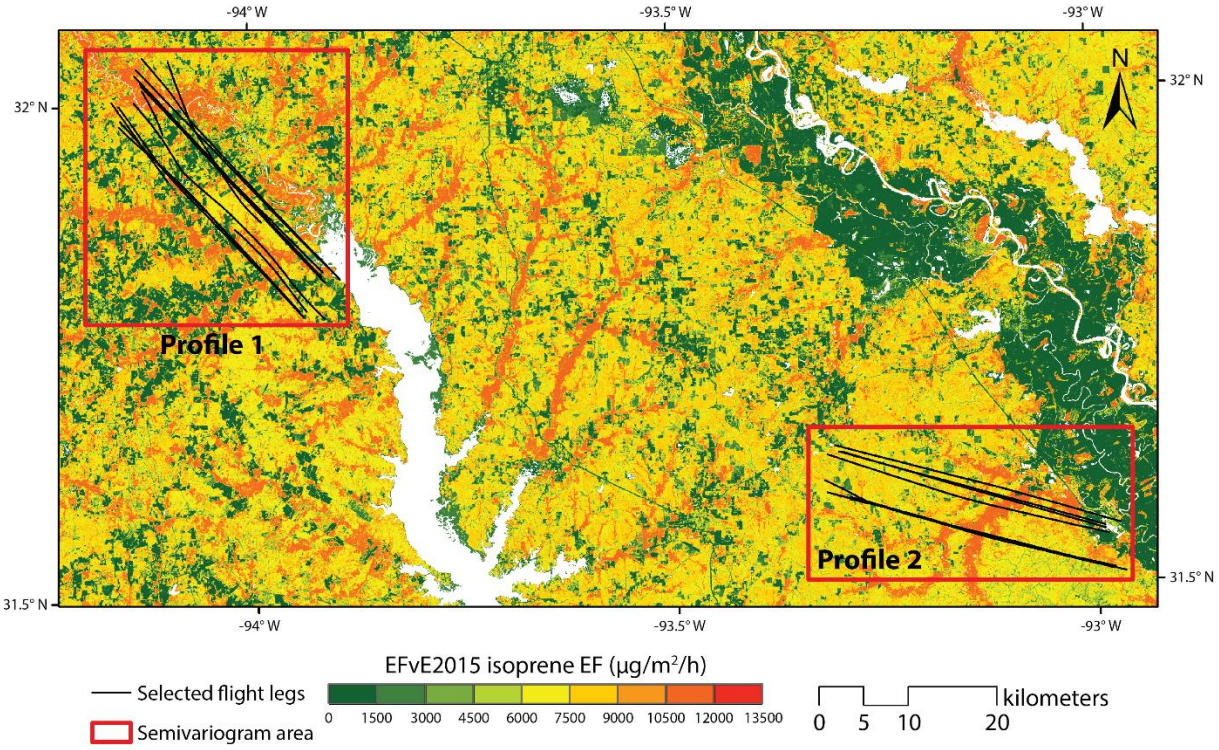

Figure 4-21. Spatial heterogeneity of EFvE2015 isoprene emission factors for the areas around two profiles.

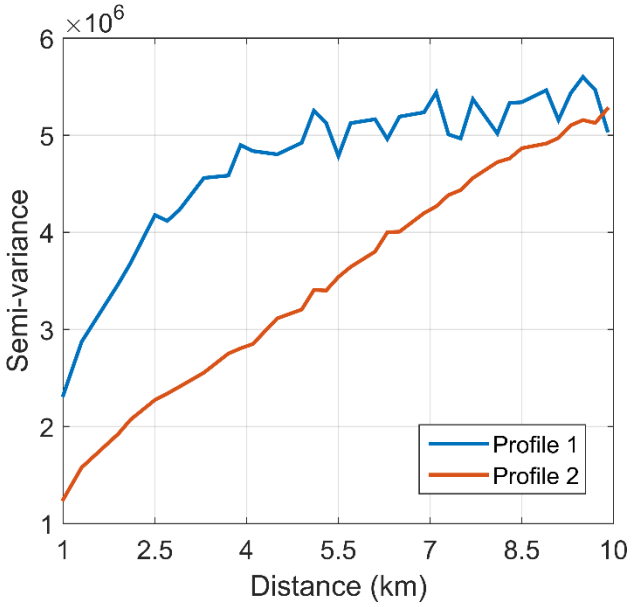

Figure 4-22. Semivariogram of EFvE2015 isoprene emission factors for the two profiles. Analysis shown is based on 900 meters resolution data.

4.4 Summary of Findings

- An updated 30-meter resolution PFT database (PFT16v2015) was developed for the continental US based on various ground survey, remote sensing and land surface model data products. The PFT16v2015 database provided the starting point for development of a high-resolution (30 m) emission factor (EF) database for the continental US. The resulting EFs were then compared with the PFT16v2011 EF database (Guenther et al., 2012). The EFs were then compared to EFs that were based on aircraft flux measurements.
- Compared with the EFv2011 data, the EFvE2015 data predicts higher isoprene emission factors in some regions in the southeastern US, with the biggest differences in north Florida, central Texas, Oklahoma and Arkansas. Higher broadleaf deciduous tree coverages are also predicted for these areas in the PFT16v2015 database. On the other hand, lower broadleaf deciduous tree coverages were predicted in PFT16v2015 database for southeast Missouri and northern Minnesota, which also has lower isoprene emission factors in the EFvE2015 database. The differences are mainly due to the incorporation of the LandFire existing vegetation type (EVT) data, which provides more spatial details than the land cover dataset used to develop the EFv2011 dataset.
- Aircraft observations were used to evaluate and constrain MEGAN emission factors. The wavelet based approach provides isoprene and monoterpene flux data at high spatial resolution. Surface fluxes of BVOCs were calculated using a vertical flux divergence correction method that assumes a linear relationship between fluxes at different altitudes.
- The estimation of EAF and airborne EF showed consistent results, and they suggest that the developed land cover EF (EFvE2015 database) reasonably captured the variations of BVOC emissions among different EVTs. We calculated mean airborne EF for isoprene using different approaches and their correlations with landcover EF (EFvE2015 database). The correlations between airborne EF calculated using different approaches and the landcover based EFvE2015 data range from 0.32 to 0.73.
- The airborne EFs calculated using WRF or using NLDAS meteorological data are considerably different. The WRF based EF values are consistently lower due to higher EAF values estimated by WRF. This is likely due to a high bias in solar radiation and temperature due to underestimates of aerosol and clouds. We have used the NLDAS data for our analysis because it includes assimilation of observed meteorology. However, the substantial differences (~37%) between the WRF and NLDAS results demonstrate the importance of having accurate meteorological observations to determine airborne EFs.

4.5 Recommendations

Despite the above mentioned uncertainties involved in this study, the aircraft measurement based EFvA2015 isoprene emission factor database is expected to be a significant improvement compared with the EFvE2011 isoprene database (Figure 4-14). It captures a large portion of isoprene emission variations among the heterogeneous southeastern US landscape, with R^2 up

to 0.73 as shown in Table 4-1, R^2 = 0.99 when excluding agriculture EVTs in Table 4-2, and R^2 = 0.76 in Figure 4-18 when using mixed layer flux data.

Therefore, we recommend using the updated LAIv2015, PFT16v2015 and EFvA2015 isoprene emission factor database for air quality modeling studies in the State of Texas. Due to data restrictions, we were not able to thoroughly evaluate the accuracy of EFvA2015 emission factor database for BVOC species other than isoprene. The case for using the aircraft based total monoterpene emission factor database is less certain and we recommend using the EFvE2015 emission factor database for BVOC species other than isoprene. It should also be noted that additional efforts are needed to further evaluate and refine the EFvA2015 database.

5.0 DEVELOPMENT OF MEGAN BIOGENIC EMISSION INVENTORIES AND INVENTORY EVALUATION USING REGIONAL PHOTOCHEMICAL MODELING

We performed photochemical modeling with default and updated MEGAN emission inventories and evaluated modeled concentrations against surface and aircraft measurements.

5.1 Modeling Strategy

We prepared model-ready MEGAN biogenic emissions based on the landcover and emission factor databases described in Sections 3 and 4 and evaluated the biogenic emission inventories using a photochemical grid model. Three biogenic emission inventories were developed for use in the photochemical modeling. The initial inventory was a base-case biogenic emission inventory, which was developed using the MEGAN v2.1 default landcover database and default emission factors (EFv2011). Then, a second biogenic emission inventory was derived from the updated high-resolution landcover database and Texas and Southeastern U.S. emission factor database EFv2015 described in Sections 3 and 4. Finally, a third biogenic emission inventory was derived from the updated high-resolution landcover database and the emission factor database EFv2015x. We compared the photochemical model concentrations for the simulations using default and updated biogenic emission inventories against observed concentrations from surface monitoring stations and the C-130 and P-3 aircraft. In Section 5, we describe the meteorological modeling that was used as an input to the MEGAN biogenic emissions modeling, the MEGAN emissions modeling, and the photochemical modeling and comparison with surface and aircraft measurements.

The Comprehensive Air quality Model with Extensions v6.1 (CAMx; ENVIRON, 2015) photochemical grid model was used to model fluxes and atmospheric concentrations of BVOCs and other relevant species. The modeling platform was adapted from a 2013 Texas ozone forecast modeling application developed by Ramboll Environ for the TCEQ (Johnson et al., 2013). The modeling domain consists of a 36 km continental-scale grid and a nested 12 km grid. The regional 12 km grid used in the forecasting project to cover Texas and surrounding states was expanded so that it encompassed nearly all of the overland flight tracks of the C-130 and P-3 made during June-July 2013 (Figure 5-1). The vertical structure of the CAMx model is shown in Figure 5-2. CAMx was run from June 1-July 15, 2013 to simulate the period when C-130 and P-3 aircraft data are available. A two-week spinup period leading up to June 1 was modeled to remove the influence of the model initial conditions. CAMx was run with Revision 2 of the CB6 chemical mechanism (CB6r2) (Yarwood et al., 2013).

The Weather Research and Forecasting (WRF) (Skamarock et al., 2008) meteorological model was used in hindcast mode to develop the meteorological fields required for input to the MEGAN biogenic emissions modeling as well as to the photochemical model. The WRF model configuration is shown in Table 5-1. The WRF domains are slightly larger than the CAMx domains (Figure 5-1) and the vertical structure of the WRF model is shown in Figure 5-2. The WRF model was run for the period April-October, 2013. The 12 km WRF modeling grid is shown in Figure 5-3. A 4 km grid focused on Houston (not shown) was present in this WRF run so it could also be used by AQRP Project 14-024. The 4 km grid was not used in Project 14-016.

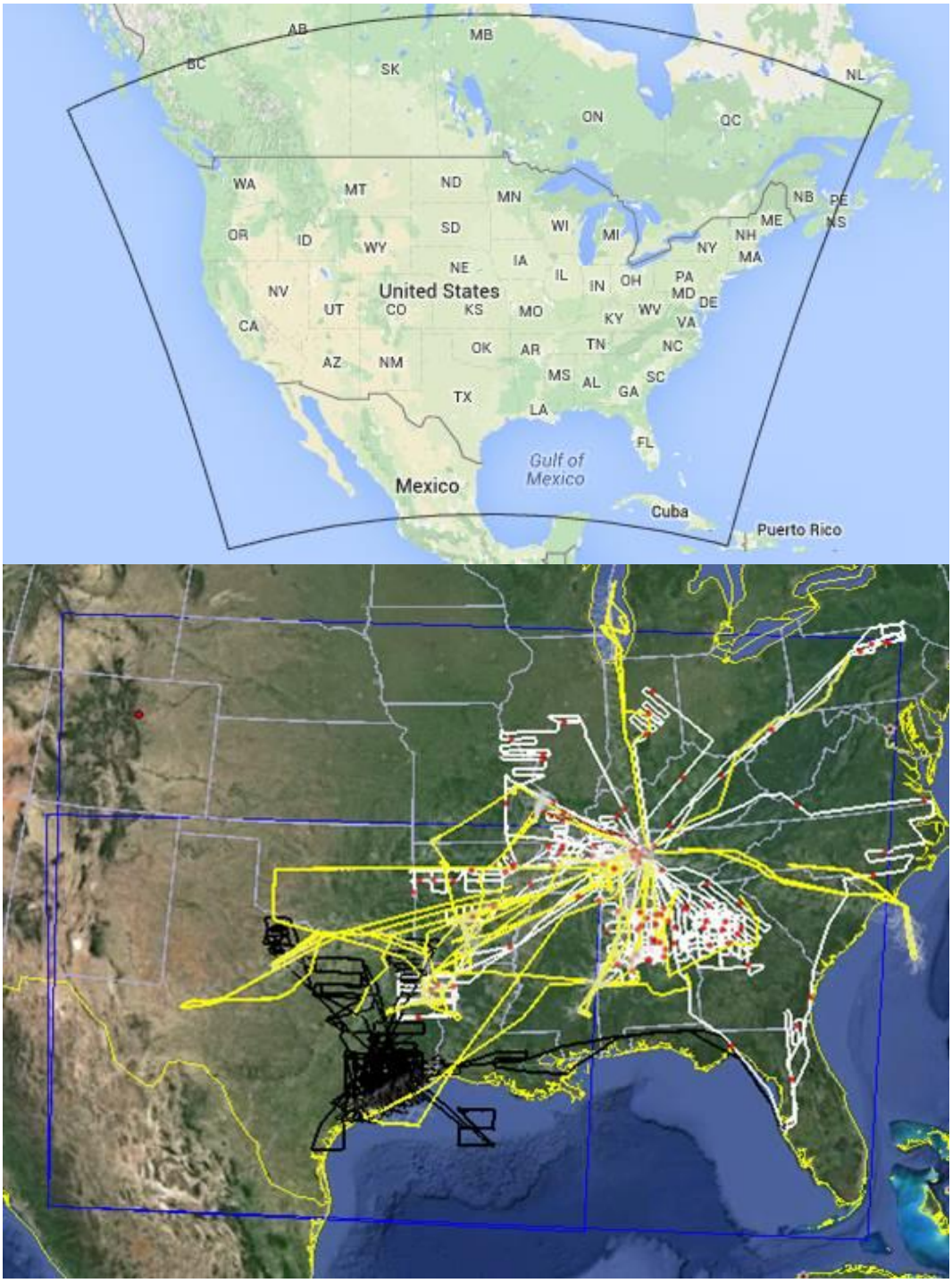

Figure 5-1. Upper panel: 36 km continental-scale modeling grid. Lower panel: 12 km CAMx modeling grid and aircraft flight paths. Aircraft flight paths: SAS C-130 (yellow), SAS P-3 (white), and TexAQS 2006 (black). TCEQ 12 km grid extent (smaller blue domain), and expanded 12 km grid (larger blue domain) used in this project.

Vertical Layer Structure

Corresponding WRF Layer	Layer Top (m AGL)	CAMx Layer	Layer Center (m AGL)	Thickness (m)
38	15179.1	28	13637.9	3082.5
36	12096.6	27	10631.6	2930.0
32	9166.6	26	8063.8	2205.7
29	6960.9	25	6398.4	1125.0
27	5835.9	24	5367.0	937.9
25	4898.0	23	4502.2	791.6
23	4106.4	22	3739.9	733.0
21	3373.5	21	3199.9	347.2
20	3026.3	20	2858.3	335.9
19	2690.4	19	2528.3	324.3
18	2366.1	18	2234.7	262.8
17	2103.3	17	1975.2	256.2
16	1847.2	16	1722.2	249.9
15	1597.3	15	1475.3	243.9
14	1353.4	14	1281.6	143.6
13	1209.8	13	1139.0	141.6
12	1068.2	12	998.3	139.7
11	928.5	11	859.5	137.8
10	790.6	10	745.2	90.9
9	699.7	9	654.7	90.1
8	609.7	8	565.0	89.3
7	520.3	7	476.1	88.5
6	431.8	6	387.9	87.8
5	344.0	5	300.5	87.1
4	256.9	4	213.8	86.3
3	170.6	3	127.8	85.6
2	85.0	2	59.4	51.0
1	33.9	1	17.0	33.9

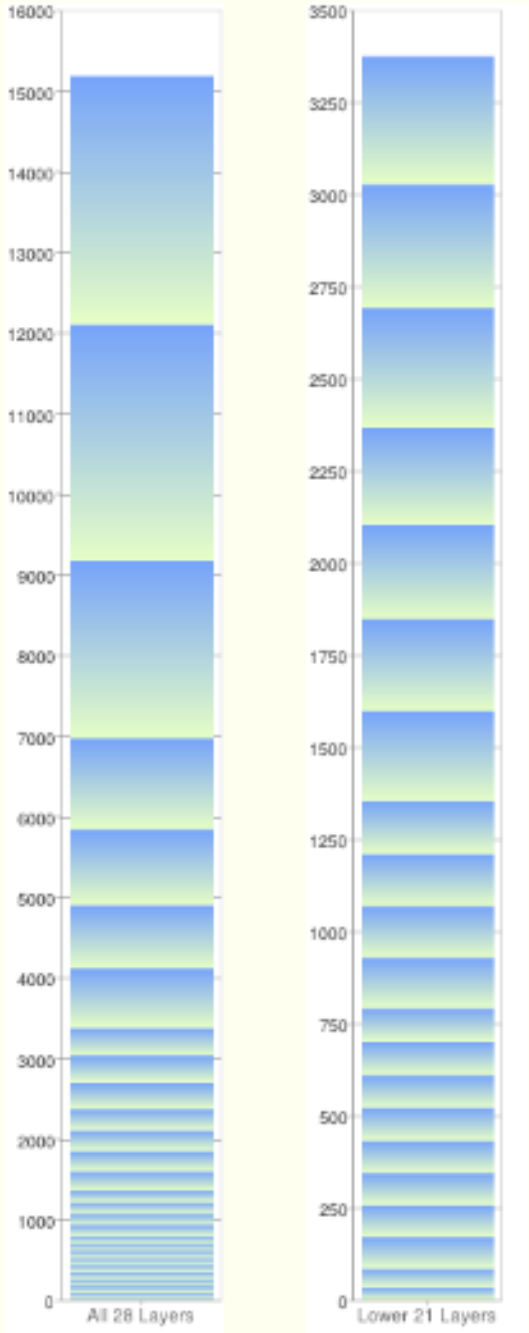

AGL - Above Ground Level.

Figure 5-2. WRF and CAMx layer structure. TCEQ figure from http://www.tceq.texas.gov/airquality/airmod/rider8/modeling/domain[1].

[1] http://www.tceq.texas.gov/airquality/airmod/data/domain

Table 5-1. WRF model configuration.

	AQRP Biogenics WRF Run Configuration
WRF version	3.6
Horizontal Resolution	36/12 km
Microphysics	WSM6
Longwave Radiation	RRTMG
Shortwave Radiation	RRTMG
Surface Layer Physics	MM5 similarity
LSM	Noah
PBL scheme	Yonsei University (YSU)
Cumulus parameterization	Kain-Fritsch
Boundary and Initial Conditions Data Source	12 km NAM analysis
Analysis Nudging Coefficients (s^{-1})	36/12 km grids
Winds	$3x10^{-4}$
Temperature	$3x10^{-4}$ (above BL only)
Mixing Ratio	$3x10^{-4}$ (above BL only)
Observation Nudging Coefficients (s^{-1})	36/12 km grids:
Winds	None
Temperature	None
Mixing Ratio	None
Miscellaneous Notes	Using KF-RRTMG interaction which feeds back subgrid cloud information to radiation scheme (36/12 km grids)

5.2 WRF Model Performance Evaluation

We evaluated the performance of the WRF model in reproducing observed weather at the surface and aloft. A graphical and statistical evaluation of model performance was carried out for winds, temperatures, humidity, the placement of frontal boundaries, and the intensity of precipitation, clouds and downward solar radiation at the Earth's surface. Output from the 12 km WRF modeling domain was compared against meteorological observations from the TCEQ's Continuous Air Monitoring Stations (CAMS), airport meteorological monitoring sites (ds472 data set), analyzed precipitation fields and satellite imagery.

In the initial WRF run completed in October 2014, the precipitation evaluation showed the presence of an artifact in the region around the 4 km grid focused on Houston. The precipitation artifact was caused by the use of the WRF 2-way nesting option on the 4 km grid. WRF was run a second time without the nested 4 km grid, and the model performance evaluation was completed as described in Section 5.3. No precipitation artifact was present in the second and final WRF run.

5.3 WRF Model Performance Evaluation Results

5.3.1 Surface Layer Wind, Temperature and Humidity

We evaluated WRF 12 km grid surface layer output fields for the period June 1-July 15, 2013 against TCEQ's Continuous Air Monitoring Stations (CAMS) stations within Texas and ds472 airport data[2] for wind, temperature and humidity data outside of Texas. WRF surface performance was assessed using the METSTAT program to generate statistics and hourly graphical model-observation comparisons for winds, temperature and humidity. We calculated bias, error and root mean square error (RMSE) statistics for wind speed, direction, temperature, and humidity. The definitions of these statistical metrics are shown in Table 5-2. Each metric was compared to performance benchmarks to evaluate how well the model performed.

Table 5-2. Statistical metrics used in WRF surface performance evaluation.

Metric	Definition[1]
Mean Bias (MB)	$\frac{1}{N}\sum_{i=1}^{N}(P_i - O_i)$
Mean Error (ME)	$\frac{1}{N}\sum_{i=1}^{N}\lvert P_i - O_i\rvert$
Normalized Mean Bias (NMB) (-100% to +∞)	$\frac{\sum_{i=1}^{N}(P_i - O_i)}{\sum_{i=1}^{N} O_i}$
Root Mean Squared Error (RMSE)	$\sqrt{\frac{\sum_{i=1}^{N}(P_i - O_i)^2}{N}}$

[1] Pi and Oi are the predicted and observed values (Oi,Pi) at the i^{th} site paired in space and time and N is the number of observed/modeled data pairs.

Emery et al. (2001) derived a set of daily performance benchmarks for typical meteorological model performance. These standards were based upon the evaluation of about 30 meteorological simulations (using a variety of regional meteorological models) since 1993 in support of air quality applications as reported by Tesche et al. (2001) and other studies. The purpose of these benchmarks was not to give a passing or failing grade to any one particular meteorological model application, but rather to put its results into the proper context of other models and meteorological data sets. Since 2001, the benchmarks have been promoted by the EPA-sponsored National Ad Hoc Meteorological Modeling Group and have been consistently relied upon to evaluate Pennsylvania State University / National Center for Atmospheric Research (MM5) and WRF model performance in many regulatory modeling projects throughout Texas and the U.S. As part of the Western Regional Air Partnership (WRAP) meteorological modeling of the western United States, including complex conditions in the Rocky Mountain Region and in Alaska, Kemball-Cook et al., (2005) proposed model performance benchmarks for complex conditions. McNally (2009) performed a reassessment of these benchmarks using WRF runs, and suggested a revision to the humidity benchmark. The determination to use simple or complex benchmarks in this evaluation was made on a regional

[2] http://rda.ucar.edu/datasets/ds472.0/

basis depending on the presence of significant terrain or local circulations (e.g. coastal sea breeze).

The benchmarks for each variable are shown in Table 5-2 If model performance falls outside one or more of these ranges, the meteorological data fields for a particular parameter are not necessarily unacceptable; however, such a result indicates that caution should be exercised in the use of such variables, and in interpreting subsequent air quality modeling based on those meteorological fields. If wind, temperature and humidity bias and error statistics are reasonably near their respective benchmarks, WRF model performance is considered acceptable.

Table 5-3. WRF performance benchmarks.

Parameter	Emery et al. (2001)	Kemball-Cook et al. (2005)	McNally (2009)
Conditions	Simple	Complex	Complex
Temperature Bias	≤ ±0.5 K	≤ ±2.0 K	≤ ±1.0 K
Temperature Error	≤ 2.0 K	≤ 3.5 K	≤ 3.0 K
Humidity Bias	≤ ±1.0 g/kg	≤ ±0.8 g/kg	≤ ±1.0 g/kg
Humidity Error	≤ 2.0 g/kg	≤ 2.0 g/kg	≤ 2.0 g/kg
Wind Speed Bias	≤ ±0.5 m/s	≤ ±1.5 m/s	(not addressed)
Wind Speed RMSE	≤ 2.0 m/s	≤ 2.5 m/s	(not addressed)
Wind Dir. Bias	≤ ±10 degrees	(not addressed)	(not addressed)
Wind Dir. Error	≤ 30 degrees	≤ 55 degrees	(not addressed)

In this near-surface model performance evaluation, we focused on wind, temperature, and humidity. In order to summarize model performance, we show soccer plots on which are displayed average performance statistics for a region over the entire modeling episode. Soccer plots are shown for wind speed bias versus wind speed RMSE, wind direction bias versus wind direction error, temperature bias versus temperature error, and humidity bias versus humidity error. The closer a data point is to the origin, the better the model's performance. Perfect model performance is indicated by a data point at (0,0). In each soccer plot, dashed lines indicate the performance benchmarks from Table 5-3. A data point that falls inside the box formed by the performance benchmarks (the "soccer goal") represents a model run that meets the benchmark. Meteorological stations are shown in Figure 5-3. Because it is not practical to present an evaluation for each site, we average model performance over the 8 geographical subdomains shown in the figure. The monthly average of the metric is compared to the performance benchmarks. Because temporal averaging can mask problems with model performance, we also present the daily average value for each metric.

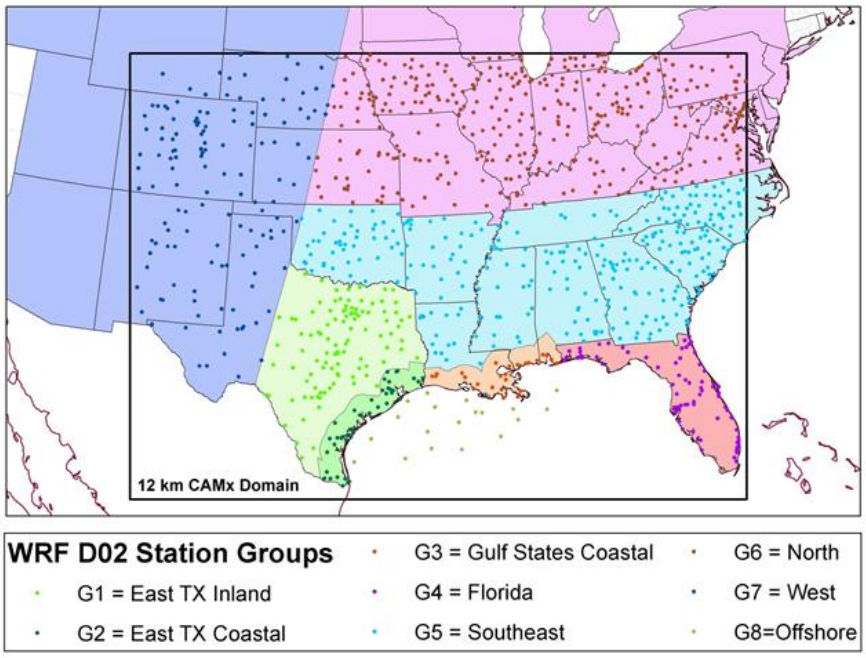

Figure 5-3. WRF surface model performance evaluation subdomains and location of ds472 airport meteorological monitoring sites.

Figure 5-4 and Figure 5-5 show soccer plots for wind speed bias and RMSE. The daily values show considerable variation about the monthly averages, but the monthly average values are within the complex benchmarks for all subdomains except west and offshore. The model has a general tendency to be biased high for wind speed, and larger values of the bias occur in subdomains near the Atlantic and Gulf Coasts. For wind direction (Figure 5-6 and Figure 5-7), most of the monthly averages fall within the complex terrain benchmark, with some of the largest values of wind direction bias occurring in East Texas at both coastal and inland sites. For temperature (Figure 5-8 and Figure 5-9), all monthly averages fall within the complex benchmarks. The model does not show a consistent pattern of warm or cold bias across subdomains. For humidity (Figure 5-10 and Figure 5-11), most subdomains fall within the complex benchmarks, with several exceptions. The offshore subdomain has an extremely strong wet bias, with all months falling outside the complex bias benchmark. The Gulf States and East Texas coastal subdomains also show a wet bias, but have more variability than the offshore subdomain, with some days showing a dry bias.

Overall, the WRF model's surface performance is neither exceptionally good nor exceptionally poor for this application, but generally falls within the complex benchmarks. Given the model's 12 km resolution, it is not surprising that the model performance lies outside the simple benchmarks for coastal and offshore regions. These regions are influenced by weather phenomena (e.g. sea breeze) that may not be well-resolved on a 12 km grid.

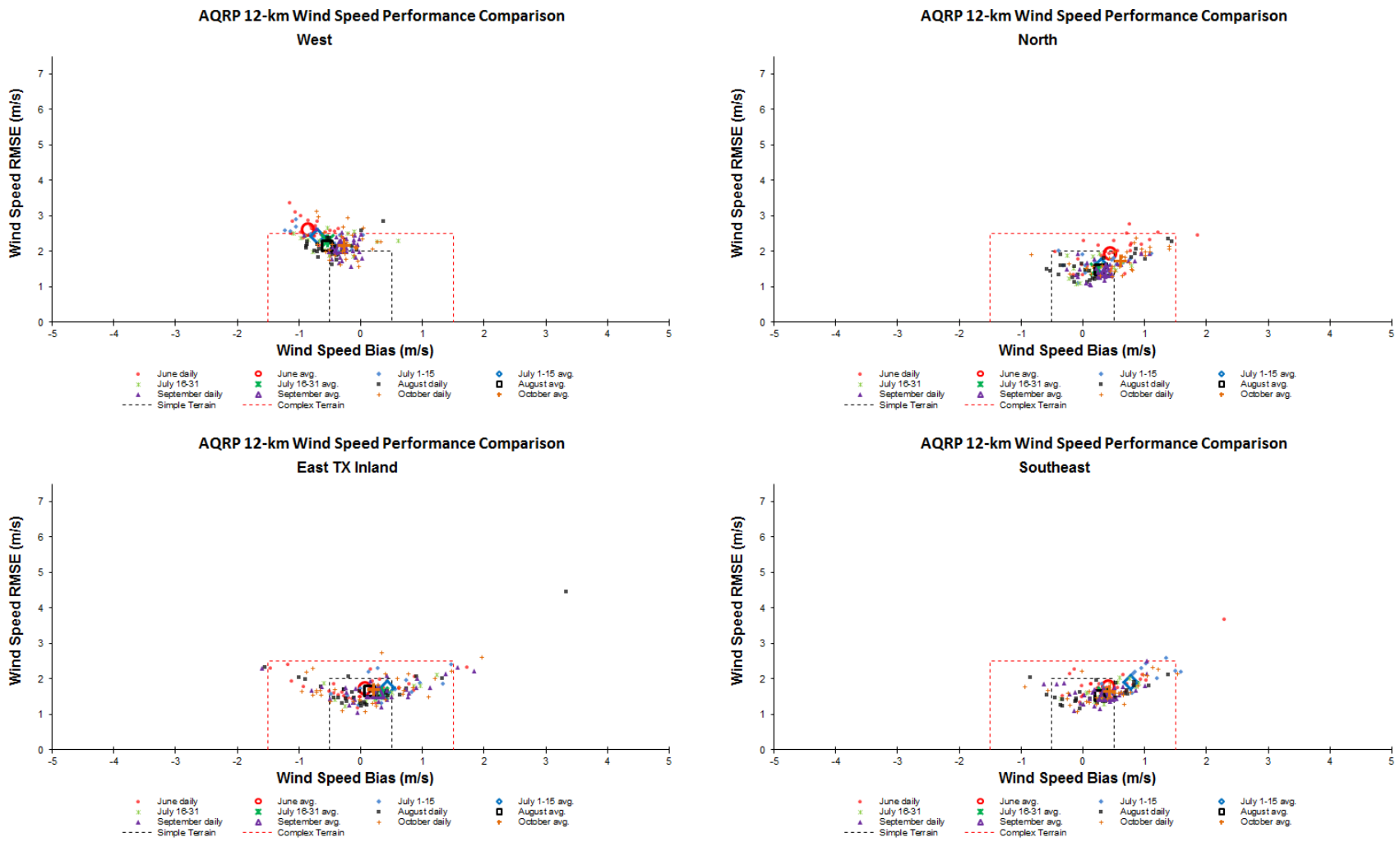

Figure 5-4. Wind speed bias and RMSE soccer plots, part 1.

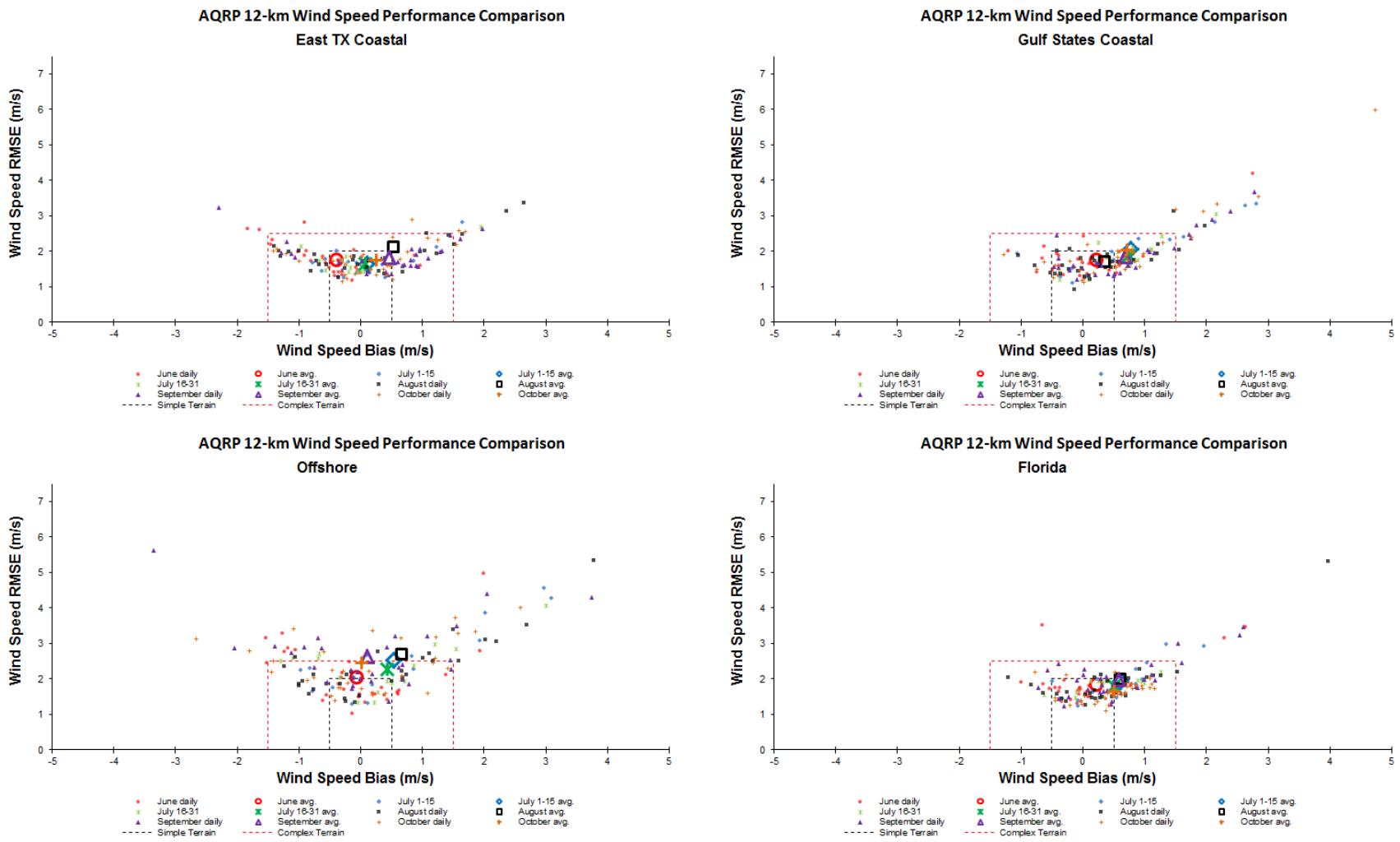

Figure 5-5. Wind speed bias and RMSE soccer plots, part 2.

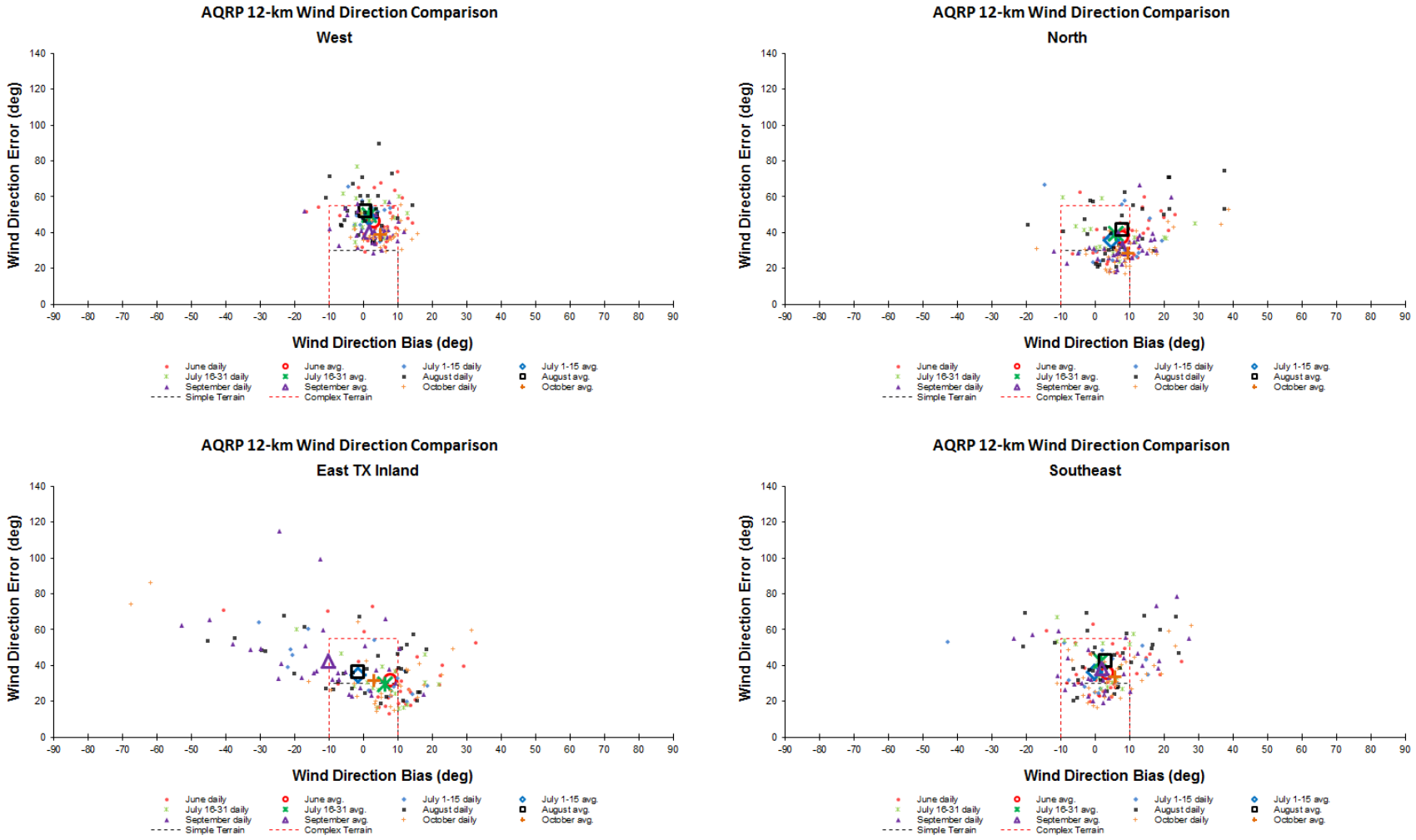

Figure 5-6. Wind direction bias and error soccer plots, part 1.

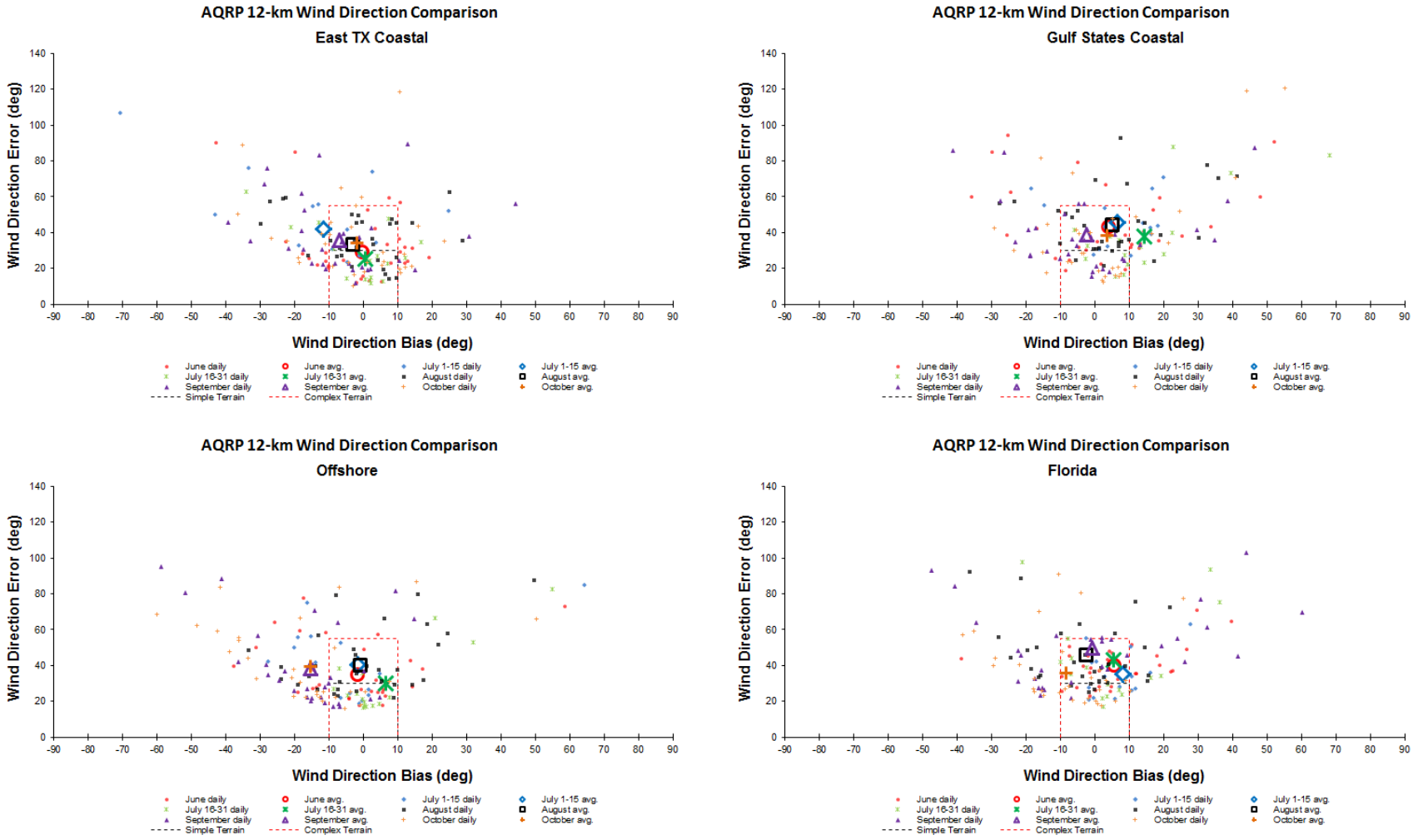

Figure 5-7. Wind direction bias and error soccer plots, part 2.

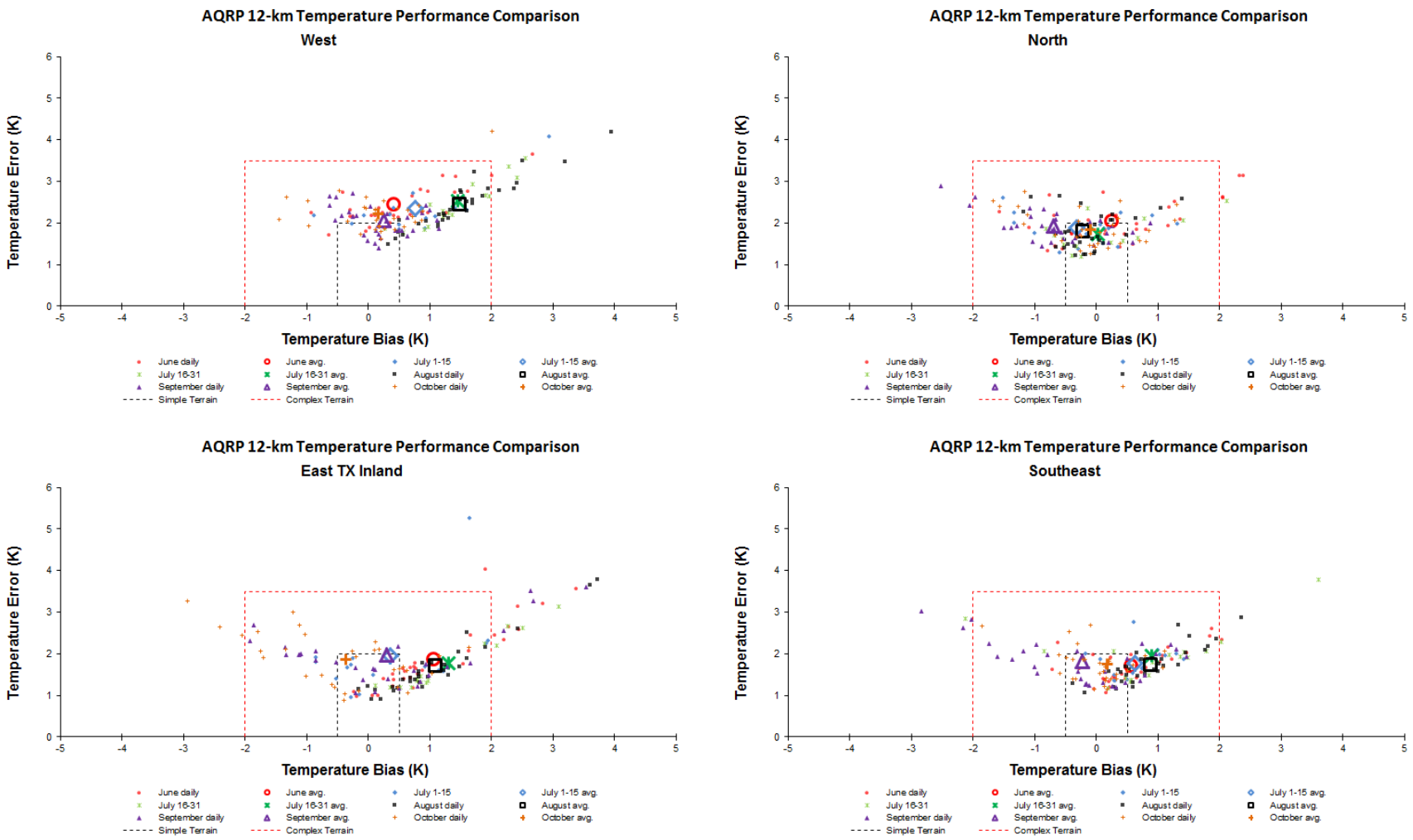

Figure 5-8. Temperature bias and error soccer plots, part 1.

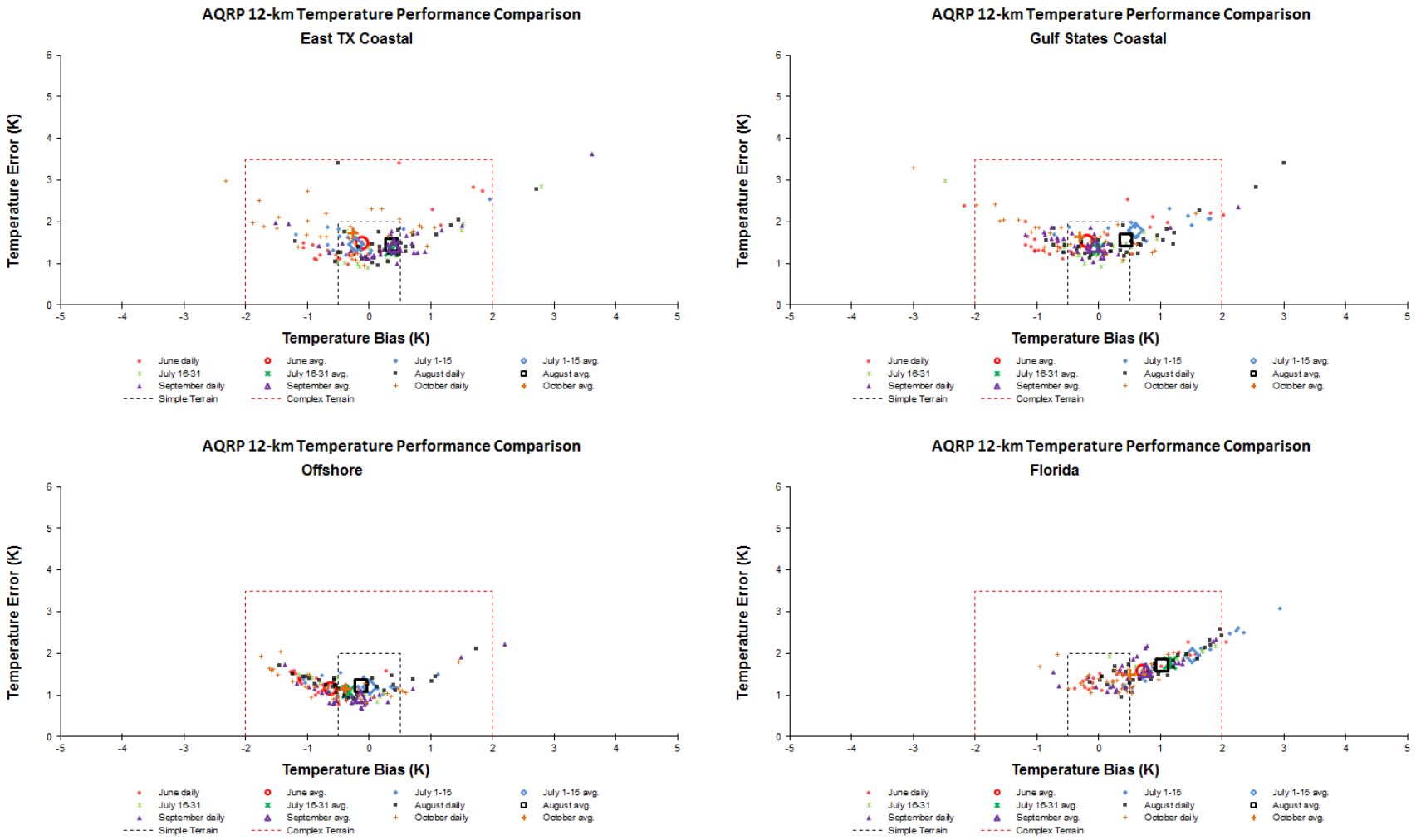

Figure 5-9. Temperature bias and error soccer plots, part 2.

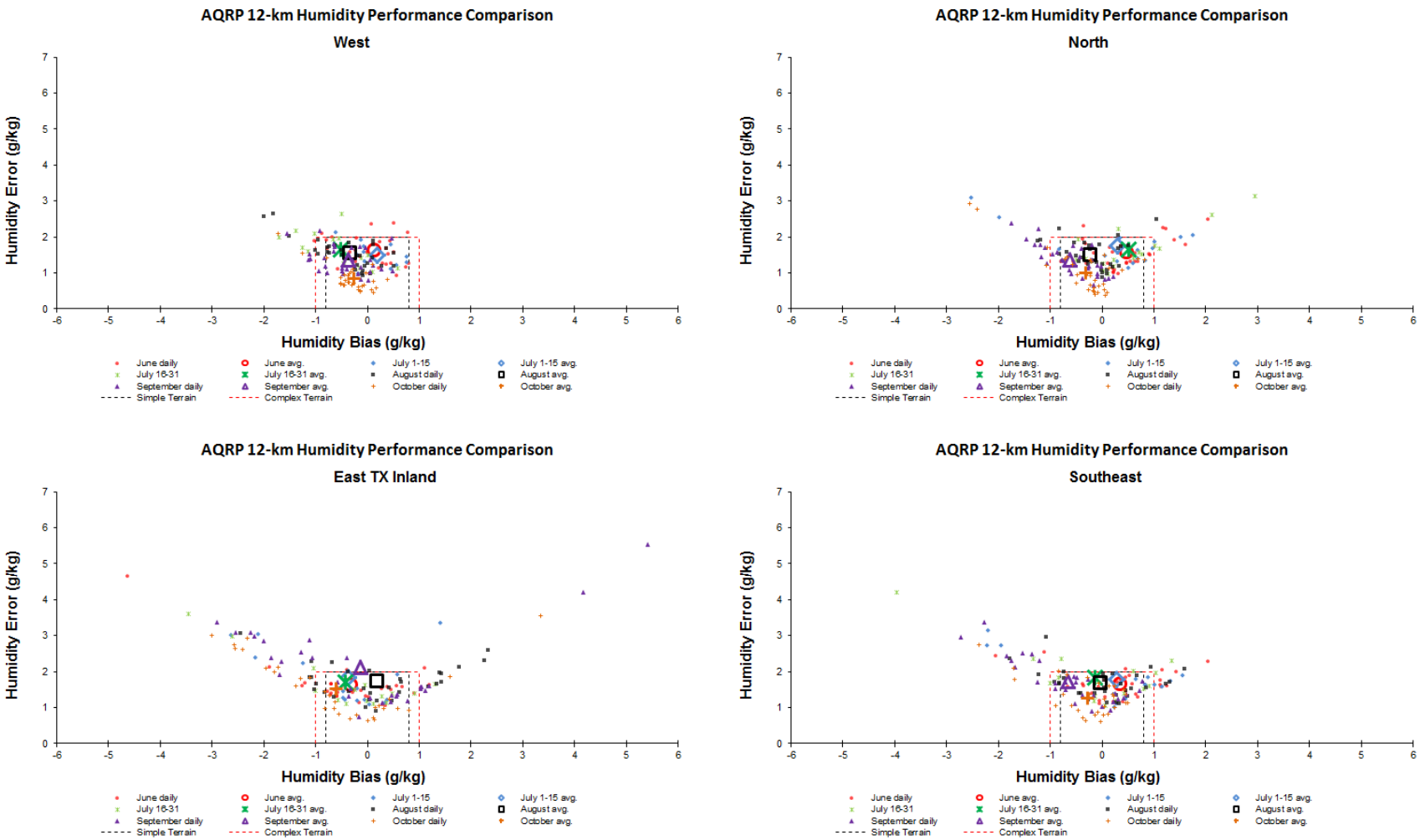

Figure 5-10. Humidity bias and error soccer plots, part 1.

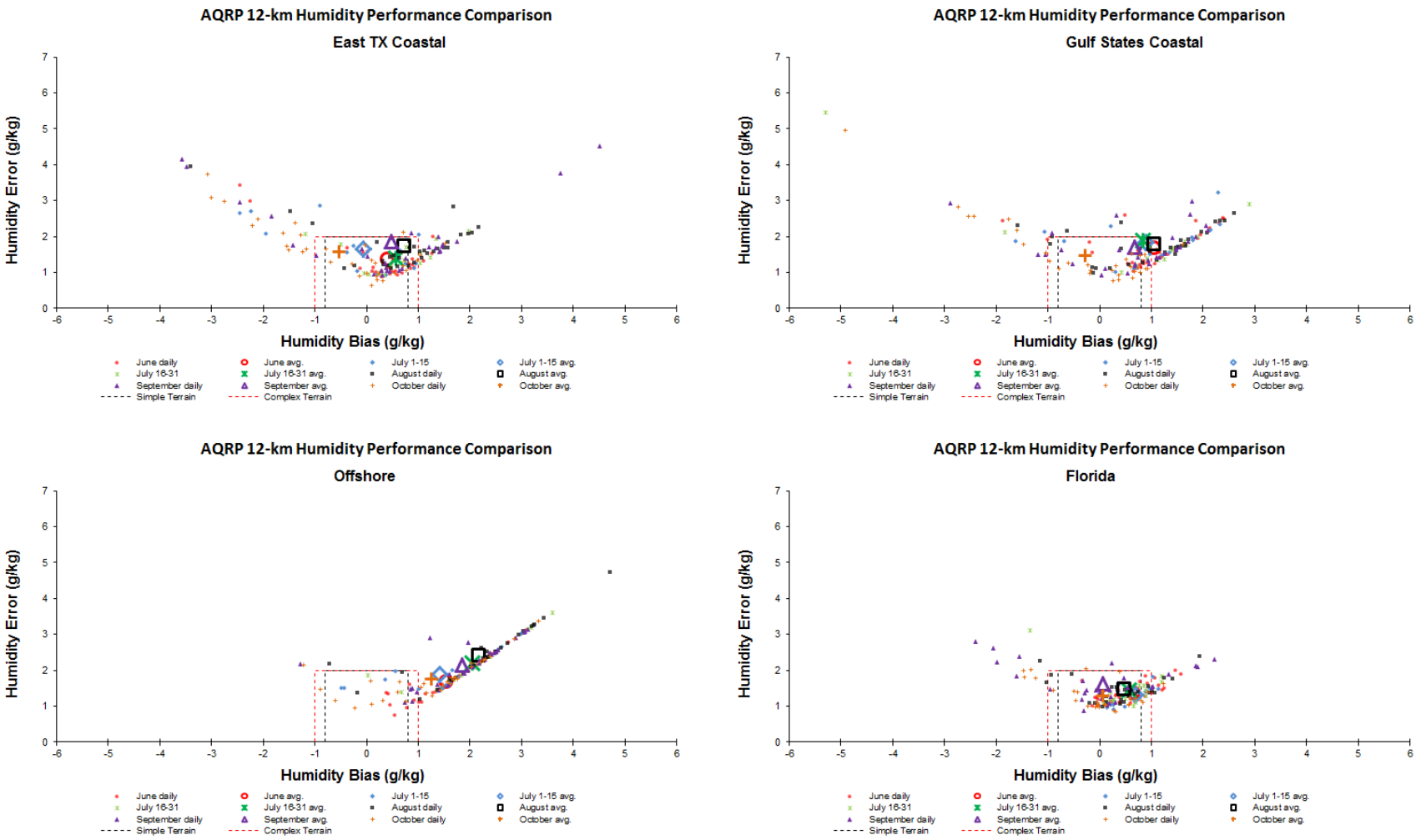

Figure 5-11. Humidity bias and error soccer plots, part 2.

5.3.2 Precipitation

The WRF 12 km grid daily precipitation totals were evaluated by comparing them with daily PRISM (Parameter-elevation Relationships on Independent Slopes Model) precipitation analysis fields. The PRISM analysis fields are based on precipitation observations from US monitoring sites and cover the continental United States and do not extend into Canada or over the ocean. The WRF precipitation fields, on the other hand, cover the entire domain, but we show WRF precipitation over land only for this comparison. Because precipitation monitoring sites tend to be located at lower elevations (e.g., airports); the PRISM observation fields may not fully capture the enhanced precipitation at high elevations due to orographic effects that could be present in the WRF simulations. Therefore, PRISM includes an elevation effect to account for orographic effects that increase precipitation over high terrain. In this section, we show precipitation results for two days to illustrate general features of WRF precipitation performance. Daily precipitation plots for the entire June 1-July 15, 2013 modeling episode are shown in Appendix A.

The WRF model shows good skill in reproducing the large-scale patterns of precipitation, which indicates that the model is successfully reproducing the development and evolution of synoptic-scale weather features. Figure 5-12 shows PRISM and WRF modeled daily precipitation totals for June 15.

PRISM Precipitation Analysis **WRF Precipitation**

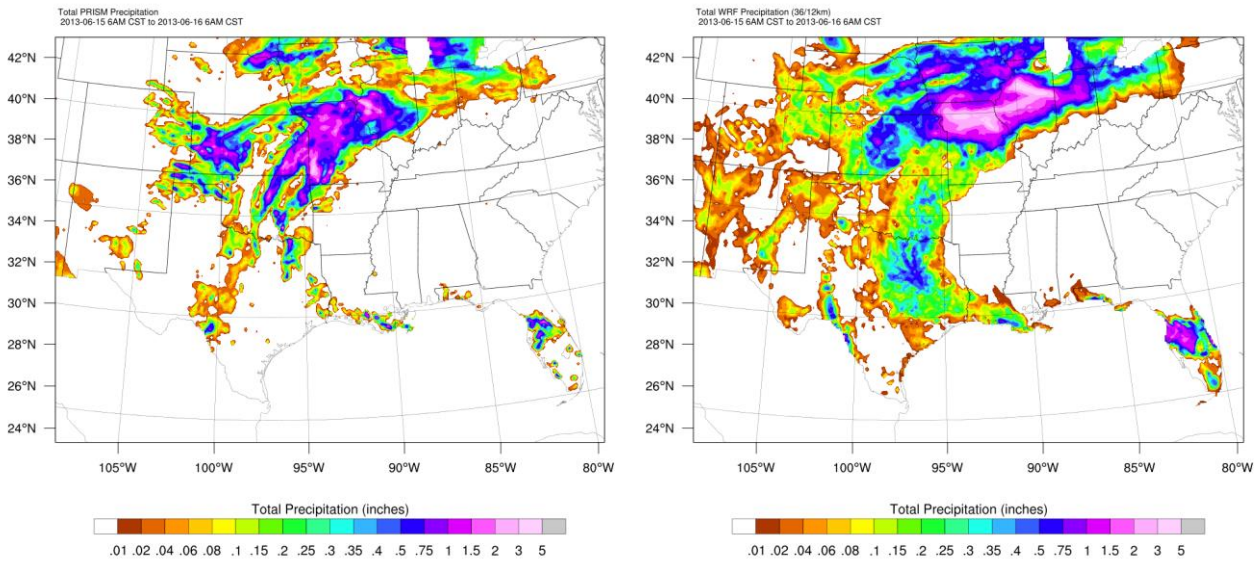

Figure 5-12. Comparison of PRISM and WRF daily total precipitation for June 15, 2013.

The model reproduces the overall pattern of precipitation, which indicates that WRF has successfully reproduced the location of the stationary fronts that stretched across the central US on this day as well as the presence of convective precipitation over Florida. The model overestimates the precipitation maximum over Missouri and Illinois and displaces it to the

north relative to the analysis. WRF also overestimates the intensity of convective precipitation over Florida as well as the spatial coverage of precipitation over New Mexico and Colorado.

In general, WRF overestimates convective precipitation, and this is more pronounced in July than in June. Figure 5-13 shows the precipitation pattern for July 5. WRF is similar to PRISM in that it reproduces areas of heavy precipitation over the eastern US and lighter precipitation over the west, with a dry region over Texas. However, WRF overestimates both the spatial coverage and intensity of convective precipitation across the Midwest and New Mexico and Colorado. Overestimates of summer convective precipitation are typical for WRF simulations and are a result of the difficulty in treating sub-grid scale convection and feedbacks between clouds and radiation for both resolved and sub-grid scale clouds. The model's lack of skill in reproducing convective precipitation patterns is indicative of the difficulty in accurately reproducing cloud fields and therefore surface shortwave radiation; this directly affects the accuracy of biogenic emissions. Next, we focus on WRF's simulation of clouds.

PRISM Precipitation Analysis **WRF Precipitation**

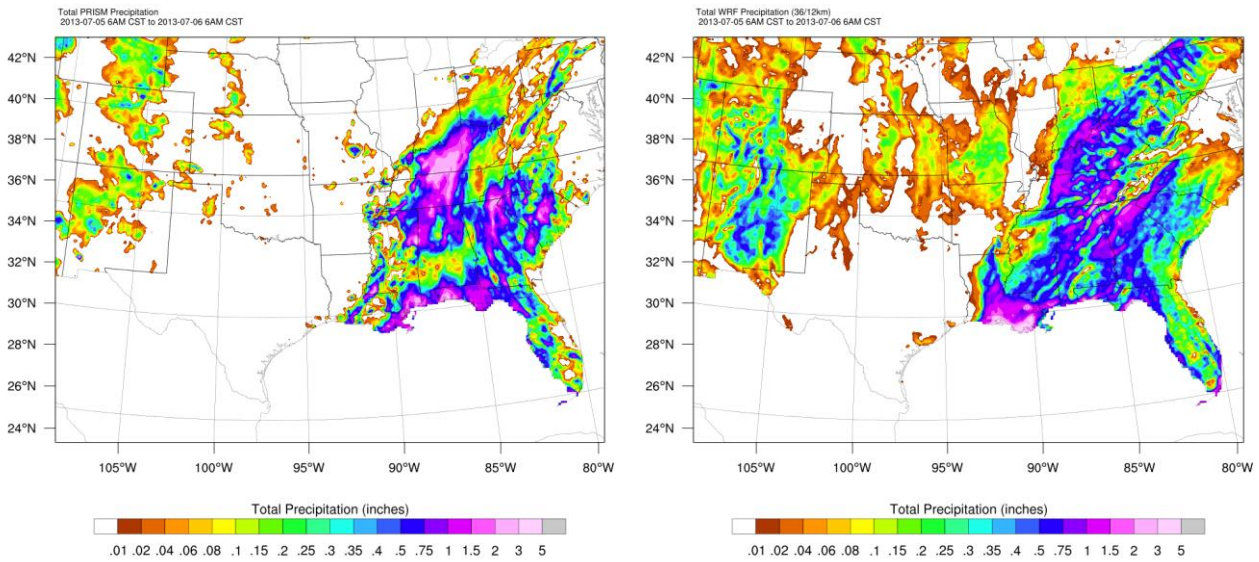

Figure 5-13. Comparison of PRISM and WRF daily total precipitation for July 5, 2013.

5.3.3 Evaluation of WRF Modeled Clouds and Downward Shortwave Radiation

To compare modeled and observed cloudiness, WRF downward shortwave radiation (DSW) at the surface was compared with the GOES 13 4 km Ch1 VIS fields from the SAS data catalog[3]. The colors in the WRF DSW plots are scaled so that areas where skies are clear (high DSW values) are dark and areas where clouds are present (low DSW) are gray. This convention was chosen so that cloudy areas show up as gray in both the satellite and the WRF panels. Hours selected for this comparison were those when the C-130 aircraft was flying racetrack patterns

[3] http://catalog.eol.ucar.edu/maps/sas

used in the emissions flux calculations. We present a single illustrative comparison below and the remaining satellite/WRF cloudiness comparisons are shown in Appendix B.

Figure 5-14 shows a comparison of the GOES visible image and the WRF DSW for July 5 at 20 UTC. The C-130 flight track is shown as a yellow line with wind barbs in the left panel. On July 5, daily maximum 8-hour average ozone values higher than 75 ppb were recorded at TCEQ CAMS monitors in the Dallas-Fort Worth, Houston-Galveston-Brazoria, and San Antonio-Austin areas in East Texas. On July 5, skies were generally partly sunny over East Texas with some widely scattered showers (Figure 5-13). The visible satellite image in Figure 5-14 shows fair weather cumulus clouds across East Texas, while the WRF model shows clear skies. This indicates that WRF is overestimating the shortwave radiation reaching the surface and would therefore overestimate PAR within the MCIP calculation that is used to provide input data for MEGAN. This WRF underestimate of observed fair weather cumulus occurred on many days during the episode in locations across the 12 km modeling domain.

GOES Satellite Visible Image **WRF DSW**

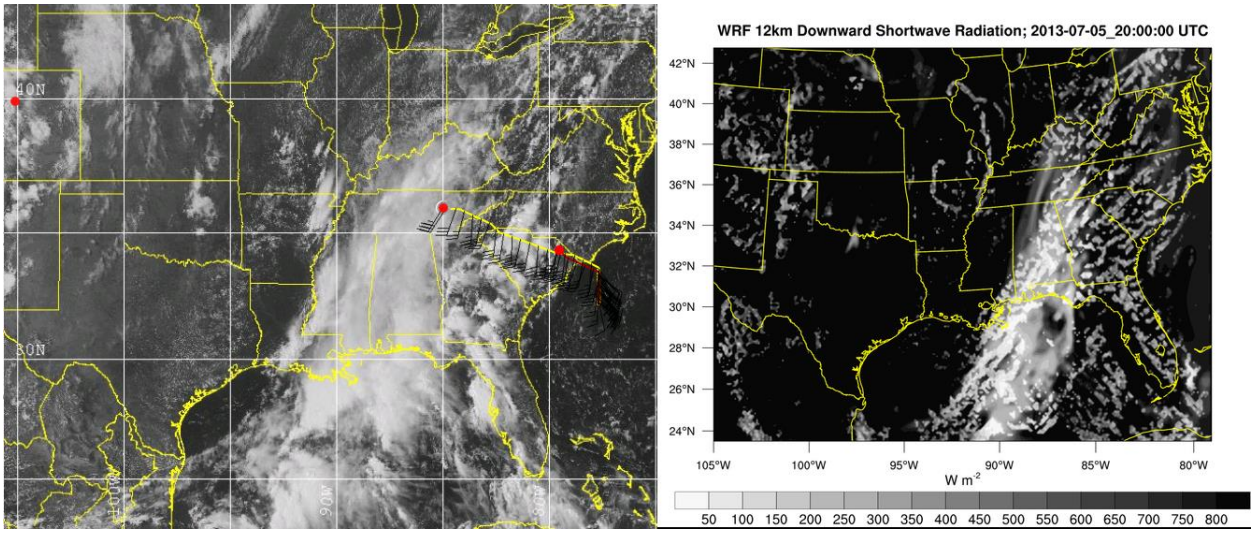

Figure 5-14. GOES visible satellite image showing C-130 flight track (left panel) and WRF DSW (right panel) for July 5, 2013, 20 UTC.

On July 5, WRF simulates the region of enhanced cloudiness extended from Louisiana northeastward to Pennsylvania, and simulated cirrus outflow from convective cells across the southeast. However, the cloud field is more concentrated into smaller, more optically thick clouds rather than the thinner, more widespread clouds that appear in the satellite image (Figure 5-14). This is related to WRF's simulation of convection, which tends to remove atmospheric instability through more intense and more widely spaced convective cells than appear in the observations, which show more numerous smaller convective cells.

Figure 5-15 through Figure 5-18 compare observed and modeled DSW at the surface for

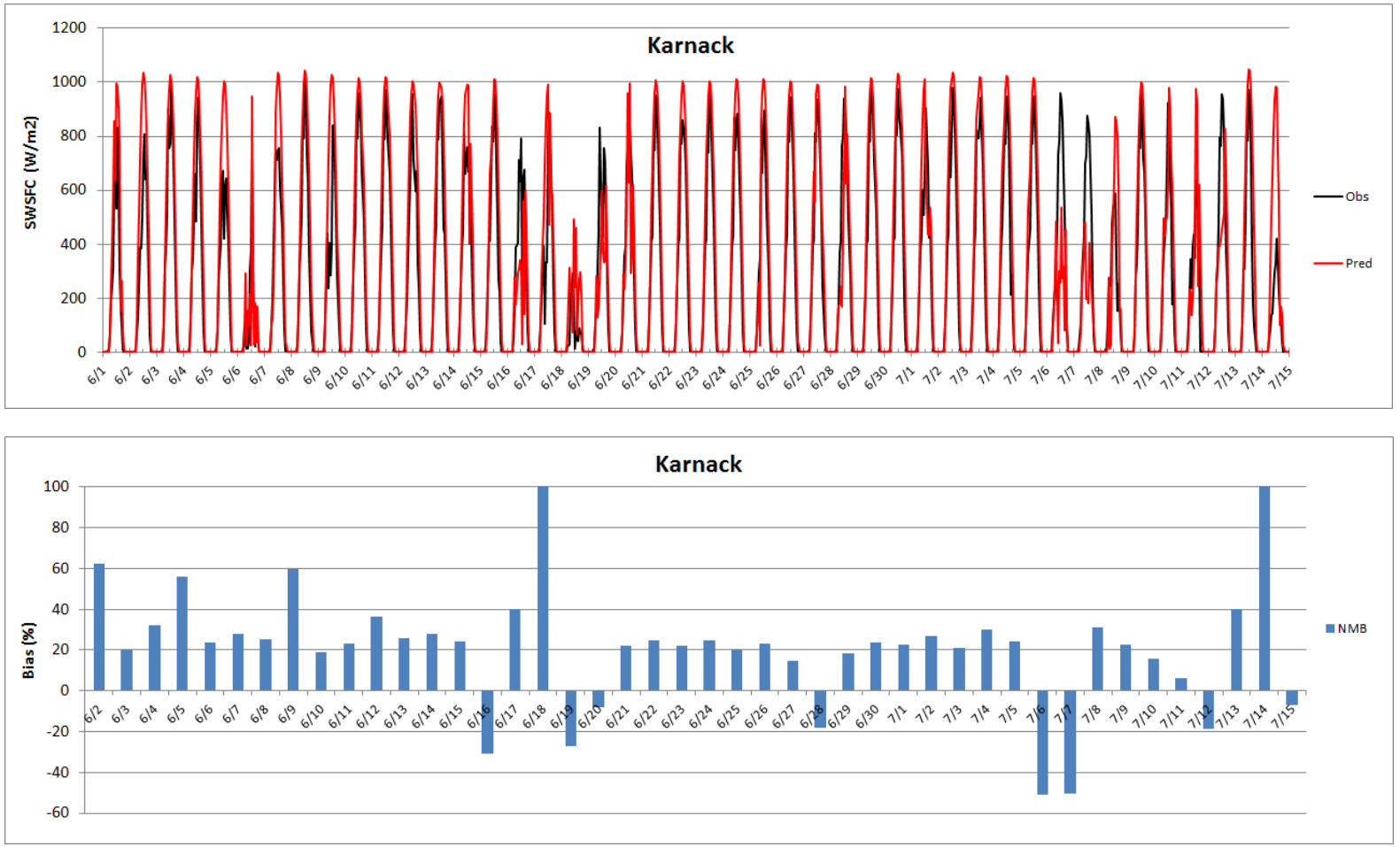

Figure 5-15. Upper panel: observed (obs) and WRF-predicted (pred) downward shortwave radiation (W m^{-2}) at the surface for the TCEQ Continuous Air Monitoring Station (CAMS) 85 site at Karnack in Northeast Texas. Lower panel: daily normalized mean bias (NMB) for downward shortwave radiation.

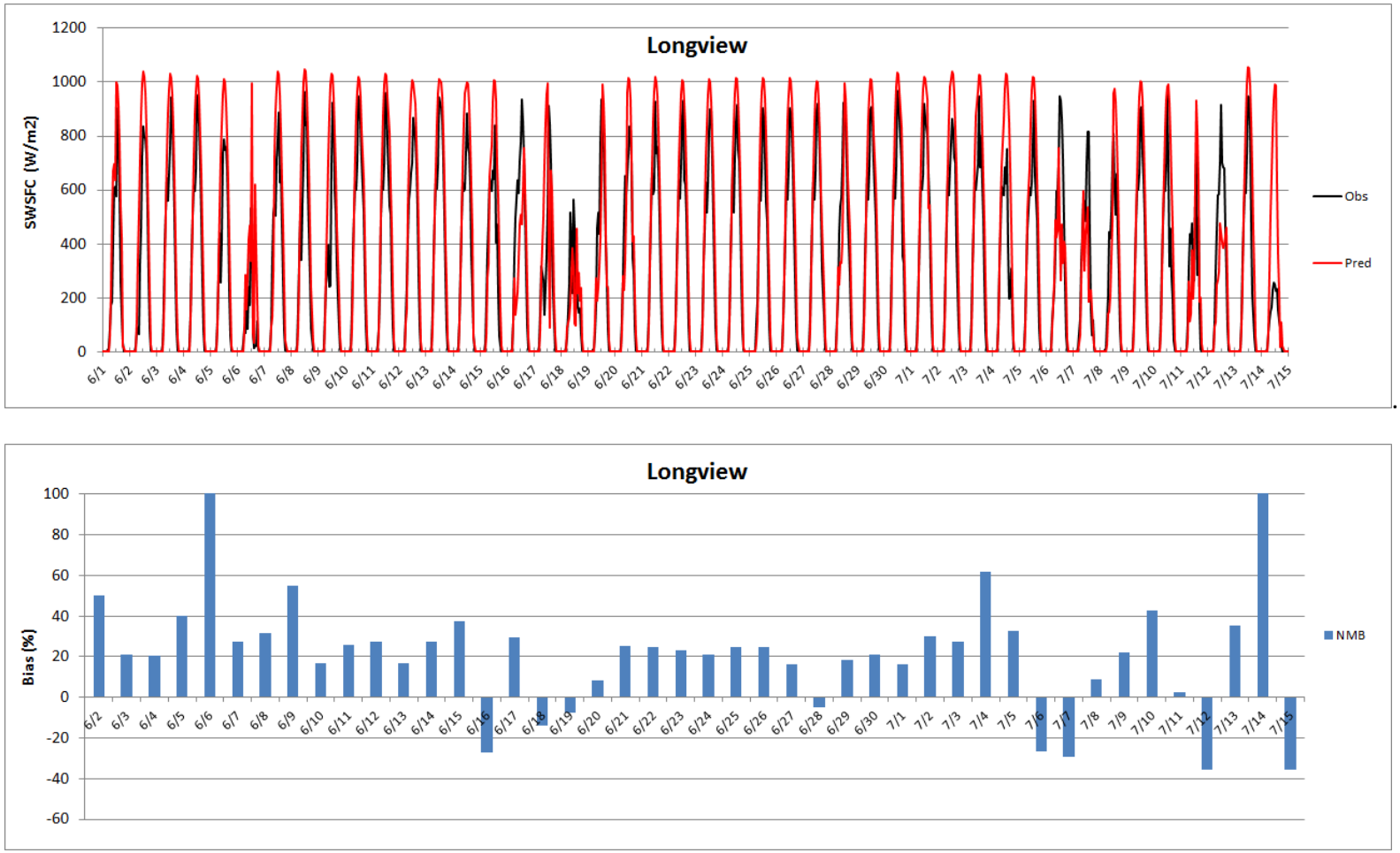

Figure 5-16. Upper panel: observed (obs) and WRF-predicted (pred) downward shortwave radiation (W m^{-2}) at the surface for the TCEQ Continuous Air Monitoring Station (CAMS) 19 site at Longview in Northeast Texas. Lower panel: daily normalized mean bias (NMB) for downward shortwave radiation.

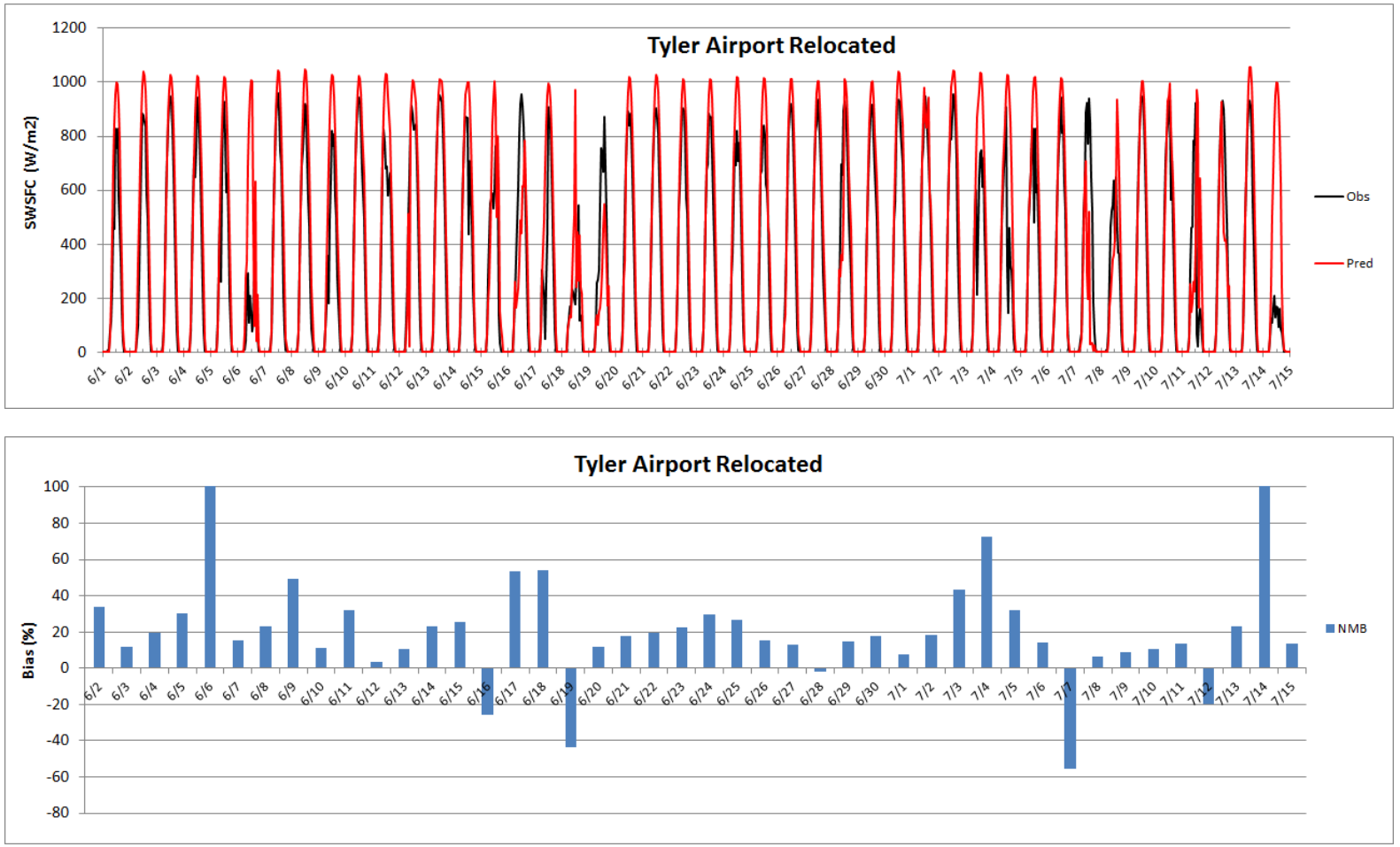

Figure 5-17. Upper panel: observed (obs) and WRF-predicted (pred) downward shortwave radiation (W m^{-2}) at the surface for the TCEQ Continuous Air Monitoring Station (CAMS) 82 site at Tyler in Northeast Texas. Lower panel: daily normalized mean bias (NMB) for downward shortwave radiation.

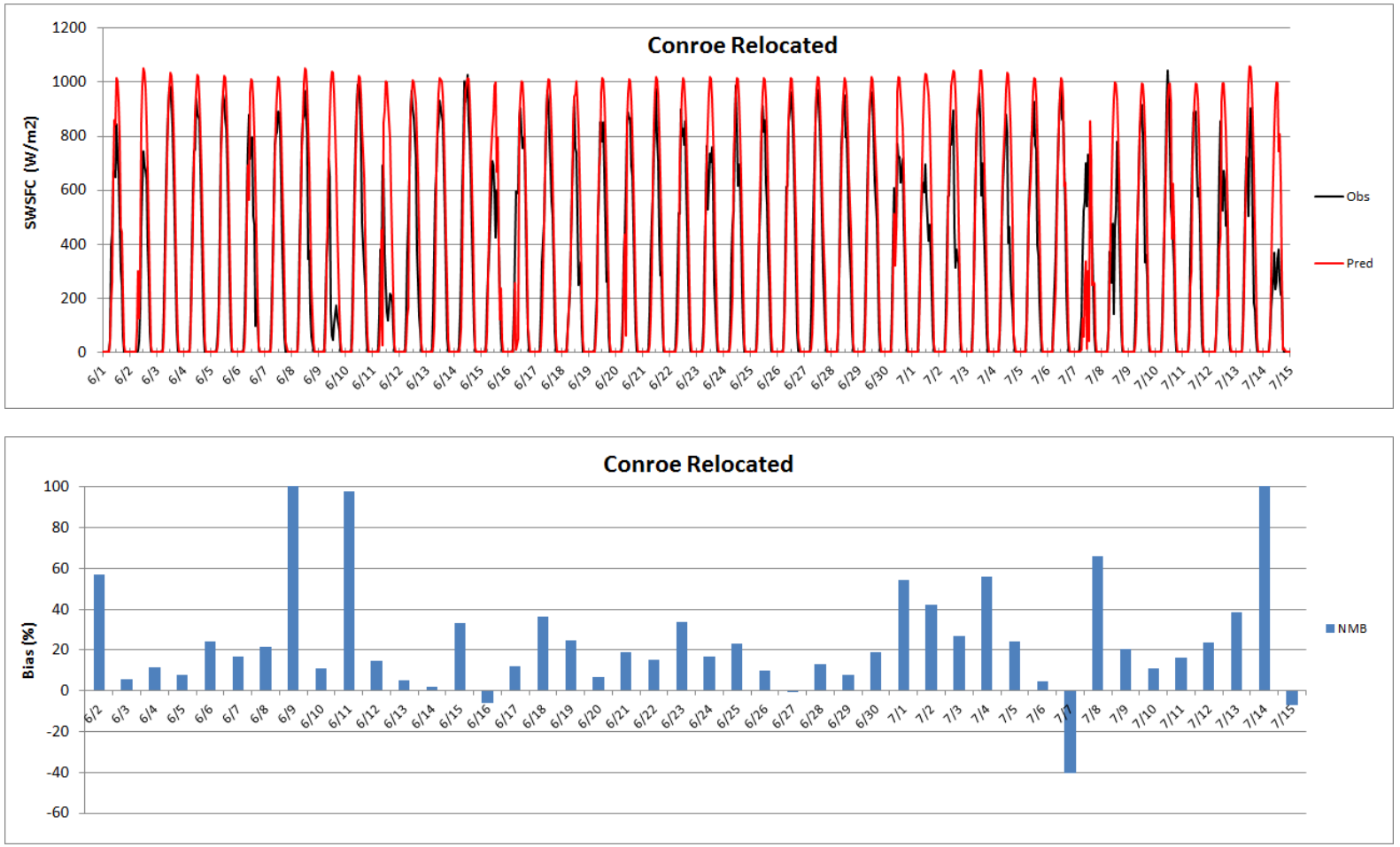

Figure 5-18. Upper panel: observed (obs) and WRF-predicted (pred) downward shortwave radiation (W m^{-2}) at the surface for the TCEQ Continuous Air Monitoring Station (CAMS) 78 site at Conroe in Houston. Lower panel: daily normalized mean bias (NMB) for downward shortwave radiation.

the TCEQ CAMS monitoring sites shown in Figure 4-19. At all four sites, WRF frequently overestimates the downwelling solar radiation at the surface. The normalized mean bias is positive on a majority of days at all four sites. All CAMS sites in Texas that monitor solar radiation were evaluated in this way with similar results (not shown).

5.3.4 Summary of WRF Model Performance

The WRF model performance in simulating surface meteorology, large scale synoptic features, precipitation and clouds is typical of summer US WRF applications at 12 km resolution. Wind, temperature and humidity performance was generally within benchmarks except at sites located offshore or along the coast. These areas may be influenced by sea breeze circulations that are not well-resolved at 12 km model resolution.

The most important finding of the WRF model performance evaluation from the point of the MEGAN emissions modeling is the overestimate of DSW at the surface. This will likely produce a high bias in PAR used as input to MEGAN and can impart a high bias to the modeled terpenoid emission estimates. The MEGAN emissions and the CAMx photochemical modeling that relies upon it should be viewed with this WRF model bias in mind.

5.4 MEGAN Emissions Modeling

5.4.1 MEGAN Modeling Configuration and Inputs

Once model performance had been evaluated, the WRF model output data was used in the development of biogenic emission inventories for the June 1-July 15, 2013 period. The MEGAN model requires information about temperature, soil moisture and solar radiation from the meteorological model. WRF model output was formatted for use by MEGAN through application of the EPA's MCIP (Meteorology-Chemistry Interface Processor) processor. Photosynthetically active radiation (PAR) data, an important input driving the MEGAN light dependency algorithm, can be derived from satellite observation or from predicted solar radiation from WRF/MCIP. However, satellite PAR observations were not available for year 2013. Instead, we used solar radiation from WRF/MCIP with a solar radiation-to-PAR conversion factor of 0.45 (Sakulyanontvittaya et al., 2012).

5.4.2 Comparison of Default and Updated MEGAN Terpenoid Emissions

We prepared three sets of model-ready MEGAN v2.1 biogenic emissions. The first inventory was a base-case biogenic emission inventory, which was developed using the MEGAN default landcover database and default emission factors (EFvE2011). Then, a second biogenic emission inventory was derived from the new high-resolution landcover database and Texas and Southeastern U.S. emission factor database EFvE2015. Finally, a third biogenic emission inventory was derived from the new high-resolution landcover database and the experimental emission factor database EFvA2015.

Figure 5-19 compares domain-wide (upper panel) and state-wide (lower panel) isoprene (ISOP) emissions in the default and the two updated MEGAN emission inventories for the 36 km RPO modeling grid and the 12 km grid. On both grids, domain-wide isoprene totals decrease in

going from the default to updated inventories. On the 12 km grid, the decrease in going from the default to the EFvE2015 inventory is relatively small (1%), while there is a much larger decrease (38%) in going to the EFvA2015 inventory. The breakdown by state shows that the decreases are not uniform in the EFvE2015 inventory; isoprene emissions decrease in Texas, Georgia and Missouri, but increase in Arkansas, Louisiana and Oklahoma. In the EFvA2015 inventory, there are large decreases in isoprene emissions relative to the default emission inventory for all states.

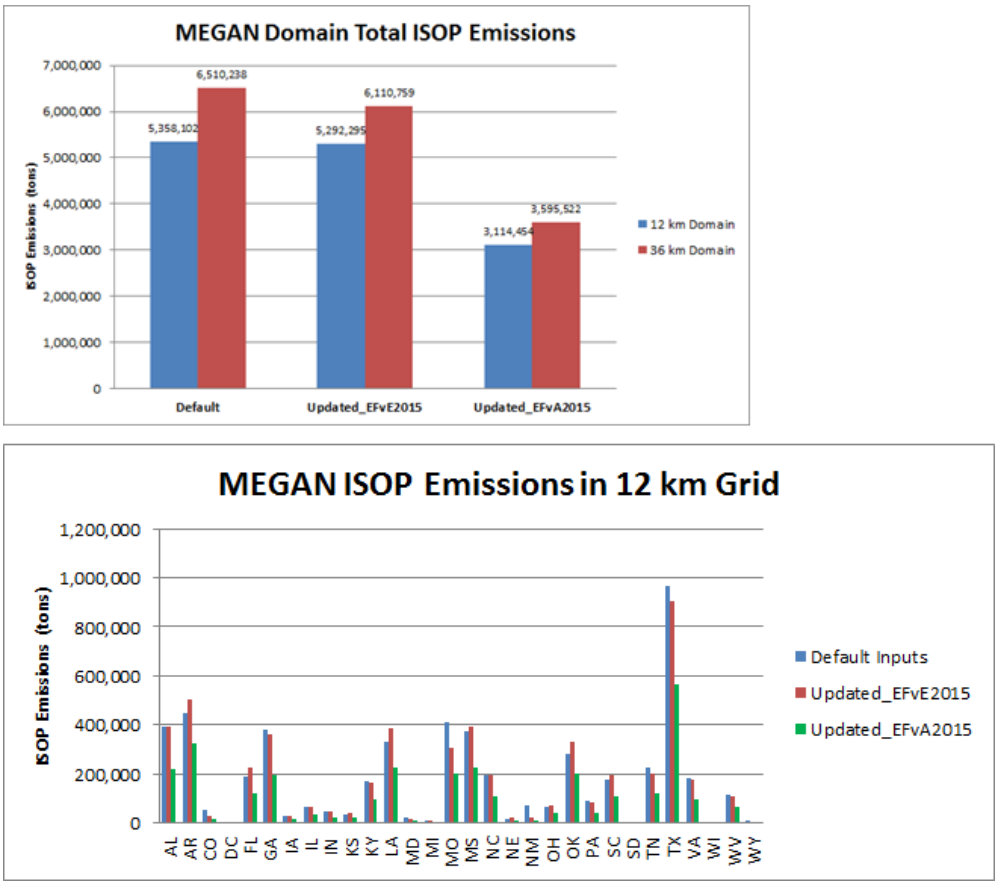

Figure 5-19. MEGAN isoprene (ISOP) emissions for the default and updated emission inventories. Upper panel: domain wide isoprene emissions in the 12 km and 36 km modeling domains. Lower panel: isoprene emission totals by state within the 12 km domain for the default and updated (EFvE2015 and EFvA2015) MEGAN inventories.

Figure 5-20 summarizes the differences among the default and the two updated episode average isoprene emission inventories. The upper left hand panel of Figure 5-20 indicates that LAIv decreased across much of the southeastern US and in east Texas in going from the default to the EFvE2015 inventory, while West Texas and the westernmost states in the 12 km modeling domain have increased LAIv in the updated inventory. The middle left hand panel of Figure 5-20 shows that the LAIv is the same in the EFvE2015 and EFvA2015 inventories.

The upper and center middle panels of Figure 5-20 show the change from the default in the isoprene emissions factor for the EFvE2015 and EFvA2015 cases. The corresponding changes in the June 1-July 15 episode average isoprene emissions are shown in the right hand panels. A large decrease in isoprene emissions in Missouri in the updated EFvE2015 inventory is evident, as is the increase in emissions in a band oriented east-west across Oklahoma and Arkansas. Increases in isoprene emissions occur in central Texas and in southeast Texas in the EFvE2015 inventory. There is a large decrease in isoprene emissions the Houston area that occurs in a region that has decreases in LAIv and EF between the default and updated EFvE2015 cases. Northern Louisiana and northern Florida also show increases in isoprene emissions in the EFvE2015 inventory.

In EFvA2015, there are widespread decreases in the isoprene emissions factor and isoprene emissions relative to the default case and the EFvE2015 case. As in the EFvE2015 case, there is an increase in emissions in a band oriented east-west across Oklahoma and Arkansas, but the extent of this band is smaller in the EFvA2015 case, and there are decreases in the isoprene emissions across most of Texas and the southeastern US. Like the EFvE2015 case, the EFvA2015 inventory shows a large decrease in isoprene emissions the Houston area relative to the default inventory.

The lower panels of Figure 5-20 show the episode average isoprene emissions for the default and updated cases. The widespread reductions in isoprene emissions relative to the default and EFvE2015 cases are apparent in the EFvA2015 case. Overall, the changes in isoprene emissions factor from the default to the EFvE2015 and EFvA2015 cases result in corresponding changes to the isoprene emission inventories. In the EFvA2015 inventory, isoprene emissions are significantly reduced across the 12 km domain relative to the default and EFvE2015 inventories.

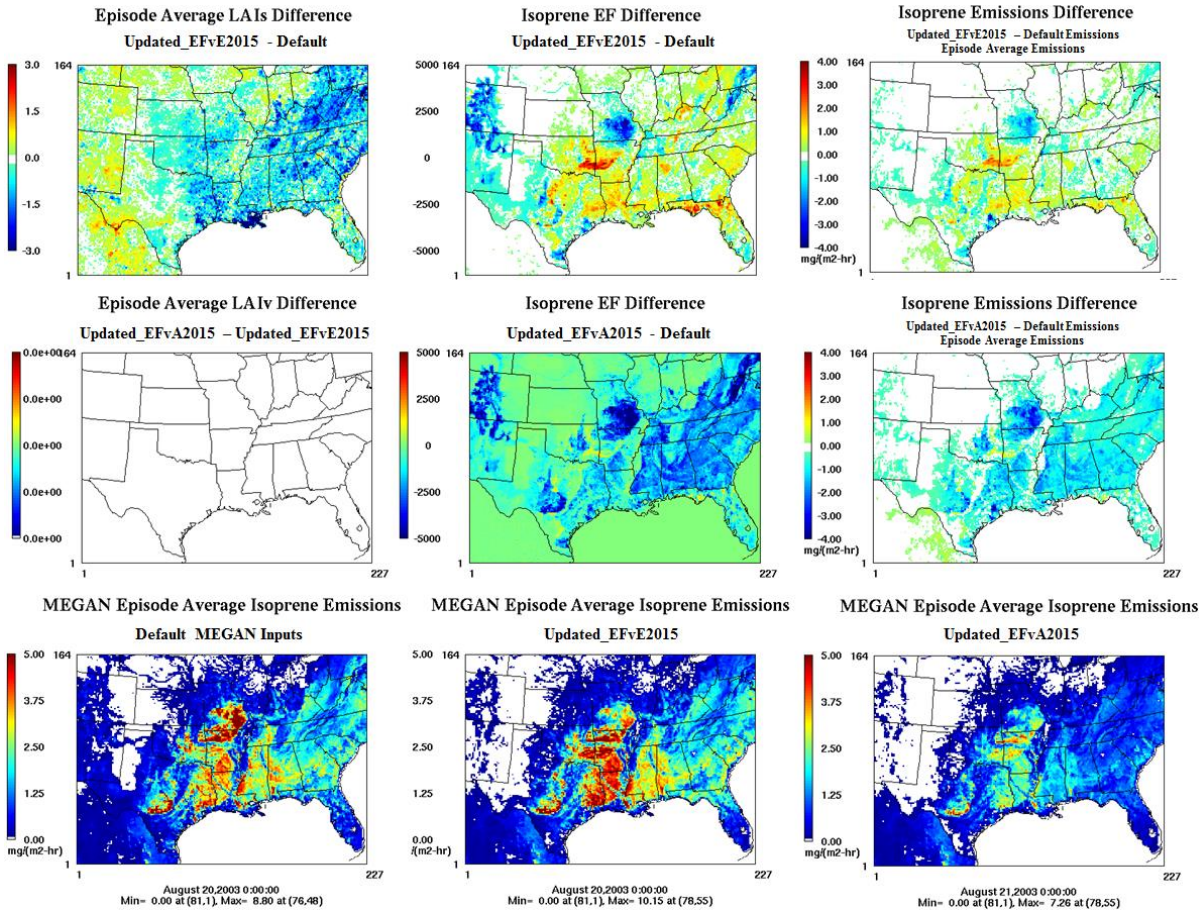

Figure 5-20. Comparison of MEGAN inputs and isoprene emissions for default, updated_EFvE2015 and updated_EFvA2015 emission inventories. Upper left: difference in episode average LAIv (EFv2015-default). Upper center: difference in isoprene emission factors (EFv2015-default). Upper right: difference in episode average isoprene emissions (EFv2015-default). Left middle: difference in episode average LAIv (EFvA2015 - EFv2015). Center middle: difference in isoprene emission factors (EFvA2015 - EFv2015. Right middle: difference in episode average isoprene emissions (EFvA2015- default). Lower left: episode average isoprene emissions (default). Lower center: episode average isoprene emissions (EFv2015). Lower right: episode average isoprene emissions (EFvA2015).

In the EFvE2015 inventory, monoterpene emissions decrease domain-wide for both the 36 km and 12 km grids (Figure 5-21). (EFvE2015 and EFvA2015 are identical for monoterpenes). The largest decrease in monoterpene emissions on both grids in EFvE2015 occurs in Texas (Figure 5-21). Florida and Missouri also show decreases. Monoterpene emissions in the updated inventory increased relative to the default inventory in Alabama, Arkansas, Louisiana, Georgia, South Carolina and Mississippi. The spatial pattern of changes in monoterpene emissions in the updated EFvE2015 inventory is shown in Figure 5-22. In Texas, there are large decreases in monoterpene emissions in west Texas and increases in east Texas, with the exception of the Houston area. The Houston area shows decreases in LAIv, EF and monoterpene emissions. There are broad areas of monoterpene emissions increases across the southeast, and decreases in Florida. There is an abrupt shift in monoterpene emissions at the US-Mexico border in the EF and the emissions.

The pattern of increases and decreases in sesquiterpene emissions in the updated inventory is similar to that of the monoterpenes (Figure 5-23).

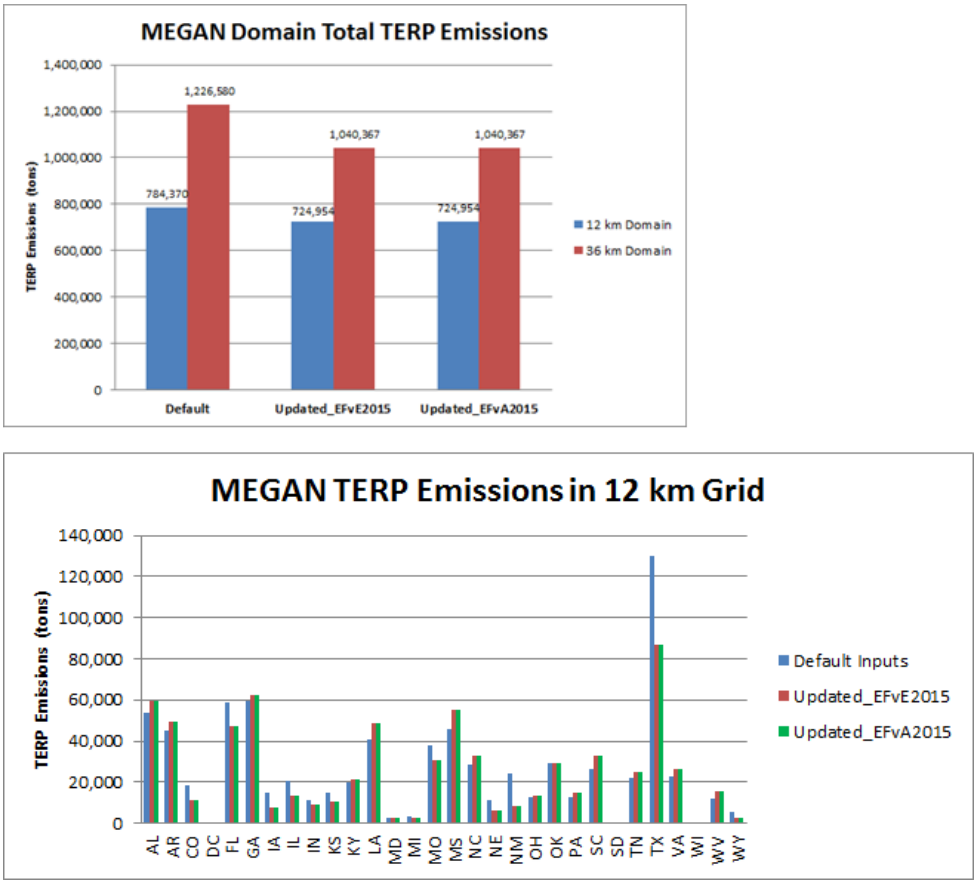

Figure 5-21. MEGAN monoterpene (TERP) emissions for the default and updated (EFvE2015 and EFvA2015) emission inventories. Upper panel: domain wide monoterpene emissions in the 12 km and 36 km modeling domains. Lower panel: monoterpene emissions totals by state within the 12 km domain for the default and updated MEGAN inventories.

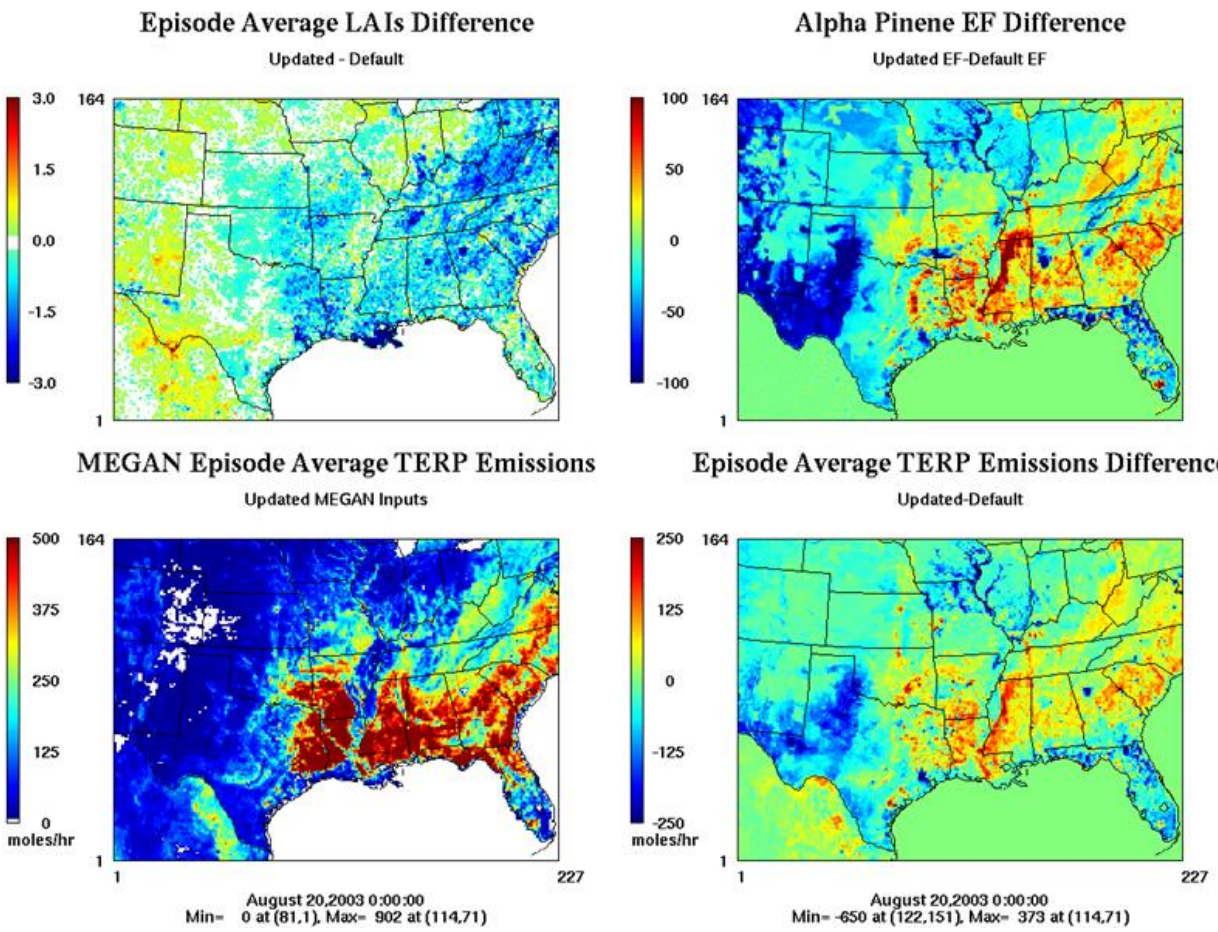

Figure 5-22. Comparison of MEGAN inputs and monoterpene emissions for default and updated emission inventories. Upper left panel: difference in episode average LAI. Upper right panel: difference in α-pinene emission factors. Lower left panel: MEGAN episode average monoterpene (TERP) emissions for updated inventory. Lower right panel: difference in episode average monoterpene emissions.

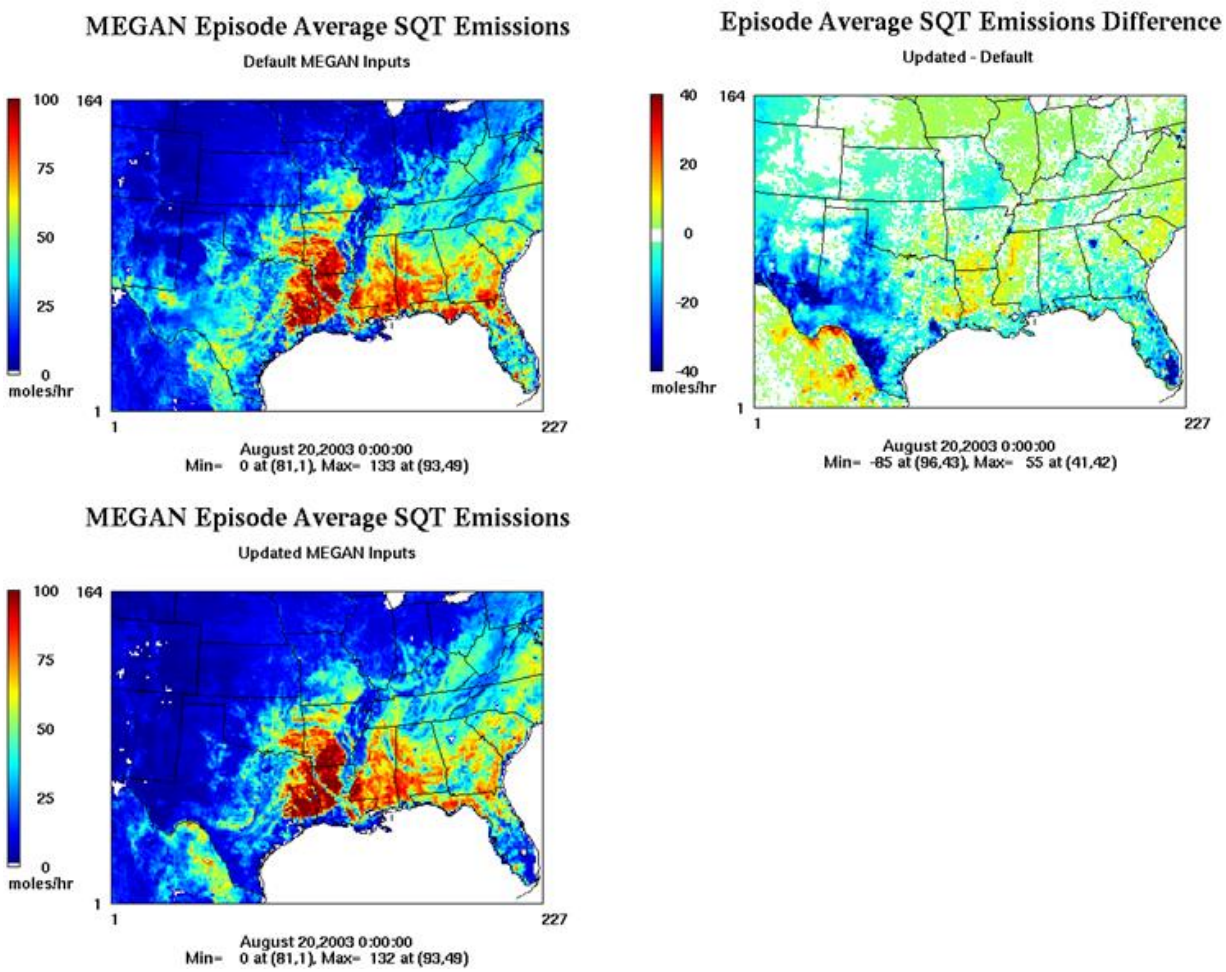

Figure 5-23. Comparison of MEGAN inputs and sesquiterpene (SQT) emissions for default and updated emission inventories. Upper left panel: MEGAN episode average sesquiterpene (TERP) emissions for default inventory. Lower left panel: MEGAN episode average monoterpene (TERP) emissions for updated inventory. Upper right panel: difference in episode average sesquiterpene emissions.

5.4.3 Comparison of MEGAN Emissions and Airborne Emission Fluxes

We extracted MEGAN emissions along the C-130 flight segments for the default and updated EFvE2015 and EFvA2015 inventories. The MEGAN emissions were paired in space and time with the aircraft data. Figure 5-24 shows the isoprene comparison for the MEGAN default and updated emission inventories. In the default inventory, isoprene emissions are higher than in aircraft fluxes for most of the racetrack flight segments. In the updated EFvE2015 emission inventory, agreement with the aircraft fluxes improves for the racetrack segments in southern Missouri, where isoprene emissions are lower in the updated inventory. For the racetrack along the Texas-Louisiana border, isoprene is reduced in the updated inventory, but emissions are still consistently higher than in the aircraft data. The same is true for the Mississippi and Alabama racetrack segments.

The EFvA2015 inventory comparison reflects the lower isoprene emissions across the southeast and Texas. Although the MEGAN isoprene emissions are still generally higher than the airborne fluxes, the EFvA2015 emissions agree more closely than the EFvE2015 emissions.

Monoterpene emissions for the MEGAN default and updated inventories are compared to airborne flux data in Figure 5-25. The default and updated MEGAN monoterpene emissions show closer agreement with the airborne fluxes in this region than the isoprene emissions, but the MEGAN monoterpene emissions are generally higher than the airborne fluxes. The changes between default and updated inventories vary along the tracks, with many of the tracks showing increases in monoterpene emissions from default to updated case. It is difficult to assess whether this improves agreement with the airborne fluxes. However, the MEGAN emissions show the same spatial pattern present in the airborne fluxes of high emissions over the Texas-Louisiana border region and Mississippi and Alabama and lower emissions over southern Missouri and western Tennessee.

The comparison between MEGAN emissions and the airborne fluxes is affected by the use of different meteorological data (WRF and NLDAS) in preparing the emissions flux estimates. In Section 4.2.2, it was noted that there are differences of ~37% between airborne fluxes developed using WRF and NLDAS data. It is possible that the MEGAN emissions estimates shown in Figure 5-25 would have shown better agreement with airborne fluxes derived using WRF data.

Isoprene Fluxes from Aircraft Data

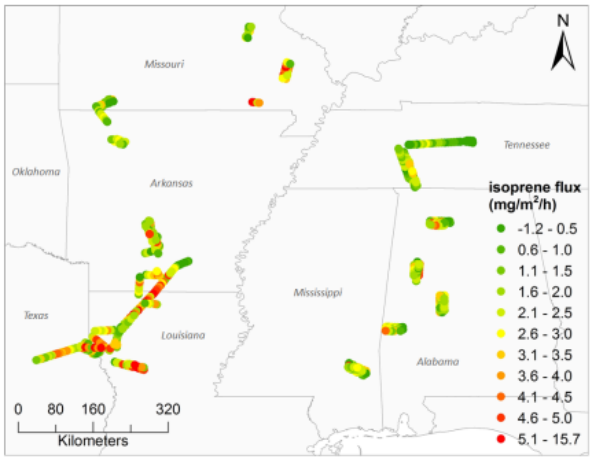

MEGAN ISOP Emissions: Default

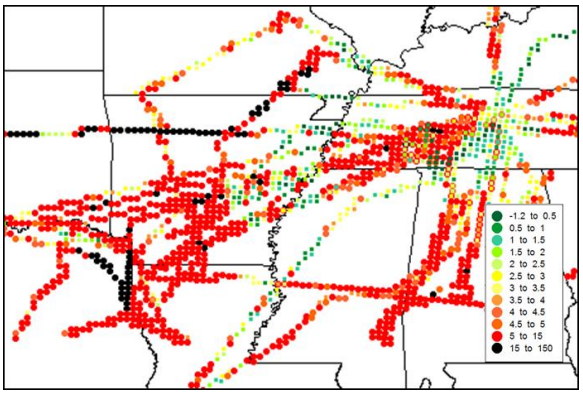

MEGAN ISOP Emissions: Updated_EFvE2015

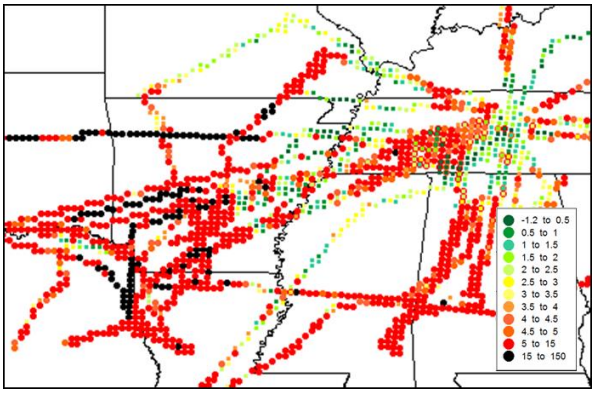

MEGAN ISOP Emissions: Updated_EFvA2015

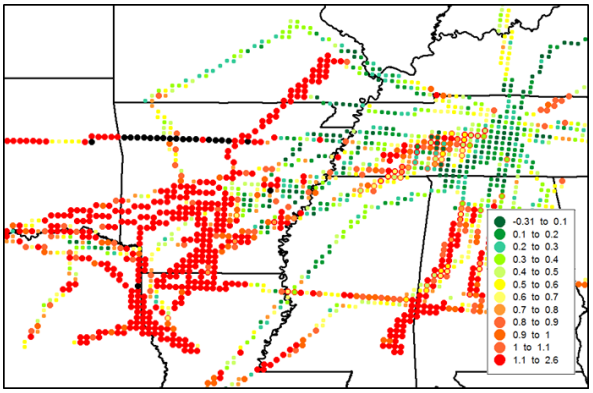

Figure 5-24. Isoprene fluxes derived from airborne data for C-130 racetrack flight segments (upper left) and MEGAN v2.1 isoprene emissions along all C-130 flight tracks for the default (upper right), updated_EFvE2015 (lower left) and updated_EFvA2015 (lower right) emission inventories. Units are mg $(m^2\text{-hr})^{-1}$ for all panels.

Monoterpene Fluxes from Aircraft Data

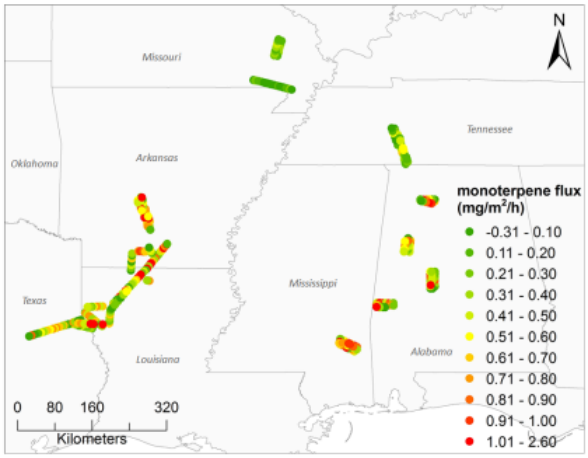

MEGAN TERP Emissions: Default

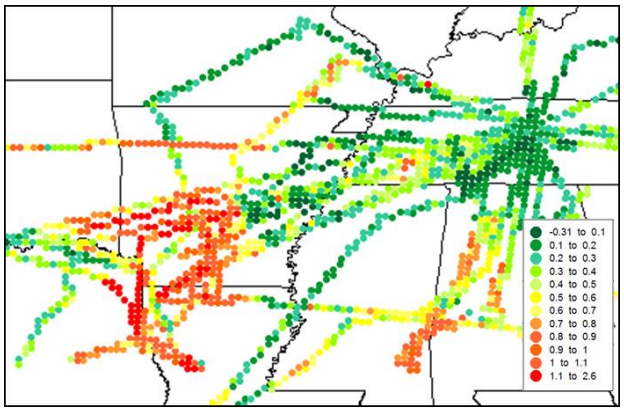

MEGAN TERP Emissions: Updated_EFv2015

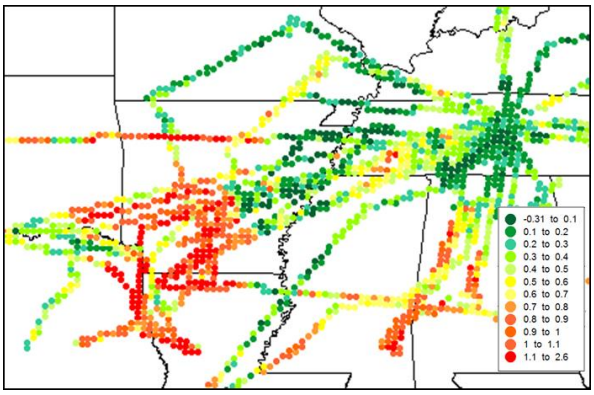

MEGAN TERP Emissions: Updated_EFvA2015

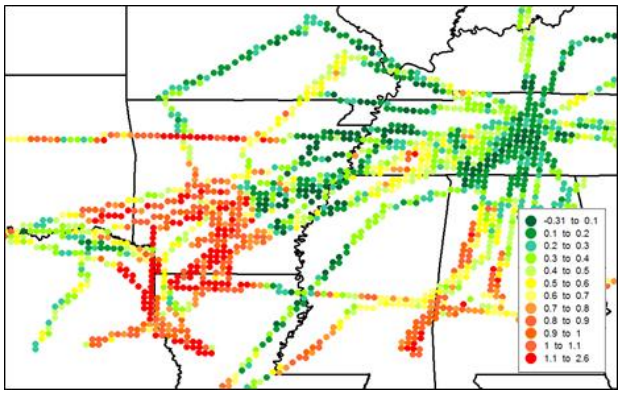

Figure 5-25. Monoterpene fluxes derived from airborne data for C-130 racetrack flight segments (upper left) and MEGAN v2.1 monoterpene emissions along all C-130 flight tracks for the default (upper right), updated_EFvE2015 (lower left) and updated_EFvA2015 (lower right) emission inventories. Units are mg $(m^2\text{-}hr)^{-1}$ for all panels.

5.4.4 Summary of MEGAN Modeling

The comparison of airborne fluxes and MEGAN emissions showed that the MEGAN isoprene emissions are higher than the airborne isoprene fluxes in both the default and updated cases. In the previous section, the dependence of the airborne EFs values on the choice of input meteorological data was discussed. The airborne fluxes in Figure 5-24 and Figure 5-25 may have shown closer agreement with the MEGAN values if consistent meteorology had been used to develop both sets of estimates. The MEGAN values were computed with the WRF run described earlier in this section that has a known high bias for shortwave radiation at the surface that can introduce a high bias into the emissions estimates.

5.5 CAMx Modeling

5.5.1 CAMx Model Configuration

The TCEQ Near-Real Time Ozone Model platform (Johnson et al., 2013) was used to model the June 1-July 15, 2013 period that encompassed all of the C-130 and P-3 flights. To model the July and September, 2013 episodes, we developed meteorological inputs for CAMx by running the WRF model in hindcast mode as described in Section 5.3. The WRF outputs were converted into CAMx model-ready inputs using the WRFCAMx preprocessor v4.3 with YSU vertical diffusivity (Kv). The Kv landuse patch was applied up to 100 m and the Kv cloud patch was also applied.

2012 day-of-week specific anthropogenic emissions were provided by the TCEQ. The 2012 emission inventory was augmented by the TCEQ with 2013 oil and gas emissions for the State of Texas. Electric generating unit emissions were typical ozone season day averages for 2012. 2013 day-specific FINN wildfire emissions (Wiedinmyer et al., 2012) were used and the fire emission modeling is described in Kemball-Cook et al. (2014).

The Zhang dry deposition scheme was used. Photolysis rates files were generated using O3MAP 2012 monthly averages from 1 degree TOMS satellite ozone column data. Land use/land cover inputs were generated using the USGS 24-category dataset and monthly LAI data from MODIS satellite were used.

Boundary conditions for the outer 36 km grid were extracted from a Goddard Earth Observing System Chemistry-Transport Model (GEOS-Chem) simulation for 2012. Monthly average values for 2012 were used for the corresponding month in 2013. Modifications were made to the GEOS-Chem boundary conditions to increase unrealistically low CO concentrations and reduce impacts from 2012 wildfires in northern Manitoba. Based on evaluation of the TCEQ Near-Real Time Ozone Model platform (Johnson et al., 2013) determined that ozone is overestimated in the GEOS-Chem model output. Therefore, we performed a flat 10 ppb ozone reduction and applied various caps to ozone precursors over the Gulf of Mexico and Atlantic Ocean in order to deplete the ozone coming onshore. The boundary condition caps are summarized in Table 5-4.

Table 5-4. Maximum concentration limits for ozone precursors applied to the 36 km boundary condition grid cells across the Gulf of Mexico, Caribbean Sea, and Atlantic Ocean south of Cape Hatteras.

Species	Description	Max. Concentration (ppb)
NO2	Nitrogen dioxide	0.05
CO	Carbon monoxide	150.0
N2O5	Dinitrogen pentoxide	0.001
HNO3	Nitric acid	0.25
PNA	Peroxynitric acid	0.001
H2O2	Hydrogen peroxide	0.5
NTR	Organic nitrates	0.01
FORM	Formaldehyde	0.25
ALD2	Acetaldehyde	0.05
ALDX	Propionaldehyde and higher aldehydes	0.02
PAR	Paraffin carbon bond (C-C)	1.0
OLE	Terminal olefin carbon bond (R-C=C)	0.01
ETHA	Ethane	1.0
MEPX	Methylhydroperoxide	0.1
PAN	Peroxyacetyl Nitrate	0.01
PANX	C3 and higher peroxyacyl nitrate	0.001
INTR	Organic nitrates from ISO2 reaction with NO	0.001
ISOP	Isoprene	0.1
ISPD	Isoprene product (lumped methacrolein, methyl vinyl ketone, etc.)	0.1
TERP	Monoterpenes	0.05
ISP	Isoprene (SOA chemistry)	0.1
TRP	Monoterpenes (SOA chemistry)	0.05
TOL	Toluene and other monoalkyl aromatics	0.02
XYL	Xylene and other polyalkyl aromatics	0.01
SO2	Sulfur dioxide	0.1
PRPA	Propane	0.5
ACET	Acetone	0.25
KET	Ketone carbon bond (C=O)	0.05
BENZ	Benzene	0.1

The CB6r2 chemical mechanism (Yarwood et al., 2012) was used in the CAMx modeling. CB6r2 differentiates organic nitrates (ON) between simple alkyl nitrates that remain in the gas-phase (providing a reservoir of NO_2) and multi-functional ONs that can partition into organic aerosols (OA). ON present in OA are then assumed to undergo hydrolysis to nitric acid. CB6r2 Includes documented OH production under low NOx conditions and evaluates well against isoprene chamber experiments at low NOx. Nevertheless, Cb6r2 may still underestimate OH production at low NOx. CB6r2 contains an explicit hydroperoxyaldehyde (HPLD) product and the lumped isoprene product species ISPD represents methyl vinyl ketone (MVK), methacrolein (MACR) and similar products.

We made the following simulations of the June 1-July 15, 2013 period with CAMx:

1. Base run: MEGAN emissions developed with default inputs EFvE2011 (Run 1)

2. Add OH production to isoprene chemistry to determine whether agreement improves for isoprene and products (Run 2)

3. Updated MEGAN emission inventory EFvE2015. MEGAN developed with updated LAIv, EF, PFT inputs described in Sections 3 and 4 inputs (Run 3)

4. Test of reduction in MEGAN isoprene emissions by a constant factor for all grid cells and times. (ISOP emissions)/2 to determine whether agreement improves for isoprene and products (Run 4)

5. Increase dry deposition of oxygenated VOCs based on SOAS measurements of Nguyen et al. (2015) (Run 5)

6. Updated MEGAN emission inventory EFvA2015. MEGAN developed with updated LAIv, EF, PFT inputs described in Sections 3 and 4 inputs (Run 6)

First, we describe the model performance evaluation method for ground level ozone and provide an overview of the results of the evaluation of the Base run (Run 1) and the updated MEGAN sensitivity tests (Run 3 and Run 6). More information on the surface ozone evaluation for the base run comparison with Run 3 and Run 6 (MEGAN sensitivity tests) is given in Appendix C. Ground level ozone performance was not evaluated for sensitivity tests 2, 4 and 5. Finally, in the remainder of Section 5, we focus on the evaluation of the base run and sensitivity tests against the C-130 and P-3 aircraft data.

5.5.2 CAMx Model Performance Evaluation Method

We evaluated CAMx against ground level ozone observations from Clean Air Status and Trends Network (CASTNET) sites for stations within the 12 km grid and outside of Texas. The CASTNET monitors are located in rural areas and this is appropriate considering the model's relatively coarse horizontal resolution. U.S. CASTNET sites are shown in Figure 5-26. We used data from the subset of these stations that had monitoring data available for the June 1-July 15, 2013 modeling period. We also evaluated ozone at rural locations in Texas using ozone measurements from TCEQ Continuous Air Monitoring Stations (CAMS). To evaluate the model's performance in simulating ground level ozone, we prepared time series of hourly observed and modeled ozone for each station for the June 1-July 15, 2013 model run. We also evaluated model performance for 8-hour average ozone against two statistical metrics. The statistical metric used in this model performance evaluation is the normalized mean bias (NMB), defined as

$$NMB = \frac{\sum_{i=1}^{N}(P_i - O_i)}{\sum_{i=1}^{N} O_i}$$

where P_i and O_i are the predicted and observed values (O_i,P_i) paired in space and time and N is the number of observed/modeled data pairs. The NMB shows whether a modeled quantity such as ozone is under- or over-predicted on average, compared with observations.

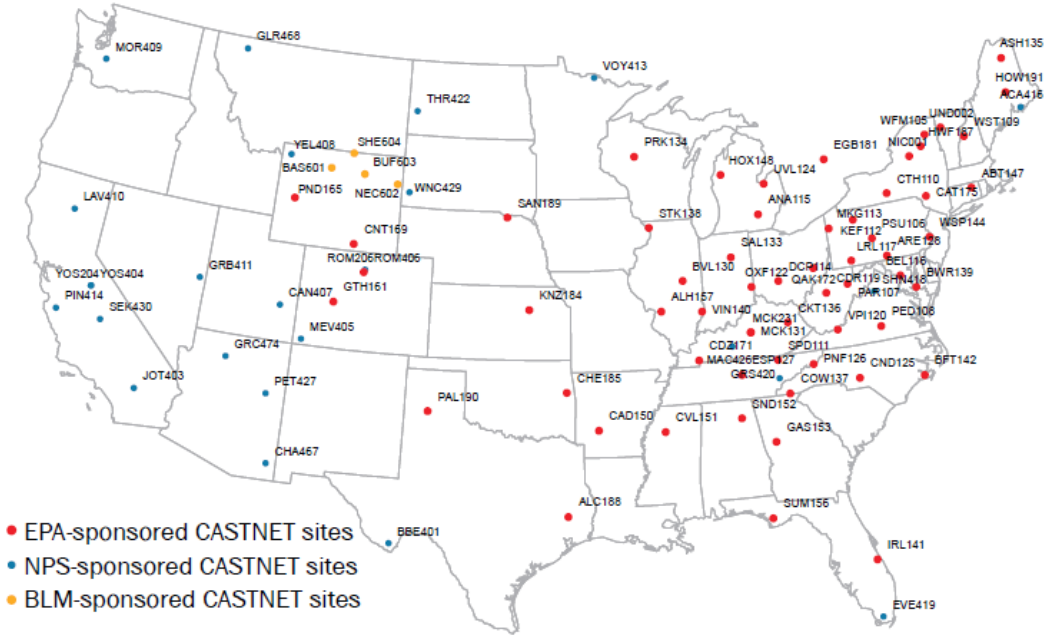

Figure 5-26. Location of CASTNet monitoring sites. EPA figure[4].

[4] http://epa.gov/castnet/javaweb/docs/CASTNET_Factsheet_2013.pdf

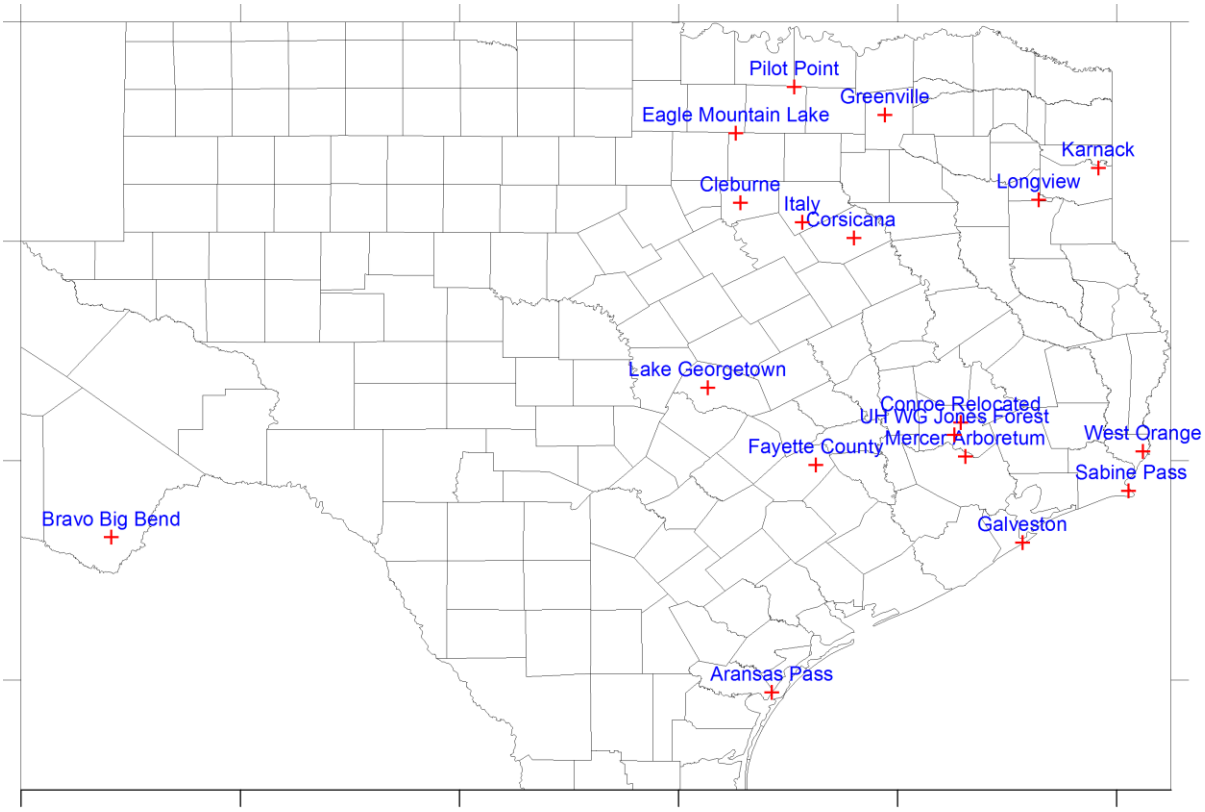

Figure 5-27. TCEQ CAMS monitoring sites used in the model performance evaluation.

5.5.3 CAMx Performance Evaluation Results

5.5.3.1 Comparison with Surface Observations

The hourly ozone time series and daily bias statistics for the CAMx evaluation against observed ozone at CASTNET and CAMS stations are shown in Appendix C and are summarized below. The model performance evaluation for surface ozone at Texas CAMS sites showed the following:

- CAMx model performance was reasonably good at rural/suburban sites in north and central Texas (e.g. Pilot Point, Cleburne). The model captured much of the variability in observed ozone on weekly and daily timescales.
- CAMx has a general high bias for ozone in east Texas that is more pronounced at coastal sites and sites near the eastern border of Texas than at sites in central Texas.
- In the CAMx run with the updated MEGAN emissions, the high bias was reduced at many Texas sites relative to the Base run.
- At CAMS sites in the Houston-Galveston-Brazoria area, the reduction in ozone in the run with updated MEGAN emissions was large, reaching values as large as 20 ppb (Figure 5-28). The effect of this reduction was to improve agreement with observations because these reductions frequently happened on days where the Base run with default MEGAN emissions had a high bias relative to observed ozone.

- At the Big Bend monitor in west Texas, CAMx did not show a consistent high bias and simulated the observed time series with good skill.
- Coastal sites such as Sabine Pass and Galveston had periods of extremely high bias where ozone was overestimated during periods of onshore flow (e.g. June 22-24 in Figure 5-28). This phenomenon may be related to the model boundary conditions, which are not specific to this episode and contain a high bias for ozone introduced by the global model (Johnson et al., 2014). The CAMx overestimates at coastal sites may also reflect the WRF model's difficulty in simulating near surface winds at coastal sites.

The model performance evaluation for surface ozone at Texas CAMS sites showed the following:

- At most CASTNet sites in the southeast, the CAMx model had an overall high bias, consistent with TCEQ's previous modeling of this region.
- The high bias was most pronounced at coastal sites such as IRL141 and SUM156 in Florida, which had consistent overestimates of ozone. These overestimates sometimes occurred during periods of onshore flow and may be related to bias in the CAMx 36 km grid boundary conditions.
- Differences between the default and updated CAMx run surface ozone at CASTNet sites were smaller than differences between the runs in east Texas, and especially those of in Houston and Northeast Texas.

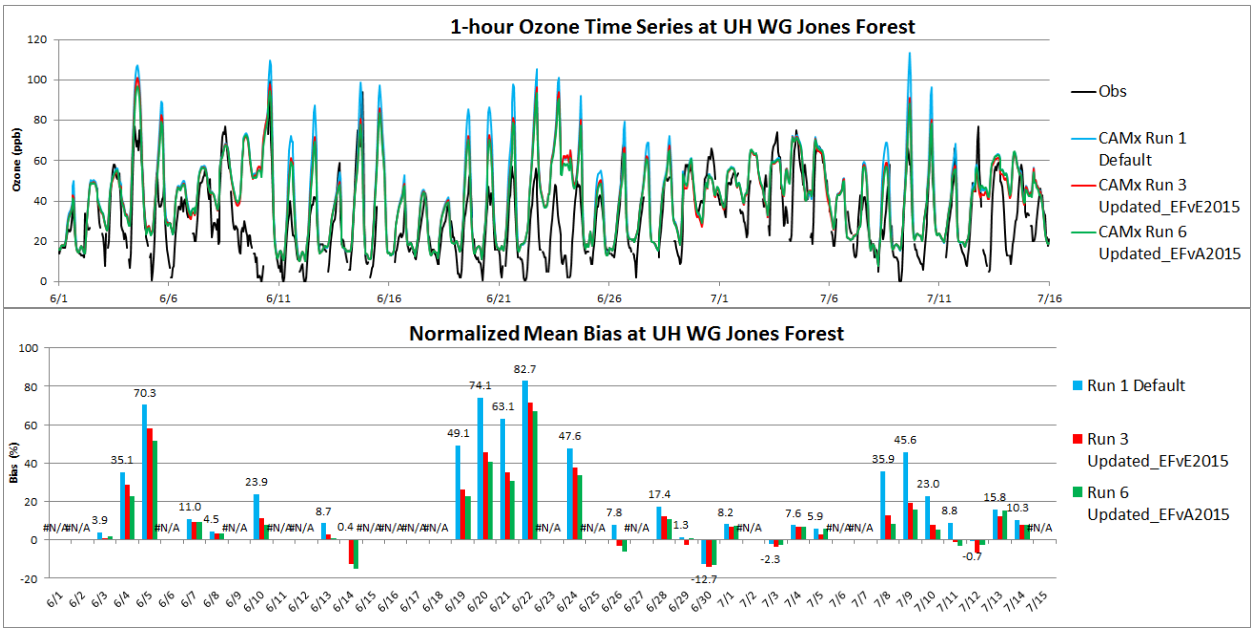

Figure 5-28. 1-hour ozone time series (upper panel) and normalized mean bias (lower panel) for the UH WG Jones Forest (CAMS 698) monitor in the Houston area. NMB was not calculated on days when observed daily maximum 8-hour ozone was < 40 ppb and these days are indicated by #N/A.

5.5.3.2 Comparison with SAS C-130 and P-3 Aircraft Data

We evaluated the CAMx base case simulation using MEGAN emissions developed with default inputs against C-130 and P-3 aircraft observations paired in time and space. For each dataset from the C-130 and P-3 (described below), we averaged all observations within each CAMx grid cell and for each hour of the simulation.

Two datasets were available for the C-130 flights. These two merged datasets combine observations from the different instruments on the aircraft to a common time base. The first dataset, mrg60, combines the data to a 1-minute time base. The time listed in the data set is the mid-point of the 1-minute average and any measurement that occurred within or overlapped the 1 minute period is included in the average and is weighted accordingly[5]. The TOGA dataset is averaged to the 2 minute time period of the Trace Organic Gas Analyzer (TOGA). The TOGA is a fast online Gas Chromatograph/Mass Spectrometer (GC/MS) that measures VOCs and other species with a measurement frequency of approximately one 30s sample every 2 minutes[6]. We compared the mrg60 and TOGA datasets to the CAMx output. The P-3 data were reported as 1 minute averages. Measured species and measurement methods used aboard the P-3 and C-130 for species analyzed in this study are shown in Table 5-5 and Table 5-6.

Table 5-5. P-3 species and measurement methods[7].

Species	Technique	Data ID
Airborne Cavity Enhanced Spectrometer (NO_2 and glyoxal)	Airborne Cavity Enhanced Spectrometer	ACES
Nitrogen Oxide, Nitrogen Dioxide, Ozone (O_3), Nitrogen Trioxide (NO_3), Dinitrogen Pentoxide (N_2O_5)	Cavity ring-down spectrometer.	CaRDS
Carbon Monoxide (CO)	Vacuum UV resonance fluorescence	CO
HNO_3, HCOOH, HONO	Chemical Ionization Mass Spectrometry (CIMS).	HNO3HCOOH
Nitric Oxide (NO)	NO/O3 Chemiluminescence.	NO
Nitrogen Dioxide (NO_2)	Photolysis and NO/O3 Chemiluminescence.	NO2
Total Reactive Nitrogen Oxides (NOy)	Au Converter and NO/O3 Chemiluminescence.	NOy
Ozone (O_3)	Chemiluminescence.	O3
Peroxyacyl Nitrates (PANs)	Chemical Ionization Mass Spectrometer (CIMS).	PANs
Sulfur Dioxide (SO_2)	Pulsed UV fluorescence.	SO2

[5] https://www2.acd.ucar.edu/campaigns/nomadss
[6] http://data.eol.ucar.edu/datafile/nph-get/373.023/Hornbrook_TOGA_VOC_Analyzer_readme.pdf
[7] http://www.esrl.noaa.gov/csd/groups/csd7/measurements/dataui/

Species	Technique	Data ID
Various VOCs using PTR-MS	Proton Transfer Reaction Mass Spectrometer (PTRMS).	VOCsPTRMS
Various VOCs using whole air sampler (WAS) (SENEX 2013 P-3)	Whole air sampler and post-flight gas chromatograph.	VOCsiWAS2

Table 5-6. C-130 Species and measurement methods[8].

CU CIMS: OH, H_2SO_4, sCIs
In Situ Chemiluminescence: NO, NO_2, O_3 Data
NSF/NCAR C-130 HONO Particulate Nitrate and Nitric Acid Data
Proton Transfer Reaction Mass Spectrometer (PTR-MS) Data
Trace Organic Gas Analyzer (TOGA) VOC Analyzer Data

5.5.3.2.1 Base Run (Run 1)

Figure 5-29 and Figure 5-30 compare the measured and modeled isoprene along the aircraft flight tracks for the C-130 mrg60 and P-3 data, respectively. In the CAMx CB6r2 chemical mechanism, isoprene is represented explicitly by the species ISOP. Isoprene was measured via PTR-MS on both aircraft. CAMx shows patterns of high and low isoprene that are similar to the aircraft observations. For example, both the modeled and the measured isoprene are relatively high in the region that includes northeast Texas, northwest Louisiana and southwestern Arkansas. Both observed and CAMx isoprene show hot spots in southeastern Missouri, central Alabama and central Georgia. Areas of low isoprene occur in the model and measurements in northern Indiana, northern Mississippi, South Carolina, northeastern Kentucky and central Texas. CAMx generally overestimates isoprene along the aircraft flight tracks. CAMx has higher isoprene in the areas where observed isoprene has its largest values (northeast Texas, northwest Louisiana, Arkansas, southeast Missouri, and western Alabama. CAMx also has relatively high isoprene values in eastern Tennessee and western North Carolina, while the observations show this to be an area of low isoprene.

The scatter plot in Figure 5-31 shows all (observed, modeled) isoprene data pairs from the C-130 and P-3 flights. Both the C-130 mrg60 and TOGA data sets are shown. Coefficient of determination (r^2) values range between 0.56 and 0.61 for CAMx and the three aircraft datasets, consistent with the overall agreement in spatial patterns between observed and modeled isoprene. However, CAMx has a pronounced high bias for isoprene relative to all three data sets, with NMB ranging from 84-113%.

[8] http://data.eol.ucar.edu/master_list/?project=SAS

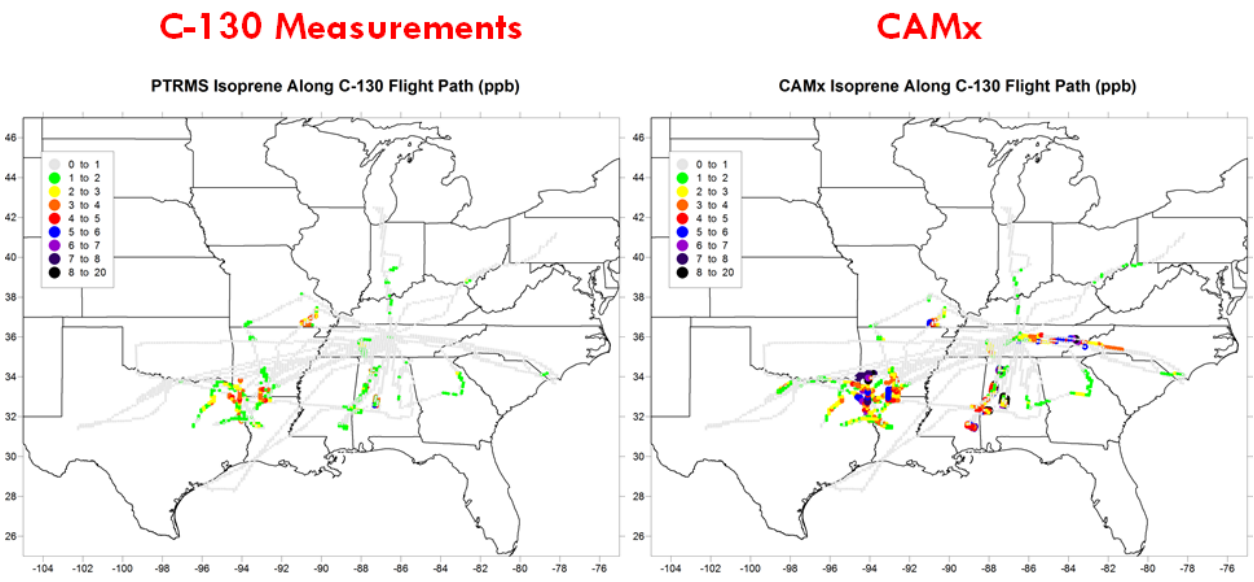

Figure 5-29. Measured and modeled isoprene along the C-130 flight tracks for the June 1-July 15, 2013 period. Left panel: C-130 mrg60 isoprene measured via PTR-MS. Right panel: CAMx isoprene (ISOP).

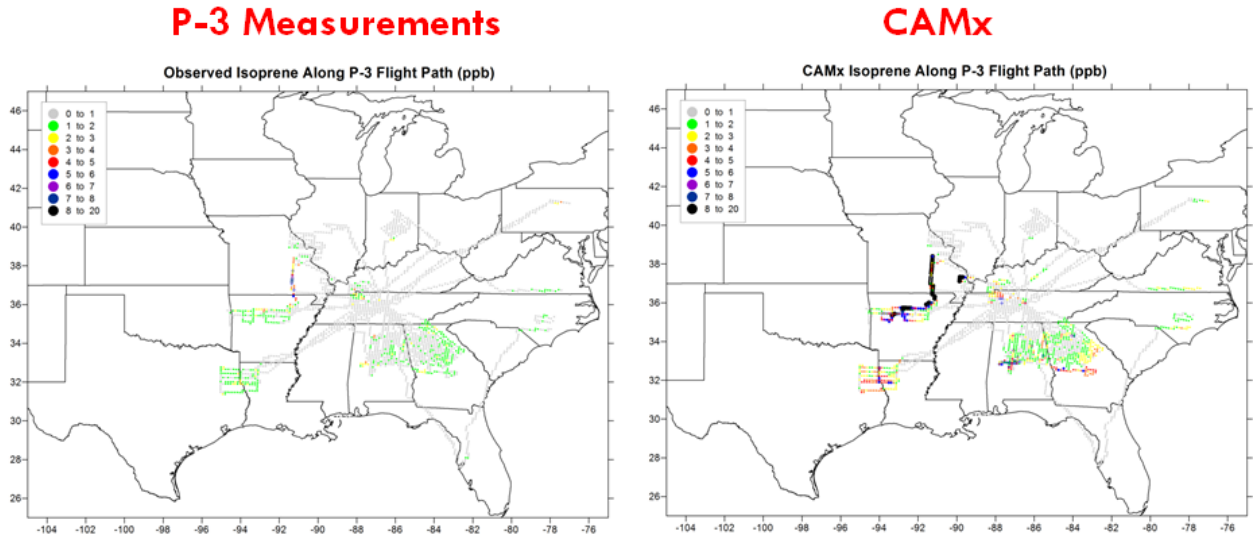

Figure 5-30. Measured and modeled isoprene along the P-3 flight tracks for the June 1-July 15, 2013 period. Left panel: P-3 isoprene measured via PTR-MS. Right panel: CAMx isoprene (ISOP).

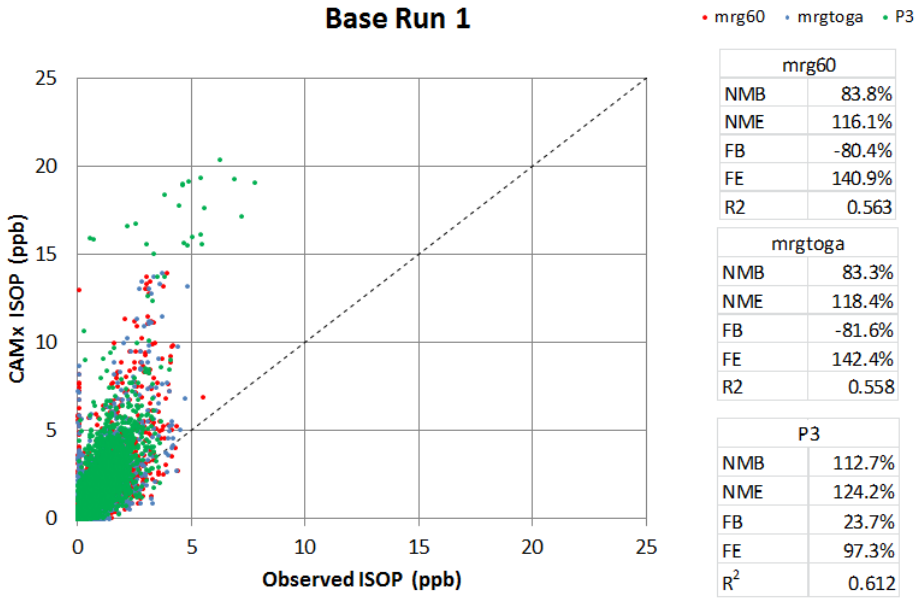

mrg60	
NMB	83.8%
NME	116.1%
FB	-80.4%
FE	140.9%
R2	0.563

mrgtoga	
NMB	83.3%
NME	118.4%
FB	-81.6%
FE	142.4%
R2	0.558

P3	
NMB	112.7%
NME	124.2%
FB	23.7%
FE	97.3%
R^2	0.612

Figure 5-31. Measured and modeled isoprene along the C-130 and P-3 aircraft flight tracks for the June 1-July 15, 2013 period.

The comparison of CAMx modeled and measured isoprene reaction products is shown in Figure 5-32. In CAMx, isoprene products are represented by the sum of ISPD and HPLD. The CB6r2 species ISPD represents isoprene products and includes lumped methacrolein (MACR) and methyl vinyl ketone (MVK). HPLD represents hydroperoxyaldehydes. The PTR-MS instrument does not distinguish MACR, MVK and HPALD and the total isoprene product measurement from the PTR-MS instrument is shown.

Figure 5-32 indicates that CAMx overestimates isoprene reaction products along the flight track for both aircraft, and this is consistent with the isoprene overestimates shown in Figure 5-29 through Figure 5-31. The bias for isoprene products is smaller than for isoprene, which implies that the chemical aging of isoprene is too slow in CAMx. It is possible that OH from isoprene could be biased low, or a high bias for isoprene could be slowing oxidation by consuming OH.

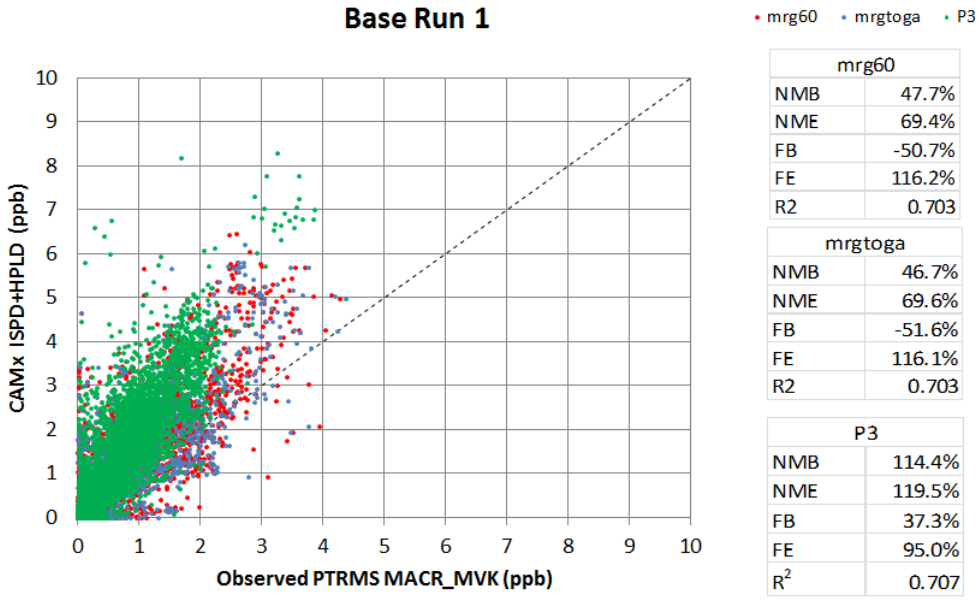

mrg60	
NMB	47.7%
NME	69.4%
FB	-50.7%
FE	116.2%
R2	0.703

mrgtoga	
NMB	46.7%
NME	69.6%
FB	-51.6%
FE	116.1%
R2	0.703

P3	
NMB	114.4%
NME	119.5%
FB	37.3%
FE	95.0%
R^2	0.707

Figure 5-32. Measured and modeled isoprene products along the C-130 and P-3 aircraft flight tracks for the June 1-July 15, 2013 period.

Figure 5-33 and Figure 5-34 compare the modeled and measured sum of monoterpenes along the C-130 and P-3 flight tracks, respectively. The scatter plot in Figure 5-35 compares measured and modeled sum of monoterpenes along both flight tracks. Values of r^2 are lower for monoterpenes than for isoprene, and mismatches between modeled and measured values are more pronounced in the C-130 measurements than in the P-3 measurements. Examples of this can be seen in the C-130 flight tracks along the northern border of West Virginia and through central Oklahoma and Indiana (Figure 5-33). The negative values of NMB indicate that CAMx monoterpene concentrations are generally less than the observed concentrations.

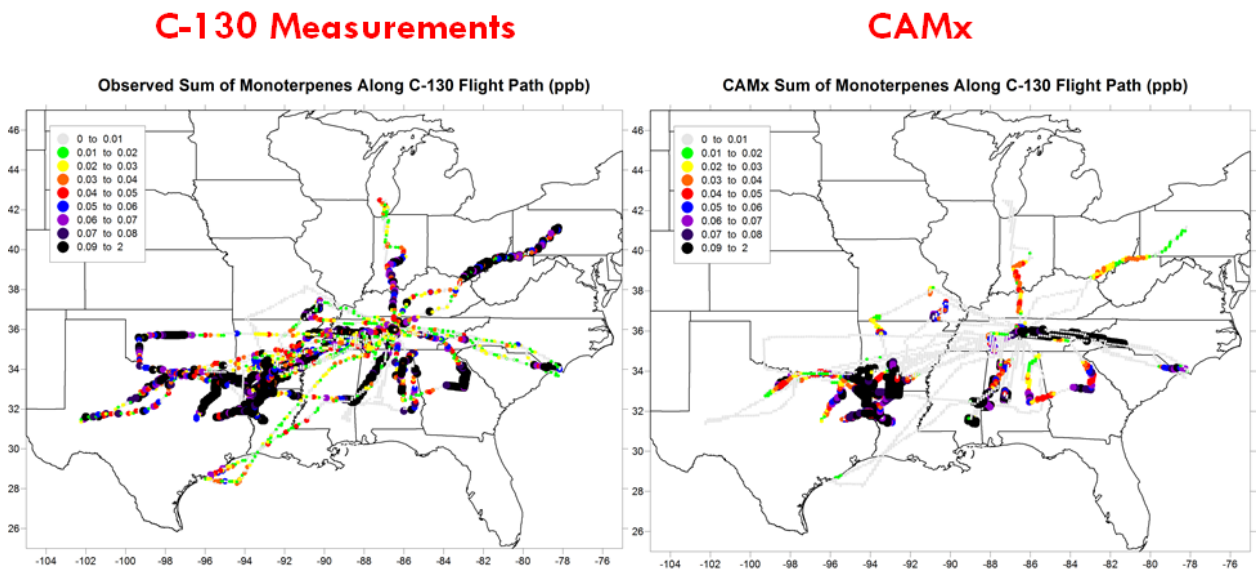

Figure 5-33. Measured and modeled monoterpenes along the C-130 flight tracks for the June 1-July 15, 2013 period. Left panel: C-130 sum of monoterpenes. Right panel: CAMx sum of monoterpenes (TERP).

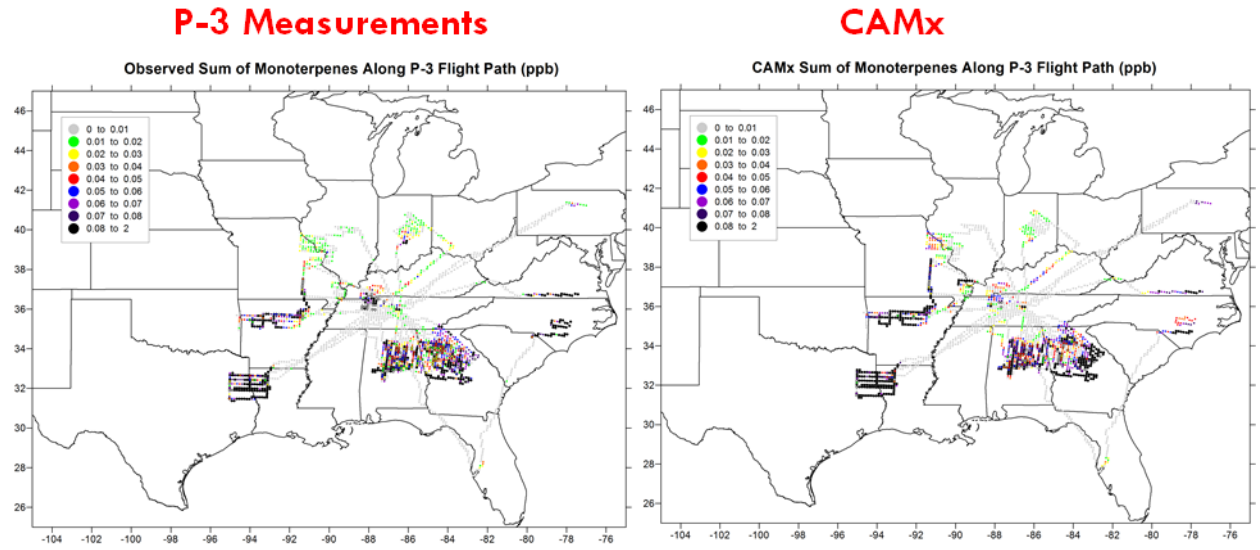

Figure 5-34. Measured and modeled isoprene along the P-3 flight tracks for the June 1-July 15, 2013 period. Left panel: P-3 sum of monoterpenes. Right panel: CAMx sum of monoterpenes (TERP).

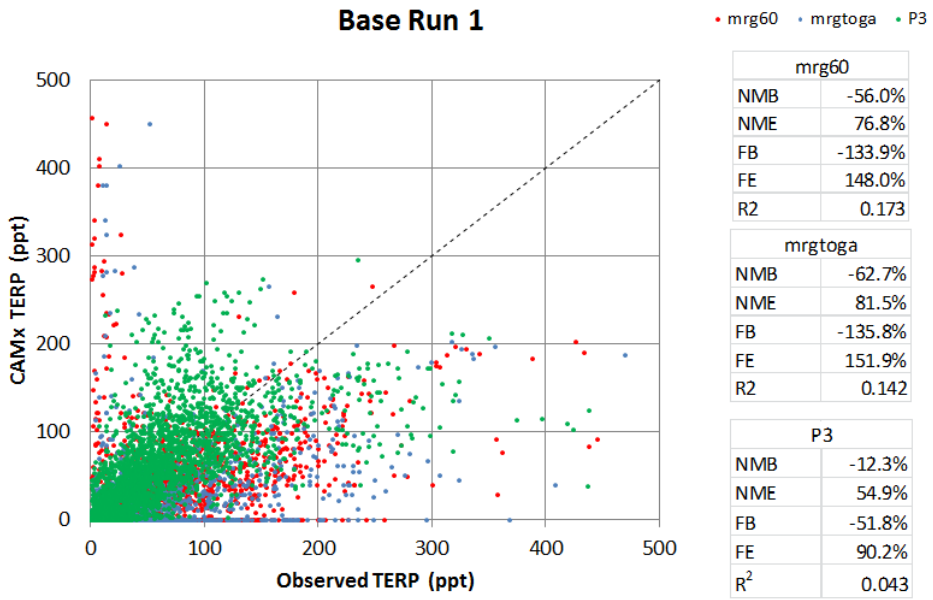

Figure 5-35. Measured and modeled sum of monoterpenes along the C-130 and P-3 aircraft flight tracks for the June 1-July 15, 2013 period. Base run.

Figure 5-36 compares measured and modeled ozone along the aircraft flight tracks. CAMx overestimates ozone along both flight tracks as indicated by the positive NMB values and the displacement of the cloud of points above the 1:1 line. R^2 values range between 0.12 and 0.22. The use of regression statistics may be inappropriate here because ozone is a relatively long-lived species with a regional background and the positive bias may be partly caused by error in the transported background due to model boundary conditions (i.e., an offset that shows up in the intercept). This is consistent with the dramatic overestimates of ozone seen in the CAMx surface performance evaluation at coastal sites during periods of onshore winds. A high bias due to boundary conditions may result from using boundary conditions that are not specific to the episode and/or bias in the global model used to develop the boundary conditions.

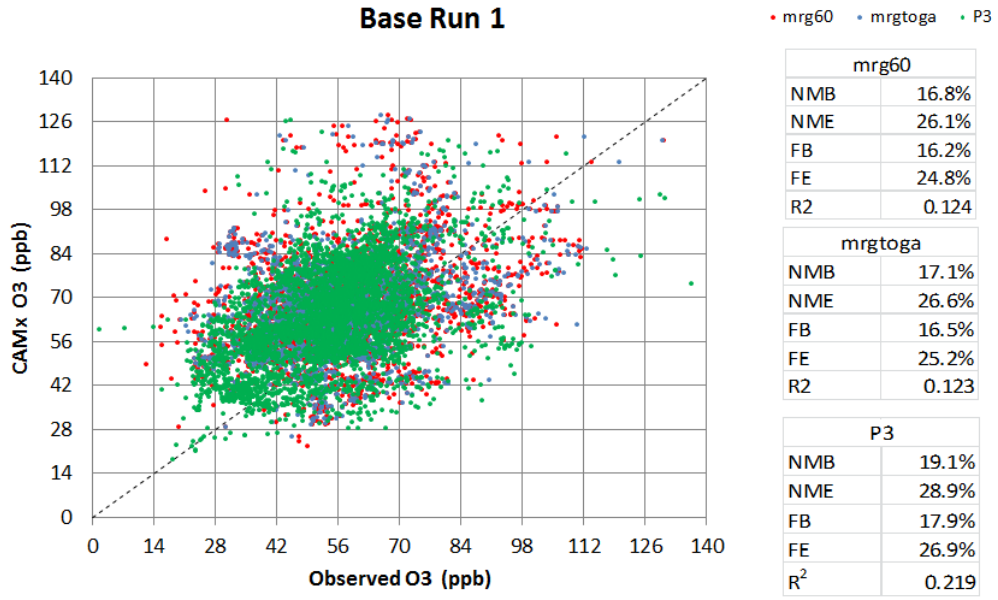

Figure 5-36. Measured and modeled ozone along the C-130 and P-3 aircraft flight tracks for the June 1-July 15, 2013 period. Base run.

CAMx model performance for OH is shown in Figure 5-37. OH was not available for all C-130 flights, and was not measured aboard the P-3. The CAMx-predicted OH is not well-correlated with the measured OH; however the accuracy of the OH measurements is a subject of current investigation and this comparison should be interpreted with caution.

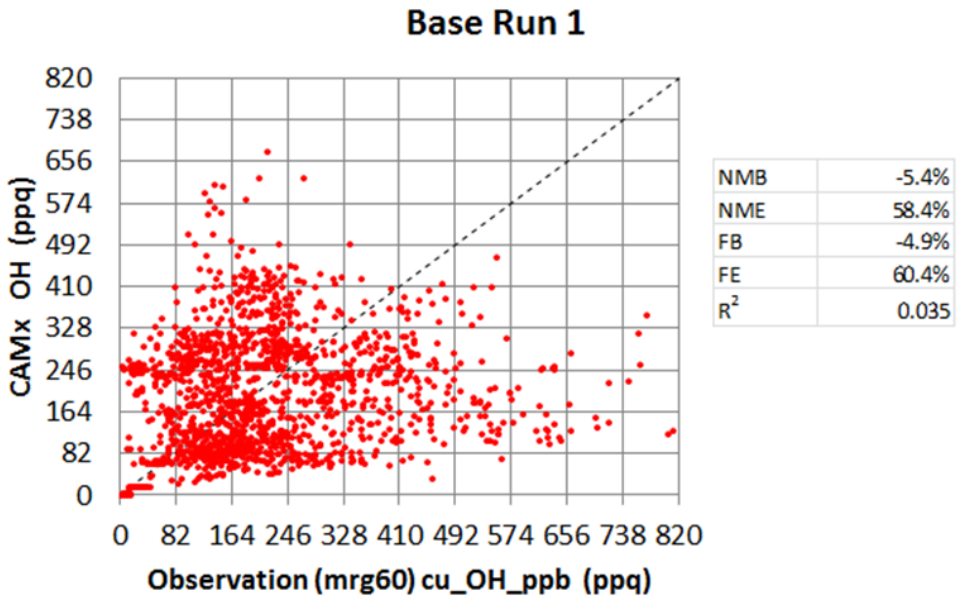

Figure 5-37. Measured and modeled OH along the C-130 aircraft flight tracks for the June 1-July 15, 2013 period. OH measurements were not available for the P-3 flight tracks. Base run.

Comparison of modeled and measured formaldehyde (HCHO) along the C-130 and P-3 flight tracks (Figure 5-38) shows results that vary by data set. CAMx overestimates HCHO along the C-130 flight track relative to the mrg60 1-minute data set (NMB of 20%), and this is consistent with the modeled overestimate of isoprene shown in Figure 5-31. CAMx shows better agreement with the TOGA dataset than with the mrg60 data. Results for the TOGA are consistent with the results of the P-3 comparison, with CAMx showing a low bias (NMB of -9.2%) relative to both the TOGA and P-3 measurements.

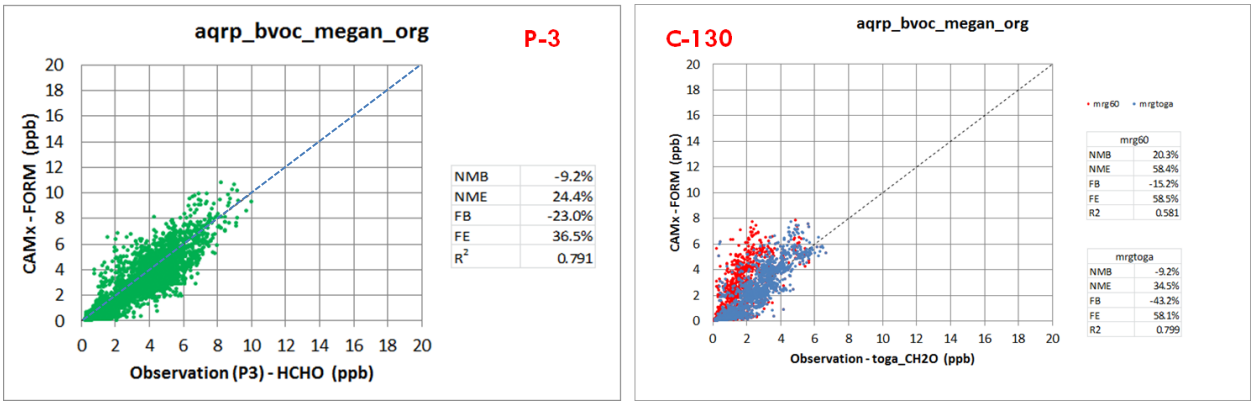

Figure 5-38. Measured and modeled formaldehyde along the P-3 (left panel) and C-130 (right panel) aircraft flight tracks for the June 1-July 15, 2013 period. Base run.

CAMx overestimates estimates acetaldehyde along flight tracks in both data sets (Figure 5-39), and this is consistent with isoprene overestimates (Figure 5-31).

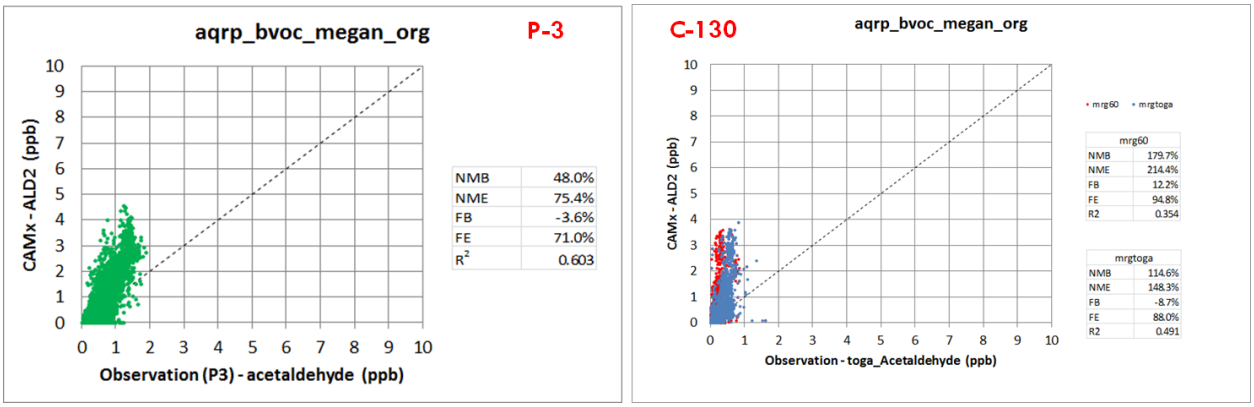

Figure 5-39. Measured and modeled acetaldehyde along the P-3 (left panel) and C-130 (right panel) aircraft flight tracks for the June 1-July 15, 2013 period. Base run.

CAMx overestimates methanol along C-130 flight track compared to the mrg60 1-minute data, and underestimates methanol compared to TOGA dataset and the P-3 data. R^2 values are greater than 0.6 for CAMx and the C-130 TOGA and P-3 methanol datasets, but R^2 is 0.29 for CAMx and the mrg60 data from the C-130. The comparison of modeled and measured acetone (Figure 5-41) shows similar results, with CAMx underestimating acetone relative to the P-3 and the C-130 TOGA acetone values, with similar R^2 values (0.4) and showing a pronounced

overestimate of the C-130 mrg60 acetone with lower R^2 (0.24). The CAMx underestimate relative to the P-3 data is consistent with the CAMx underestimate of propane relative to P-3 measurements that is shown later on in this section.

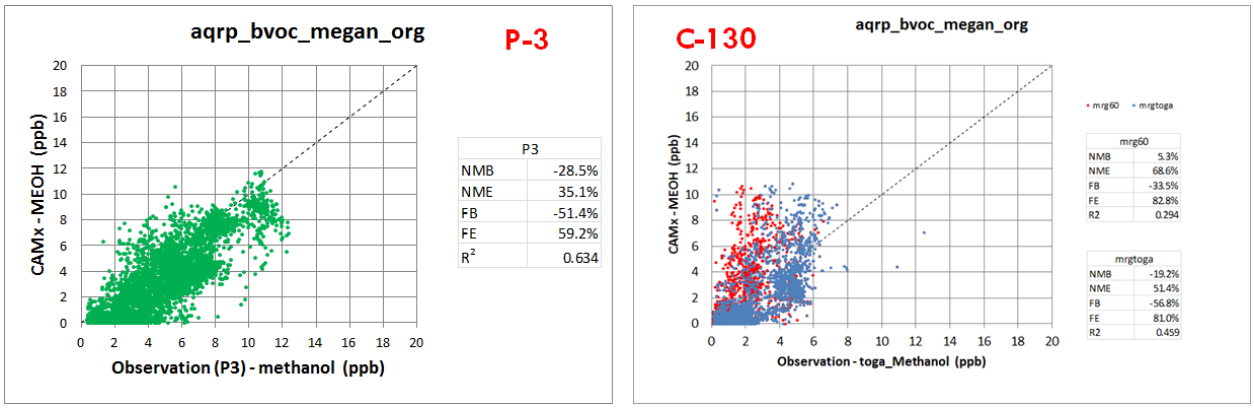

Figure 5-40. Measured and modeled methanol along the P-3 (left panel) and C-130 (right panel) aircraft flight tracks for the June 1-July 15, 2013 period. Base run.

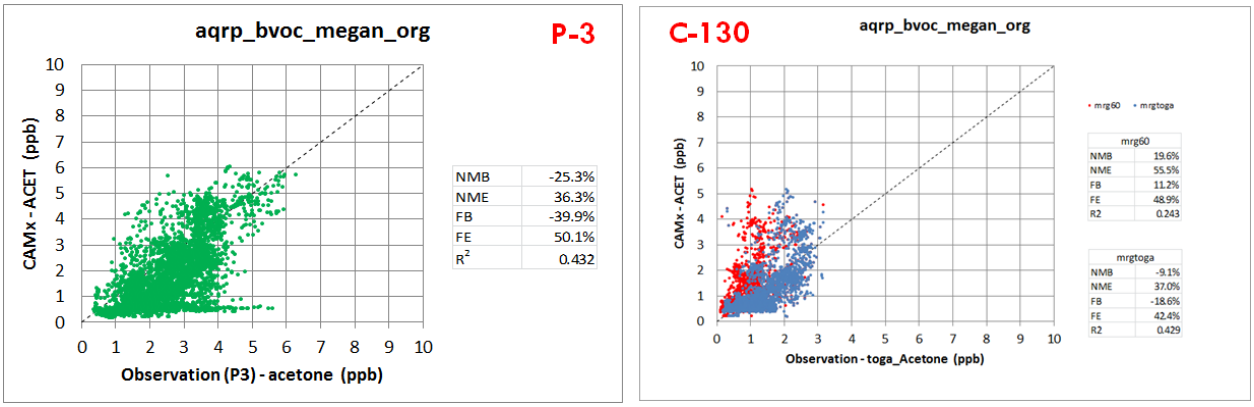

Figure 5-41. Measured and modeled acetone along the P-3 (left panel) and C-130 (right panel) aircraft flight tracks for the June 1-July 15, 2013 period. Base run.

Figure 5-42 and Figure 5-43 compare modeled and measured NO_2 for the C-130 and P-3 aircraft data, respectively. In both figures, the region of the NO_2 scale from 0 to 2 ppb has been expanded in the left panel to show additional detail. Both aircraft were most often in low NOx ($NO_2 < 0.5$ ppb) environments, although plumes containing higher values were encountered. Agreement with CAMx is reasonably good for values of $NO_2 < 0.5$ ppb, but the right panels of both Figure 5-42 and Figure 5-43 indicate that the aircraft encountered NOx plumes that were not captured by the model, which has horizontal resolution of 12 km.

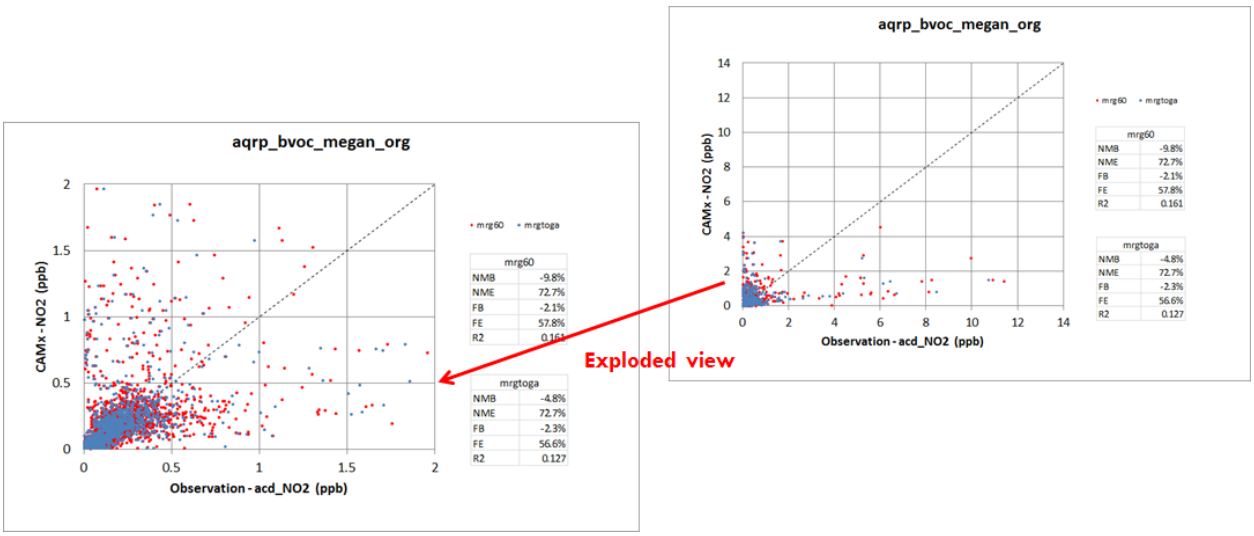

Figure 5-42. Measured and modeled NO_2 along the C-130 aircraft flight tracks for the June 1-July 15, 2013 period. Base run.

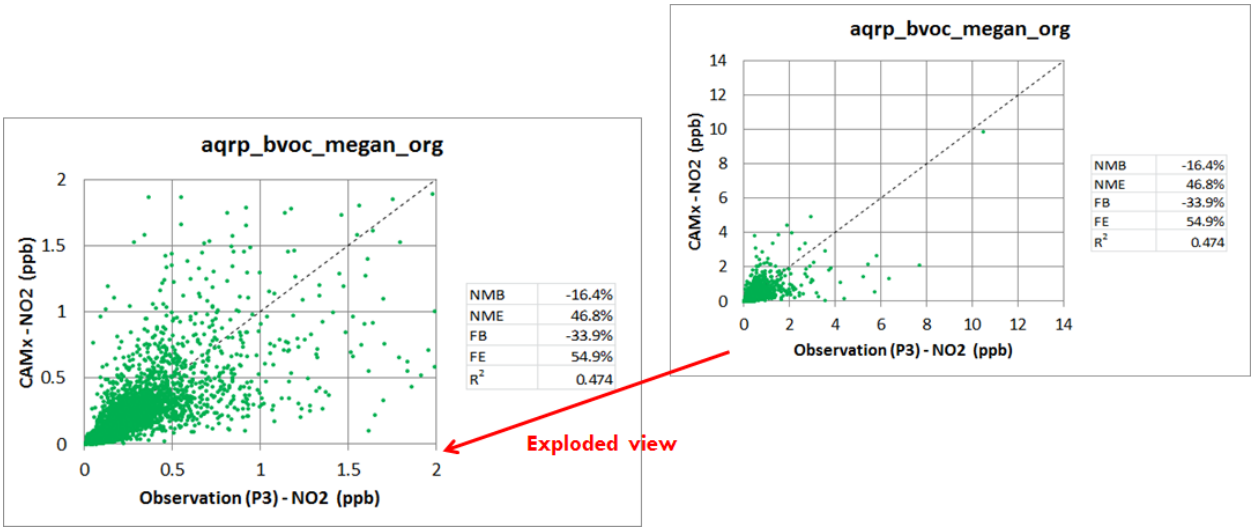

Figure 5-43. Measured and modeled NO_2 along the P-3 aircraft flight tracks for the June 1-July 15, 2013 period. Base run.

For nitric acid (HNO_3), the model performance comparison is strikingly different when CAMx is compared to the P-3 and C-130 data (left and right panels of Figure 5-44, respectively). Compared to the C-130 data, CAMx has a large positive bias (>200%) and a very low R^2 (0.15). The model's positive bias is smaller (8%) for when compared to the P-3 data, although the R^2 value is still quite low (0.34). Aboard the C-130, HNO_3 was measured via a Long-Path Absorption Photometric (LPAP) detector, which appears to have lower sensitivity than the CIMS instrument aboard the P-3.

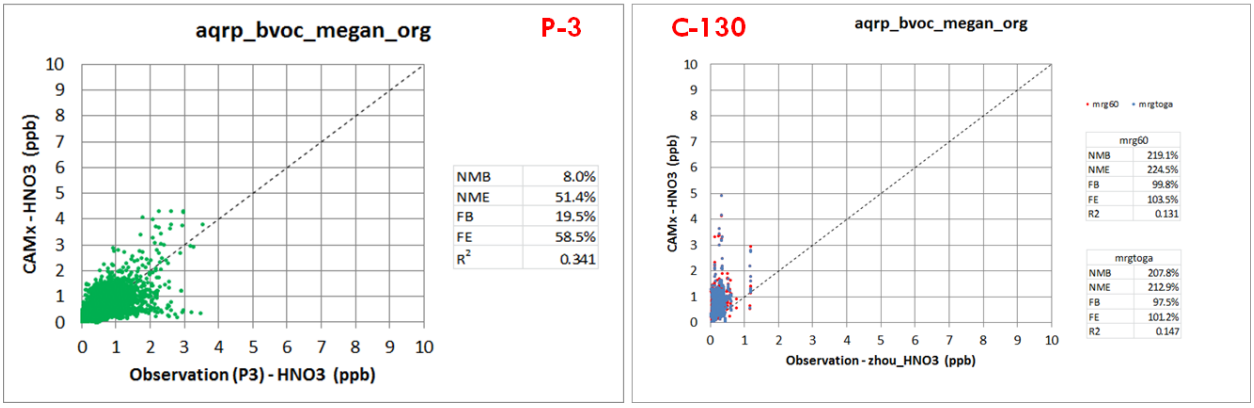

Figure 5-44. Measured and modeled HNO_3 along the P-3 (left panel) and C-130 (right panel) aircraft flight tracks for the June 1-July 15, 2013 period. Base run.

When compared to the P-3 PAN measurements (left panel of Figure 5-45), CAMx has a pronounced high bias (39%), although the R^2 is relatively high at 0.58. There is reasonably good agreement for NOy, with a small positive bias (8.8%) and R^2 of 0.55.

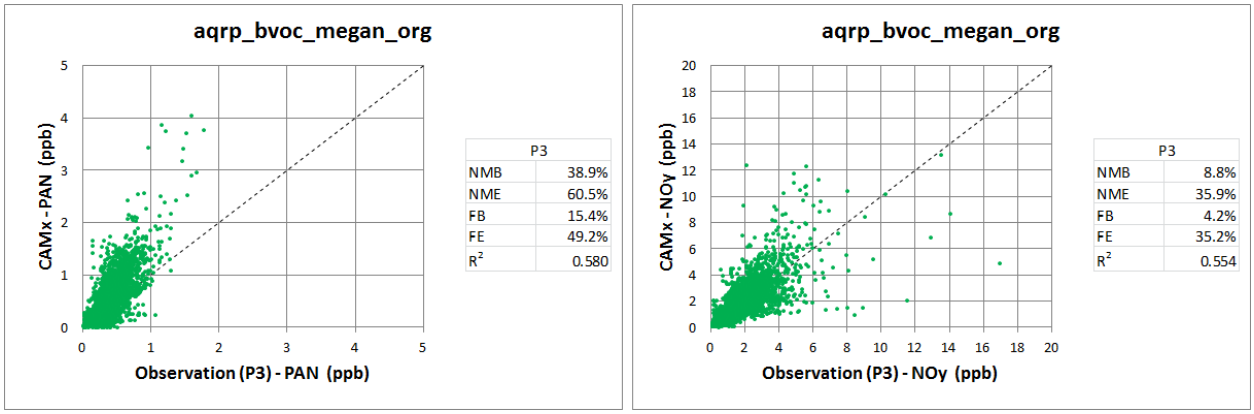

Figure 5-45. Measured and modeled PAN (left panel) and NOy (right panel) along the P-3 aircraft flight tracks for the June 1-July 15, 2013 period. Base run.

For SO_2, agreement between CAMx and the P-3 measurements is better for lower values of SO_2 (left panel of Figure 5-46). Higher observed values of SO_2 associated with localized plumes are not well-captured in the model. The model has an overall high bias and R^2 is low, at 0.19. Agreement is better for CO (right panel of Figure 5-46), for which the model has a slight low bias and reasonably good skill (r^2 of 0.60).

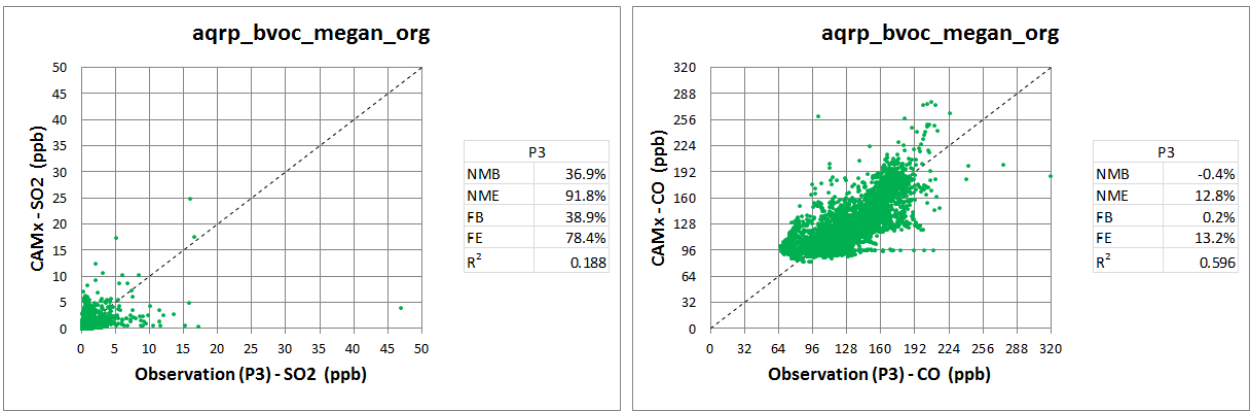

Figure 5-46. Measured and modeled SO_2 (left panel) and CO (right panel) along the P-3 aircraft flight tracks for the June 1-July 15, 2013 period. Base run.

For benzene (Figure 5-47) there is reasonable agreement between modeled and measured values except over hot spots. This could be due to sources that are not present in the model or misalignment of the modeled plume. The highest values observed values of benzene occurred when the aircraft flew over fires and regions of oil and gas development and production. Both are unlikely to be well represented in the model.

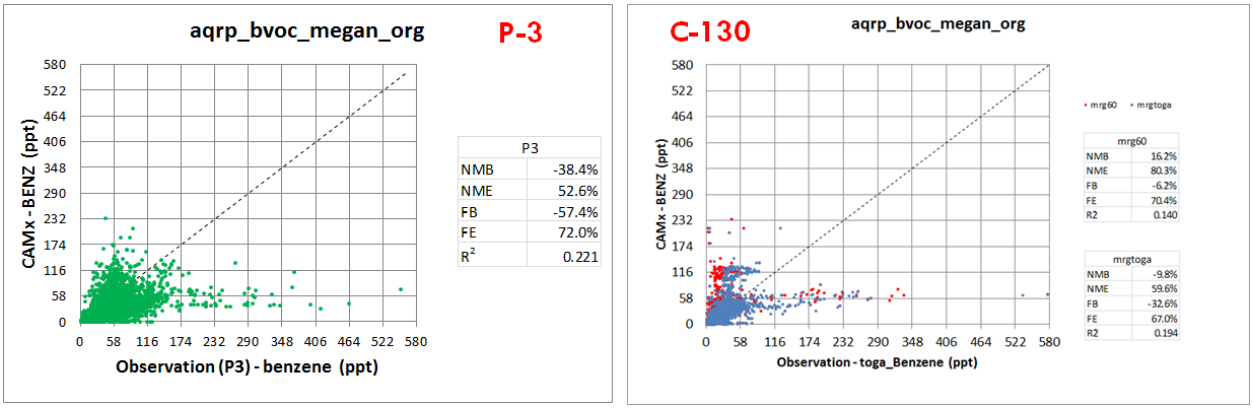

Figure 5-47. Measured and modeled benzene along the P-3 (left panel) and C-130 (right panel) aircraft flight tracks for the June 1-July 15, 2013 period. Base run.

CAMx underestimates propane along the C-130 flight track. This result is consistent with a previous CAMx comparison with INTEX-A propane data (Kemball-Cook et al., 2012). The r^2 of 0.4 shows some skill in modeling spatial distribution of propane sources, however, the magnitude of the propane concentrations is underestimated. This suggests that propane emissions may be underestimated regionally. An important source of propane and ethane emissions which is broadly distributed across the modeling domain is oil and gas exploration and production. The extent to which emissions from oil and gas exploration and production are well-characterized in current emission inventories is a subject of ongoing research (e.g. Petron et al., 2012; Ahmadov, 2015).

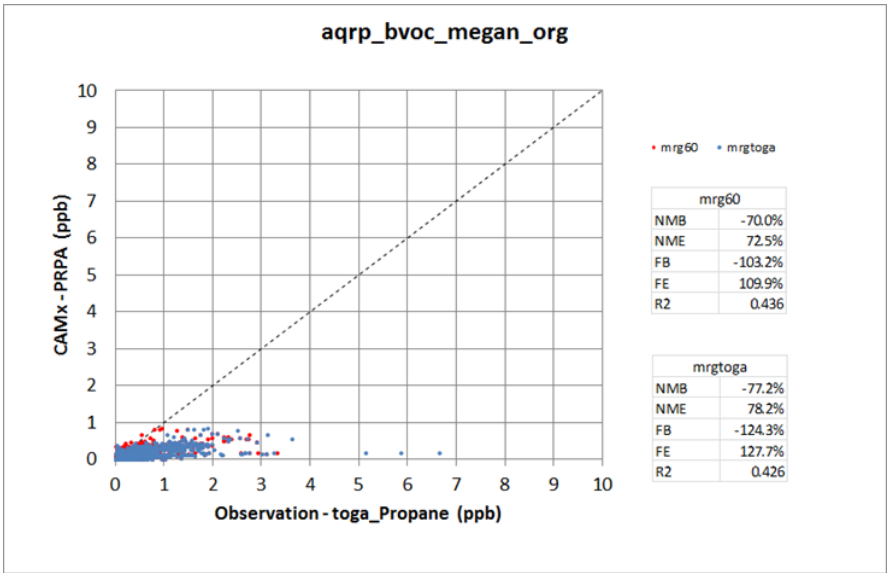

Figure 5-48. Measured and modeled propane along the C-130 aircraft flight tracks for the June 1-July 15, 2013 period. Base run.

5.5.4 CAMx Sensitivity Testing

5.5.4.1 OH Chemistry Sensitivity Test (Run 2)

In this sensitivity test, we altered the CB6r2 chemical mechanism to increase the production of OH from the breakdown of isoprene following the mechanism of Peeters et al. (2013). The purpose of the test was to gauge the model's response to an isoprene mechanism that represents an upper limit on the production of OH from isoprene. CB6r2 reaction 163 shown below in Figure 5-49 was replaced with an updated reaction 163 and reactions 217-220 were added.

163	HPLD = OH + ISPD	Photolysis
Becomes:		
163	HPLD = OH + HO2 + PCLD	Photolysis
217	PCLD = 2 OH + OKET	Photolysis (set J = 0.1 x JNO2)
218	PCLD + NO3 = HNO3 + ISPD	k = 6.00E-12 exp(-1860/T)
219	OKET + HO2 = CO + C2O3 + 2 OH	k = 1.0E-11
220	OKET = CO + C2O3	Photolysis (set J = MGLY)

PCLD has formula C5H5O4 and deposits like HPLD
OKET has formula C4H4O2 and deposits like HPLD

Figure 5-49. Changes to CB6r2 for OH sensitivity test.

Where the standard CB6r2 scheme produces one OH from isomerization, this scheme produces 4 OH. Figure 5-50 shows that this change to the chemical mechanism reduces the high bias in isoprene products from 47% in the Base Run 1 to 15% in the OH sensitivity test for the two C-

130 data sets. In the P-3 comparison, the high bias is reduced from 114% in the Base run to 62% in the Run 2 sensitivity test. The r^2 value is approximately 0.7 for Base and OH sensitivity runs for all three datasets. Increasing OH production from isoprene therefore reduces but does not eliminate the high bias in isoprene products.

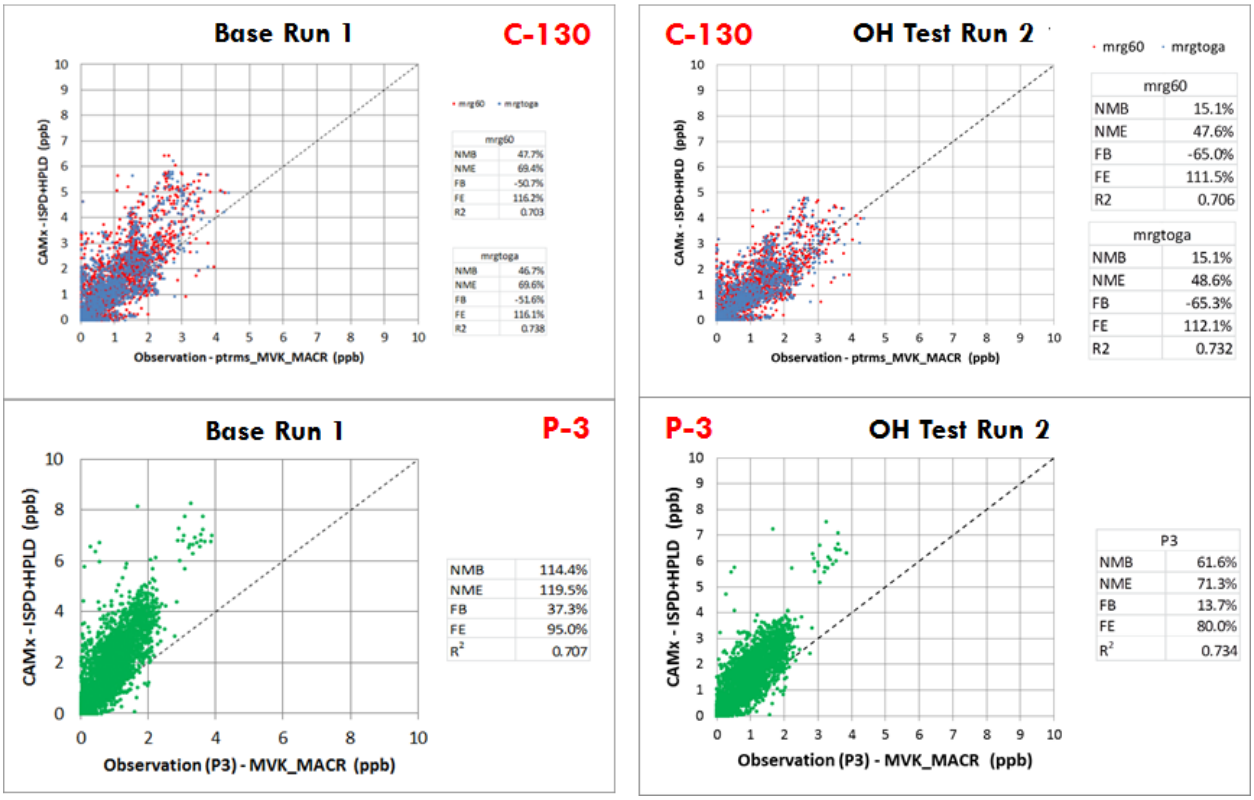

Figure 5-50. Measured and modeled isoprene products along the C-130 (upper panels) and P-3 (lower panels) aircraft flight tracks for the June 1-July 15, 2013 period. Results for Base Run 1 shown in left panels and results for the OH sensitivity test (Run 2) are shown in the right panels.

5.5.4.2 Updated EFvE2015 MEGAN Emissions (Run 3)

We ran CAMx for the June 1-July 15, 2013 episode in a configuration identical to the Base run (Run 1), except that we substituted the MEGAN emission inventory developed using updated EFvE2015 inputs (described in Sections 3 and 4) for the MEGAN inventory developed with default inputs. We then evaluated the CAMx outputs against the C-130 and P-3 data and compared the results to those of the Base run. Figure 5-51 shows that isoprene is overestimated in both the Base Run 1 and in Run 3 in both the C-130 and P-3 data sets, and that the high bias increases from 84% in the Base run to 104% in the Run 3 sensitivity test with updated EFvE2015 MEGAN emissions.

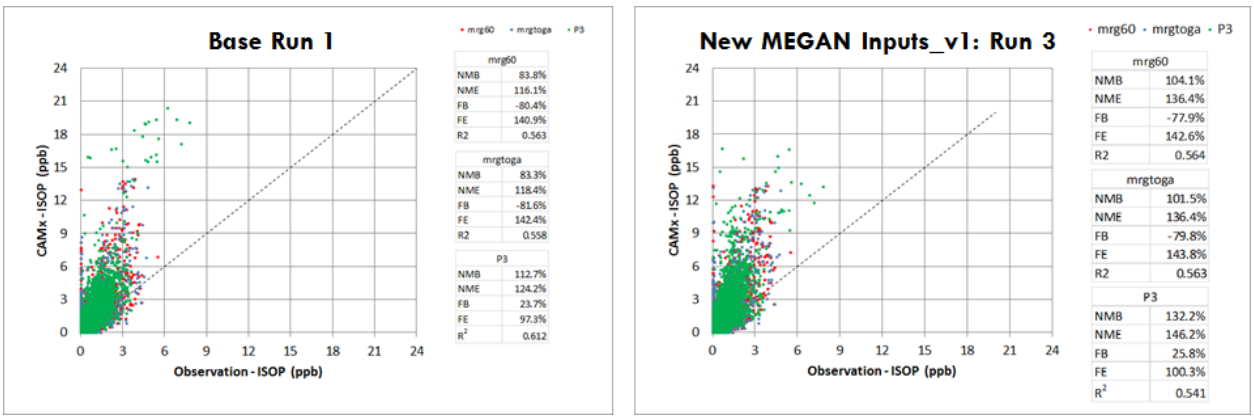

Figure 5-51. Measured and modeled isoprene along the C-130 and P-3 aircraft flight tracks for the June 1-July 15, 2013 period. Left panel: Base Run 1. Right panel: Run 3 sensitivity test with updated EFvE2015 MEGAN emissions.

Monoterpenes are underestimated in Base Run 1 and in Run 3 in both C-130 and P-3 data sets, but the magnitude of the low bias decreases in the Run 3 sensitivity test for the C-130 data and changes to a small positive bias for the P-3 data (Figure 5-52). R^2 values increase slightly for all three data sets but remain relatively low, ranging from 0.5 to 0.21 in Run 3.

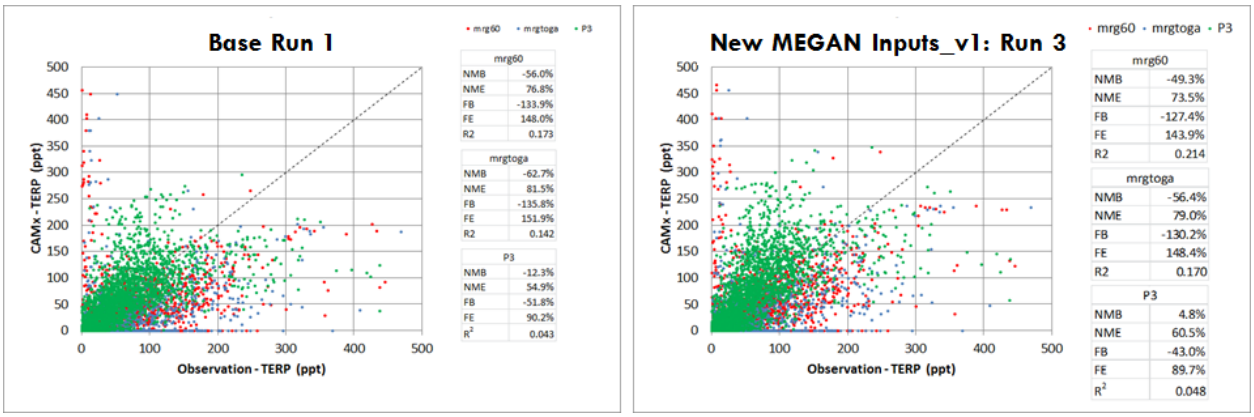

Figure 5-52. Measured and modeled sum of monoterpenes along the C-130 and P-3 aircraft flight tracks for the June 1-July 15, 2013 period. Left panel: Base Run 1. Right panel: Run 3 sensitivity test with updated EFvE2015 MEGAN emissions.

5.5.4.3 Isoprene Emissions Reduction Sensitivity Test (Run 4)

Based on the high bias for isoprene noted in Base Run 1 (Figure 5-31), we divided the MEGAN isoprene emissions by a factor of 2 for all grid cells and times and reran CAMx in the same configuration as Base Run 1 except for the change to the isoprene emissions (Run 4). In contrast to the high bias for isoprene in Base Run 1, isoprene is underestimated in Run 4 in both the C-130 and P-3 data sets and r^2 degrades slightly, as expected based on the brute force nature of the sensitivity test. For the P-3 data, the CAMx Base Run 1 high bias for isoprene products (114%) changed to a low bias of -7% in the Run 4 sensitivity test as a result of the lower isoprene emissions and atmospheric concentrations (Figure 5-53). For the C-130 data,

the CAMx bias for isoprene products changed from 48% to -33% (Figure 5-54). The reduction in the magnitude of bias for isoprene products suggests in this sensitivity test suggests that the MEGAN isoprene emissions are overestimated in the default case.

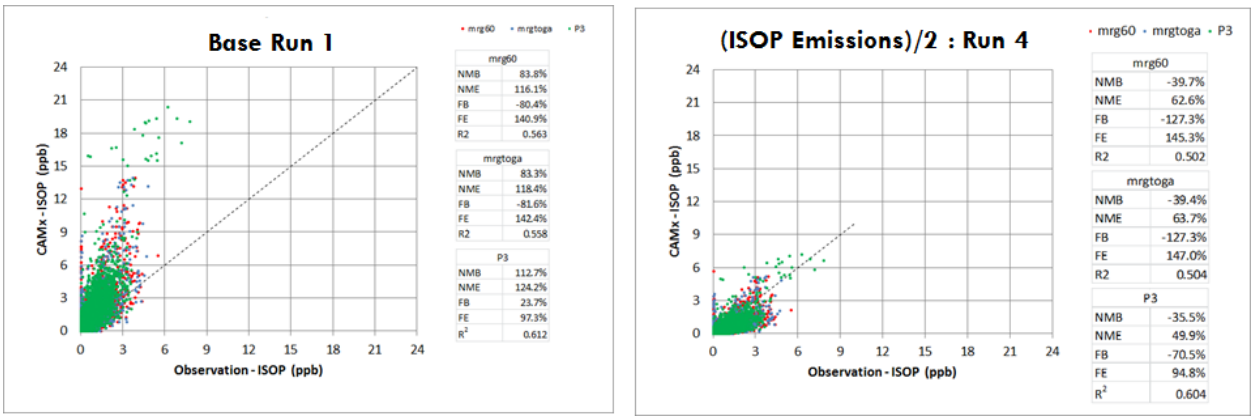

Figure 5-53. Measured and modeled isoprene along the C-130 and P-3 aircraft flight tracks for the June 1-July 15, 2013 period. Results for Base Run 1 shown in left panels and results for the ISOP/2 sensitivity test (Run 4) are shown in the right panels.

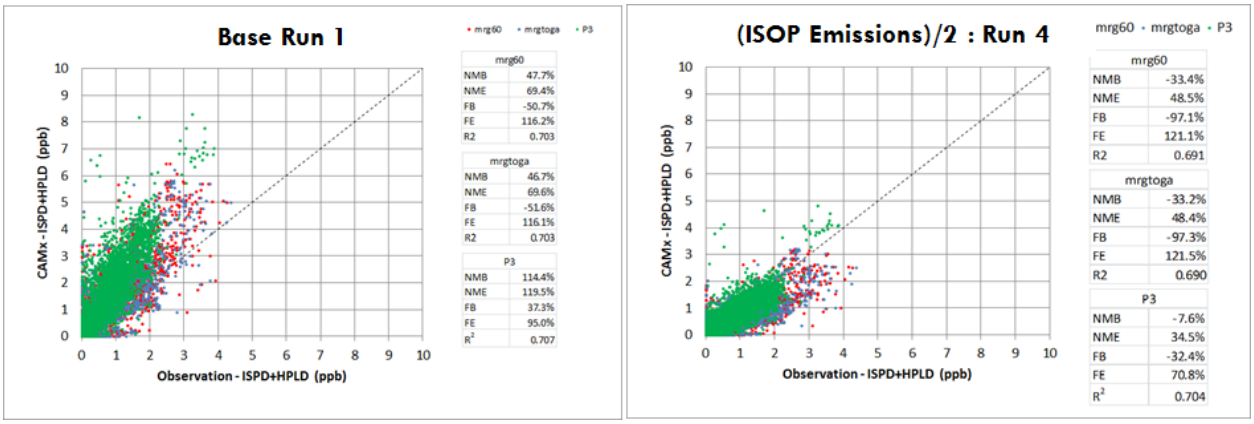

Figure 5-54. Measured and modeled isoprene products along the C-130 and P-3 aircraft flight tracks for the June 1-July 15, 2013 period. Results for Base Run 1 shown in left panels and results for the ISOP/2 sensitivity test (Run 4) are shown in the right panels.

5.5.4.4 Dry Deposition Velocity Sensitivity Test

BVOCs are removed from the atmosphere via dry deposition and accurate simulation of this process is important for modeling atmospheric concentrations of terpenoid species. In June 2013, Nguyen et al. (2015) measured dry deposition velocities for 16 biogenic trace gases in an Alabama forest during the Southern Oxidant and Aerosol Study (SOAS). We evaluated the CAMx Base Run 1 run dry deposition velocities, V_d, against the measurements of Nguyen et al. (2015) and this comparison showed V_d was greatly underestimated for some isoprene products (Figure 5-55).

The CAMx deposition calculation for gases uses an "Rscale" factor to adjust the surface resistance to zero for strong acids (e.g., HNO_3). We performed a sensitivity test to dry deposition of oxygenated VOC species by setting Rscale to zero for the following species:

- EPOX (Epoxide formed from ISPX reaction with OH)
- HPLD (hydroperoxyaldehyde)
- INTR (Organic nitrates from ISO2 reaction with NO)
- ISPX is already zero (Hydroperoxides from ISO2 reaction with HO2)

We also changed the Henry's Law constant for NTR2 (multi-functional organic nitrates) to $2x10^6$. This has no influence on oxidants, but provides a diagnostic of whether the Henry's Law constant increase is sufficient to produce agreement in deposition velocity for an isoprene nitrate-like species.

For the comparison of modeled and measured V_d, we took a daytime average from 10:00-15:00 local time and compared against measured and GEOS-Chem values reported in Nguyen et al. (2015) (Figure 5-55). There were large increases in V_d in the CAMx sensitivity test due to the change in the Rscale factors for HPLD, EPOX, INTR and NTR2.

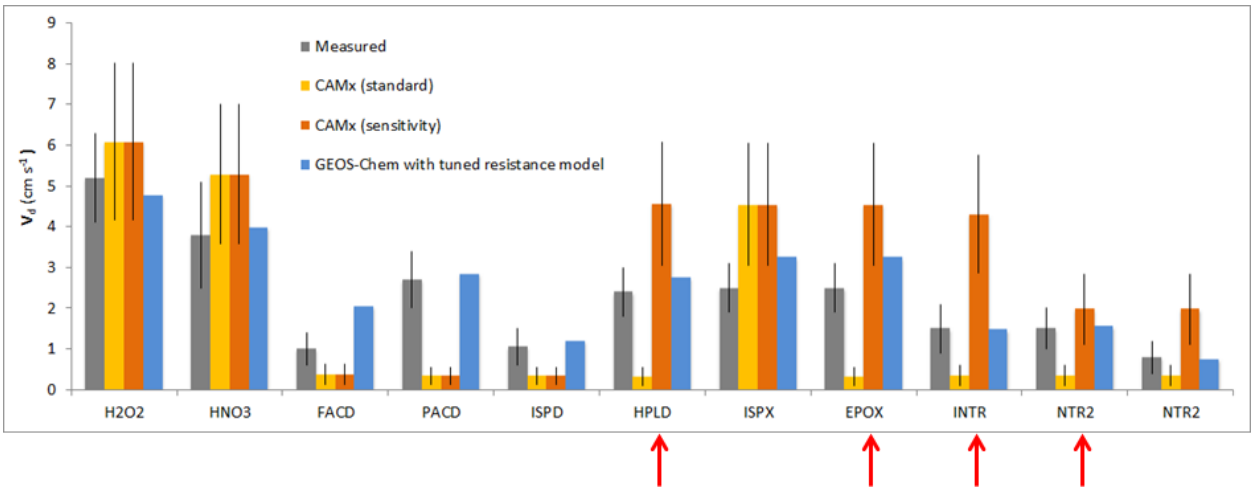

Figure 5-55. Daytime mean V_d from measured values from SOAS (Nguyen et al. 2015), CAMx Base Run 1 (standard), the CAMx Run 5 sensitivity test and GEOS-Chem using a tuned resistance model, as reported in Nguyen et al. (2015).

We compared the CAMx mean V_d diurnal cycle with the measured diurnal cycles reported in Nguyen et al. (2015) for ISPX and EPOX (Figure 5-56), HPLD and INTR and isoprene products (Figure 5-57). There is much closer agreement with observations in Run 5 compared with the Base Run 1 for all species. However, in Run 5, the morning increase and evening decrease in V_d are too rapid in CAMx, which contributes to the V_d overestimates shown in Figure 5-55.

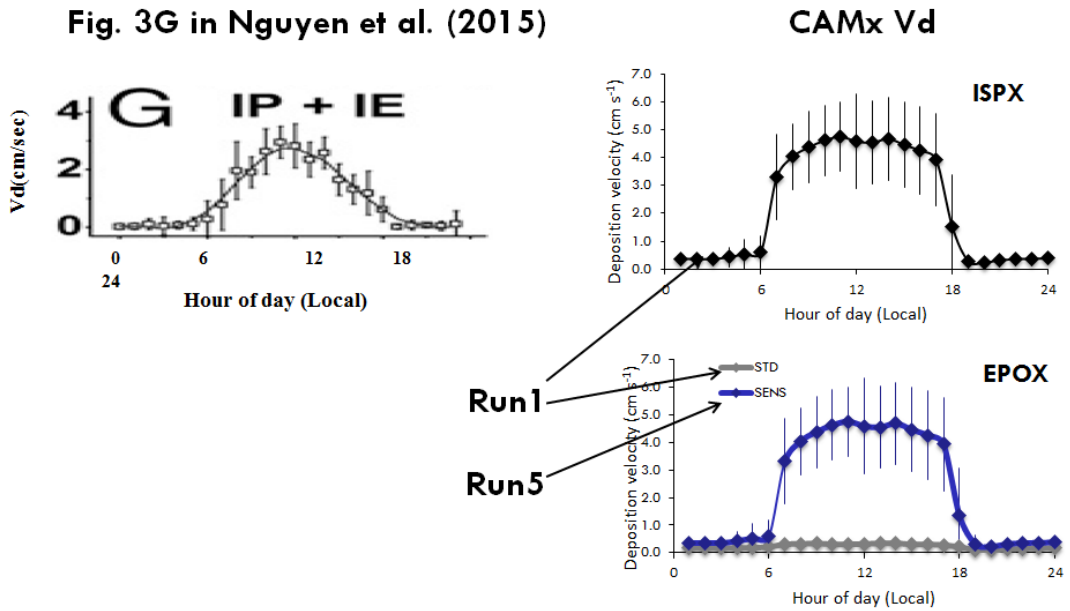

Figure 5-56. V_d diurnal cycle evaluation for ISPX and EPOX. Note that Rscale is already set to zero for ISPX so results for Run 1 and Run 5 are identical for ISPX. For Nguyen et al. (2015) results, IP+IE is the sum of isoprene hydroxy hydroperoxides and epoxydiols (ISOPOOH + IEPOX).

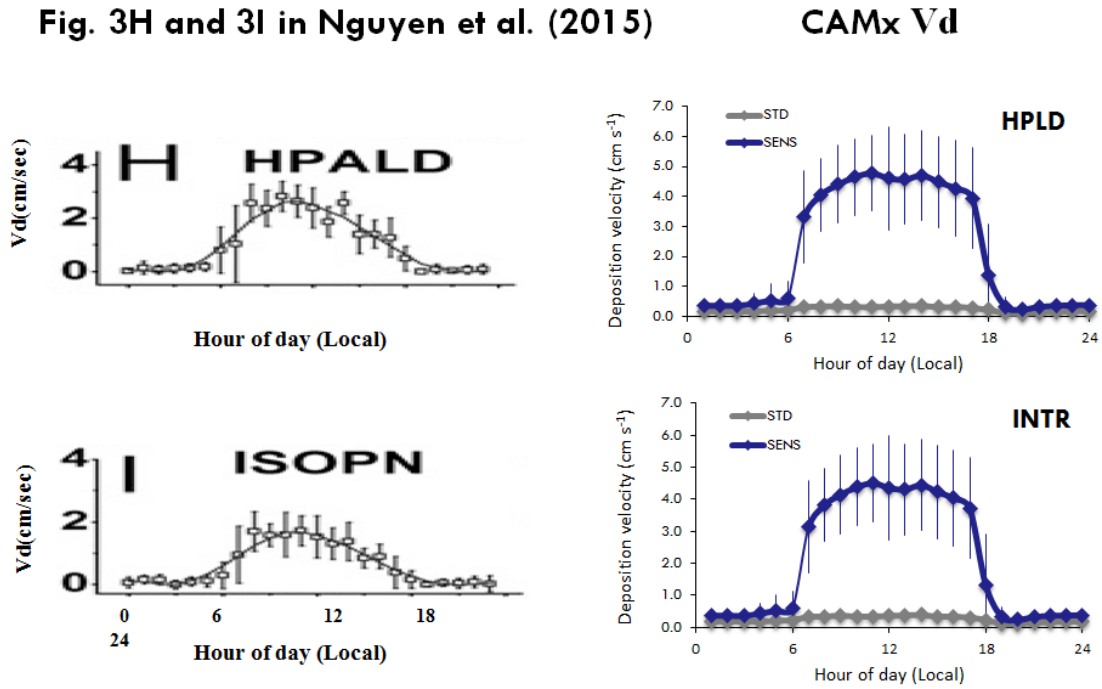

Figure 5-57. V_d diurnal cycle evaluation for hydroperoxyaldehydes (abbreviated HPALD and HPLD) and isoprene hydroxy nitrates (abbreviated ISOPN for Nguyen et al. [2015] results).

The effects of changes to dry deposition in Run 5 on modeled ozone and isoprene and monoterpenes species were small; Run 5 results were nearly identical to the Base Run 1 and are not shown. A statistical summary of the results of the comparison for ozone and other species against aircraft data for Run 5 is shown in Figure 5-64 through Figure 5-67.

5.5.4.5 Updated EFvA2015 MEGAN Emissions Sensitivity Test (Run 6)

This test is similar to that performed in Run 3, except that we substituted the MEGAN emission inventory developed using updated EFvA2015 inputs (described in Sections 3 and 4) for the MEGAN inventory developed with default EFvE2011 inputs (Base, Run 1). We then evaluated the CAMx outputs against the C-130 and P-3 data and compared the results to those of the Base Run 1 and Run 3.

Figure 5-58 shows that isoprene is overestimated in both the Base Run 1 and in Run 3 in both the C-130 and P-3 data sets, but the high bias decreases from 84%-113% in the Base run and 104%-132% in the Run 3 sensitivity test with updated EFvE2015 MEGAN emissions to the range -5% to -16% in the Run EFvA2015 sensitivity test. This indicates that the use of the EFvA2015 emission factors for isoprene improves the CAMx model's ability to reproduce the isoprene concentrations measured by the P-3 and C-130 aircraft. Although the high bias seen in Base Run 1 and EFvE2015 Run 3 is reduced in EFvA2015 Run 6, Run does not show an improvement in correlation between observed and modeled values. R^2 values worsen slightly in Run 6 relative to Base Run 1 and Run 3.

Figure 5-59 shows that Run 6, like Base Run 1, reproduces many of the observed variations of isoprene (higher isoprene concentrations over Northeast Texas, lower concentrations over northern Mississippi), and that the CAMx overestimates of isoprene in the Base Run are improved in Run 6. However, there are regions where the model's skill in reproducing observed isoprene does not improve in Run 6. For example, both model runs predict high isoprene over eastern Tennessee, where the observations show low values.

Figure 5-60 indicates that the use of the EFvA2015 emission factors in MEGAN emissions greatly reduces the high bias for isoprene products seen in Base Run 1 and Run 3 (EFv2015). In Run 6, the bias ranges between -16% and 14%. The R^2 value in Run 6 is comparable to that of Run 3 and both are slightly lower than in the Base Run 1. The high bias for acetaldehyde seen in Run 1 is neutralized with Run 6 bias ranging from -20% to +15% depending on aircraft (Figure 5-65; Figure 5-67).

In Figure 5-61, the evaluation for monoterpenes is shown. Performance in Run 6 is comparable to that of the Base Run 1. As for the other sensitivity tests, modeled ozone was not significantly affected in Run 6 (Figure 5-62). OH was measured aboard the C-130 aircraft only, and none of the three simulations was skilful in simulating the observed OH (R^2 is less than 0.1 for all three runs shown in Figure 5-63). However, the OH measurements are regarded as uncertain. In Run 6, there is a small high bias for OH (9%) compared to the low bias (-5%-7%) seen in Base Run 1 and Run 3. It is not clear whether Run 6 represents improved or worsened performance for OH.

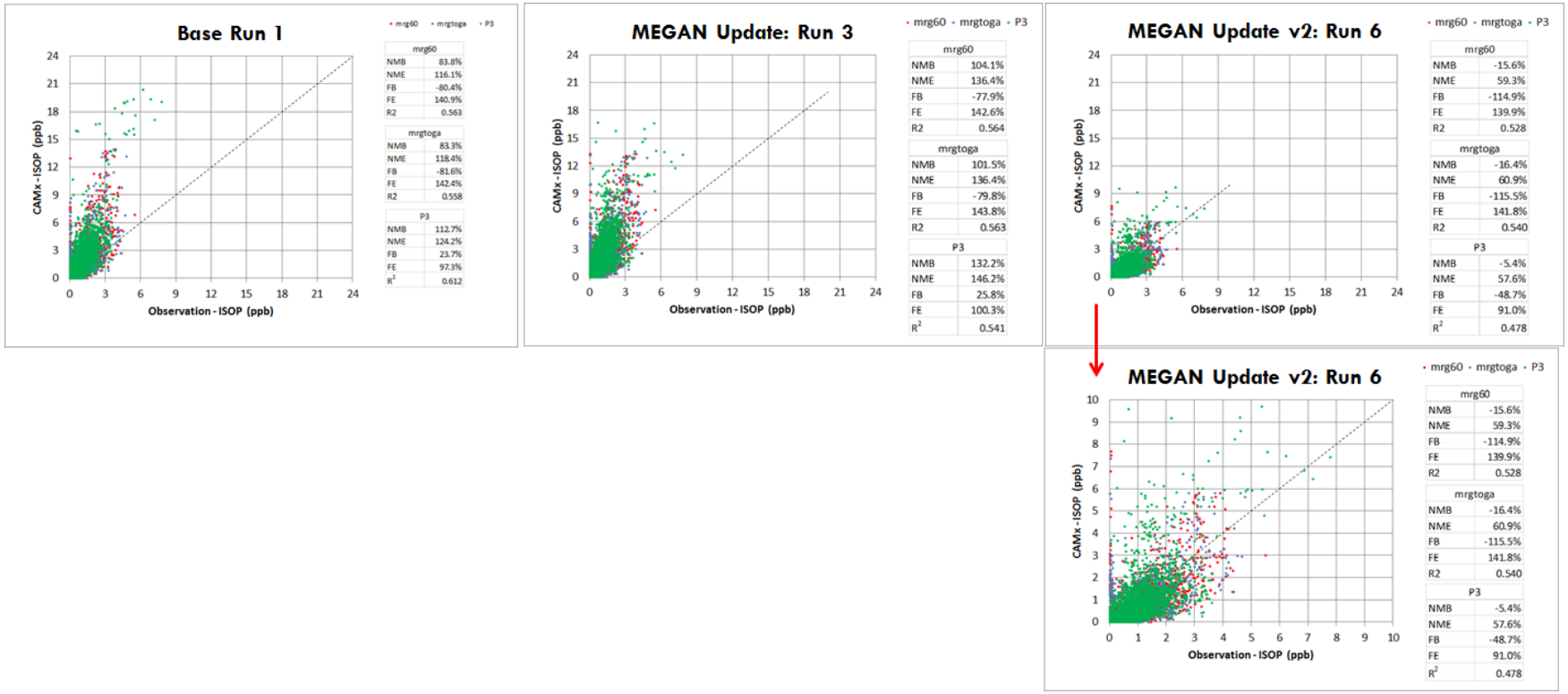

Figure 5-58. Measured and modeled isoprene along the C-130 (mrg60 and mrgtoga data sets) and P-3 aircraft flight tracks for the June 1-July 15, 2013 period. Results for Base Run 1 shown in left panel and results for the Updated_EFvE2015 MEGAN inputs sensitivity test (Run 3) are shown in the center panel. Upper and lower right panels are results for the Updated_EFvA2015 MEGAN inputs sensitivity test (Run 6). Lower right panel shows same data as upper right panel but on scales with lower maxima.

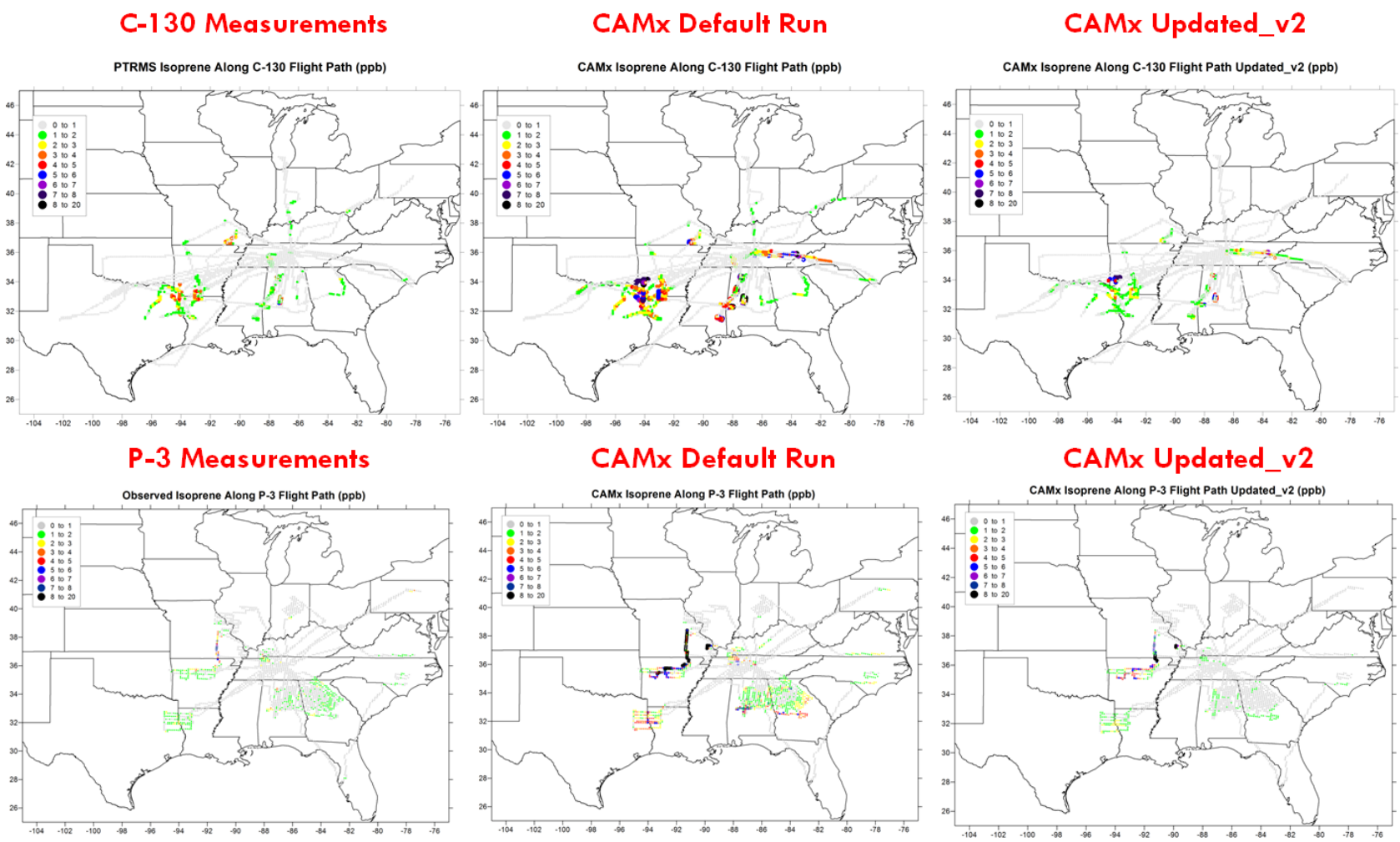

Figure 5-59. Measured and modeled isoprene along the C-130 (upper panels) and P-3 (lower panels) flight tracks for the June 1-July 15, 2013 period. Center panels are CAMx default run (Run 1) and right panels are CAMX updated_EFvA2015 run (Run 6).

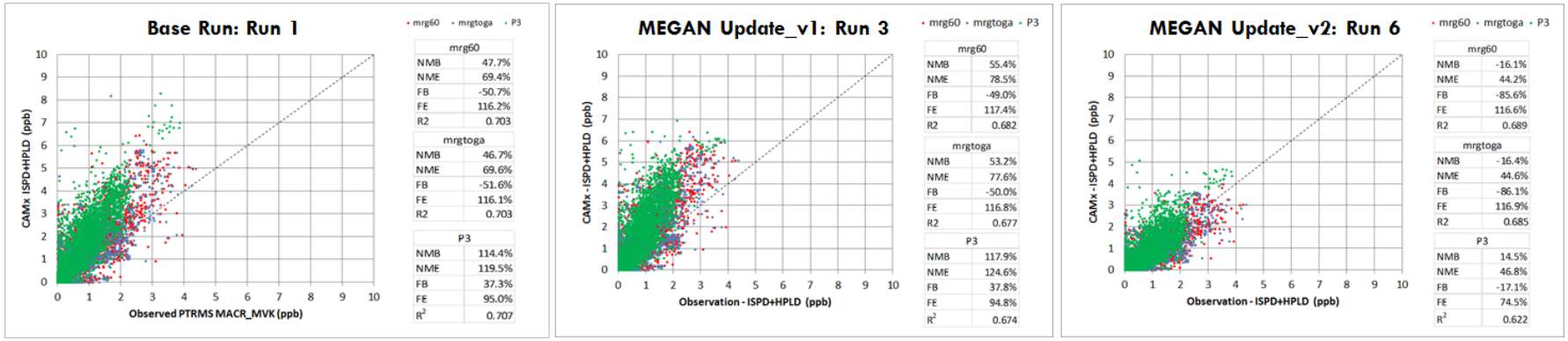

Figure 5-60. Measured and modeled isoprene products along the C-130 and P-3 aircraft flight tracks for the June 1-July 15, 2013 period. Results for Base Run 1 shown in left panel and results for the Updated_EFvE2015 MEGAN inputs sensitivity test (Run 3) are shown in the center panel. Upper and lower right panels are results for the Updated_EFvA2015 MEGAN inputs sensitivity test (Run 6).

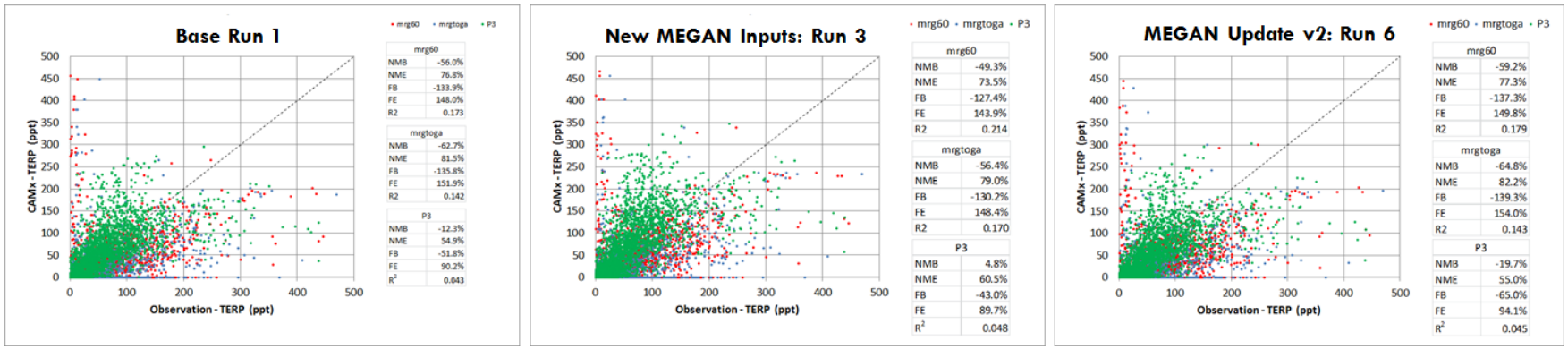

Figure 5-61. Measured and modeled monoterpenes along the C-130 (mrg60 and mrgtoga data sets) and P-3 aircraft flight tracks for the June 1-July 15, 2013 period. Results for Base Run 1 shown in left panel and results for the Updated_EFvE2015 MEGAN inputs sensitivity test (Run 3) are shown in the center panel. Upper and lower right panels are results for the Updated_EFvA2015 MEGAN inputs sensitivity test (Run 6).

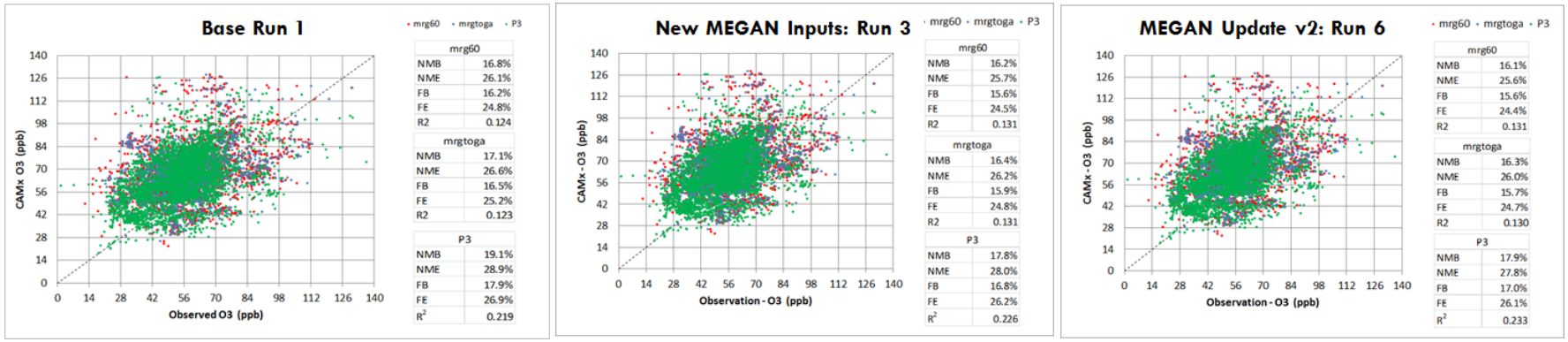

Figure 5-62. Measured and modeled ozone along the C-130 (mrg60 and mrgtoga data sets) and P-3 aircraft flight tracks for the June 1-July 15, 2013 period. Results for Base Run 1 shown in left panel and results for the Updated_EFvE2015 MEGAN inputs sensitivity test (Run 3) are shown in the center panel. Upper and lower right panels are results for the Updated_EFvA2015 MEGAN inputs sensitivity test (Run 6).

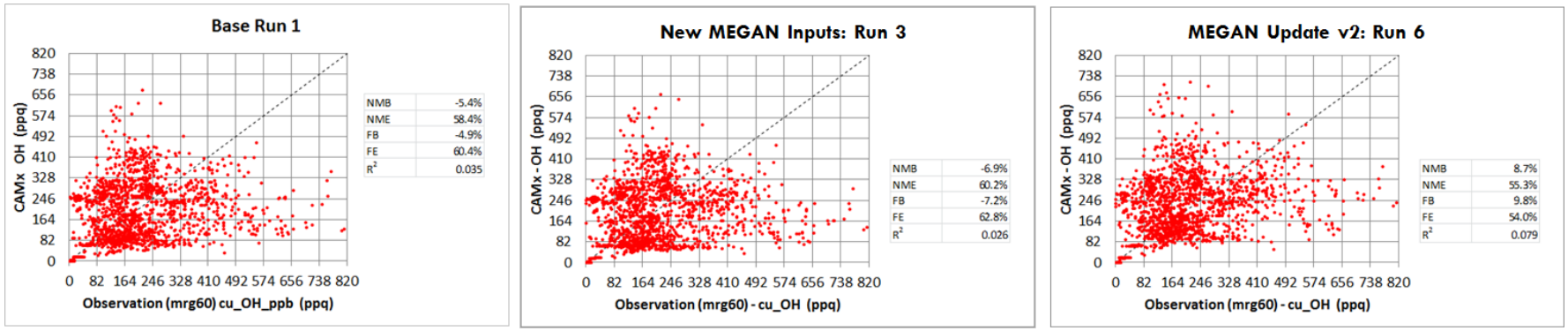

Figure 5-63. Measured and modeled OH along the C-130 aircraft flight tracks for the June 1-July 15, 2013 period. Results for Base Run 1 shown in left panel and results for the Updated_EFvE2015 MEGAN inputs sensitivity test (Run 3) are shown in the center panel. Upper and lower right panels are results for the Updated_EFvA2015 MEGAN inputs sensitivity test (Run 6)

5.5.5 Summary of CAMx Modeling

CAMx model performance in the Base Run and the sensitivity tests is summarized in Figure 5-64 through Figure 5-67, which indicate how the NMB varied among the different CAMx runs as the model results were compared to measurements made aboard the C-130 and P-3 aircraft.

The best overall performance for the subset of species (isoprene, isoprene products, sum of monoterpenes, ozone, OH) shown in Figure 5-64 and Figure 5-66 occurred in the EFvA2015 isoprene emissions sensitivity test (Run 6). In Run 3, the sensitivity test with updated MEGAN emissions EFv2015, the CAMx bias for monoterpenes improved, but the overall bias for isoprene, isoprene products and OH increased. The NMB for ozone was nearly unchanged across all CAMx runs, which indicates that modeled ozone along the aircraft flight track was not sensitive to changes in the specification of the biogenic emissions, changes to isoprene chemical mechanism or rates of OVOC deposition. Modeled ozone shows persistent overestimates that are caused by other processes which are currently not well understood.

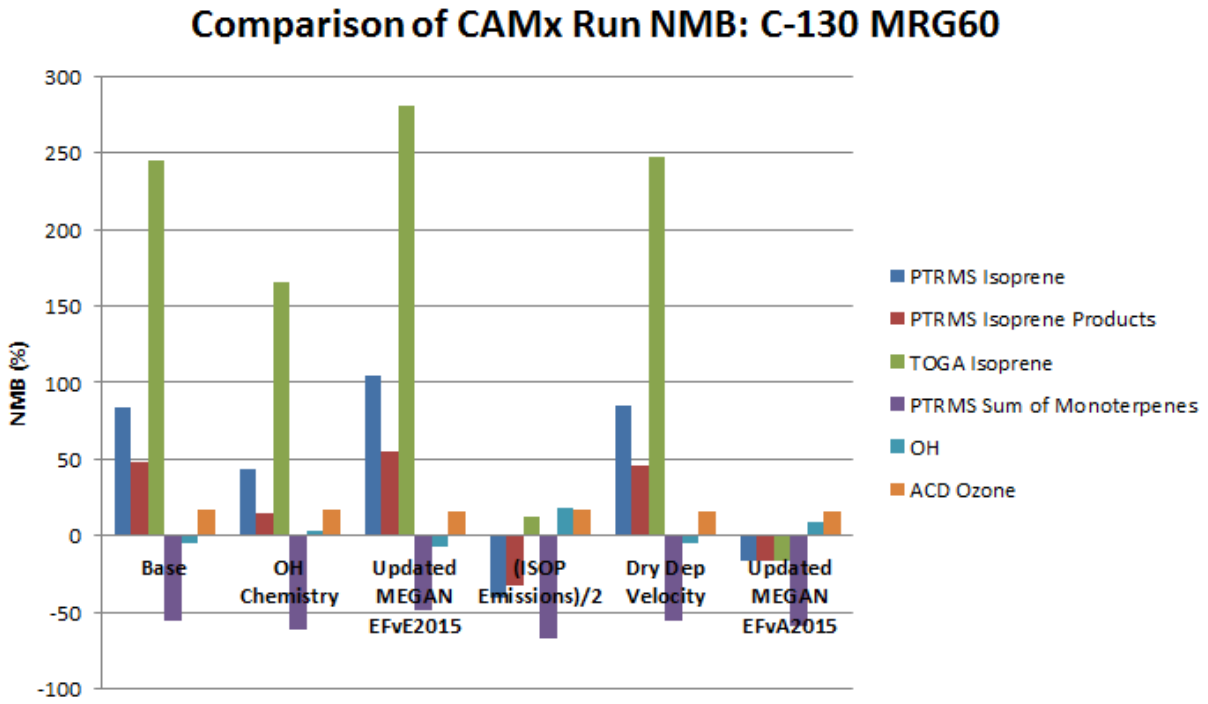

Figure 5-64. Summary of variation of NMB for the CAMx Base Run and sensitivity test results when model results were compared to C-130 measurements for a subset of key species. ACD indicates measurements made via chemiluminescence detection.

	Mean Normalized Bias (%)					
	Run 1	Run 2	Run 3	Run 4	Run 5	Run 6
Species	Base	OH Chemistry	Updated MEGAN EFvE2015	(ISOP Emissions)/2	Dry Dep Velocity	Updated MEGAN EFvA2015
PTRMS Isoprene	84	43	104	-40	85	-16
TOGA Isoprene	245	165	280	12	247	-16
PTRMS Isoprene Products	48	15	55	-33	46	-16
ACD Ozone	17	17	16	17	16	16
PTRMS Sum of Monoterpenes	-56	-61	-49	-67	-56	-59
OH	-5	3	-7	18	-5	9
TOGA Formaldehyde	20	24	22	-10	19	-26
PTRMS Methanol	-54	-55	-48	-57	-54	18
TOGA Methanol	5	4	23	-0.5	5	-10
TOGA Acetone	20	14	20	0.5	19	-20
TOGA Benzene	16	13	17	8	16	-14
Zhou HNO3	219	224	211	250	201	234
ACD NO2	-10	-17	-13	-5	-11	-9
ACD NO	-22	-30	-24	-13	-23	-17
TOGA Acetaldehyde	180	155	202	103	177	-20
PTRMS Acetaldehyde	-42	-48	-39	-60	-43	6

|MNB| < |MNB of Run 1|
|MNB| > |MNB of Run 1|
< 1% change in MNB

Figure 5-65. Summary of variation of NMB for the CAMx Base Run and sensitivity test results when model results were compared to C-130 mrg60 measurements. ACD indicates species measurement made via chemiluminescence detection.

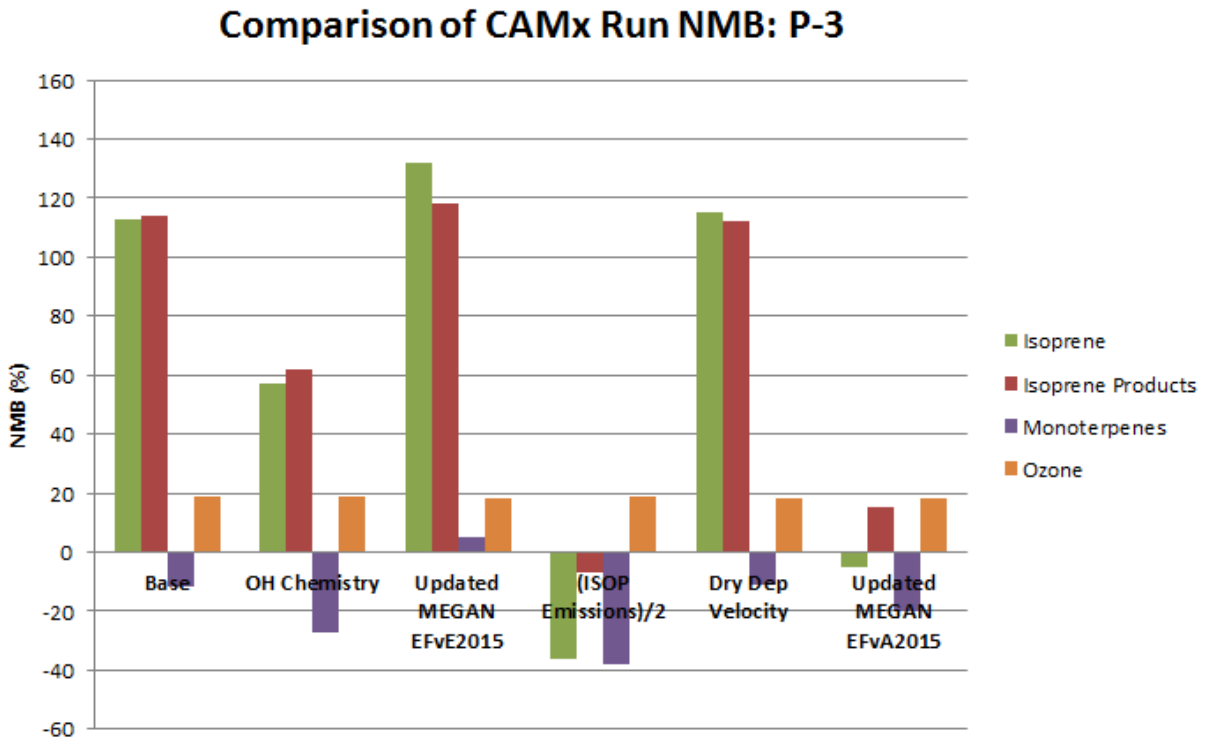

Figure 5-66. Summary of variation of NMB for the CAMx Base Run and sensitivity test results when model results were compared to P-3 measurements.

Species	Mean Normalized Bias (%)					
	Run 1	Run 2	Run 3	Run 4	Run 5	Run 6
	Base	OH Chemistry	Updated MEGAN EFvE2015	(ISOP Emissions)/2	Dry Dep Velocity	Updated MEGAN EFvA2015
Isoprene	113	57	132	-36	115	-5
Isoprene Products	114	62	118	-7	112	15
Ozone	19	19	18	19	18	18
Ozone CARDS	24	24	23	24	23	23
Monoterpenes	-12	-27	5	-38	-11	-20
SO2	37	34	37	30	37	32
Formaldehyde	-9	-7	-10	-36	-11	-31
Methanol	-29	-30	-15	-33	-29	-19
NOy	9	11	6	10	0.4	7
Acetone	-25	-30	-25	-41	-26	-38
Benzene	-38	-41	-38	-44	-38	-42
HNO3	8	10	6	21	-0.5	16
NO2 ACES	6	-2	4	15	4	11
NO2 CARDS	-25	-31	-26	-19	-27	-21
NO	-22	-31	-23	-8	-22	-13
NO CaRDS	-62	-65	-62	-55	-62	-57
PAN	39	54	34	21	34	21
Acetaldehyde	48	31	55	-0.1	47	15
CO	-0.4	0.3	0	-6	-0.8	-4.2
HONO	-87	-86	-86	-79	-87	-80
N205	-86	-78	-72	-26	-84	-22

	|MNB| < |MNB of Run 1|
	|MNB| > |MNB of Run 1|
	< 1% change in MNB

Figure 5-67. Summary of variation of NMB for the CAMx Base Run and sensitivity test results when model results were compared to P-3 measurements. ACES indicates measurements made with airborne cavity enhanced spectrometer. CARDS indicates measurements made with cavity ringdown absorption spectrometer. ACD indicates measurements made via chemiluminescence detection.

5.6 Summary of Findings

- Comparison of WRF modeled surface downward shortwave radiation (DSW) with visible satellite images for the C-130 flights indicated that, despite the simulation of sub-grid cloud-radiation feedback, WRF underestimated the observed cloud field and overestimated DSW. Underestimating clouds and overestimating the available shortwave radiation very likely introduced a high bias in the MEGAN isoprene emissions through a high bias in PAR and affected the partitioning of surface heat and moisture fluxes.
- The default and updated MEGAN biogenic emission inventories were compared against aircraft flux data and then evaluated using a photochemical grid model. The evaluation of the isoprene and monoterpene emissions against aircraft flux data showed that the MEGAN v2.1 isoprene emissions were consistently higher than the aircraft flux data calculated along the C-130 racetrack flight segments. This was true for both the default and updated MEGAN emission inventories.
- The default and updated MEGAN monoterpene emissions showed closer agreement with the airborne fluxes than the isoprene emissions, but the MEGAN monoterpene emissions were also generally higher than the airborne fluxes. The MEGAN monoterpene emissions had a spatial pattern similar to the airborne fluxes,

- The comparison between MEGAN emissions and the airborne fluxes is affected by the use of different meteorological data (WRF and NLDAS) in preparing the emissions flux estimates.
- The CAMx model has a high bias for surface ozone that is most pronounced at coastal sites during periods of onshore flow. This suggests that the model is affected by bias in the model boundary conditions for ozone and/or precursors.
- Using both default and updated MEGAN inventories, CAMx spatial patterns of high and low isoprene concentrations were similar to those of the aircraft observations.
- CAMx generally overestimates isoprene along the aircraft flight tracks with bias of 84% in the default MEGAN emissions and 104% in the updated case.
- Although the CAMx modeled high bias for isoprene relative to aircraft observations increased in the run using the updated MEGAN emissions, the CAMx model's performance in simulating ground level ozone improved in the Houston area. The updated MEGAN inventory has significantly lower isoprene emissions in the Houston area, and this appears to reduce ground level ozone, bringing the model into closer agreement with observations.
- Kota et al. (2015) compared the gridded MEGAN isoprene emissions factor for the region north of Houston with isoprene emission factor estimates derived from a field study and found that the MEGAN emission factor was higher. Kota et al. determined that the overestimated emission factor caused a high bias in modeled isoprene concentrations in their Community Multiscale Air Quality (CMAQ) model simulation, but the isoprene overestimates did not significantly influence modeled ozone; this is in contrast to results of our CAMx simulations, in which changes in Houston area isoprene emissions strongly affected modeled ozone.
- Outside of the Houston area and monitoring sites near the eastern border of Texas, the changes in surface ozone due to the change in the MEGAN emission inventory were relatively small.
- In the CAMx runs using default and updated MEGAN emissions, modeled monoterpene concentrations were generally lower than the observed concentrations along the P-3 and C-130 flight tracks. Values of the coefficient of determination were lower for monoterpenes than for isoprene. In the run with updated MEGAN emissions, the magnitude of the CAMx model's low bias for monoterpenes was reduced relative to the run with default emissions.
- Three additional CAMx sensitivity tests were carried out.
    1. We altered the CB6r2 chemical mechanism to increase the production of OH from the breakdown of isoprene following the mechanism of Peeters et al. (2013). The purpose of the test was to gauge the model's response to an isoprene mechanism that represents an upper limit on the production of OH from isoprene. Increasing OH production from isoprene reduces but does not eliminate the high bias in isoprene products.

    2. Based on the high bias for isoprene noted in the CAMx run that used default MEGAN emissions, we reduced the MEGAN isoprene emissions by a factor of 2 for all grid cells and times and reran CAMx. For the P-3 data, the CAMx Base run high bias for isoprene

products (114%) changed to a low bias of -7% in the sensitivity test as a result of the lower isoprene emissions and atmospheric concentrations. For the C-130 data, the CAMx bias for isoprene products changed from 48% to -33%. The reduction in the magnitude of bias for isoprene products in this sensitivity test suggests that the MEGAN isoprene emissions are overestimated in the default case.

3. In June 2013, Nguyen et al. (2015) measured dry deposition velocities (V_d) for biogenic trace gases in an Alabama forest during the Southern Oxidant and Aerosol Study (SOAS). Comparison of CAMx V_d against the measurements showed Vd was underestimated in the model. We increased CAMx dry deposition of these species to improve agreement with the SOAS measurements. The effects of this test on modeled ozone and isoprene and monoterpenes species were small.

- The best overall performance among all CAMx runs for a subset of species (isoprene, isoprene products, sum of monoterpenes, ozone, OH) occurred in the sensitivity test in which isoprene emissions were decreased by a factor of two. The CAMx bias for ozone was nearly unchanged across all CAMx runs.
- In the sensitivity test with updated MEGAN emissions, the CAMx bias for monoterpenes improved, but the overall bias for isoprene, isoprene products and OH increased. This result taken together with the high bias in MEGAN isoprene emissions compared to the aircraft fluxes, suggests that MEGAN isoprene emissions are overestimated in both the default and updated inventories.

6.0 CONCLUSIONS AND RECOMMENDATIONS FOR FUTURE WORK

Below, we provide a summary of findings of this study. As of the writing of this draft, we are completing work on the study. We have developed a new MEGAN biogenic emission inventory and will compare it with airborne fluxes and evaluate its effect on the CAMx modeling. This work will be completed in time for the results to be included in the Final Report. Conclusions from the study will be presented in the Final Report. Below, we present a summary of findings and preliminary recommendations for future work.

6.1 Summary of Findings

- Using a wavelet based approach, fluxes of isoprene and total monoterpenes were estimated using turbulence and proton transfer reaction-mass spectrometry (PTR-MS) measurements made onboard the C-130 aircraft during the 2013 SAS field campaign.
- As expected, the highest isoprene fluxes were observed over broadleaf tree dominated woodland areas, while higher monoterpene fluxes were observed over areas such as longleaf pine woodland in Missouri and conifer and hardwood plantations in Louisiana, Texas, Arkansas and Alabama. The forests in these areas generally have higher fractions of high monoterpene emitting trees such as pines.
- Subsampling was also performed for select C-130 flight legs to simulate VOC observations as collected during SAS on the P-3 aircraft, which used a much longer sampling interval (15 s versus 0.6 s on average for the C-130). The increased sampling interval in the P-3 data added significant uncertainty and error to calculated fluxes for sampling intervals greater than a few seconds. Therefore, Fast Fourier Transform and wavelet based approaches were determined not to be suitable for analyzing VOC fluxes from the P-3 aircraft data in heterogeneous regions.
- Instead, a mass balance approach was used to estimate isoprene emission fluxes from the NOAA P-3 and C-130 data. The emission fluxes derived from the aircraft measurements using the mass balance approach were compared with emissions calculated using the BEIS3 and MEGAN2 models. For the purpose of these comparisons, the emissions were calculated along the flight tracks using the temperature and photoactive radiation (PAR) measured onboard the aircraft.
- Isoprene emissions calculated from BEIS3.12, BEIS3.13, MEGAN2.0, MEGAN2.1 and the MEGAN_E2015 and MEGAN_A2015 models developed in this project were compared to those calculated using the mass balance approach with measured isoprene mixing ratios from the following studies: SENEX (the NOAA contribution to the SAS campaign), NOMADSS, TexAQS2000, TexAQS2006, ICARTT2004 and SOS1999. The comparison showed that in general, MEGAN gives higher emissions than BEIS, but that the MEGAN_E2015 and MEGAN_A2015 models developed here provide emissions that are much closer to BEIS results. The results from the C-130 (NOMADSS) and P-3 (SENEX) measurements during SAS compared very similarly with the emissions inventories. In general, the emissions according to BEIS3.12 and the MEGAN_A2015 and MEGAN_E2015 models are closest to the emissions estimated from the measurements. However, the uncertainties in the emissions estimated

from the measurements are significant and do not allow a decision to be made as to which emissions model is more accurate.

- We developed an updated LAI database for all of North America based on the 2013 MODIS (MOderate Resolution Imaging Spectroradiometer) satellite product (MCD15A2.005) and applied maximum green vegetation fraction from USGS (http://landcover.usgs.gov/green_veg.php), which is also based on MODIS remote sensing products.
- An updated 30-meter resolution PFT database (PFT16v2015) was developed for the continental US based on various ground survey, remote sensing and land surface model data products. The PFT16v2015 database provided the starting point for development of a high-resolution (30 m) emission factor (EF) database for the continental US. The resulting EFs were then compared with the PFT16v2011 EF database (Guenther et al., 2012). The EFs were then compared to EFs that were based on aircraft flux measurements.
- Compared with the EFv2011 data, the EFvE2015 data predicts higher isoprene emission factors in some regions in the southeastern US, with the biggest differences in north Florida, central Texas, Oklahoma and Arkansas. Higher broadleaf deciduous tree coverages are also predicted for these areas in the PFT16v2015 database. On the other hand, lower broadleaf deciduous tree coverages were predicted in PFT16v2015 database for southeast Missouri and northern Minnesota, which also has lower isoprene emission factors in the EFvE2015 database. The differences are mainly due to the incorporation of the LandFire existing vegetation type (EVT) data, which provides more spatial details than the land cover dataset used to develop the EFv2011 dataset.
- Aircraft observations were used to evaluate and constrain MEGAN emission factors. The wavelet based approach provides isoprene and monoterpene flux data at high spatial resolution. Surface fluxes of BVOCs were calculated using a vertical flux divergence correction method that assumes a linear relationship between fluxes at different altitudes.
- The estimation of EAF and airborne EF showed consistent results, and they suggest that the developed land cover EF (EFvE2015 database) reasonably captured the variations of BVOC emissions among different EVTs. We calculated mean airborne EF for isoprene using different approaches and their correlations with landcover EF (EFvE2015 database). The correlations between airborne EF calculated using different approaches and the landcover based EFvE2015 data range from 0.32 to 0.73.
- The airborne EFs calculated using WRF or using NLDAS meteorological data are considerably different. The WRF based EF values are consistently lower due to higher EAF values estimated by WRF. This is likely due to a high bias in solar radiation and temperature due to underestimates of aerosol and clouds. We have used the NLDAS data for our analysis because it includes assimilation of observed meteorology. However, the substantial differences (~37%) between the WRF and NLDAS results demonstrate the importance of having accurate meteorological observations to determine airborne EFs.
- Comparison of WRF modeled surface downward shortwave radiation (DSW) with visible satellite images for the C-130 flights indicated that, despite the simulation of sub-grid cloud-radiation feedback, WRF underestimated the observed cloud field and overestimated DSW.

Underestimating clouds and overestimating the available shortwave radiation very likely introduced a high bias in the MEGAN isoprene emissions through a high bias in PAR and affected the partitioning of surface heat and moisture fluxes.

- The default and updated MEGAN biogenic emission inventories were compared against aircraft flux data and then evaluated using a photochemical grid model. The evaluation of the isoprene and monoterpene emissions against aircraft flux data showed that the MEGAN v2.1 isoprene emissions were consistently higher than the aircraft flux data calculated along the C-130 racetrack flight segments. This was true for both the default and updated MEGAN emission inventories.
- The default and updated MEGAN monoterpene emissions showed closer agreement with the airborne fluxes than the isoprene emissions, but the MEGAN monoterpene emissions were also generally higher than the airborne fluxes. The MEGAN monoterpene emissions had a spatial pattern similar to the airborne fluxes,
- The comparison between MEGAN emissions and the airborne fluxes is affected by the use of different meteorological data (WRF and NLDAS) in preparing the emissions flux estimates.
- The CAMx model has a high bias for surface ozone that is most pronounced at coastal sites during periods of onshore flow. This suggests that the model is affected by bias in the model boundary conditions for ozone and/or precursors.
- Using both default and updated MEGAN inventories, CAMx spatial patterns of high and low isoprene concentrations were similar to those of the aircraft observations.
- CAMx generally overestimates isoprene along the aircraft flight tracks with bias of 84% in the default MEGAN emissions and 104% in the updated case.
- Although the CAMx modeled high bias for isoprene relative to aircraft observations increased in the run using the updated MEGAN emissions, the CAMx model's performance in simulating ground level ozone improved in the Houston area. The updated MEGAN inventory has significantly lower isoprene emissions in the Houston area, and this appears to reduce ground level ozone, bringing the model into closer agreement with observations.
- Kota et al. (2015) compared the gridded MEGAN isoprene emissions factor for the region north of Houston with isoprene emission factor estimates derived from a field study and found that the MEGAN emission factor was higher. Kota et al. determined that the overestimated emission factor caused a high bias in modeled isoprene concentrations in their Community Multiscale Air Quality (CMAQ) model simulation, but the isoprene overestimates did not significantly influence modeled ozone; this is in contrast to results of our CAMx simulations, in which changes in Houston area isoprene emissions strongly affected modeled ozone.
- Outside of the Houston area and monitoring sites near the eastern border of Texas, the changes in surface ozone due to the change in the MEGAN emission inventory were relatively small.
- In the CAMx runs using default and updated MEGAN emissions, modeled monoterpene concentrations were generally lower than the observed concentrations along the P-3 and C-

130 flight tracks. Values of the coefficient of determination were lower for monoterpenes than for isoprene. In the run with updated MEGAN emissions, the magnitude of the CAMx model's low bias for monoterpenes was reduced relative to the run with default emissions.

- Three additional CAMx sensitivity tests were carried out.
  4. We altered the CB6r2 chemical mechanism to increase the production of OH from the breakdown of isoprene following the mechanism of Peeters et al. (2013). The purpose of the test was to gauge the model's response to an isoprene mechanism that represents an upper limit on the production of OH from isoprene. Increasing OH production from isoprene reduces but does not eliminate the high bias in isoprene products.

  5. Based on the high bias for isoprene noted in the CAMx run that used default MEGAN emissions, we reduced the MEGAN isoprene emissions by a factor of 2 for all grid cells and times and reran CAMx. For the P-3 data, the CAMx Base run high bias for isoprene products (114%) changed to a low bias of -7% in the sensitivity test as a result of the lower isoprene emissions and atmospheric concentrations. For the C-130 data, the CAMx bias for isoprene products changed from 48% to -33%. The reduction in the magnitude of bias for isoprene products in this sensitivity test suggests that the MEGAN isoprene emissions are overestimated in the default case.

  6. In June 2013, Nguyen et al. (2015) measured dry deposition velocities (V_d) for biogenic trace gases in an Alabama forest during the Southern Oxidant and Aerosol Study (SOAS). Comparison of CAMx V_d against the measurements showed Vd was underestimated in the model. We increased CAMx dry deposition of these species to improve agreement with the SOAS measurements. The effects of this test on modeled ozone and isoprene and monoterpenes species were small.

- The best overall performance among all CAMx runs for a subset of species (isoprene, isoprene products, sum of monoterpenes, ozone, OH) occurred in the sensitivity test in which isoprene emissions were decreased by a factor of two. The CAMx bias for ozone was nearly unchanged across all CAMx runs.
- In the sensitivity test with updated MEGAN emissions, the CAMx bias for monoterpenes improved, but the overall bias for isoprene, isoprene products and OH increased. This result taken together with the high bias in MEGAN isoprene emissions compared to the aircraft fluxes, suggests that MEGAN isoprene emissions are overestimated in both the default and updated inventories.

6.2 Conclusions

Below, we present conclusions drawn from the results of this study.

- Accurate meteorological input data, especially PAR and temperature, are critical for accurate BVOC emission calculations. Bias in weather model simulation of clouds and shortwave radiation introduces bias into the MEGAN emissions. Standard WRF simulations

may result in considerable high bias in solar radiation and temperature due to model treatment of clouds. NLDAS appears to be better but also leads to overestimates. It should also be noted that bias in the PAR and temperature used to estimate emission factors from measured emissions will also introduce bias into the calculated emission factors. Data assimilation approaches (satellite and/or in-situ observations) are recommended for improving these inputs and they should be evaluated by comparison to observations.

- Landcover inputs (LAI and vegetation type) are also critical for BVOC emission modelling. LAI can vary considerably between years and we recommend using the provided 2013 LAI data for 2013 simulations and use the provided scripts and approach to calculate LAI for other years. We also recommend using the vegetation type distributions developed for this project.
- Emission factors are another key variable for BVOC emission modelling. We recommend using the new (aircraft based) isoprene emission factors (EFvA2015) developed for this project for BVOC emission modelling since both the eddy covariance and mixed layer approaches indicate this. However, more work still needs to be done to verify these emission factors. There is less evidence that the monoterpenes should be changed so we do not recommend changing the emission factors for monoterpenes from EFvE2015 to EFvA2015 at this time.

6.3 Recommendations for Future Work

- We need to reconcile the substantial differences between leaf-scale, tower-scale and aircraft-scale emission estimates as well as comparisons to satellite based emission estimates.
- As is the case with most BVOC studies, we have focused on only a few compounds but there is evidence that other “unmeasured” compounds play an important role in atmospheric chemistry (e.g. Di Carlo et al., 2004; Goldstein and Galbally, 2007; Park et al., 2013; Jardine et al., 2015). New analytical techniques provide an opportunity for determining whether there are other important compounds and also for characterizing the contribution of these compounds (Pankow et al., 2012). New techniques include high sensitivity, high resolution, accurate mass, full scan MS (TOF and Orbitrap) and better approaches to minimize artifacts and losses (whole air sampling, removing oxidants with reactive alkenes.
- BVOC response to stress is an important but not well known component of BVOC emission models. The processes controlling BVOC emission response to stress should be quantified and evaluated with long-term above canopy flux measurements.
- A good understanding of hydroxyl (OH) radical concentrations in forest environments is essential for modelling BVOC concentrations and for the interpretation of the measurements of BVOC fluxes. However, several detailed measurements have yielded significantly higher concentrations than can be explained using the known chemical reactions. Resolving this issue is important to advance the understanding of the effect of BVOC emissions on radical levels and ozone formation.

- Accurate meteorological data (PAR and temperature) is critical for accurate BVOC emission calculations. Bias in the WRF model's simulation of clouds and shortwave radiation introduces bias into the MEGAN emissions. The magnitude of this bias can be assessed by comparison of MEGAN emissions calculated along the aircraft flight track using temperatures and PAR measured aboard the aircraft with MEGAN emissions calculated using WRF model temperatures and PAR. Improvements to the WRF model treatment of clouds and radiation that enable it to provide accurate inputs to MEGAN are needed for development of accurate BVOC emission inventories for photochemical modeling.
- SOAS dry deposition velocity measurements were very useful in constraining CAMx model dry deposition of oxygenated VOCs. Dry deposition measurements for other species/locations would be very helpful in improving models.

7.0 AUDITS OF DATA QUALITY

During this study, we performed Quality Assurance/Quality Control (QA/QC) procedures to ensure that all data and products generated are of known and acceptable quality. QA/QC procedures were performed in accordance with the Category III Quality Assurance Project Plan (QAPP) that was completed at the beginning of the study. In a Category III Project, data audits must be performed for at least 10% of the data sets and a report of QA findings must be given in the final report (this document). A technical systems audit is not required. In Section 7, we report on the findings of our QA audits during this project.

7.1 Aircraft Data

100% of the aircraft data used in this study have undergone extensive QA/QC by the research groups who collected the data during the SAS Study. The NOAA and PNNL teams reviewed more than 10% of the aircraft data for quality assurance purposes before using the data for the analysis presented in Sections 2-4. Aircraft data were evaluated against the quality metrics outlined in the QAPP and were found to be of acceptable quality for use in this study.

7.2 LAI and PFT Data

A member of the PNNL team who did not develop the MEGAN input LAI and PFT data reviewed more than 50% of the developed data for quality assurance purposes and determined that the data were acceptable and suitable for use in this study. Where new data sets were developed as part of this study, they were compared with existing data sets (for example, see section 3.2.2 for comparison of new and existing PFT data sets).

7.3 MEGAN Emissions Modeling Data

The MEGAN model was run by Ramboll Environ using inputs developed by PNNL. Three sets of MEGAN emissions were developed using three sets of PNNL inputs which differed only in the EF data used: EFvE2011, EFvE2015 and EFvA2015. The Ramboll Environ team member who performed the initial MEGAN modeling using EFvE2011 inputs documented steps taken to obtain and process the MEGAN inputs, file paths to all inputs and outputs and provided a brief summary of the results. The documentation was used in the subsequent MEGAN modeling with EFvE2015 and EFvA2015 inputs to ensure consistency in methods. Once the MEGAN modeling was completed, a Ramboll Environ team member who had not performed the MEGAN modeling reviewed the modeling scripts for accuracy and then reviewed the model outputs. For the ISOP and TERP species, model outputs for 10% of the episode days were reviewed using the PAVE visualization tool for completeness and compared with observations as well as the episode mean values reported in this document. All data for these days were examined for values that were outliers or otherwise unreasonable and none were found. A second Ramboll Environ team member reviewed ISOP and TERP outputs for each day for the entire episode and found all values were reasonable. For other MEGAN output species such as SQT, NO, MEOH and FORM, model outputs for 10% of the episode days were reviewed using the PAVE visualization tool for completeness and consistency with episode averages as well as

the range of modeled values-no comparisons with observations were made. The MEGAN output data were determined to be correctly developed and complete and therefore suitable for the purposes of this study.

7.4 WRF Meteorological Modeling Data

The WRF model run output was evaluated against observed winds, temperatures, humidity and precipitation for all hours for 100% of episode days to ensure that the model had been run correctly and provided a reasonable simulation of atmospheric conditions during the modeling period. The model output data were evaluated against the quality metrics described in the QAPP. This evaluation is described in Section 5.3. A Ramboll Environ team member who did not perform the WRF modeling reviewed the WRF model scripts to ensure that the model had been run correctly. The WRF modeling was determined to have been carried out correctly and the model results to be suitable for use in the MEGAN emissions modeling and the CAMx air quality modeling.

7.5 CAMx Modeling Data

All CAMx runs were evaluated against aircraft and surface measurements to ensure that the model had been run correctly and provided a reasonable simulation of the chemical species of interest in this study. This evaluation is described in Section 5.5. Additional QA/QC checks were performed to ensure that the modeling was performed correctly. A member of the research team who did not conduct the modeling or air quality model input data processing reviewed animations of the model-ready emissions for NO, NO2, ISOP, and TERP using PAVE for 10% of the episode days. Spatial patterns of emissions were reviewed and the reasonableness of emissions values was assessed. No outliers or missing data were found and the emissions inputs were deemed acceptable for use in the CAMx modeling.

A member of the Ramboll Environ team who did not conduct the modeling or air quality model input data processing reviewed all CAMx modeling and post-processing scripts for accuracy as well as consistency among the Base Run and sensitivity tests. For 10 % of episode days, CAMx output for each hour of the day was reviewed using PAVE animations for the following species: O3, NO2, TERP, SQT, ISOP, FORM, ACET, ALD2, BENZ, CO, MEOH, HNO3, PAN, SO2, and PRPA. The modeling outputs were determined to be of acceptable quality and suitable for use in this study.

8.0 REFERENCES

Ahmadov, R., McKeen, S., Trainer, M., Banta, R., Brewer, A., Brown, S. S., Edwards, P. M., de Gouw, J. A., Frost, G. J., Gilman, J. B., Helmig, D., Johnson, B., Karion, A., Koss, A., Langford, A., Lerner, B., Olson, J., Oltmans, S., Peischl, J., Petron, G., Pichugina, Y., Roberts, J. M., Ryerson, T., Schnell, R., Senff, C., Sweeney, C., Thompson, C., Veres, P., Warneke, C., Wild, R., Williams, E. J., Yuan, B. and Zamora, R.: Understanding high wintertime ozone pollution events in an oil and natural gas-producing region of the western US, *Atmos. Chem. Phys*., 15, 411–429, doi:10.5194/acpd-14-20295-2014, 2015.

Alapaty, K., J. A. Herwehe, T. L. Otte, C. G. Nolte, O. R. Bullock, M. S. Mallard, J. S. Kain, and J. Dudhia. 2012. Introducing subgrid-scale cloud feedbacks to radiation for regional meteorological and climate modeling, *Geophys. Res. Lett*., 39, L24809, doi:10.1029/2012GL054031.

Daly, C., M. Halbleib, J.I. Smith, W.P. Gibson, M.K. Doggett, G.H. Taylor, J. Curtis, P.P. Pasteris 2008. Physiographically sensitive mapping of climatological temperature and precipitation across the conterminous United States. *Int. J. Climatol.,* (http://prism.nacse.org/documents/Daly2008_PhysiographicMapping_IntJnlClim.pdf).

Di Carlo, P., W.H. Brune, M. Martinez, H. Harder, R. Lesher, X.R. Ren, T. Thornberry, M.A. Carroll, V. Young, P.B. Shepson, D. Riemer, E. Apel and C. Campbell 2004. Missing OH reactivity in a forest: Evidence for unknown reactive biogenic VOCs. *Science*. 304:722-725.

Ehhalt, D. H. and Rohrer, F.: Dependence of the OH concentration on solar UV, *J. Geophys. Res.*, 105, 3565–3571, 2000.

ENVIRON, 2013. The Comprehensive Air quality Model with extensions (CAMx) homepage, http://www.CAMx.com.

Garrigues, S., Allard, D., Baret, F., and Weiss, M.: Quantifying spatial heterogeneity at the landscape scale using variogram models, Remote Sensing of Environment, 103, 81-96, 2006.

Goldstein, A.H. and Galbally, I.E. 2007. Known and unexplored organic constituents in the earth's atmosphere. *Environ. Sci. & Tech.* 41(5), 1514-1521.

Guenther, A., Karl, T., Harley, P., Wiedinmyer, C., Palmer, P., & Geron, C. (2006). Estimates of global terrestrial isoprene emissions using MEGAN (Model of Emissions of Gases and Aerosols from Nature). *Atmospheric Chemistry and Physics Discussions, 6*(1), 107-173.

Guenther, A. (2013), Biological and Chemical Diversity of Biogenic Volatile Organic Emissions into the Atmosphere, ISRN Atmospheric Sciences, 2013(doi: 10.1155/2013/786290).

Guenther, A. B., X. Jiang, C. L. Heald, T. Sakulyanontvittaya, T. Duhl, L. K. Emmons, and X. Wang (2012), The Model of Emissions of Gases and Aerosols from Nature version 2.1 (MEGAN2.1): an extended and updated framework for modeling biogenic emissions, *Geosci. Model Dev*., 5(6), 1471-1492.

Hasel, M., C. Kottmeier, U. Corsmeier, and A. Wieser. 2005. Airborne measurements of turbulent trace gas fluxes and analysis of eddy structure in the convective boundary layer over complex terrain. *Atmospheric Research* 74 (1-4):381-402.

Herwehe, J.A., K. Alapaty, T.L. Spero, C.G. Nolte, 2014. Increasing the credibility of regional climate simulations by introducing subgrid-scale cloud-radiation interactions. *J. Geophys. Res.*, 119, 5317-5330, doi:10.1002/2014JD021504.

Hildebrandt-Ruiz, L. and G. Yarwood 2013. Interactions between Organic Aerosol and NOy: Influence on Oxidant Production. Final report for AQRP project 12-012.

Jardine, A.B., Jardine, K.J., Fuentes, J.D., Martin, S.T., Martins, G., Durgante, F., Carneiro, V., Higuchi, N., Manzi, A.O. and Chambers, J.Q. (2015) Highly reactive light-dependent monoterpenes in the Amazon. *Geophys. Res. Lett.* 42(5), 1576-1583.

Jin, S., Yang, L., Danielson, P., Homer, C., Fry, J., & Xian, G. (2013). A comprehensive change detection method for updating the National Land Cover Database to circa 2011. *Remote Sensing of Environment, 132*, 159-175.

Johnson, J., P. Karamchandani, G. Wilson, and G. Yarwood, 2013. TCEQ Ozone Forecasting System. Prepared for Mark Estes, TCEQ. November.

Karl, T., E. Apel, A. Hodzic, D. D. Riemer, D. R. Blake, and C. Wiedinmyer 2009. Emissions of volatile organic compounds inferred from airborne flux measurements over a megacity, *Atmos. Chem. Phys*., 9(1), 271-285.

Karl, T., P. K. Misztal, H. H. Jonsson, S. Shertz, A. H. Goldstein, and A. B. Guenther. 2013. Airborne flux measurements of BVOCs above Californian oak forests: Experimental investigation of surface and entrainment fluxes, OH densities and Dahmköhler numbers. *J. Atmos. Sci.*, 70, 3277–3287.

Kemball-Cook, S.R., Y. Jia, R. C. Emery, R. Morris, 2005. "Alaska MM5 Modeling for the 2002 Annual Period to Support Visibility Modeling." Prepared for the Western Regional Air Partnership, Denver CO. September.

Kemball-Cook, S., T. Pavlovic, J. Johnson, L. Parker, D.J. Rasmussen, J. Zagunis, L. Ma, G. Yarwood, 2014. Analysis of Wildfire Impacts on High Ozone Days in Houston, Beaumont, and Dallas-Fort Worth in 2012 and 2013. Final Report: Work Order 582-11-10365-FY14-19. Prepared for the Texas Commission on Environmental Quality, Austin, TX; by ENVIRON International Corporation, Novato, CA, July.

Kim, S. W., Barth, M. C. and Trainer, M.: Influence of fair-weather cumulus clouds on isoprene chemistry, *J. Geophys. Res.-Atmos*., 117(D10), D10302, doi:10.1029/2011JD017099, 2012.

Kota, S.-H., G. Schade, M. Estes, D. Boyer, and Q. Ying, 2015. Evaluation of MEGAN predicted biogenic isoprene emissions at urban locations in Southeast Texas. *Atmos. Env*. V. 110, p. 54–64.

Lenschow, D., Mann, J., & Kristensen, L. (1994). How long is long enough when measuring fluxes and other turbulence statistics? *Journal of Atmospheric and Oceanic Technology*, 11(3), 661-673.

Mauder, M., Desjardins, R. L., & MacPherson, I. (2007). Scale analysis of airborne flux measurements over heterogeneous terrain in a boreal ecosystem. *Journal of Geophysical Research: Atmospheres (1984–2012), 112*(D13).

McNally, D. E., 2009. 12 km MM5 Performance Goals. Presentation to the Ad-Hoc Meteorology Group. June 25, 2009. Available at: http://www.epa.gov/scram001/adhoc/mcnally2009.pdf.

Misztal, P., Karl, T., Weber, R., Jonsson, H., Guenther, A. B., & Goldstein, A. H. (2014). Airborne flux measurements of biogenic isoprene over California. *Atmospheric Chemistry and Physics, 14*(19), 10631-10647.

NatureServe. (2009). International Ecological Classification Standard: Terrestrial Ecological Classifications (N. C. Databases., Trans.). Arlington, VA, U.S.A.

Nguyen, T., J. D. Crounse, A. P. Teng, J. M. St. Clair, F. Paulot, G. M. Wolfe, and P. O. Wennberg. 2015. Rapid deposition of oxidized biogenic compounds to a temperate forest. PNAS. www.pnas.org/cgi/doi/10.1073/pnas.1418702112.

Oleson, K. W., Lawrence, D. M., Bonan, G. B., Drewniak, B., Huang, M., Koven, C. D., . . . Yang, Z.-L. (2013). Technical Description of version 4.5 of the Community Land Model (CLM) (N. E. S. Laboratory, Trans.). Boulder, Colorado. U.S.A: National Center for Atmospheric Research.

Pankow, J.F., Luo, W., Melnychenko, A.N., Barsanti, K.C., Isabelle, L.M., Chen, C., Guenther, A.B. and Rosenstiel, T.N. (2012) Volatilizable Biogenic Organic Compounds (VBOCs) with two dimensional Gas Chromatography-Time of Flight Mass Spectrometry (GC × GC-TOFMS): sampling methods, VBOC complexity, and chromatographic retention data. *Atmos. Meas. Tech*. 5(2), 345-361.

Park, J.H., Goldstein, A.H., Timkovsky, J., Fares, S., Weber, R., Karlik, J. and Holzinger, R. (2013) Active Atmosphere-Ecosystem Exchange of the Vast Majority of Detected Volatile Organic Compounds. *Science* 341(6146), 643-647.

Peeters, J., Nguyen, S.V., Nguyen, T.L., Stavrakou, T., Müller, J.-F., 2013. Hydroxyl radical regeneration in isoprene oxidation: the upgraded mechanism LIM1. Presentation to ACCENT Meeting, Urbino, Italy.

Peeters, J., Müller, J.-F., Stavrakou, T., Nguyen, V.S., 2014. Hydroxyl radical recycling in isoprene oxidation driven by hydrogen bonding and hydrogen tunneling: The upgraded LIM1 mechanism. *J. Phys. Chem*. A 118, 8625-8643.

Pétron, Gabrielle, Gregory Frost, Benjamin R. Miller, Adam I. Hirsch, Stephen A. Montzka, Anna Karion, Michael Trainer, Colm Sweeney, Arlyn E. Andrews, Lloyd Miller, Jonathan Kofler, Amnon Bar-Ilan, Ed J. Dlugokencky, Laura Patrick, Charles T. Moore Jr., Thomas B. Ryerson, Carolina Siso, William Kolodzey, Patricia M. Lang, Thomas Conway, Paul

Novelli, Kenneth Masarie, Bradley Hall, Douglas Guenther, Duane Kitzis, John Miller, David Welsh, Dan Wolfe, William Neff, and Pieter Tans, (2012). Hydrocarbon emissions characterization in the Colorado Front Range: A pilot study. *J. Geophys. Res*., V. 117, D04304, doi:10.1029/2011JD016360.

Popescu, S.C., R. Sheridan, N.W. Ku, and S. Srinivasan. 2011. Urban Vegetation for Biogenic Emissions, Report on TCEQ Grant # 582-5-64593-FY11-29. Prepared for Clint Harper, TCEQ Air Quality Division.

Sakulyanontvittaya, T., G. Yarwood, and A. Guenther. 2012. Improved biogenic emission inventories across the West. Prepared for: Western Governors' Association, 1600 Broadway, Suite 1700, Denver, CO 80202.

Warneke, C., de Gouw, J. A., Del Negro, L., Brioude, J., McKeen, S., Stark, H., Kuster, W. C., Goldan, P. D., Trainer, M., Fehsenfeld, F. C., Wiedinmyer, C., Guenther, A. B., Hansel, A., Wisthaler, A., Atlas, E. L., Holloway, J. S., Ryerson, T. B., Peischl, J., Huey, L. G. and Case Hanks, A. T.: Biogenic emission measurement and inventories determination of biogenic emissions in the eastern United States and Texas and comparison with biogenic emission inventories, *J. Geophys. Res.-Atmos.,* 115, D00F18, doi:10.1029/2009JD012445, 2010.

Wiedinmyer, C., Akagi, S. K., Yokelson, R. J., Emmons, L. K., Al-Saadi, J. A., Orlando, J. J., and Soja, A. J.: The Fire INventory from NCAR (FINN): a high resolution global model to estimate the emissions from open burning, Geosci. Model Dev., 4, 625-641, doi:10.5194/gmd-4-625-2011, 2011.

Yarwood, G., H. Gookyoung, W.P.L. Carter, G.Z. Whitten. 2012. "Environmental Chamber Experiments to Evaluate NOx Sinks and Recycling in Atmospheric Chemical Mechanisms." Final Report prepared for the Texas Air Quality Research Program, University of Texas, Austin, Texas (AQRP Project 10-042, February 2012).